



**HAL**  
open science

# Graphene based nanofluids : development, characterization and application for heat and energy systems

Samah Hamze

► **To cite this version:**

Samah Hamze. Graphene based nanofluids : development, characterization and application for heat and energy systems. Mechanical engineering [physics.class-ph]. Université de Rennes, 2020. English. NNT : 2020REN1S010 . tel-03033677

**HAL Id: tel-03033677**

**<https://theses.hal.science/tel-03033677>**

Submitted on 1 Dec 2020

**HAL** is a multi-disciplinary open access archive for the deposit and dissemination of scientific research documents, whether they are published or not. The documents may come from teaching and research institutions in France or abroad, or from public or private research centers.

L'archive ouverte pluridisciplinaire **HAL**, est destinée au dépôt et à la diffusion de documents scientifiques de niveau recherche, publiés ou non, émanant des établissements d'enseignement et de recherche français ou étrangers, des laboratoires publics ou privés.

# THESE DE DOCTORAT DE

L'UNIVERSITE DE RENNES 1

ECOLE DOCTORALE N° 602  
*Sciences pour l'Ingénieur*  
Spécialité : *Energétique, Thermique et Combustion*

Par

**Samah HAMZE**

## **Graphene based nanofluids: development, characterization and application for heat and energy systems**

Thèse présentée et soutenue à l'Université de Rennes 1, le 15 octobre 2020  
Unité de recherche : Laboratoire de Génie Civil et Génie Mécanique  
Thèse N° :

### **Rapporteurs avant soutenance :**

Leonor HERNÁNDEZ LÓPEZ  
Alina ADRIANA MINEA

Professeur, Universitat Jaume I, Espagne  
Professeur, Technical University Gheorghe Asachi, Roumanie

### **Composition du Jury :**

Examineurs : Stefan VAN VAERENBERGH  
Josefa FERNÁNDEZ PÉREZ  
Alina ADRIANA MINEA  
Leonor HERNÁNDEZ LÓPEZ

Professeur, Université Libre de Bruxelles, Belgique  
Professeur, University of Santiago de Compostela, Espagne  
Professeur, Technical University Gheorghe Asachi, Roumanie  
Professeur, Universitat Jaume I, Espagne

Dir. de thèse : Thierry MARÉ  
Co-dir. de thèse : Patrice ESTELLÉ

Maître de Conférences HDR, Université de Rennes 1  
Maître de Conférences, Université de Rennes 1

### **Invité(s)**

Brigitte VIGOLO

Chargé de Recherche CNRS, IJL, Université de Lorraine



*“Science opens an infinite path for the human mind and launches it, through a series of countless steps, onto the asymptote of truth.”*

**Paul Bert**



# Acknowledgements

First of all, I would like to thank my thesis director Dr. Thierry MARÉ, and my co-director Dr. Patrice ESTELLÉ, without whom this work could not have been carried out. I would like to say that I have had the best possible supervision to carry out the hard work that is the thesis. During these three years, they (especially Dr. Patrice ESTELLÉ) were able to lavish me with their knowledge, their great availability, their extreme patience, their humour, their kindness, and above all their unfailing support from the beginning to the end of this thesis.

I would like to warmly thank our collaborators at the *Institut Jean Lamour* especially Dr. Brigitte VIGOLO and Dr. Nawal BERRADA, and all the team who worked with us on this project: Dr. Alexandre DESFORGES, Dr. Dominique BEGIN, Dr. Florentin MICHAUX, Dr. Jaafar GHANBAJA and Dr. Jérôme GLEIZE. Thank you for the countless discussions and for all the little and big moments that contributed to the success of this work.

I thank all the jury members. Sincere thanks to Pr. Stefan VAN VAERENBERGH, president of the jury and examiner of this thesis. I am extremely grateful to Pr. Josefa FERNÁNDEZ PÉREZ and Dr. Brigitte VIGOLO for examining this work. I am very warmly grateful to Pr. Alina ADRIANA MINEA and Pr. Leonor HERNÁNDEZ LÓPEZ for giving me the benefit of their expertise by agreeing to judge this work and to devote time to the examination of this manuscript.

I would like to warmly thank all the staff of the IUT of the University of Rennes 1 for having welcomed me during these three years of thesis and in particular Pr. Christophe LANOS, director of the Laboratory of Civil Engineering and Mechanical Engineering (LGCGM), and my colleagues especially Nourhan MORTADA, Naima BOUMEDIENE, Damien GAUDREL and Moussa KA for their good mood, their kindness and their encouragements.

Another people that I would like to thank very much for all the time we've been working on together is Abdussamet SUBASI, associate professor at the Istanbul Technical University, Turkey, and David CABALEIRO, doctor at the University of Vigo, Spain, and his team of work, especially Pr. Luis LUGO. Thank you very much for your availability, your advice, your encouragement, and especially your kindness.

## *Acknowledgements*

---

And what would those years have been like without the support of my family and friends?

I want to thank my family, my brothers and sisters, for supporting me. Unfortunately, the distance did not allow us to see each other often, thank you for always being there to support me.

A huge thank you to my friends: Farah, Soumaya, Lina, Nourhan, Marwan, Queen, Naima, Nour, Asseel, Ali, Hassan... who believe in me and help me to move forward and be who I am.

These last lines will allow me to show my deepest love and gratitude to my dear mother. Thank you for your devotion to me and for all the sacrifices made to get me here. Thank you for always supporting me...

# Summary

<b>Nomenclature.....</b>	<b>1</b>
<b>Résumé.....</b>	<b>3</b>
<b>I- Introduction.....</b>	<b>13</b>
I.1- Research context.....	14
I.2- Objectives.....	16
I.3- Structure.....	17
I.4- References.....	18
<b>II- General information on graphene nanofluids.....</b>	<b>21</b>
II.1- Introduction.....	22
II.2- Definition.....	22
II.2.1- Base fluids.....	23
II.2.2- Nanoadditives.....	25
II.3- Proposal process of new nanofluids.....	28
II.3.1- Nanofluid design.....	29
II.3.1.1- Nanoparticles synthesis and characterization.....	29
II.3.1.2- Nanofluid preparation.....	37
II.3.1.3- Stability.....	39
II.3.2- Thermophysical profile.....	42
II.3.2.1- Thermal conductivity.....	44
II.3.2.2- Rheology and Dynamic viscosity.....	49
II.3.2.3- Isobaric heat capacity.....	58
II.3.2.4- Density.....	60
II.3.2.5- Surface tension.....	61
II.3.3- Heat transfer performance.....	65

II.3.3.1- Qualitative approach.....	66
II.3.3.2- Quantitative approach.....	67
II.4- Conclusion.....	70
II.5- References.....	71
<b>III- Materials and experimental methods.....</b>	<b>83</b>
III.1- Introduction.....	84
III.2- Presentation of the nanofluids used.....	84
III.3- Graphene synthesis.....	86
III.4- Graphene characterization.....	88
III.5- Nanofluid preparation.....	89
III.6- Nanofluid stability.....	92
III.7- Thermophysical properties of nanofluids: measurement techniques, experimental protocol and validation.....	93
III.7.1- Thermal conductivity.....	93
III.7.2- Isobaric heat capacity.....	97
III.7.3- Dynamic viscosity.....	98
III.7.4- Density.....	102
III.7.5- Surface tension.....	105
III.8- Conclusion.....	106
III.9- References.....	107
<b>IV- Characterization of FLG based nanofluids and their thermophysical properties: results and discussion.....</b>	<b>111</b>
IV.1- Introduction.....	112
IV.2- Few-Layer Graphene-Based Nanofluids with Enhanced Thermal Conductivity.....	114
IV.3- Isobaric heat capacity.....	136

IV.4- Volumetric properties and surface tension of few-layer graphene nanofluids based on a commercial heat transfer fluid.....	144
IV.5- Shear flow behavior and dynamic viscosity of few-layer graphene nanofluids based on propylene glycol-water mixture.....	163
IV.6- Conclusion.....	176
<b>V- Thermal performance of stable FLG nanofluids: qualitative approach.....</b>	<b>179</b>
V.1- Introduction.....	180
V.2- Laminar regime.....	180
V.3- Turbulent regime.....	186
V.4- Conclusion.....	191
V.5- References.....	192
<b>VI - General conclusion and perspectives.....</b>	<b>193</b>
<b>Appendix.....</b>	<b>199</b>



# Nomenclature

$k$	Thermal conductivity [ $\text{W}\cdot\text{m}^{-1}\cdot\text{K}^{-1}$ ]
$T$	Temperature [K]
$\eta$	Dynamic viscosity [mPa.s]
$C_p$	Isobaric heat capacity [ $\text{J}\cdot\text{g}^{-1}\cdot\text{K}^{-1}$ ]
$\varphi_v$	Volume fraction
$\varphi_m$	Mass fraction
$\rho$	Density [ $\text{kg}\cdot\text{m}^{-3}$ ]
$ST$	Surface tension [ $\text{mN}\cdot\text{m}^{-1}$ ]
$C_k$	Coefficient of thermal conductivity improvement
$C_\eta$	Coefficient of dynamic viscosity improvement
$Mo$	Mouromsteff number
$Re$	Reynolds number
FLG	Few layer graphene
SEM	Scanning electron microscopy
TEM	Transmission electron microscopy
HRTEM	High-resolution transmission electron microscopy
FFT	Fast Fourier Transform
IFFT	Inverse Fast Fourier Transform
TrX	Triton X-100
P123	Pluronic® P-123
GA	Gum Arabic
AAD	Absolute average deviation [%]
DW	Distilled water
$\dot{\gamma}$	Shear rate [ $\text{s}^{-1}$ ]
$\sigma$	Shear stress [Pa]
CMC	Critical micelle concentration
$\alpha_p$	Isobaric thermal expansivity [ $\text{K}^{-1}$ ]

## *Nomenclature*

---

St. Dev.	Standard deviation
$a_i$	Fitting parameters
R	Cone and plate diameter [m]
$\alpha$	Cone angle [°]
$\dot{W}$	Pumping power consumption
FOM	Figure of merit
GO	Graphene oxide
rGO	Reduced graphene oxide
GQD	Graphene quantum dots
CVD	Chemical vapor deposition
LPE	Liquid phase exfoliation
Subscripts	
$np$	Nanoparticles
$nf$	Nanofluid
$sft$	Surfactant
$tyf$	Tyfocor
$bf$	Base fluid
Symbols	
↑	Increase
→	Stable or constant
↓	Decrease

# Résumé

Dans notre vie quotidienne, le transfert de la chaleur et de l'énergie constitue la base de nombreux processus industriels. L'épuisement progressif des énergies fossiles conduit à améliorer et optimiser les rendements de ces échanges par de nouveaux procédés. Les « nanofluides » peuvent s'inscrire dans ce cadre pour être l'outil de transfert thermique et énergétique de nos jours et dans l'avenir. Ils apparaissent comme un sujet de recherche mondial en raison de leur potentiel, et ils peuvent être utilisables dans les échangeurs de chaleur, les systèmes énergétiques, les capteurs solaires, les appareils électroniques, en substitution des liquides caloporteurs traditionnels.

Qu'est-ce qu'un nanofluide ? Et quelles sont ses propriétés intéressantes qui le rendent important dans ce domaine ? Les nanofluides sont constitués des nanoparticules (des particules de taille nanométrique  $< 100$  nm) qui ont une forme déterminée (sphériques, cylindriques...), dispersées dans un fluide de base avec ou sans présence d'un surfactant qui aide si nécessaire à la dispersion des nanoparticules dans le fluide et à leur stabilité. Les nanoparticules peuvent être de type métallique (Cu, Ag, Au...), des oxydes ( $Al_2O_3$ , CuO,  $SiO_2$ ,  $TiO_2$ ...), des nanotubes de carbone (CNT), graphène, etc...

L'idée est d'améliorer les propriétés thermiques des fluides caloporteurs en y insérant une phase solide de conductivité thermique très élevée, ainsi les nanofluides présentent une conductivité thermique significativement plus élevée que les fluides de base qui augmente avec l'augmentation de la concentration de nanoparticules. Dans leur développement et leur exploitation, il convient de trouver un compromis entre de meilleures propriétés thermiques tout en maîtrisant leur viscosité (qui ne doit pas être trop importante dans les échangeurs par exemple) et leur stabilité qui doit être assurée, sans quoi les propriétés peuvent être modifiées. Plusieurs paramètres peuvent jouer un rôle dans l'efficacité des nanofluides comme la concentration et la nature des nanoparticules, leur densité, leur type, leur taille, leur aspect, la température, le fluide de base, la présence d'un surfactant, etc...

Parmi les familles de nanoparticules, les nanomatériaux à base de carbone (nanotubes de carbone, graphène, diamant...) sont d'un intérêt majeur en raison de leurs excellentes propriétés thermiques intrinsèques et qui permettent d'obtenir des nanofluides plus performants que ceux préparés avec

## Résumé

des nanoparticules d'oxyde métallique par exemple. C'est pourquoi notre projet se focalise sur les nanofluides à base de carbone et le graphène plus spécifiquement.

Ce projet s'inscrit aussi dans une collaboration avec l'Institut Jean Lamour de Nancy, spécialisé dans les propriétés chimiques des matériaux à base de carbone et de graphène. C'est dans cet organisme que sont préparés les nanofluides dédiés à notre étude. Plus largement, notre projet contribue également à l'European COST Action NanoUptake OC-2015-1-19591, « Overcoming Barriers to Nanofluids Market Uptake », puisqu'il vise au développement et à l'exploitation pratique de nanofluides.

Nous présentons dans cette thèse une étude complète sur les nanofluides à base de graphène à quelques couches (FLG), y compris la synthèse du FLG, la préparation des nanofluides à base de FLG et l'étude de leur stabilité, ainsi que l'évaluation expérimentale de leurs propriétés thermophysiques en fonction de la concentration en graphène, du type de surfactant utilisé et de la température. Finalement, sur la base de ces résultats et par une approche qualitative, le potentiel applicatif des nanofluides dans des systèmes énergétiques est déterminé pour sélectionner le meilleur candidat.

Les feuillets de graphène sont synthétisés par une méthode originale d'exfoliation mécanique de graphite expansé dans de l'eau assistée par des agents de surface biosourcés, tels que l'acide tannique, comme montre la figure 1. Les molécules d'acide tannique viennent ainsi s'intercaler entre les feuillets et favoriser leur séparation.

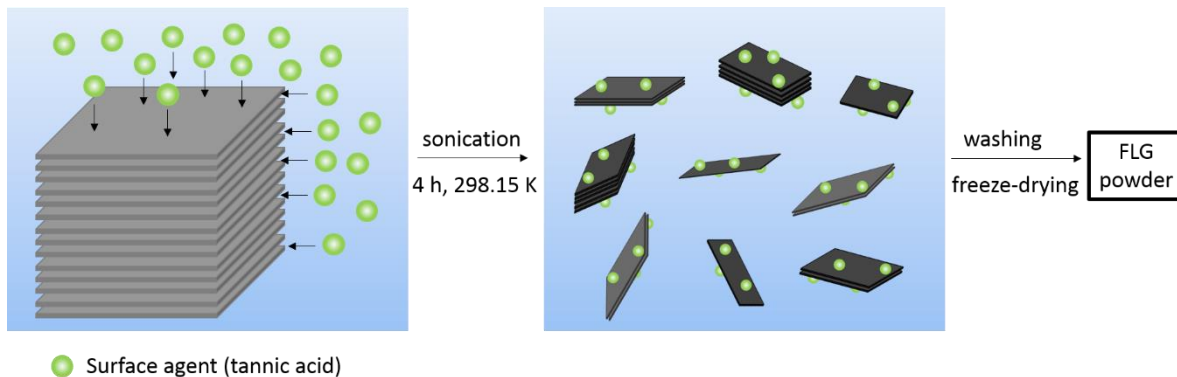


**Figure 1.** Schéma de la méthode d'exfoliation mécanique en milieu aqueux assistée par l'acide tannique [1].

La caractérisation morphologique et structurale de FLG synthétisé est étudiée à la fois par microscopie électronique à balayage (MEB) et à transmission (MET) et par spectroscopie Raman.

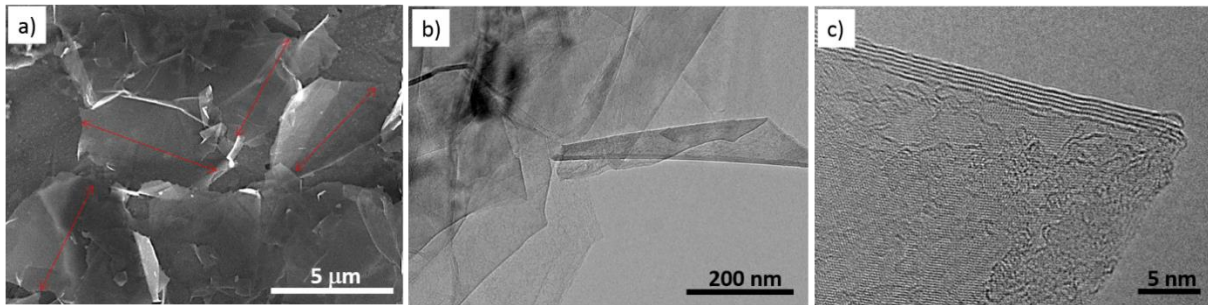


**Figure 2.** Images MEB (a) et MET (b et c) du FLG synthétisé [1].

La figure 2 montre les images MEB et MET du matériel graphique synthétisé. Les images d'observation à faible grossissement du MEB (Fig. 2a) et du MET (Fig. 2b) montrent que le matériau préparé se présente sous la forme de très fines feuilles d'environ 3 à 5 couches d'une épaisseur généralement comprise entre 1 et 2 nm (image typique illustrée dans la Fig. 2c), ce qui signifie que la méthode d'exfoliation utilisée produit de préférence du FLG. La taille latérale moyenne des feuilles de FLG est d'environ 5 µm, comme le montre la Fig. 2a. Les feuillets de graphène ont été caractérisés aussi par la spectroscopie Raman qui a montré que le rapport d'intensité  $I_D/I_G$  du graphite est supérieur à celui du FLG, ce qui signifie que ce dernier était de haute qualité structurale. En accord avec la spectroscopie Raman, des caractérisations MET à haute résolution, transformée de Fourier rapide, et transformée de Fourier rapide inverse ont montré que le FLG utilisé a une excellente qualité structurale avec son réseau d'atomes de carbone en nid d'abeille qui était bien visible.

Les nanofluides ont été préparés par la méthode de deux étapes où surfactants non ioniques (Triton X-100, Pluronic® P-123 et Gomme Arabique), un mélange commercial d'eau et de propylène glycol (Tyfocor® LS) et une teneur massique en FLG de 0,05 à 0,5% ont été utilisés, avec un rapport surfactant:FLG égal à 2 pour toutes les concentrations testées. La préparation est réalisée avec une sonde à ultrason en contrôlant les temps de sonication et la température des échantillons. Les échantillons à faible concentration en graphène sont obtenus par dilution de la solution la plus concentrée.

## Résumé

La stabilité statique des nanofluides à base de FLG a été suivie dans le temps par des observations visuelles et des analyses au Turbiscan. Le Turbiscan a permis de mesurer l'évolution de la sédimentation dans les nanofluides à base de FLG préparés avec le Triton X-100 et le Pluronic® P123 (Fig. 3b). Dans le cas de ces deux séries de nanofluides, le comportement de la sédimentation n'a pas été modifié par la concentration en FLG. La sédimentation complète a été plus rapide pour le Triton X-100 que pour le Pluronic® P123. La sédimentation des nanoparticules de FLG a été achevée après un jour avec le Triton X-100, tandis qu'avec le Pluronic® P123, la sédimentation du FLG a été atteinte 3 jours après la préparation du nanofluides (Fig. 3b). Une analyse fiable n'a pas été possible avec la gomme arabique alors que ce nanofluides a été visuellement observé plus stable que les deux autres.

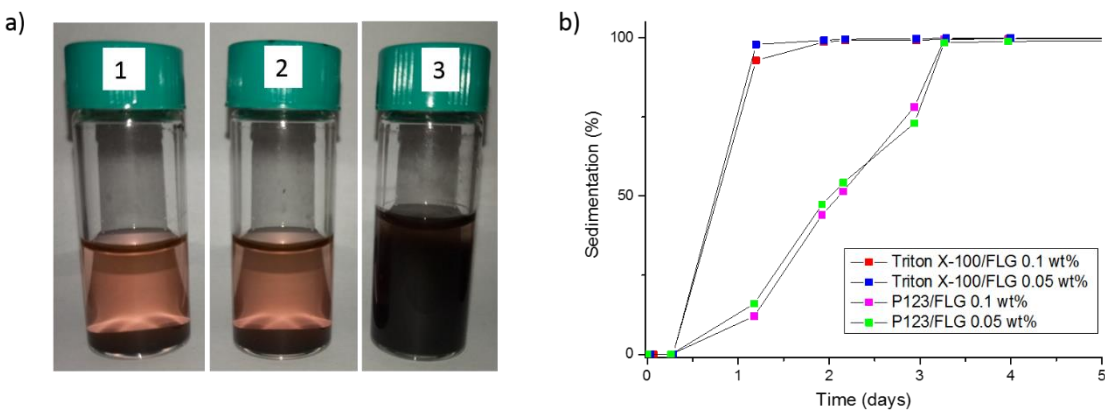


**Figure 3.** a) Photos de nanofluides à base de FLG avec 0,1 % en masse de FLG et (1) Triton X-100, (2) Pluronic® P-123 et (3) Gomme Arabique comme agent tensioactif 6 jours après leur préparation. b) Niveau de sédimentation du Turbiscan pour les nanofluides à base de FLG avec Triton X-100 et Pluronic® P-123 pour 0,05 et 0,1 % en masse de FLG [1].

Les mesures des propriétés thermo-physiques des trois séries de nanofluides à base de FLG sont effectuées dans la plage de température de 283,15 à 323,15 K. La conductivité thermique des fluides de base et des nanofluides a été évaluée avec un dispositif THW-L2 (Thermtest Inc., Canada) en utilisant la méthode du fil chaud transitoire. Les résultats ont montré que l'ajout du surfactant n'a pas d'effet significatif sur la conductivité thermique du Tyfocor® LS. A propos des nanofluides, l'ajout de FLG a amélioré la conductivité des fluides de base avec le Triton X-100, Pluronic® P-123 et Gomme Arabique par un taux maximal de 23,9%, 18,3% et 21,5%,

respectivement. Cette amélioration a été obtenue pour les nanofluides de concentration la plus élevée (0,5 % en masse), et elle est indépendante de la température. Un exemple à la température 283,15 K de la conductivité relative à toutes les concentrations volumiques est présenté dans la figure 5.

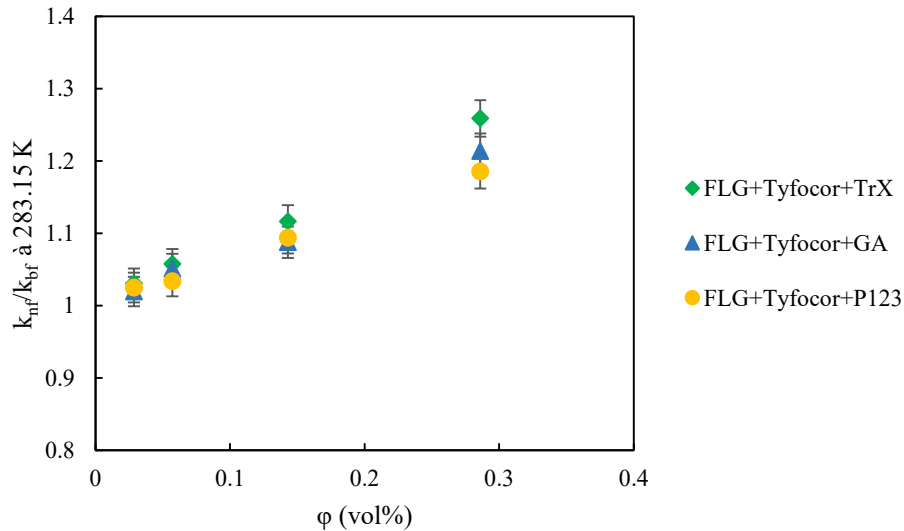


**Figure 5.** La variation de la conductivité thermique relative des nanofluides avec le Triton X-100, Pluronic® P-123 et Gomme Arabique en fonction de la concentration volumique de FLG à 283,15 K.

La conductivité thermique des nanofluides préparés a été comparée à plusieurs modèles et il a été démontré que l'amélioration de la conductivité thermique des nanofluides à base de graphène est régie par des effets combinés tels que la taille du FLG, la résistance thermique à l'interface du FLG, l'épaisseur et leur rapport de planéité.

Les mesures de la chaleur spécifique de FLG, des surfactants, du Tyfocor® LS, des fluides de base et des nanofluides ont été faites avec un Calorimètre Différentiel à Balayage DSC-Q2000 (TA Instruments, New Castle, USA) entre 283,15 K et 323,15 K. Les résultats ont montré que ni l'ajout du surfactant, ni l'ajout de FLG n'a un effet significatif sur la chaleur spécifique du Tyfocor® LS. Une comparaison entre les valeurs expérimentales de la chaleur spécifique et les valeurs calculées à l'aide de la loi de mélange montre que cette dernière peut décrire d'une manière adéquate les résultats expérimentaux des fluides de base et des nanofluides (voir Fig. 6).

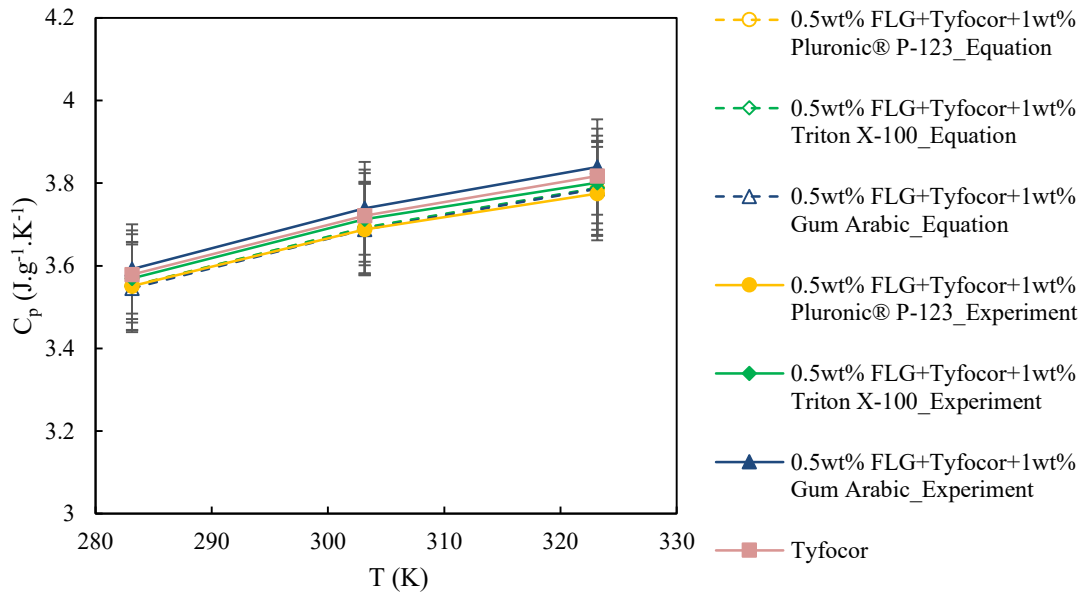


**Figure 6.** La variation de la chaleur spécifique des nanofluides de la concentration maximale, 0,5 % en masse de FLG, avec le Triton X-100, Pluronic® P-123 et Gomme Arabique, trouvé expérimentalement et par calcul en utilisant la loi de mélange, en fonction de la température.

Les densités du Tyfocor® LS, du Triton X-100 liquide, et de chaque mélange tensioactif+Tyfocor® LS utilisé comme fluide de base ainsi que les nanofluides préparés à base de FLG ont été déterminées expérimentalement au moyen d'un densimètre DMA 501 (Anton Paar, Autriche). La densité du FLG a été mesurée à température ambiante à l'aide d'un pycnomètre à gaz Quantachrome Ultrapyc 1200e (Quantachrome Instruments, Anton Paar, USA) travaillant avec de l'hélium sous un mode d'impulsion adapté aux poudres. Les densités du Pluronic® P-123 et Gomme Arabique ont été prises de la littérature. Il a été observé que la densité des nanofluides et des fluides de base préparés diminue avec la température avec une tendance similaire. De plus, il a été trouvé que l'ajout de surfactant n'a pas d'effet significatif sur l'évolution de la densité par rapport au Tyfocor® LS seul, sauf pour l'ajout de 0,5 et 1 % en masse de Gomme Arabique dans le Tyfocor® LS, pour lequel la densité augmente de 0,18 et 0,36%, respectivement. Les résultats montrent aussi que la densité des nanofluides diminue légèrement pour les plus faibles concentrations de FLG et augmente pour les concentrations les plus élevées. Les résultats sont similaires pour les trois séries de nanofluides étudiés. Un exemple à 303,15 K de la densité relative des nanofluides en fonction de la concentration massique de FLG est présenté dans la figure 7.

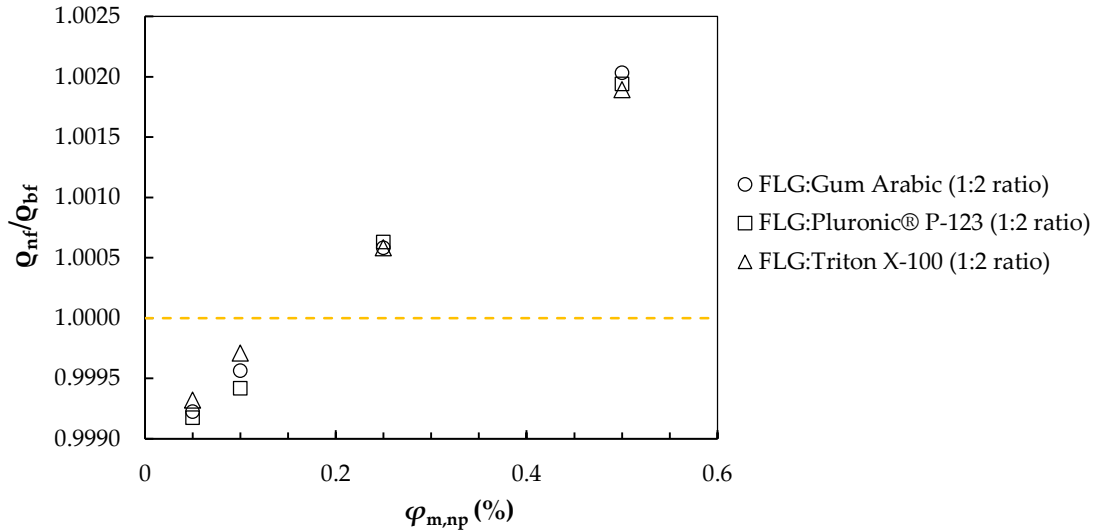


**Figure 7.** La densité relative des nanofluides, qui est définie comme le rapport de la densité des nanofluides à la densité des fluides de base correspondants, en fonction de la concentration massique de FLG à 303,15 K [2].

L'évolution de la densité des nanofluides à base de FLG en fonction de la température et de la concentration en FLG est bien prédite par l'équation de la moyenne pondérée de la densité, en tenant compte des densités de tous les composants.

À partir des résultats de la densité expérimentale, les effets de la température, de la nature et de la concentration des surfactants, ainsi que la concentration massique de FLG sur le coefficient d'expansion thermique isobare ont également été évalués. Il a été démontré que le coefficient d'expansion thermique isobare, qui augmente avec la température, est similaire pour les tous les fluides de base sans aucun effet distinct de l'agent de surface utilisé. Contrairement aux fluides de base, une diminution de cette propriété a été remarquée en présence de FLG avec tous les fluides de base utilisés.

Pour la tension de surface du Tyfocor® LS, des fluides de base et des nanofluides, un analyseur de goutte tombante DSA-30 de KRÜSS GmbH (Hambourg, Allemagne) a été utilisé pour effectuer les mesures. La tension de surface des nanofluides est plus sensible au type de tensioactif et à sa teneur en fonction de leur concentration critique de micelles (CMC). L'ajout de tensioactif a diminué la tension de surface du Tyfocor® LS, sauf dans le cas de la Gomme Arabique. Pour les nanofluides étudiés, cette propriété a évolué d'une manière variable en fonction du tensioactif utilisé et de la teneur en FLG. L'ajout de FLG peut induire une augmentation ou ne pas modifier

fortement la tension de surface. Par exemple, par rapport au Tyfocor® LS, la tension de surface des nanofluides est inférieure à celle du Tyfocor® LS dans le cas des tensioactifs Triton X-100 et Pluronic® P-123 et elle est supérieure dans le cas de la Gomme Arabique. Un exemple des résultats d'une série, celle avec le Pluronic® P-123, est présenté dans la figure 8.

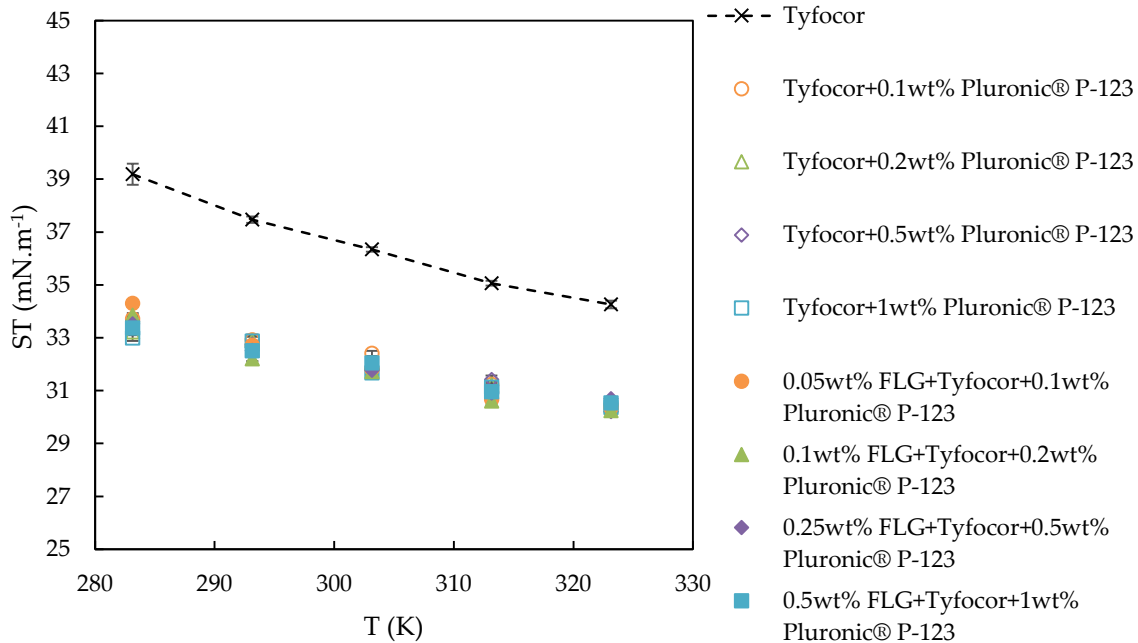


**Figure 8.** La variation de la tension de surface du Tyfocor® LS, des fluides de base et des nanofluides correspondants en fonction de la température [2].

Les études de viscosité dynamique ont été réalisées avec un rhéomètre rotatif Malvern Kinexus Pro de Malvern Instruments Ltd. (Malvern, Royaume-Uni) équipé d'une géométrie cône-plan appropriée pour étudier les suspensions colloïdales de faible viscosité. Au-delà de l'évaluation de la viscosité dynamique des nanofluides, l'étude montre que la température, le cisaillement et la durée du cisaillement jouent un rôle important sur la stabilité des nanofluides sous écoulement en fonction du surfactant et de la concentration en graphène. Les nanofluides avec le Pluronic® P-123 sont plus stables sous cisaillement que les deux autres séries. L'ajout de la concentration de FLG la plus élevée (0,5 % en masse) avec la présence du surfactant augmente la viscosité du Tyfocor® LS jusqu'à 19,9 %, 34,5 % et 121,6 % dans le cas de Pluronic® P-123, Triton X-100 et Gomme Arabique à 283,15 K, 283,15 K et 303,15 K, respectivement. Un exemple de la viscosité

relative (par rapport au mélange Tyfocor® LS+surfactant) des trois séries à 283,15 K est présenté dans la figure 9.

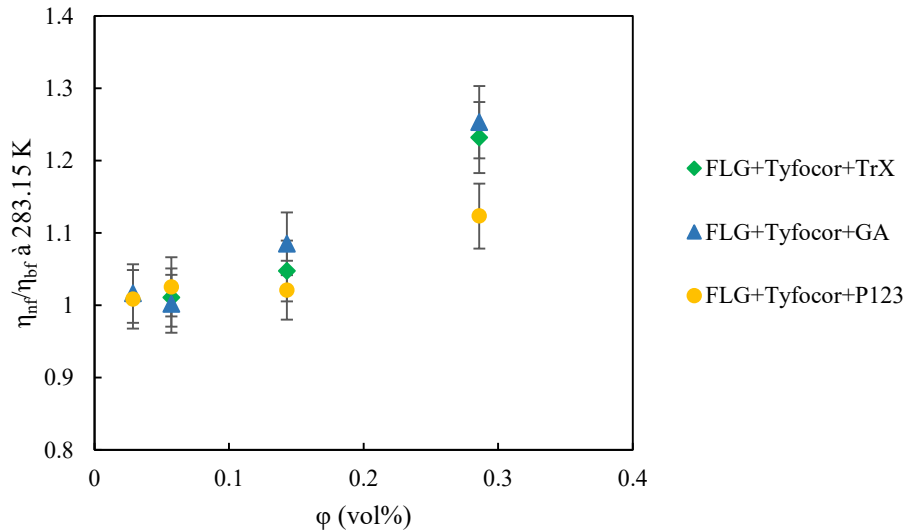


**Figure 9.** Variation de la viscosité relative des nanofluides avec Triton X-100, Pluronic® P-123, et Gomme Arabique en fonction de la concentration volumique de FLG à 283,15 K.

Enfin, pour les nanofluides stables sous cisaillement, l'évolution de la viscosité dynamique avec la température a été corrélée au modèle de Vogel-Fulcher-Tammann (VFT) [3].

En se basant sur les résultats de ces études, une approche théorique a été utilisée pour évaluer, dans un premier temps, les avantages offerts par les nanofluides à base de FLG, qui sont stables sous cisaillement, par rapport au Tyfocor® LS. Cette approche peut être utilisée pour prévoir les conditions expérimentales et les teneurs en particules qui tendraient vers un bilan énergétique favorable et identifier les nanofluides qui pourraient être testés dans des conditions réelles d'échange thermique. L'étude des performances de transfert de chaleur des nanofluides stables de FLG à base de Tyfocor® LS avec l'utilisation de Triton X-100, Pluronic® P-123, et de la Gomme Arabique comme tensioactifs a montré que la série de Pluronic® P-123 est la meilleure pour une utilisation possible dans un échangeur de chaleur entre 283,15 K et 323,15 K, en particulier la concentration volumique 0,143% qui correspond à la teneur massique 0,25%, sous écoulement laminaire et turbulent. De plus, les résultats de la tension de surface affirme aussi ce choix comme les nanofluides avec le Pluronic® P-123 ont les tensions de surface les plus faibles par rapport au Tyfocor® LS.

Dans le prolongement de ces travaux, il serait pertinent d'étudier les performances thermiques du ou des nanofluides sélectionnés en utilisant une approche quantitative, alors en réalisant des expériences dans un échangeur de chaleur et en étudiant ses performances en situation réelle. En outre, en ce qui concerne la stabilité des nanofluides, différentes actions pourraient être effectuées. Il sera intéressant de déterminer la nature des agents de corrosion et de vieillissement existant dans le fluide commercial utilisé, Tyfocor® LS, et d'évaluer leur influence sur la stabilité des nanofluides. Un développement des nanofluides similaires en remplaçant ce fluide de base par un mélange de composés purs de propylène glycol et d'eau avec le même rapport en masse (40:60)% pourrait aider dans ce sens. En outre, une étude des interactions entre les feuillets de graphène et les tensioactifs et le fluide de base pourrait être réalisée. Bien sûr, le graphène de haute qualité à quelques couches étudié et utilisé dans ce travail peut être employé pour produire des nanofluides avec différents fluides de base et/ou tensioactifs, et la présente étude pourrait être étendue à une gamme de températures plus large. Enfin, la vaste base de données expérimentale des propriétés thermo-physiques des nanofluides produits dans le cadre de ce travail peut être utilisée pour des recherches numériques dans différentes configurations.

## Références

- [1] S. Hamze *et al.*, “Few-Layer Graphene-Based Nanofluids with Enhanced Thermal Conductivity,” *Nanomaterials*, vol. 10, no. 7, p. 1258, Jun. 2020, doi: 10.3390/nano10071258.
- [2] S. Hamze *et al.*, “Volumetric Properties and Surface Tension of Few-Layer Graphene Nanofluids Based on a Commercial Heat Transfer Fluid,” *Energies*, vol. 13, no. 13, p. 3462, Jul. 2020, doi: 10.3390/en13133462.
- [3] S. Hamze *et al.*, “Shear flow behavior and dynamic viscosity of few-layer graphene nanofluids based on propylene glycol-water mixture,” *Journal of Molecular Liquids*, vol. 316, p. 113875, Oct. 2020, doi: 10.1016/j.molliq.2020.113875.

# Chapter I- Introduction

I.1- Research context.....	14
I.2- Objectives.....	16
I.3- Structure.....	17
I.4- References.....	18

## I.1- Research context

Energy consumption is one of the fundamental bases for the daily activity of societies in the 21<sup>st</sup> century. In the last century, the world energy demand has exponentially increased, mainly due to transport rising, energy-dependent human quotidian actions, population growth and industrial development [1]. So the growth in energy consumption pushes us to make an energy transition, which requires a research effort focused on the development of innovative, intelligent, durable, and effective solutions. Heat transfer plays an important role in many industrial processes, such as electronic devices, refrigerators, heat exchangers, solar energy systems, heating and cooling of buildings... Consequently, improving heat transfer is a key parameter, one solution consist of enhancing the thermal properties of usual heat transfer fluids.

Based on the fact that solids have intrinsic thermal properties higher than conventional heat transfer fluids as water, ethylene glycol, propylene glycol and engine oil (see Table I.1), the introduction of millimetric and micrometric solid particles in the fluids to enhance their thermal properties was initiated in the last decades of the 20<sup>th</sup> century.

**Table I.1.** Thermal conductivity of different materials [13–16].

	<i>Thermal conductivity (W.m<sup>-1</sup>.K<sup>-1</sup>)</i>
<b>Conventional fluids <sup>a</sup></b>	
<i>Water</i>	<i>0.613</i>
<i>Ethylene glycol</i>	<i>0.253</i>
<i>Propylene glycol</i>	<i>0.203</i>
<i>Engine oil</i>	<i>0.145</i>
<b>Metallic solids <sup>b</sup></b>	
<i>Silver</i>	<i>429</i>
<i>Copper</i>	<i>401</i>
<i>Aluminium</i>	<i>237</i>
<b>Non-metallic solids <sup>b</sup></b>	
<i>Graphene</i>	<i>~ 3000-5000</i>
<i>Diamond</i>	<i>~ 2300</i>
<i>Pure graphite</i>	<i>~ 2000</i>
<i>Silicon</i>	<i>148</i>
<i>Alumina</i>	<i>40</i>
<sup>a</sup> At 300 K	
<sup>b</sup> At room temperature	

More recently, the concept of “nanofluids” was introduced in 1995 by Choi *et al.* [2] who proposed the use of nanosized particles, which make the solution more stable than in the case of bigger particles because of the size effect and the Brownian motion of the nanoparticles in the fluid [3]. Since that time, this topic and related issues are of growing interest worldwide [4–12], due to the large number of applications where nanofluids could be used in replacement of common fluids (Figure I.1).

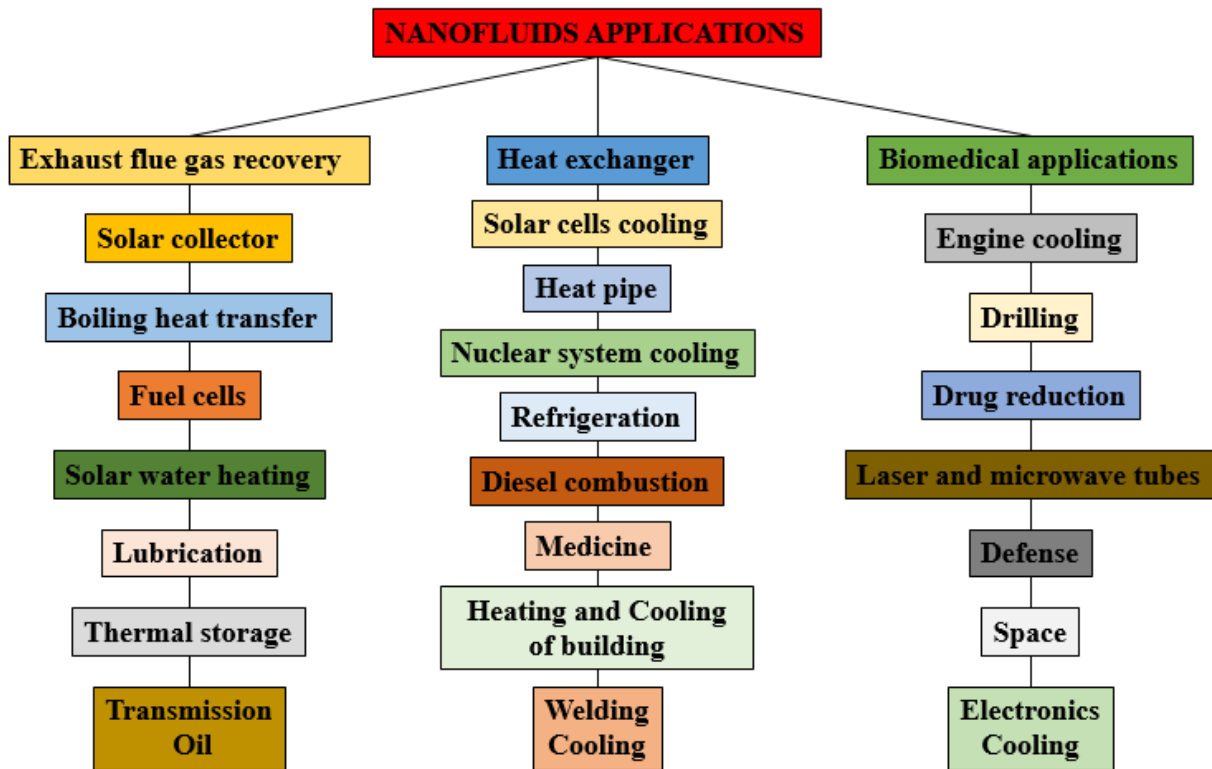


**Figure I.1.** General applications of nanofluids [17].

The key issue of nanofluid research, in view of applications, is to prepare stable solutions, to increase the thermal conductivity of the liquid, without a large increase in viscosity. Many factors can affect the thermal conductivity of a nanofluid, like the other thermophysical properties, such as particle size, particle shape, concentration of nanoparticles, and addition of surfactant. For that, different types of nanofluids that differ by the base fluid, and/or by the type of the nanoparticles such as metal oxide [18–22], metallic nanoparticles [23,24], or carbon nanomaterials [25–31] have been studied. Since the discovery of graphene [32], this material has found many interesting

applications, as it has many excellent physical, chemical, and mechanical features [7]. Quite naturally, the development of graphene-based nanofluids started a few years ago because of the high intrinsic thermal conductivity of graphene compared to other types of nanoparticles and carbon-based materials (see Table I.1). Thus, graphene appears as a promising candidate for nanofluid preparation and applications. Such a development, with a comprehensive characterization of graphene and graphene-based nanofluids, is the aim of this PhD thesis.

This project was performed within the Laboratoire de Génie Civil et Génie Mécanique (LGCGM) from Université de Rennes 1, whose activities in the field of nanofluids are more than ten years old, particularly with carbon-based nanofluids. It is also part of a strong collaboration with the *Institut Jean Lamour* in Nancy, specialized in the chemical properties of carbon and graphene-based materials. The nanofluids dedicated to our study were prepared in this institute. More broadly, our project contributed to the recently completed European COST Action NanoUptake OC-2015-1-19591, "Overcoming Barriers to Nanofluids Market Uptake". It should be finally noted that, before the comprehensive study about few-layer graphene nanofluids reported in this manuscript, preliminary studies and tests have been carried out with graphene oxide and reduced graphene oxide as well as with carbon nanotubes without obtained convincing results in terms of both stability and thermal conductivity enhancement. However, these results were a great source of information and they have led to some publications [33,34].

## **I.2- Objectives**

The general objectives of this study are described as following:

1. Synthesis of suitable graphene nanomaterials for obtaining stable heat transfer nanofluids.
2. Characterization of the synthesized nanopowders to analyze their morphology, size and structural quality.
3. Preparation of different concentrations of nanofluids by dispersing the synthesized graphene in a base fluid employed in heat transfer applications to obtain stable nanofluids with the help of surfactants.
4. Characterization and stability of the prepared nanofluids.

5. Experimental determination of the thermal conductivity of the base fluids and the prepared nanofluids in a wide range of temperatures and concentrations.
6. Performing complete rheological tests for all base fluids and nanofluids.
7. Determining the density, surface tension, and heat capacity of the base fluids and nanofluids.
8. Modelling the studied thermophysical properties.
9. Analyzing the heat transfer performance for the selected nanofluids for heat transfer applications.
10. Evaluation and discussion of the obtained results for all the analyzed nanofluids in the function of composition parameters and temperature, and determination of general conclusions.

### **I.3- Structure**

The second chapter of the thesis presents a bibliographical synthesis allowing a better understanding of the current knowledge in the development of graphene-based nanofluids, including graphene production methods, and their thermo-physical properties, and a description of the different models of the literature often used for the estimation of thermo-physical properties (thermal conductivity, dynamic viscosity, density...). The analysis of this work allows us to identify the different parameters that can influence the thermal and hydrodynamic properties of graphene-based nanofluids.

Thus, the third chapter presents, after a detailed description of the graphene production and characterization methods, nanofluids used and how they were prepared and evaluated in terms of stability, the experimental systems and devices used for experimental characterization of the thermo-physical properties, thermal conductivity, dynamic viscosity, density, surface tension, and isobaric heat capacity of nanofluids. The experimental procedures and the determination of measurement uncertainties are also detailed.

In the fourth chapter, we present the main results of the thesis, including the full characterization of graphene, the stability of nanofluids, at rest and under shear and the thermophysical properties of nanofluids tested (thermal conductivity, dynamic viscosity, density, etc). In this chapter, we also present an analysis of the results to evaluate the influence of the type of surfactant,

temperature, and volume fraction of graphene. These results are also compared and discussed with some existing models. This was done in the form of published articles.

The fifth chapter proposes a theoretical qualitative approach to evaluate the heat transfer potential of the stable nanofluids in a heat exchanger.

The main conclusions and perspectives of this work will be finally presented in the last chapter.

## I.4- References

1. H.F. Matare, *Energy: facts and future*, CRC Press, Boca Raton, FL, USA, 2018.
2. S.U.S. Choi, J.A. Eastman, *Enhancing thermal conductivity of fluids with nanoparticles*, International Mechanical Engineering Congress and Exhibition, Argonne National Lab, USA 1995, pp. 99–105.
3. Haddad, Z.; Abid, C.; Oztop, H.F.; Mataoui, A. A review on how the researchers prepare their nanofluids. *International Journal of Thermal Sciences* **2014**, *76*, 168–189, doi:10.1016/j.ijthermalsci.2013.08.010.
4. Safaei, M.R.; Ranjbarzadeh, R.; Hajizadeh, A.; Bahiraei, M.; Afrand, M.; Karimipour, A. Effects of cobalt ferrite coated with silica nanocomposite on the thermal conductivity of an antifreeze: New nanofluid for refrigeration condensers. *International Journal of Refrigeration* **2019**, *102*, 86–95, doi:10.1016/j.ijrefrig.2018.12.007.
5. Nazari, S.; Safarzadeh, H.; Bahiraei, M. Experimental and analytical investigations of productivity, energy and exergy efficiency of a single slope solar still enhanced with thermoelectric channel and nanofluid. *Renewable Energy* **2019**, *135*, 729–744, doi:10.1016/j.renene.2018.12.059.
6. Sardarabadi, H.; Zeinali Heris, S.; Ahmadpour, A.; Passandideh-Fard, M. Experimental investigation of a novel type of two-phase closed thermosyphon filled with functionalized carbon nanotubes/water nanofluids for electronic cooling application. *Energy Conversion and Management* **2019**, *188*, 321–332, doi:10.1016/j.enconman.2019.03.070.
7. Bahiraei, M.; Heshmatian, S. Graphene family nanofluids: A critical review and future research directions. *Energy Conversion and Management* **2019**, *196*, 1222–1256, doi:10.1016/j.enconman.2019.06.076.
8. Qi, C.; Liu, M.; Tang, J. Influence of triangle tube structure with twisted tape on the thermo-hydraulic performance of nanofluids in heat-exchange system based on thermal and exergy efficiency. *Energy Conversion and Management* **2019**, *192*, 243–268, doi:10.1016/j.enconman.2019.04.047.
9. Bellos, E.; Tzivanidis, C. Investigation of a nanofluid-based concentrating thermal photovoltaic with a parabolic reflector. *Energy Conversion and Management* **2019**, *180*, 171–182, doi:10.1016/j.enconman.2018.11.008.
10. Yen, P.-H.; Wang, J.-C. Power generation and electric charge density with temperature effect of alumina nanofluids using dimensional analysis. *Energy Conversion and Management* **2019**, *186*, 546–555, doi:10.1016/j.enconman.2019.03.005.
11. Karimipour, A.; Bagherzadeh, S.A.; Goodarzi, M.; Alnaqi, A.A.; Bahiraei, M.; Safaei, M.R.; Shadloo, M.S. Synthesized CuFe<sub>2</sub>O<sub>4</sub>/SiO<sub>2</sub> nanocomposites added to water/EG: Evaluation of the thermophysical properties beside sensitivity analysis & EANN. *International Journal*

- of Heat and Mass Transfer* **2018**, *127*, 1169–1179, doi:10.1016/j.ijheatmasstransfer.2018.08.112.
12. Bahiraei, M.; Ahmadi, A.A. Thermohydraulic performance analysis of a spiral heat exchanger operated with water–alumina nanofluid: Effects of geometry and adding nanoparticles. *Energy Conversion and Management* **2018**, *170*, 62–72, doi:10.1016/j.enconman.2018.05.061.
  13. S.K. Das, S.U. Choi, W. Yu, T. Pradeep, *Nanofluids: science and technology*, John Wiley & Sons, Hoboken, NJ, USA, 2007.
  14. Mallan, G.M.; Michaelian, M.S.; Lockhart, F.J. Liquid thermal conductivities of organic compounds and petroleum fractions. *Journal of Chemical & Engineering Data* **1972**, *17*, 412–415, doi:10.1021/je60055a028.
  15. Hone, J.; Whitney, M.; Piskoti, C.; Zettl, A. Thermal conductivity of single-walled carbon nanotubes. *Physical Review B* **1999**, *59*, R2514–R2516, doi:10.1103/PhysRevB.59.R2514.
  16. Hu, J.; Ruan, X.; Chen, Y.P. Thermal Conductivity and Thermal Rectification in Graphene Nanoribbons: A Molecular Dynamics Study. *Nano Letters* **2009**, *9*, 2730–2735, doi:10.1021/nl901231s.
  17. Arshad, A.; Jabbal, M.; Yan, Y.; Reay, D. A review on graphene based nanofluids: Preparation, characterization and applications. *Journal of Molecular Liquids* **2019**, *279*, 444–484, doi:10.1016/j.molliq.2019.01.153.
  18. Yasinskiy, A.; Navas, J.; Aguilar, T.; Alcántara, R.; Gallardo, J.J.; Sánchez-Coronilla, A.; Martín, E.I.; De Los Santos, D.; Fernández-Lorenzo, C. Dramatically enhanced thermal properties for TiO<sub>2</sub>-based nanofluids for being used as heat transfer fluids in concentrating solar power plants. *Renewable Energy* **2018**, *119*, 809–819, doi:10.1016/j.renene.2017.10.057.
  19. Yiamsawas, T.; Dalkilic, A.S.; Mahian, O.; Wongwises, S. Measurement and Correlation of the Viscosity of Water-Based Al<sub>2</sub>O<sub>3</sub> and TiO<sub>2</sub> Nanofluids in High Temperatures and Comparisons with Literature Reports. *Journal of Dispersion Science and Technology* **2013**, *34*, 1697–1703, doi:10.1080/01932691.2013.764483.
  20. Angayarkanni, S.A.; Philip, J. Review on thermal properties of nanofluids: Recent developments. *Advances in Colloid and Interface Science* **2015**, *225*, 146–176, doi:10.1016/j.cis.2015.08.014.
  21. Lee, S.; Choi, S.U.-S.; Li, S.; Eastman, J.A. Measuring Thermal Conductivity of Fluids Containing Oxide Nanoparticles. *Journal of Heat Transfer* **1999**, *121*, 280–289, doi:10.1115/1.2825978.
  22. Mahian, O.; Kianifar, A.; Heris, S.Z.; Wongwises, S. Natural convection of silica nanofluids in square and triangular enclosures: Theoretical and experimental study. *International Journal of Heat and Mass Transfer* **2016**, *99*, 792–804, doi:10.1016/j.ijheatmasstransfer.2016.03.045.
  23. Gómez-Villarejo, R.; Martín, E.I.; Navas, J.; Sánchez-Coronilla, A.; Aguilar, T.; Gallardo, J.J.; Alcántara, R.; De los Santos, D.; Carrillo-Berdugo, I.; Fernández-Lorenzo, C. Ag-based nanofluidic system to enhance heat transfer fluids for concentrating solar power: Nano-level insights. *Applied Energy* **2017**, *194*, 19–29, doi:10.1016/j.apenergy.2017.03.003.
  24. Navas, J.; Sánchez-Coronilla, A.; Martín, E.I.; Teruel, M.; Gallardo, J.J.; Aguilar, T.; Gómez-Villarejo, R.; Alcántara, R.; Fernández-Lorenzo, C.; Piñero, J.C.; et al. On the enhancement of heat transfer fluid for concentrating solar power using Cu and Ni nanofluids: An

- experimental and molecular dynamics study. *Nano Energy* **2016**, *27*, 213–224, doi:10.1016/j.nanoen.2016.07.004.
25. Seong, H.; Kim, G.; Jeon, J.; Jeong, H.; Noh, J.; Kim, Y.; Kim, H.; Huh, S. Experimental Study on Characteristics of Grinded Graphene Nanofluids with Surfactants. *Materials* **2018**, *11*, 950, doi:10.3390/ma11060950.
  26. Naddaf, A.; Zeinali Heris, S. Experimental study on thermal conductivity and electrical conductivity of diesel oil-based nanofluids of graphene nanoplatelets and carbon nanotubes. *International Communications in Heat and Mass Transfer* **2018**, *95*, 116–122, doi:10.1016/j.icheatmasstransfer.2018.05.004.
  27. Kamatchi, R., & Kannan, K. G. (2018). An aqua based reduced graphene oxide nanofluids for heat transfer applications: synthesis, characterization, stability analysis, and thermophysical properties. *INTERNATIONAL JOURNAL OF RENEWABLE ENERGY RESEARCH*, *8*(1), 313-319.
  28. Bahaya, B.; Johnson, D.W.; Yavuzturk, C.C. On the Effect of Graphene Nanoplatelets on Water–Graphene Nanofluid Thermal Conductivity, Viscosity, and Heat Transfer Under Laminar External Flow Conditions. *Journal of Heat Transfer* **2018**, *140*, doi:10.1115/1.4038835.
  29. Hussien, A.A.; Abdullah, M.Z.; Yusop, N.M.; Al-Nimr, M.A.; Atieh, M.A.; Mehrali, M. Experiment on forced convective heat transfer enhancement using MWCNTs/GNPs hybrid nanofluid and mini-tube. *International Journal of Heat and Mass Transfer* **2017**, *115*, 1121–1131, doi:10.1016/j.ijheatmasstransfer.2017.08.120.
  30. Manasrah, A.D.; Al-Mubaiyedh, U.A.; Laui, T.; Ben-Mansour, R.; Al-Marri, M.J.; Almanassra, I.W.; Abdala, A.; Atieh, M.A. Heat transfer enhancement of nanofluids using iron nanoparticles decorated carbon nanotubes. *Applied Thermal Engineering* **2016**, *107*, 1008–1018, doi:10.1016/j.applthermaleng.2016.07.026.
  31. Etefaghi, E.; Ghobadian, B.; Rashidi, A.; Najafi, G.; Khoshtaghaza, M.H.; Pourhashem, S. Preparation and investigation of the heat transfer properties of a novel nanofluid based on graphene quantum dots. *Energy Conversion and Management* **2017**, *153*, 215–223, doi:10.1016/j.enconman.2017.10.010.
  32. Novoselov, K.S. Electric Field Effect in Atomically Thin Carbon Films. *Science* **2004**, *306*, 666–669, doi:10.1126/science.1102896.
  33. Hamze S., Berrada N., Desforges A., Vigolo B., Gleize J., Ghanbaja J., Maré T., Cabaleiro D., and Estellé P. Dynamic viscosity of purified MWCNT water and water-propylene glycol based nanofluids, *Heat transfer Eng.*, accepted.
  34. Berrada, N.; Hamze, S.; Desforges, A.; Ghanbaja, J.; Gleize, J.; Maré, T.; Vigolo, B.; Estellé, P. Surface tension of functionalized MWCNT-based nanofluids in water and commercial propylene-glycol mixture. *Journal of Molecular Liquids* **2019**, *293*, 111473, doi:10.1016/j.molliq.2019.111473.

# Chapter II- General information on graphene nanofluids

II.1- Introduction.....	22
II.2- Definition.....	22
II.2.1- Base fluids.....	23
II.2.2- Nanoparticles.....	25
II.3- Proposal process of new nanofluids.....	28
II.3.1- Nanofluid design.....	29
II.3.1.1- Nanoparticles synthesis and characterization.....	29
II.3.1.2- Nanofluid preparation.....	37
II.3.1.3- Stability.....	39
II.3.2- Thermophysical profile.....	42
II.3.2.1- Thermal conductivity.....	44
II.3.2.2- Rheology and Dynamic viscosity.....	49
II.3.2.3- Isobaric heat capacity.....	58
II.3.2.4- Density.....	60
II.3.2.5- Surface tension.....	61
II.3.3- Heat transfer performance.....	65
II.3.3.1- Qualitative approach.....	66
II.3.3.2- Quantitative approach.....	67
II.4- Conclusion.....	70
II.5- References.....	71

## **II.1- Introduction**

The basic fluids often used in heat transfer applications have very low thermal conductivities, which sometimes limit their capacity to heat transfer. The use of nanofluids is likely to bring very significant gains in thermal performance. To develop more efficient heat transfer fluids, and to better understand the physical mechanisms involved in the use of nanofluids, a great deal of research has been carried out on this new generation of fluids.

This chapter aims to provide an overview of the literature background about graphene-based nanofluids that are the subject of this research work.

## **II.2- Definition**

Nanofluids are colloidal solutions made up of nano-sized particles (tens to hundreds of nanometers in at least one dimension) [1] suspended in a carrier liquid. This type of solution is a subject of great interest since the discovery of their special thermal properties. Indeed, base fluids often used in cooling or heating applications have very low thermal conductivities that limit their heat transfer capacity. The idea is then to insert solid nanoparticles of very high thermal conductivity into the base liquids, to increase the effective thermal conductivity of the mixture and thus improve their thermal performance. An example of graphene-based nanofluid is shown in Figure II.1.



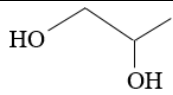
**Figure II.1.** Photograph of a graphene oxide aqueous nanofluid [2].

### **II.2.1- Base fluids**

Water, glycols (in particular ethylene glycol) and mixtures of both, as well oils are the common heat transfer fluids employed in heating and cooling applications [3–6]. So, they are logically the most used fluids to produce nanofluids. Some important properties about water and propylene glycol liquids, that compose the commercial base fluid used in this study, are provided in the following.

Water (H<sub>2</sub>O), molecules consist of hydrogen and oxygen atoms joined by covalent bonds, is an inorganic compound. At atmospheric conditions, it does not have any color, odor or taste [7]. As its molecules create hydrogen bonds with other molecules easily, and because of its strong polarity, water was identified as a good solvent. Besides, water can be freely mixed with other liquids (alcohols for example) [8]. Regarding its physical properties (see Table II.1), water presents some unusual behaviors. At atmospheric pressure, its density decreases with temperature in the majority of the liquid-state range, as usual, while it increases from the freezing point to 277 K [9]. While heat capacity usually increases with temperature, a minimum value occurs in case of water at around 308 K. Furthermore, most liquids under higher pressures become more viscous while the viscosity of water shows a minimum as a function of pressure [9].

**Table II.1.** Physical properties of water and propylene glycol [10,11].

		<i>Water</i>	<i>Propylene glycol</i>
<b>Chemical formula</b>		$H_2O$	$C_3H_8O_2$
<b>Structural formula</b>			
<b>Molecular mass (g.mol<sup>-1</sup>)</b>		18.02	76.09
<b>Density (kg.m<sup>-3</sup>)</b>	At 293.15 K	998.2	1036
<b>Specific heat (kJ.kg<sup>-1</sup>.K<sup>-1</sup>)</b>	At 293.15 K	4.184	2.481
<b>Viscosity (mPa.s)</b>	At 273.15 K	–	243
	At 293.15 K	1.00	60.5
	At 313.15 K	0.653	18.0
<b>Refractive index</b>	At 293.15 K	1.3333	1.4329
<b>Freezing point (K)</b>		273	214
<b>Boiling point (K)</b>	At 101.3 kPa	373	460
	At 6.67 kPa	311	389
	At 1.13 kPa	284	358
<b>Vapor pressure (Pa)</b>	At 293.15 K	2.4	9.3

Propylene glycol or propane-1,2-diol ( $C_3H_8O_2$ ), molecules consist of carbon, hydrogen and oxygen atoms, is an organic compound. At atmospheric pressure and room temperature, it is an odorless and colorless viscous liquid with low toxicity and a slightly sweet taste. Propylene glycol is mainly industrially produced at elevated pressure and temperature by the hydration of propylene oxide. It is used in different applications as the production of foods, polyester resins, personal care, products, drugs, and cosmetics, among others [12]. It is extensively used in heat transfer applications as de-icing fluids, a part of antifreeze mixtures as a green replacement of ethylene glycol [12]. Because of their much lower toxicity [13], they are more suitable for the heat transfer applications which need an indirect contact with food, natural resources or liquids for human consumption, used as a secondary working fluid in the geothermal collection, solar thermal energy or food industry. Among their physical properties (see Table II.1 and Figure II.2), we can note that propylene glycol has a great hygroscopicity and has a freezing point lower than that of ethylene glycol and water. Nevertheless, as shown in Figure II.2, for the same volume concentrations of propylene glycol and ethylene glycol in water, similar freezing points were obtained.

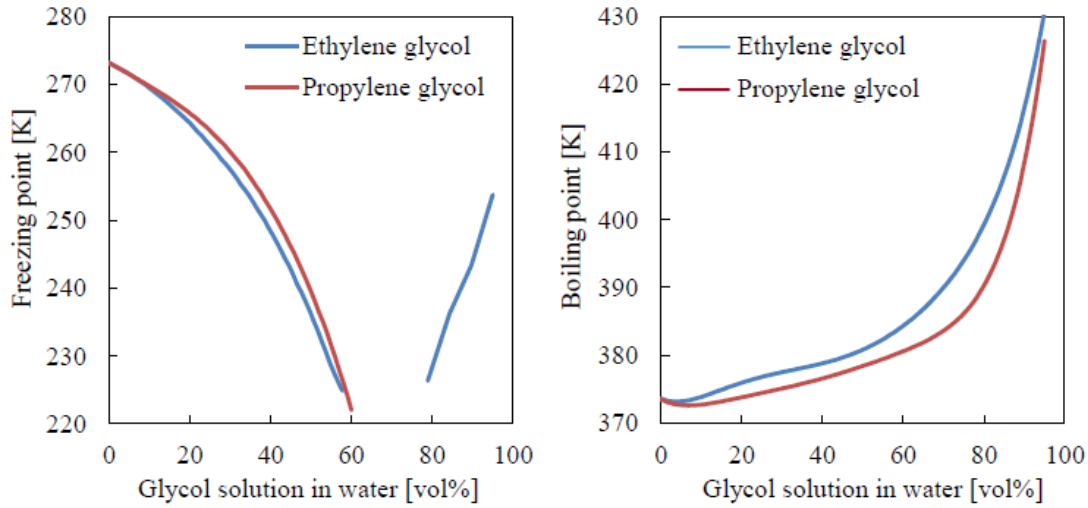


**Figure II.2.** Freezing and boiling points of glycoled waters at different ethylene glycol and propylene glycol volume concentrations [10].

## II.2.2- Nanoparticles

The production of new nanomaterials and nanoparticles is a growing field of research, so only the most commonly used nanoparticles in heat transfer applications are briefly mentioned here. In general, while a classification by nanoparticle nature is also used, nanoparticles can be divided into three broad categories according to their shape (Figure II.3):

- Spherical nanoparticles, for which several types of materials can be used in their manufacture. These spherical nanoparticles can thus be based on metals (copper Cu, iron Fe, gold Au, silver Ag...) or metal oxides (aluminium oxide  $\text{Al}_2\text{O}_3$ , copper oxide CuO, titanium oxide  $\text{TiO}_2$ ...).
- Nanotubes (carbon nanotubes NTC, titanium nanotubes, silicon nanotube, boron nitride...).
- Nanosheets (graphene nanosheets, graphene oxide nanosheets, reduced graphene oxide nanosheets...).
- Some other shapes like triangular, cubic, hexagonal, oval, helical, prism and rod nanoparticles can be accounted.

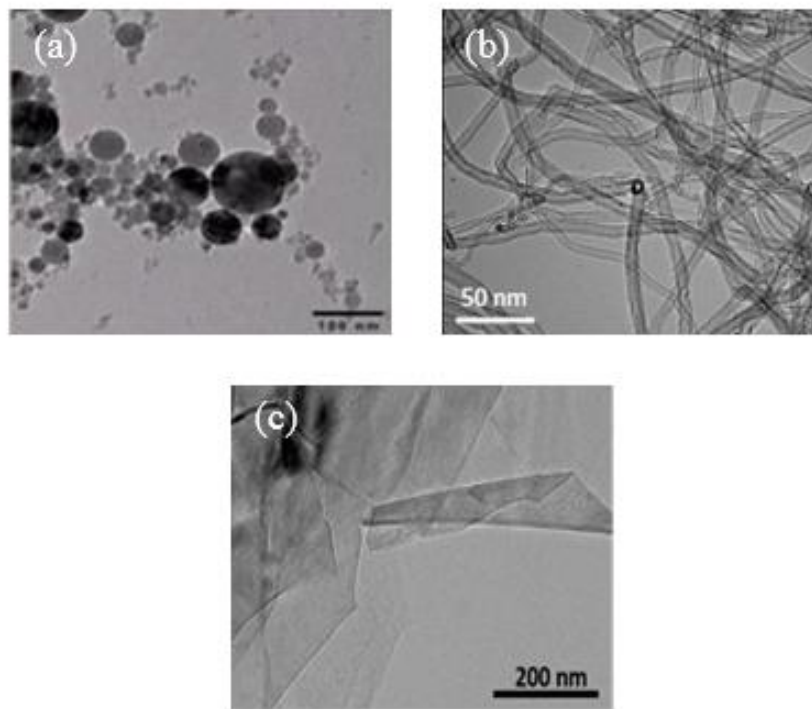


**Figure II.3.** TEM images of some examples of nanoparticles: spherical nanoparticles [14] (a), carbon nanotubes [15] (b), and graphene nanosheets (c).

As the name suggests, graphene, “the mother of all graphitic forms of carbon” [16], is obtained from graphite and is a simple two-dimensional sheet consisting of carbon atoms arranged in a hexagonal pattern. Expectations around this material can be explained by its exceptional properties:

- It consists of a single atomic layer of hexagonal mesh with a thickness (in the order of carbon atom) of 70 picometers, i.e. one-millionth of a human hair [16].
- It is considered to be the thinnest and lightest material (0.77 milligrams per square meter).
- It is among the strongest materials known to date as it has Young's modulus close to  $\sim 1000$  GPa and a fracture limit of 130 GPa.
- Its elasticity modulus is high in the order of  $\sim 0.25$  TPa [17].
- It has a high intrinsic thermal conductivity  $\sim 5000$  W.m<sup>-1</sup>.K<sup>-1</sup> (measured for single-layer graphene) [18]. For comparison, the thermal conductivity of copper is 400 W.m<sup>-1</sup>.K<sup>-1</sup>.
- Its theoretical specific surface area is  $\sim 2630$  m<sup>2</sup>.g<sup>-1</sup> [19].

- It is impermeable to standard gases, including Helium [20].
- Its electrical conductivity is  $\sim 2000000 \text{ cm}^2 \cdot \text{V}^{-1} \cdot \text{s}^{-1}$  or  $200 \text{ S} \cdot \text{m}^2 \cdot \text{C}^{-1}$  [21].
- Its melting point is above 3000 degrees Celsius [22].

Graphene nanoparticles have many advantages over the other types of nanoparticles [23–25]. For example, they have very high thermal conductivity, they are more stable, they can be easily synthesized, and they have a larger surface area to volume ratio which enhance the heat transferability. All these reasons make graphene a really good candidate for nanofluid design.

There are different types of graphene-based nanoparticles as pristine graphene, graphene oxide, reduced graphene oxide, and graphene quantum dots as shown in Figure II.4.

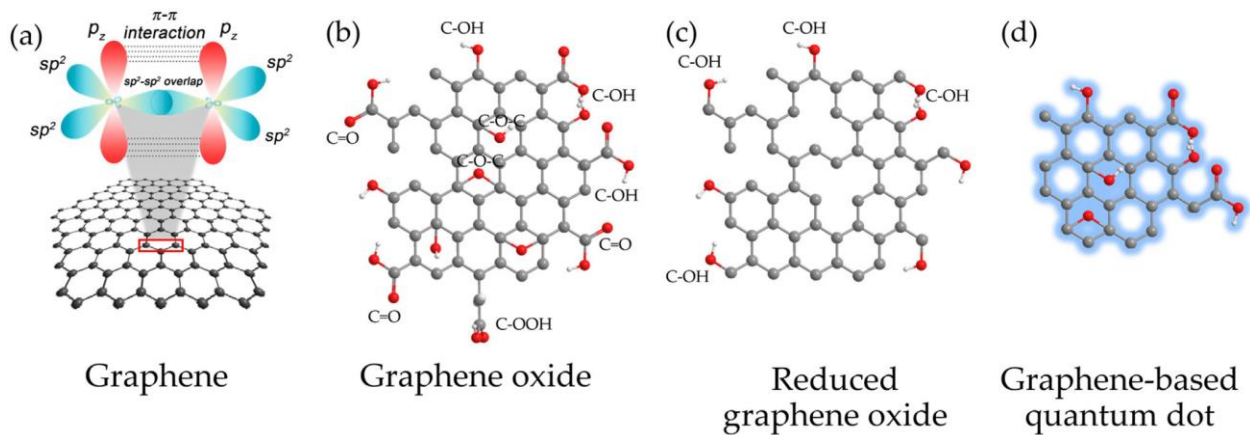


**Figure II.4.** Structures of graphene-based materials: pristine graphene (purely arranged carbon atoms) with  $sp^2$ -hybridized carbon atoms (a), and the chemically modified graphene, including GO (b), rGO (c) and GQD (d) [26].

Graphene oxide (GO), which is called also graphitic acid [27], was discovered in 1859. It is also a two-dimensional material. Graphene oxide is the oxidized form of graphene, with O functional groups decorating the  $sp^2$  C basal plane. Contrary to hydrophobic graphene, GO is hydrophilic due to the presence of the oxygen functional groups, so it can be dispersed in water solution.

Reduced graphene oxide (rGO) is the form of graphene oxide that is processed by thermal, chemical and other methods to reduce the oxygen-containing groups.

Graphene quantum dots (GQDs) are zero-dimensional members in the carbon family and are considered usually as a chopped fragment from a graphene sheet [28].

Graphene-based nanomaterials are classified based on three fundamental features ( $C/O$  atomic ratio, average lateral dimensions, and the number of layers) as shown in Figure II.5.

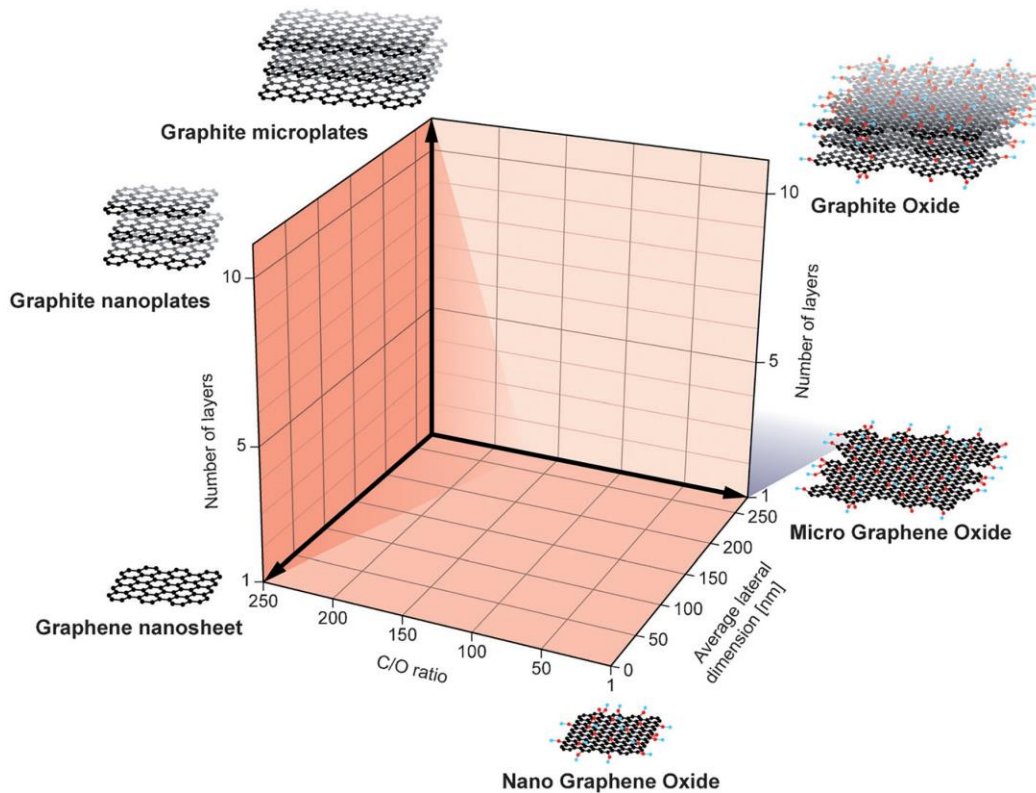


**Figure II.5.** Classification for different graphene-type materials based on the lateral dimensions, the  $C/O$  ratio and the number of layers, from Ref. [29], reused with permission from John Wiley and Sons.

### II.3- Proposal process of new nanofluids

To develop new nanofluids for heat transfer applications, three main phases are required: nanofluid design, characterization of thermophysical properties of nanofluids, and analysis of their heat transfer performance, as shown in Figure II.6. In addition to these steps of development, a trade-off between stability, an increase in thermal properties and performance and management of viscosity increase has to be aimed for practical issues.

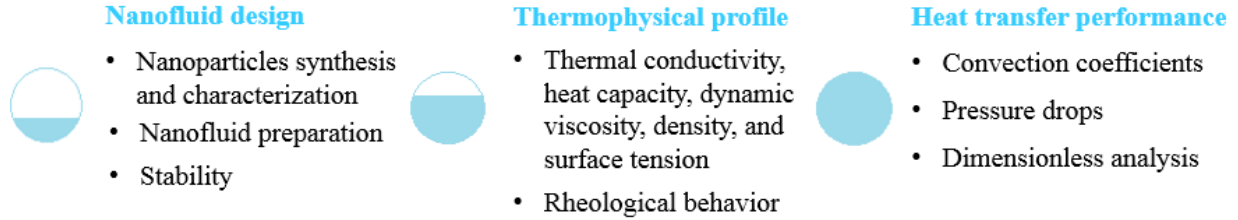


**Figure II.6.** Main steps of the proposal process of new graphene nanofluids for heat transfer applications.

### II.3.1- Nanofluid design

The design phase of the nanofluids plays a very important role in any experimental analysis of their thermophysical properties and heat transfer performance. The concentration accuracy of each component of the nanofluid, the precision of the characterization of the dimensions, shape or morphology of the nanoadditives used and the homogeneity and stability of the suspensions are all key parameters.

#### II.3.1.1- Nanoparticles synthesis and characterization

##### II.3.1.1.1- Synthesis of graphene-based nanomaterials

To fulfil the need for industry and academia for high-quality graphene in bulk quantities, many preparation methods have been proposed. In the literature, a list of synthesis strategies of graphene has been reported and few of them are adopted by graphene supplying industries. The methods are as follows [24]: mechanical exfoliation, chemical vapor deposition (CVD), liquid-phase exfoliation (LPE), electrochemical exfoliation, chemical reduction of GO, and bottom-up synthesis.

##### *a) Mechanical exfoliation*

This method is based on the top-down approach where graphene nanosheets can be produced by the direct exfoliation of pristine, expanded or oxidized graphite. The method known as scotch exfoliation of graphite or micromechanical cleavage of graphite constitutes the first experimental method that was used for the production of graphene nanosheets (see Figure.II.7).

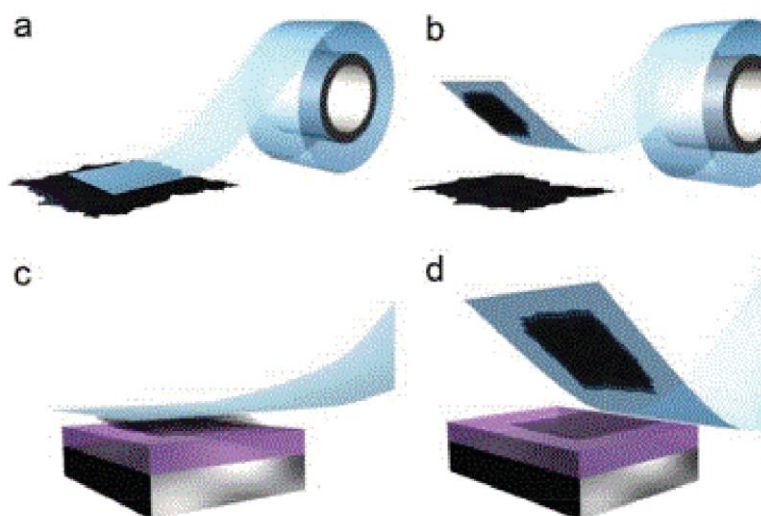


**Figure II.7.** (a-d) The steps of graphene synthesis from graphite exfoliation with scotch [30].

This discovery was made by Novoselov *et al.* in 2004 [16]. This approach is very efficient to obtain nanosheets with excellent crystalline quality but its extremely low yield makes it impossible to consider for production on an industrial scale.

### ***b) Chemical vapor deposition***

This method consists of producing the graphene layer by chemical vapor deposition (CVD) on a metal substrate. There are different metals which are used for this method such as cobalt (Co) [31], platinum (Pt) [32], nickel (Ni) [33] and copper (Cu) [34]. The gaseous sources generally used for this type of deposition are hydrocarbons such as methane, acetylene or ethylene, which decompose when they come into contact with the surface of metals to form graphene layers. Figure II.8 shows the formation of graphene by CVD from a drop of gallium (Ga) localized on a tungsten (W) substrate [30].

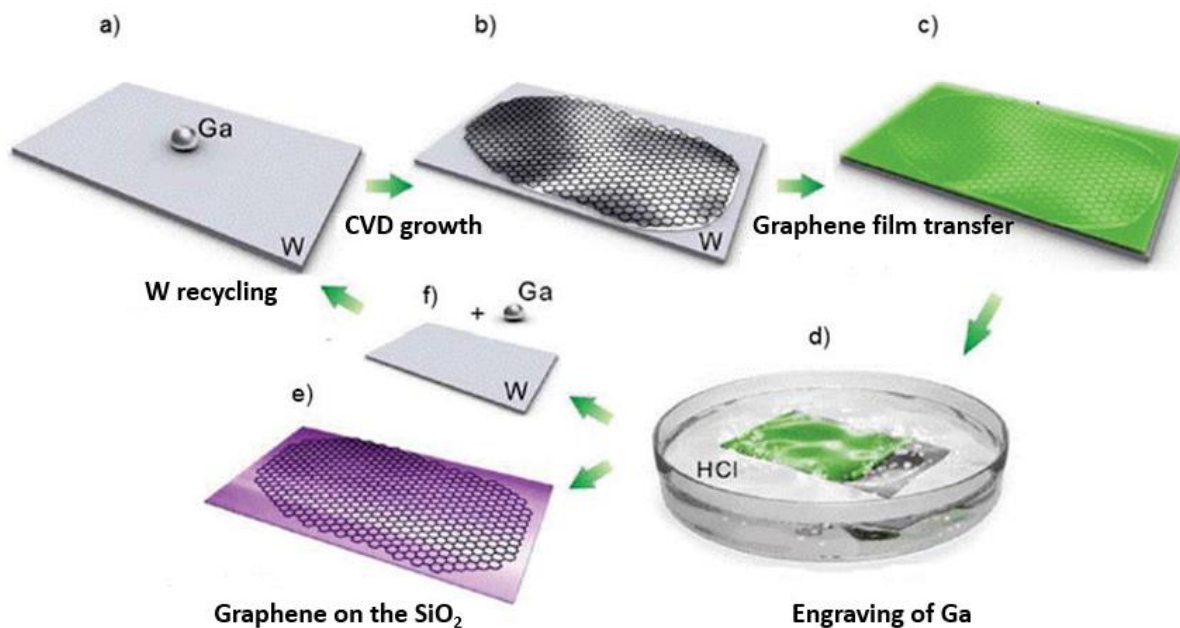


**Figure II.8.** Different stages of graphene growth on a drop of gallium (Ga) supported on a substrate (W): a) a drop of Ga placed on a support sheet (W), b) CVD growth of the graphene on the surface of liquid Ga, c) the graphene is coated with a layer of PMMA by spin-coating, d) coating of the graphene with PMMA and separation from the tungsten sheet driven by the  $H_2$  bubbles produced at the interface between the graphene and the Ga-W substrate, e) the graphene is transferred to a  $SiO_2/Si$  substrate and f) the tungsten foil is reused as a Ga support [30].

The advantage of this method is its low cost and reproducibility. The specific surface area of the graphene synthesized by this method is around  $2600 \text{ m}^2/\text{g}$  according to the literature. This value is higher than that of graphene synthesized by the mechanical exfoliation method. Nevertheless, this specific surface area depends on the size of the metal film used, the temperature and pressure which are key elements for growth [32].

### *c) Liquid phase exfoliation*

The chemical route is the most suitable technique for a large application scale in the field of composite materials because it allows the exfoliation of the graphite sheets and their subsequent functionalization [35–43]. The use of intercalating agents and surfactants generally increases the interlayer space between the graphene sheets within the graphite. Indeed, surfactants play an

important role in the exfoliation and stabilization of graphene in polar solvents such as water (Figure II.9).

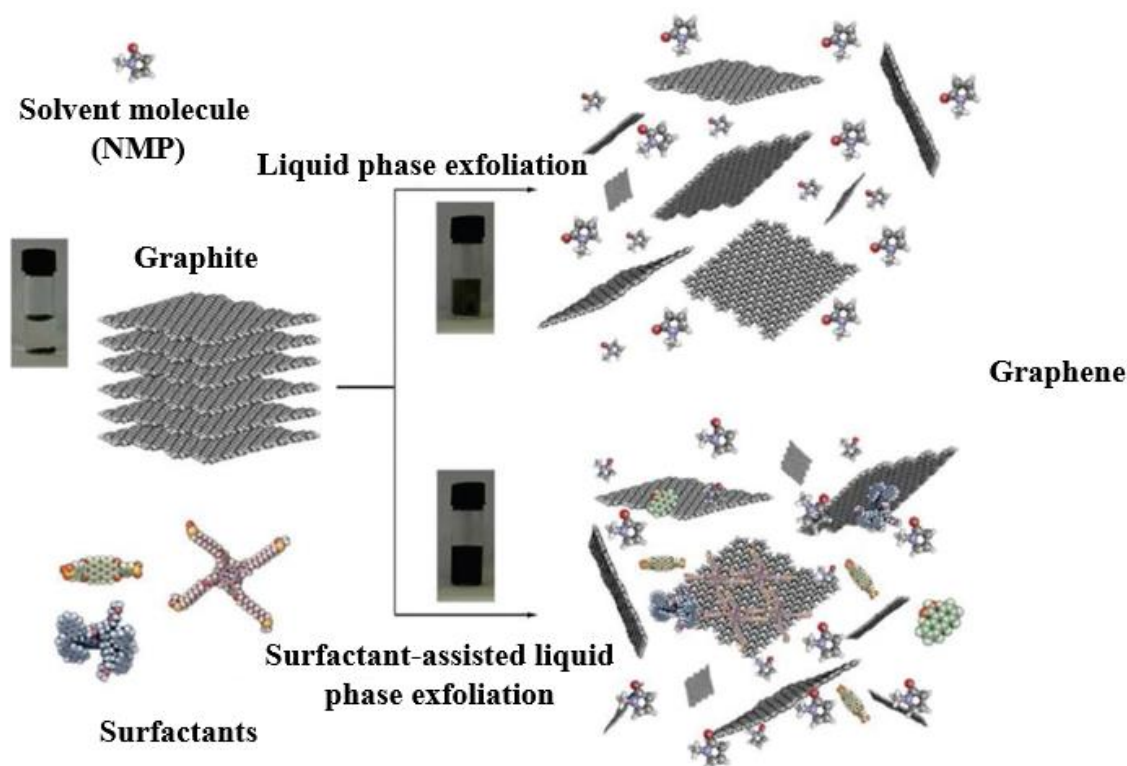


**Figure II.9.** Graphite exfoliation in solution in the presence (or not) of surfactants [36].

For example, Bepete *et al.* [44] carried out the dispersion of graphite in water to obtain graphene monolayers. In order to obtain a stable homogeneous dispersion of the monolayers in water, negatively charged graphene solutions were solubilized in tetrahydrofuran (THF) with degassed water followed by evaporation of the organic solvent.

#### ***d) Electrochemical exfoliation***

Electrochemical exfoliation of graphite in the presence of ionic liquids has been developed as an effective technique for the production of functionalized graphene nanosheets in large quantities. The advantage of this method is that it allows the production of functionalized graphene nanosheets with imidazolium groups that can assist the dispersion of the nanosheets in aprotic solvents [45].

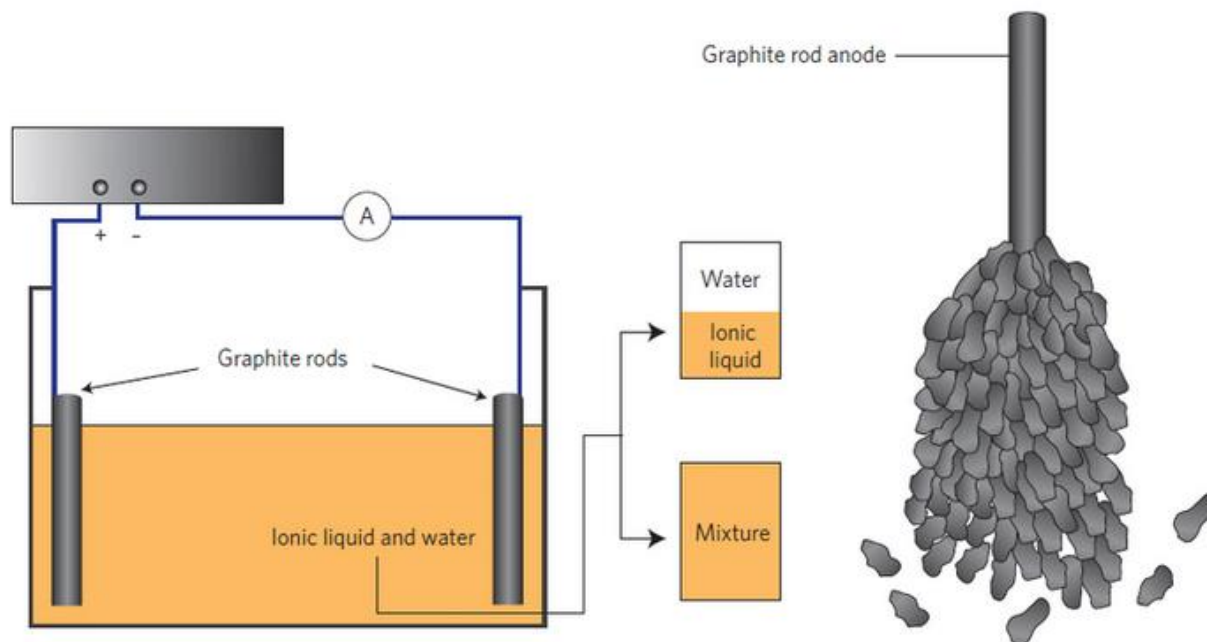


**Figure II.10.** Schematic representation of electrochemical exfoliation (right); exfoliation of chemically modified graphene from a graphite anode [45].

The aim of the electrochemical exfoliation is, first of all, to intercalate molecules or ions between the graphene sheets to separate them by breaking the van der Waals interactions which make graphite exist. In a second time, exfoliation generates the graphene nanosheets (see Figure II.10).

#### *e) Chemical reduction of graphene oxide*

In chemical reduction methods, a stable dispersion of GO is produced and followed by a reduction of the exfoliated graphene oxide nanosheets (Figure II.11). However, stable dispersions of GO are obtainable by using water or organic solvents using a sonication treatment or mechanical agitation. Chemical reduction allows removing, at least partially, oxygen-containing groups present on the surface and the edges of the GO.

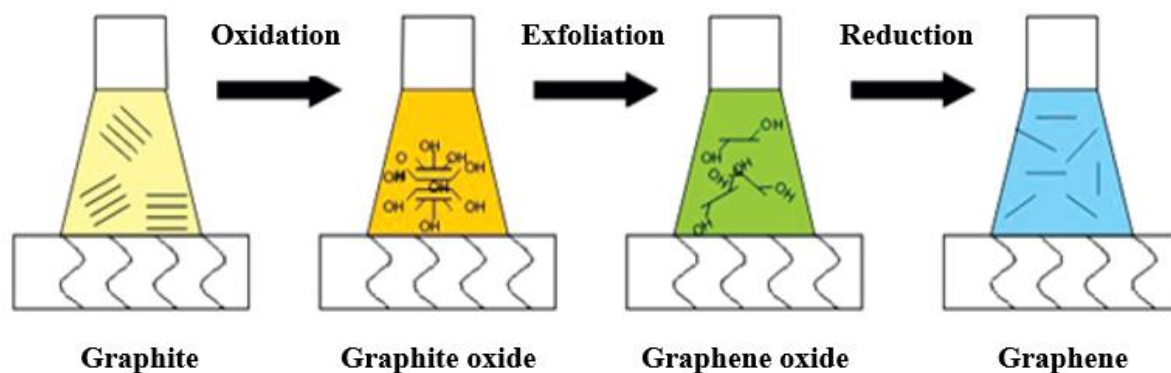


**Figure II.11.** Schematic representation of the oxidation/exfoliation/reduction process of graphite into graphene nanosheets [46].

Colloidal suspensions of GO and its organically treated version can be chemically reduced to graphene nanosheets by using different chemical reducing agents such as hydrazine hydrate [47–49], dimethylhydrazine [50], sodium borohydride followed by hydrazine [51], hydroquinone [52], UV-irradiated  $\text{TiO}_2$  [53], sulfur-containing compounds [54], Vitamin C [55], iron atoms [56] and sodium hydroxide [57].

#### *f) Bottom-up synthesis*

The bottom-up approach is an alternative method to prepare graphene nanosheets, where graphene molecules are synthesized starting from small and atomically-precise building blocks [58]. Coupling sites are needed for these building blocks. They can be stimulated from the outside to assemble to the next structural units. The process is usually performed at high temperatures where the structural variants are produced, and then part of them are separated to produce the desired structure. The control of the resolution with an atomic precision which allows obtaining very high-quality graphene is the major advantage of this method. Its main disadvantage is the constraint in the handling and transfer of the material produced, as well as the few possibilities for larger-scale replication due to the limitations of uniformity and order on a large scale.

#### **Summary of the synthesis methods**

Each method produces graphene nanomaterial with different characteristics and has different possibilities for upscaling. Raccichini *et al.* [59] summarized the advantages and the drawbacks of each method. They also evaluated different methods of graphene production based on the most

important aspects of the graphene synthesized, purity and quality, and each method, cost, yield and scalability. Their results are presented in Figure II.12. We can see that each method has different characteristics in terms of yield and therefore the selection of the method must be made each time, depending on the application for which the graphene will be used. For example, graphene oxide reduction, which is widely used in the literature, has a very high yield and scalability; however the purity and quality of the material produced is quite low. Inversely, some LPE method may have a low yield but produce high-quality graphene, and can be easily scaled up that makes this method interesting for nanofluid production.

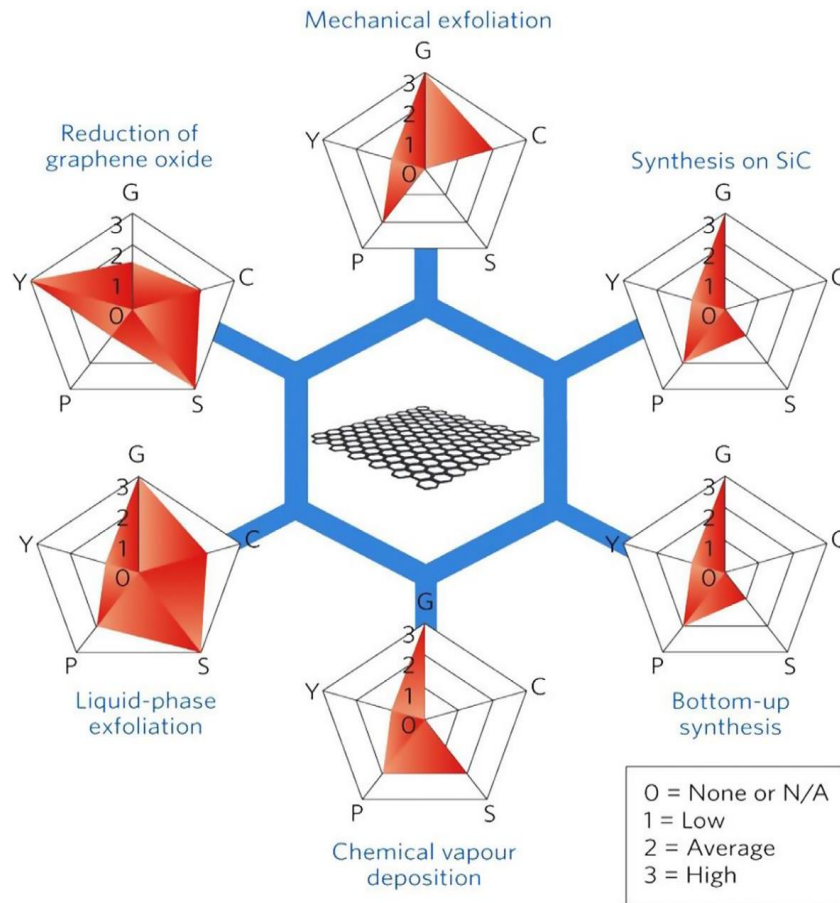


**Figure II.12.** The key characteristics of the most common methods of graphene production in a scale of 0-3; The letters refer to (G) the graphene quality, (C) the cost of production (a low value corresponds to the high cost of production), (S) the scalability, (P) the purity and (Y) the yield of each preparation route. Reproduced with permission from [59].

### **II.3.1.1.2- Nanopowder characterization**

As a first step, parameters as shape, size, crystallinity, purity, contamination and surface area of nanoparticles must be investigated in depth from a complete characterization. This section describes some of the most nanopowder characterization methods employed: SEM, TEM (and HRTEM), Raman spectroscopy, and temperature-programmed desorption (TPD).

#### ***a) Scanning electron microscopy***

SEM allows the visualization of nanomaterials by providing a comprehensive view (over several microns). It is a technique used to obtain enlarged images (magnification between 50000 and 350000) and high resolution (0.4 to 20 nm) of the surface of a wide range of materials and thus to derive morphological characteristics, size, diameter or surface appearance. A beam of accelerated electrons under vacuum sweeps the sample and the electron-matter interaction leads to re-emitted particles. Once detected and interpreted, these particles called secondary electrons in the classical mode of observation, are used to image the surface topography of the studied sample [60].

#### ***b) Transmission electron microscopy***

TEM is a powerful tool for characterizing local structural properties of nanomaterials, making it possible in particular to characterize defects, the grain boundaries... An electron beam emitted by Joule effect by heating a filament of tungsten is accelerated to a voltage between 50 kV and 200 kV and passes through the thin layer of material. This interaction results in the emission of various types of particles analyzed in a precise imaging mode. The image is formed by selecting by the sufficiently large objective diagram, the transmitted beam and one or more diffracted beams. A phase-contrast is obtained which depends on the atomic number of the chemical species. Thus, light particles that scatter little and therefore transmit electrons well appear clear; this is the case for carbon nanomaterials. Conversely, those that diffuse a lot, such as metallic impurities, will be very dark [60]. HRTEM is a TEM imaging mode that allows the crystallographic structure of a sample to be imaged at the atomic level [61].

#### ***c) Raman spectroscopy***

Raman spectroscopy is a technique that was discovered by Sir C. V. Raman and Krishnan, they were the first to observe the phenomenon of inelastic diffusion in 1928 [62]. The light was passed

through a photographic filter to create monochromatic light, and it was observed that a small portion of this light changed frequency. This type of analysis allows, among other things, the acquisition of information concerning molecular vibrations that can lead to the identification of the chemical structure of both organic and inorganic compounds and their quantification.

**d) Temperature programmed desorption**

Widely used in heterogeneous catalysis, thermo-programmed desorption (or temperature-programmed desorption, temperature-programmed spectroscopy, TPD or TPS) is a technique for studying the species (physically or chemically) adsorbed on the surface of a solid which consists of heating a catalyst sample previously covered with adsorbed molecules to observe the desorption of these molecules caused by the rise in temperature.

### II.3.1.2- Nanofluid preparation

There are two main methods for producing nanofluids:

**a) One-step method**

The one-step or single-step method consists of producing the nanoparticles in the base fluid (see Figure II.13). Less industrial, it can only be used for certain nanofluids but prevents agglomeration and oxidation of the nanoparticles. For example, one of the green methods for metal nanoparticle preparation is laser ablation technique which offers a unique tool for nanoparticle nanofabrication [63]. Another example of the one-step process is condensing a metal vapor in a reactor to form nanoparticles on a film of liquid at low vapor pressure.

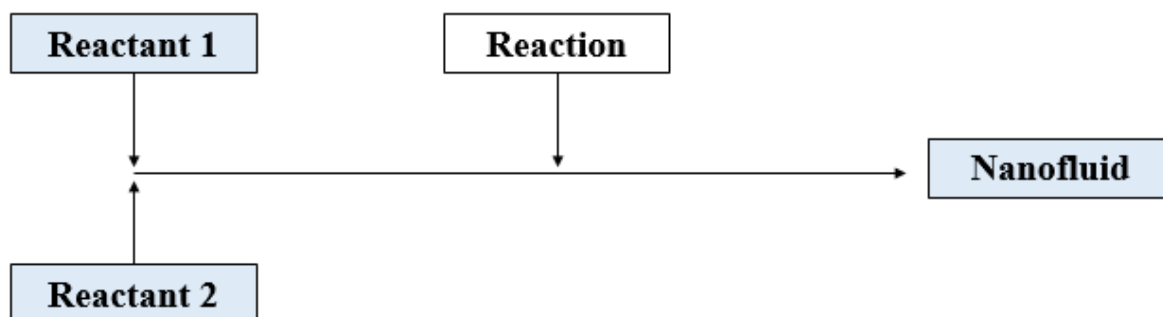


**Figure II.13.** One-step method stages for preparing nanofluids [64].

**b) Two-step method**

The two-step method is to first produce the nanoparticles and then disperse them in the base fluid (see Figure II.14). To break up the agglomerates and to ensure good dispersion, strong mechanical action using a rotary agitator and ultrasound are often required. Besides, to prevent agglomeration due to the attraction forces between the particles, electrostatic repulsion forces are used by charging the particle surface by adapting the pH value (covalent approach). Steric repulsion forces can also be used by using molecules adsorbed onto the surface (non-covalent approach).

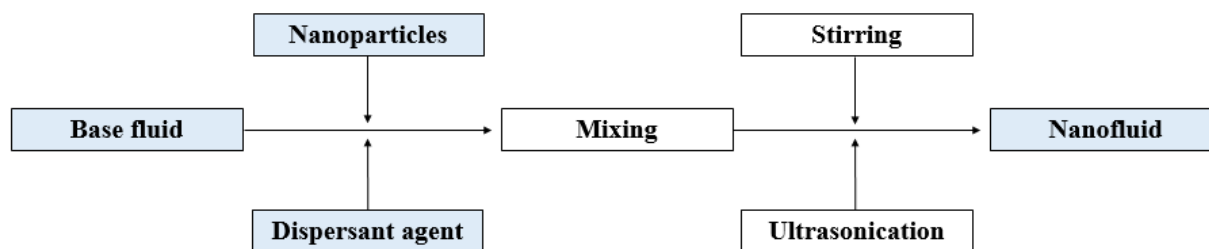


**Figure II.14.** Two-step method stages for preparing nanofluids [64,65].

The two-step method is the most widely used method for the preparation of nanofluids, especially those based on graphene. It has economic advantages and allows the preparation of nanofluids in large quantities due to the expanded industrial production of nanoparticles.

The behavior of graphene nanosheets in dispersion is governed by two types of interaction: electrostatic interactions (attractive or repulsive) between the particles themselves, and hydrodynamic interactions between the particles and the base liquid. Some interactions oppose each other while others accumulate. In addition, graphene nanosheets are distinguished by their high aspect ratio and specific surface area, which results in strong van der Waals attractive forces that can cause the aggregation and arrangement of particles in aggregates. The main difficulty encountered with this type of nanofluid is to disperse graphene homogeneously over time. On the other hand, graphene nanosheets are hydrophobic and tend to agglomerate and sediment in water and some base liquids. The stability and quality of dispersion of graphene-based nanofluids are key characteristics that significantly influence their properties.

Also, the preparation of graphene suspension is generally accompanied by mechanical and/or chemical processes, mainly related to the use of surfactant, which respectively homogenizes the

distribution of graphene in the base liquid and enhances the stability of the suspension. Mechanical techniques consist of applying a strong mechanical action using a rotary or ultrasonic agitator, breaking up agglomerates if present and ensuring the dispersion of particles in the solution. However, the duration and intensity of mechanical mixing can have negative effects on the properties of the graphene. Prolonged agitation or too much agitation can break graphene nanosheets. Thus, it is important to control these mechanical actions in order to ensure good dispersion of graphene nanosheets without reducing and/or modifying their structures and therefore their thermal properties.

Chemical techniques make it possible to limit agglomerates due to the forces of attraction between particles by adding surfactants (or dispersants) that modify the surface properties of these particles. Indeed, the molecules of the surfactants are adsorbed on the surface of the graphene nanosheets and form a sort of sprawling barrier that limits their proximity at very short distances and minimizes the van der Waals-type attraction forces. The surfactants can be classified according to their charge, in four main classes: cationic, anionic, amphoteric and non-ionic compounds [66]. Following their manufacture, the stability of nanofluids and the dispersion state of graphene in the suspension are usually studied. The main methods used in this area are described below.

### **II.3.1.3- Stability**

In addition to simple visual observations, several techniques are used to evaluate the stability and dispersion state of graphene within the base liquid. Among the most used in the literature, one can mention sedimentation and centrifugation methods, Zeta potential analysis, UV-visible spectrophotometry, and TEM or SEM.

#### ***a) Sedimentation and centrifugation processes***

In the sedimentation and centrifugation process, the density and size of sediments formed under the excitation of an external force may be a good indicator of the nanofluid stability [67]. The change in concentration and size of the supernatant particles is recorded as a function of time under external excitation. The nanofluid is considered stable when this change in concentration/size of the nanoparticles remains constant over time. This method is very simple to implement but requires a long observation period compared to other methods [68].

**b) Zeta potential analysis**

Zeta potential is an important element in controlling the electrostatic dispersion of graphene-like other nanoparticles. This technique makes it possible to measure, by electrical conductivity, the surface charges or the zeta potential of graphene nanosheets within the base liquid, and to determine thus the importance of inter-particles repulsive and attractive forces. The electrostatic potential exerted by the surface charge varies progressively within a zone called an electric double layer. The most commonly used model to describe the structure of the electric double layer (Gouy-Chapman-Stern-Grahame model) [69], suggests that this reorganization leads to the formation of two distinct zones: the compact layer (or Stern layer) and the diffuse layer (Figure II.15). The thickness of the latter varies in particular with the ionic force of the solution and decreases when the ionic force increases.

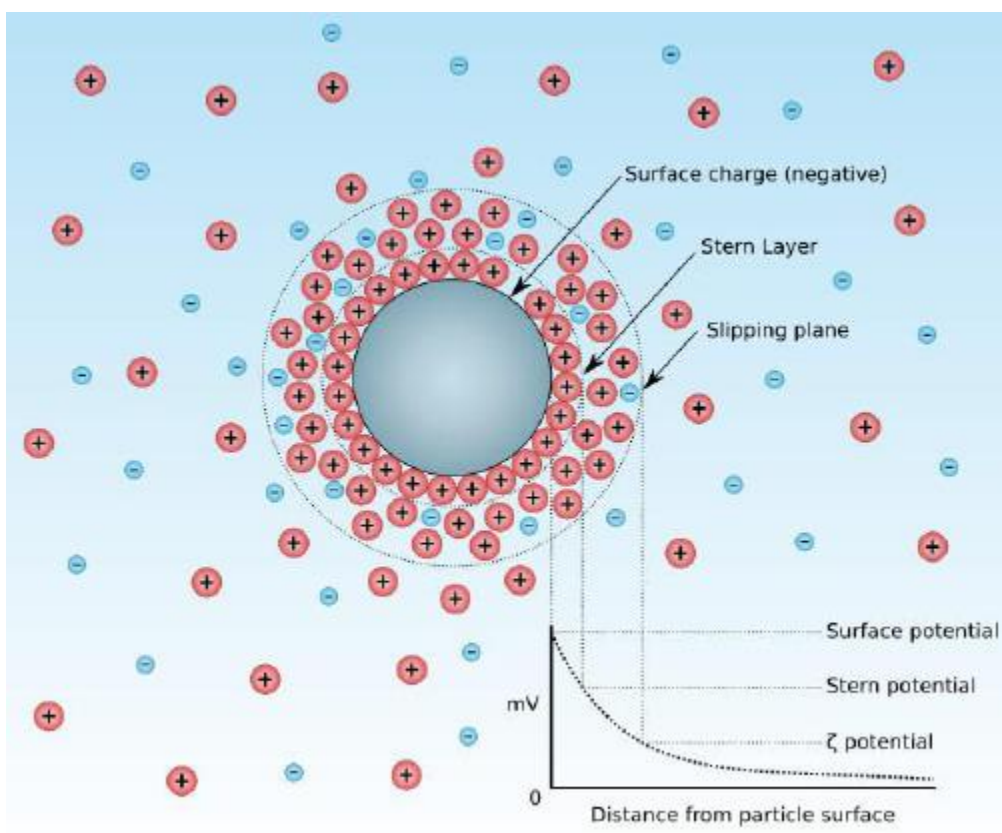


**Figure II.15.** Zeta potential diagram [70].

When the particle surface potential is below a critical value of -30mV or above +30mV (Figure II.16), inter-particle repulsive forces are predominant and the solution can be considered stable [69].

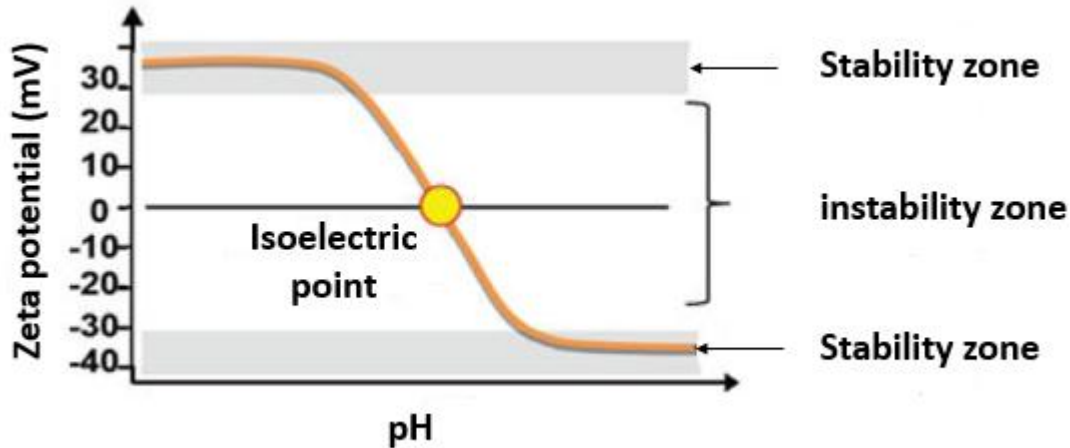


Figure II.16. Zeta potential of a solution [69].

The analysis of the Zeta potential allows also a mean particle size distribution of the particles in suspension to be evaluated.

**c) UV-Visible Absorbance Spectrophotometry**

It is a quantitative analysis technique that consists of measuring the absorbance of a medium as a function of wavelength and studying its evolution over time. The more concentrated the solution, the greater the intensity of the absorbed radiation within the limit of the proportionality between concentration and absorbance announced by Beer-Lambert's law. In the case of nanoparticles suspended in a base liquid, the spectrophotometry UV-visible is of particular interest for indicating the state of dispersion of the particles as well as the presence or absence of agglomerates based on the intensity of the absorbed or transmitted beam. Indeed, the variation in the concentration and size of the supernatant particles over time, and thus the stability evolution, is detected by measuring the absorbance of suspensions [71].

**d) TEM or SEM**

Transmission or Scanning Electron Microscopy allows the observation of elements at the atomic scale, especially their sizes, shapes and distributions. These processes do not allow the

measurement of nanoparticles in real situations in suspension in a base liquid, as measurements are usually performed on previously dried samples. Nevertheless, these techniques provide information relevant to the structure of nanoparticles and the network that they can form after dispersion. They can be used at first sight to control the formation and size of aggregates within nanofluid [72].

Finally, it should be noted that the efficiency of UV-visible spectrophotometry and TEM or SEM depends on the transparency of the medium studied. In the case of graphene-based nanofluids for which the opacity increases progressively with the graphene fraction, it is sometimes necessary to dilute these suspensions to study them. This may eventually lead, in the case of nanofluids with high graphene fractions, to test a solution that is not necessarily representative.

After a description of the methods used for graphene production and characterization and graphene-based nanofluids preparation and stability analysis, the next part of this chapter focuses on the state of knowledge of the thermophysical properties and thermal behavior of these nanofluids.

### **II.3.2- Thermophysical profile**

One of the objectives of this work is the experimental characterization of thermophysical properties of graphene-based nanofluids for determining their performance as a heat transfer fluid for their potential use in a heat exchanger. It is, therefore, necessary to identify and analyze the main approaches already developed and existing in the literature on both the theoretical and experimental design for the evaluation of thermal conductivity, dynamic viscosity, density, surface tension and isobaric heat capacity of graphene-based nanofluids.

Thermal conductivity, dynamic viscosity, surface tension, density, and isobaric heat capacity are significant for analyzing heat exchange performance [73–75]. The absorbed heat flow or transmitted by fluid in the balance of heat transfer between fluids is assumed to be the product of its isobaric heat capacity by its mass flow rate by the temperature difference between its entry and exit in the considered control volume. Nanoparticles have lower thermal capacities than those of thermal fluids, so less energy will be required to raise the temperature in nanofluids. From the experimental volume flow rate of fluids, their mass flow rate can be determined using their density value. Since most solid nanoparticles usually have densities higher than those of base fluids, the

densities of nanofluids are expected to increase with increasing nanoparticle content. The dispersion of solid nanoadditives in a fluid will also change its viscosity and therefore the flow regime may be affected. So the viscosity increase will require higher velocities to achieve turbulence flow where convective heat transfer coefficients are improved. In addition, higher viscosities result in greater pressure drops and, consequently, pumping powers increase [73,76,77]. Thus, a complete thermophysical profile characterization is required to accurately determine the fluid's thermal behavior. Besides, extensive studies on the dependencies of all these properties on the nanoparticles (type, shape, size and concentration) and the base fluid are required (Figure II.17).

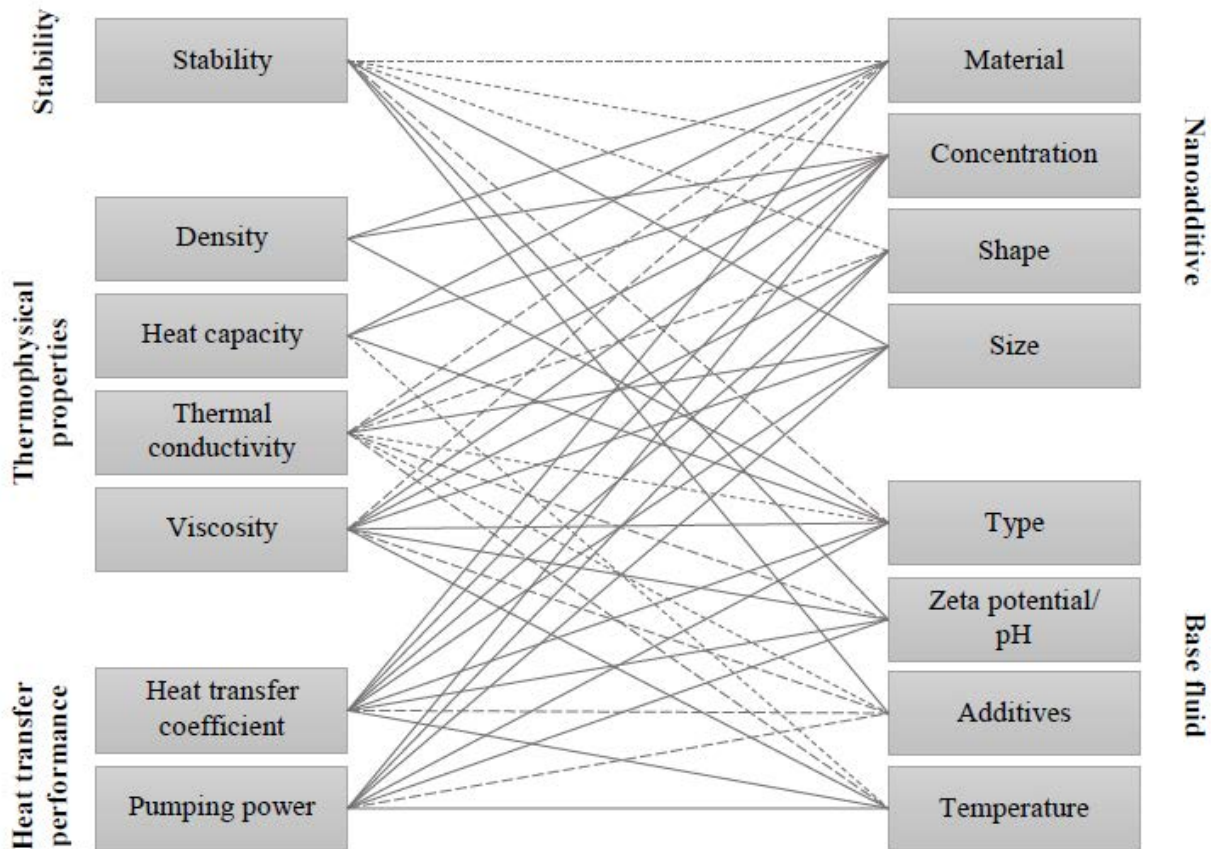


**Figure II.17.** Relations between the different properties of nanofluid and the design parameters of nanoparticles and base fluid. Weak (---), medium (---) and strong (—) dependence [78,79].

### II.3.2.1. Thermal conductivity

Thermal conductivity,  $k$  ( $\text{W}\cdot\text{m}^{-1}\cdot\text{K}^{-1}$ ), is the ability of a material to conduct or transmit heat. It is defined by the International Union of Pure and Applied Chemistry IUPAC [80] as the amount of tensor that binds heat flux ( $q$ ) to a temperature gradient ( $\Delta T$ ),  $k = -q/\Delta T$ . Thermal conductivity is a very important property for improving the thermal performance of a heat transfer fluid. Thermal diffusivity, the relation between thermal conductivity, density and heat capacity, governs the thermal transport in a fluid, confirming the essential role of these properties in thermal performance [81]. The synthesis of nanofluids meets the need to improve and amplify the thermal conductivity of liquids. Therefore, a lot of work has been carried out to measure but also to predict and explain this improvement.

From the literature [82], it has been noted that several factors as particle size and shape, temperature, motion, material, concentration, and purity level can affect the thermal conductivity of nanofluids, as shown in Figure II.18.

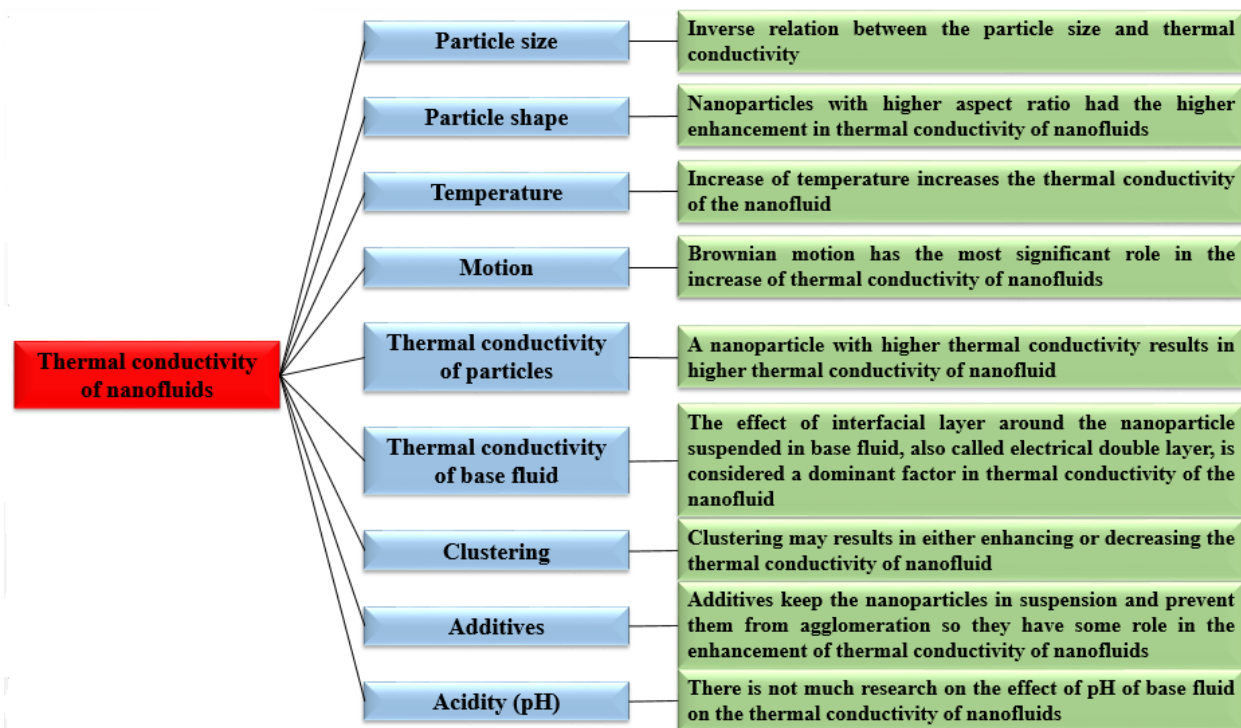


Figure II.18. Parameters that affect the thermal conductivity of nanofluids [2,83].

### II.3.2.1.1. Theoretical models

Several theoretical or empirical models have been used for comparison purpose or to explain the thermal conductivity enhancement of graphene-based nanofluids. In this section, we present some of these models, as shown in Table II.2.

**Table II.2.** Some theoretical or empirical models for the thermal conductivity of graphene nanofluids.

Authors	Equation	Key parameters	Remarks
Hamilton and Crosser [84]	$\frac{k_{eff}}{k_{bf}} = \frac{k_{np} + (n-1)k_{bf} - (n-1)(k_{bf} - k_{np})\varphi}{k_{np} + (n-1)k_{bf} - (k_{bf} - k_{np})\varphi}$	$k_{np}, k_{bf}, \varphi$	To determine the effective thermal conductivity of two heterogeneous component systems having different shapes, composition and particle sizes. The empirical shape factor, $n = 3/x$ , $x$ is the sphericity of the particle.
Hasselman and Johnson [85]	$\frac{k_{eff}}{k_{bf}} = \frac{k_{np}(1+2\gamma) + 2k_{bf} + 2(k_{np}(1+\gamma) - k_{bf})\varphi}{k_{np}(1+2\gamma) + 2k_{bf} - (k_{np}(1+\gamma) - k_{bf})\varphi}$ where $\gamma = \frac{r_K}{r_{np}}$ is a dimensionless parameter and $r_K$ here is the Kapitza radius: $r_K = R_K k_{bf}$ , where $R_K$ is the Kapitza or thermal boundary resistance.	$k_{np}, k_{bf}, \varphi$	To determine the effective thermal conductivity of a composite by introducing a thermal barrier resistance at the material interface with dilute concentrations of dispersed components of flat, cylindrical, and spherical configurations.
Nan <i>et al.</i> [86]	$\frac{k_{eff,11}}{k_{bf}} =$ $\frac{k_{eff,22} [ 2 + \varphi \{ \beta_{11}(1-L_{11})(1-\langle \cos^2 \theta \rangle) + \beta_{33}(1-L_{33})(1-\langle \cos^2 \theta \rangle) \} ]}{2 - \varphi \{ \beta_{11}L_{11}(1+\langle \cos^2 \theta \rangle) + \beta_{33}L_{33}(1-\langle \cos^2 \theta \rangle) \}}$ $\frac{k_{eff,33}}{k_{bf}} =$ $\left[ \frac{1 + \varphi \{ \beta_{11}(1-L_{11})(1-\langle \cos^2 \theta \rangle) + \beta_{33}(1-L_{33})(1-\langle \cos^2 \theta \rangle) \}}{1 - \varphi \{ \beta_{11}L_{11}(1-\langle \cos^2 \theta \rangle) + \beta_{33}L_{33}\langle \cos^2 \theta \rangle \}} \right]$ with, $\beta_{ii} = \frac{k_{ii} - k_{bf}}{k_{bf} + L_{ii}(k_{ii} - k_{bf})}$ and $\langle \cos^2 \theta \rangle = \frac{\int \rho(\theta) \cos^2 \theta \sin \theta d\theta}{\rho(\theta) \sin \theta d\theta}$	$= k_{np}, k_{bf}, \varphi$	To determine the effective thermal conductivity of arbitrarily shaped composite particles such as misoriented ellipsoids, flat plates, continuous fibers and spheres, using an efficient average approach based on Kapitza's resistance. <sup>1</sup>
Wang <i>et al.</i> [87]	$\frac{k_{nf}}{k_{bf}} = 1 + 21.487\varphi - 91.30\varphi^2$	$T, k_{bf}, \varphi$	To determine the thermal conductivity of graphene (GNPs) nanofluids based on a mixture of water and ethylene glycol knowing the volume fraction and the temperature.
Wiener [88]	$k_{nf} = \varphi_v k_{np} + (1 - \varphi_v) k_{bf}$	$k_{np}, k_{bf}, \varphi_v$	To determine the thermal conductivity of nanofluids using the thermal conductivity of base fluid, of nanoparticles and the concentration.

<sup>1</sup> The general form of this model reduces in presence of graphene as it will be explained in chapter IV.

For example, the thermal conductivity of graphene-based nanofluids was experimentally investigated by Yu *et al.* [89], Khosrojerdi *et al.* [90], Kole and Dey [91], Hadadian *et al.* [92], Kamatchi *et al.* [93] and Mehrali *et al.* [94], and the results were in a good agreement with Nan's model [86] who generalized Maxwell model [95] (used for spherical and well-dispersed particles) including the effects of finite interfacial resistance and particle geometry.

Hamilton-Crosser model [84] postulates that when the ratio of particle thermal conductivity to liquid thermal conductivity is higher than 100, the particle shape turns into a key factor. The sphericity of nanoparticles is defined as the ratio of the surface area of a sphere with the same volume than the particles to the surface area of the particles. Vallejo *et al.* [96] measured the thermal conductivity of functionalized graphene nanofluids based on propylene glycol-water mixture and compared the experimental results with Hamilton-Crosser model. A good agreement with this model was achieved considering a sphericity value around  $\sim 0.27$ .

In addition, to predict their experimental results, Vallejo *et al.* [96] used the upper Wiener bound [88], also named as parallel model, which has been previously adapted to heterogeneous materials [97] and then applied in the field of nanofluid by Cabaleiro *et al.* [98]. The authors obtained a noticeable agreement between the reported results and those found by this model and the deviation value was about 3.1%.

Because of the relevance of some of these models in previous works about graphene-based nanofluids, they could be possibly used in the present study for comparison purpose with experimental data.

### **II.3.2.1.2. Previous experimental work**

The thermal conductivity of graphene-based nanofluids has been the subject of several studies. A significant increase in the thermal conductivity of graphene nanofluids has often been observed.

For example, few-layer graphene nanofluids based on polymer solutions were studied by Sun *et al.* [99]. Their thermal conductivity measurements showed a quasi-constant enhancement  $\sim 25\%$  in the temperature range 10-60°C for low nanofluid concentration of 0.055 vol.% for the nanofluid P20/G/EtOH.

Amiri *et al.* [100] investigated the case of monolayer graphene/water nanofluids with different weight concentrations in the range of 0.001-0.01%. The authors found a thermal conductivity increase with the rise of temperature from 20 to 50°C. The obtained thermal conductivity enhancement of nanofluids was more than 25% for the highest weight fraction of 0.01% at different temperatures.

On the other hand, Amiri *et al.* [101] focused on a highly crumpled few-layer graphene dispersed in water where a Gum Arabic was mixed with the nanoparticles by a ratio of 1:0.5. A thermal conductivity enhancement of 42.5% was found with increasing the nanofluids weight concentration from 0 to 0.01% at 50°C. In addition, the authors obtained an increase in thermal conductivity by 8.6%, 20.8%, 23.8%, and 21.9% for the base fluid and nanofluids concentrations 0.001wt.%, 0.005wt.%, and 0.01wt.% with the rise of temperature in the range 20-50°C, respectively.

Some other works on thermal conductivity of graphene-based nanofluids are also detailed in the following table (Table II.3).

**Table II.3.** A detailed summary of graphene-based nanofluids: nanoparticles (Nps), particle size (PS), synthesis methods (SM), based fluids (BF), surfactants (Sfts), preparation methods (PM), concentrations (Conc.), PH, characterization techniques (CT), and thermal conductivity enhancement [2].

Authors	Nps	PS	SM	BF	Sfts	PM	Conc.	PH	CT	Findings
Sun <i>et al.</i> [99]	Few layer graphene (less than five)	500-1.5 $\mu\text{m}$	Exfoliation of graphite	Polymer solutions	N/A	Two step method	0.055vol.%	N/A	UV-vis spectroscopy, optical microscopy, SEM, TEM, HRTEM, Raman spectroscopy, TGA, XRD, EDX	Quasi-constant thermal conductivity enhancement by about 25% was obtained.
Amiri <i>et al.</i> [100]	Single layer graphene (SGr)	$\approx$ few hundred square nm, t < 1nm	In situ exfoliation and functionalization of graphene	Distilled water	N/A	Two step method	0.001-0.01wt.%	N/A	FTIR, Raman spectroscopy, TGA, XPS, TEM, FESEM, AFM, UV-vis spectroscopy, transient hot wire method	The thermal conductivity was increased by more than 25% for the highest concentration.
Amiri <i>et al.</i> [101]	Highly crumpled few layer graphene	N/A	Exfoliation of graphite in the presence of liquid-phase using microwave-assisted methods	Water	Gum Arabic	Two step method	0-0.01wt.%	N/A	FTIR, Raman spectroscopy, XRD, XPS, FESEM, TEM, SAED	Thermal conductivity enhancement by 42.5% for the highest concentration.
Cabaleiro <i>et al.</i> [102]	Graphene nanoplatelets (GNPs)	$\approx 4 \mu\text{m}$	Supplied by manufacturer	Water+EG	NH <sub>4</sub> OH solution	Two-step method	0.10-0.50wt.%	2-10	SEM, TEM, Zeta potential test, UV-vis spectroscopy, DLS	The thermal conductivity was increased up to 5% with mass

## Chapter II - General information on graphene nanofluids

											concentration of GNPs.
Mehrali <i>et al.</i> [103]	Graphene nanoplatelets (GNPs)	t=2nm d=2μm	Supplied by manufacturer	DW	Not used	Two-step method	0.025%, 0.05%, 0.075%, 0.1%	N/A	N/A		An enhancement of thermal conductivity between 12% and 28% was found.
Amiri <i>et al.</i> [104]	Graphene nanoplatelets (GNPs)	t=0.55-3.74nm, d=0.5-3μm	Supplied by manufacturer	DI water	COOH, SDBS	Two-step method	0.025wt.%, 0.05wt.%, 0.1 wt.%	N/A	TEM, FTIR		The thermal conductivity was obtained higher by GNP-COOH/water than the GNP-SDBS/Water nanofluid. A maximum thermal conductivity of ≈ 0.83W/mK was achieved at 50°C for the highest concentration of GNP-COOH nanofluid.
Park and Kim [105]	Graphene (GE)	t=6-8nm, d=5-15μm	Supplied by manufacturer	DW	Not used	Two-step method	0.001-0.01%	N/A	Transient hot wire method, SEM		The authors found an increase in thermal conductivity by 5.47% and 4.45%.
Jyothirmayee Aravind and Ramaprabhu [106]	Graphene nanosheets (GNSs)	N/A	Hummers method	EG, DI water	Not used	Two-step method	0.008%, 0.055%, 0.083%, 0.11%, 0.138%	10	TEM, FT-IR, EDX		An enhancement in thermal conductivity by 6.5% and 13.6% was obtained for GNSs/EG and GNSs/DI water nanofluid respectively at 25°C.
Yu <i>et al.</i> [89]	Graphene nanosheets (GNSs)	t=0.7-1.3nm	Modified Hummers method	EG	SDBS	Two-step method	0.01-0.05wt.%	N/A	Transient hot wire method, TEM, FT-IR, AFM,		The authors obtained an enhancement in thermal conductivity by 86% at 5.0 vol.% of GNS.
Mehrali <i>et al.</i> [94]	Graphene nanoplatelets (GNPs)	t=2nm, d=45μm	Supplied by manufacturer	DW	Not used	Two-step method	0.025wt.%, 0.05wt.%, 0.07wt.%, 0.1wt.%	10	Zeta potential test, XPS, TEM, XRD, UV-vis spectrometer,		Thermal conductivity increase by 27.64% was determined.
Ghozatloo <i>et al.</i> [107]	Graphene nanosheets (GNSs)	t=500nm	CVD	DI water	N/A	Two-step method	0.01-0.05wt.%	7	Raman spectroscopy, SEM, TEM, FT-IR		Thermal conductivity enhancement was found at 25°C of 13.5% and 12.5% at 0.05% and 0.03%, respectively.

Lee and Rhee [108]	Graphene nanoplatelets (GNPs)	N/A	Supplied by manufacturer	EG	Not used	Two-step method	0.5vol.%, 1vol.%, 2vol.%, 3vol.%, 4vol.%	N/A	Raman spectroscopy, XRD, HRTEM, FT-IR, UV-vis spectroscopy	The authors obtained at 90°C an increasing in the thermal conductivity ratio by 1.030-1.332 for 0.5-4% concentration.
--------------------	-------------------------------	-----	--------------------------	----	----------	-----------------	--	-----	--	---

So, we can see that graphene-based nanofluids have a good thermal conductivity enhancement that mainly depends on the type of graphene nanoparticles. For example, graphene nanosheets that have a minimum number of sheets have better thermal properties. And by comparison to the other graphene types, graphene oxide nanosheets are less advantageous than pristine graphene. The reason is that the groups that contain the polar oxygen atoms, even if in terms of a facilitated aqueous nanofluid, they bring positive effects, but they bring also a disadvantage with a very significant decrease in conductivity of the sheets. Therefore, the efficient removal of these oxygen species to prepare a rGO is very important for all applications related to linear and nonlinear conductive nanoparticles [109]. But the reduction process of GO cannot eliminate perfectly all the oxygen atoms, that is why a direct preparation of graphene nanosheets is preferable.

### II.3.2.2. Rheology and Dynamic viscosity

#### II.3.2.2.1- Rheology

Rheology is defined by the science of the deformations and flows of matter [110], the resulting stresses and the efforts required to achieve them. It is based on the basics of continuous media mechanics to locally determine stresses and deformations within matter. Dynamic viscosity is one of the rheological behavior characterizing parameters of material under certain conditions. A simple example considering the movement of a fluid enclosed between two parallel planes, one is at rest and the other is animated with a velocity  $V$  (Figure II.19). The displacement is communicated by tangential friction between the parallel layers. It is assumed that the fluid layers bound to the stationary plane have zero velocity (non-slip hypothesis). Two quantities will allow quantifying the shear:

The shear rate  $\dot{\gamma}$  (expressed in  $s^{-1}$ ) which represents the variation in velocity between the boundary layers with the distance between these layers. This quantity is equal to the ratio of the shear velocity  $V$  to the sheared thickness.

The shear stress  $\sigma$  (expressed in Pa) which defines the force exerted tangentially between fluid layers.

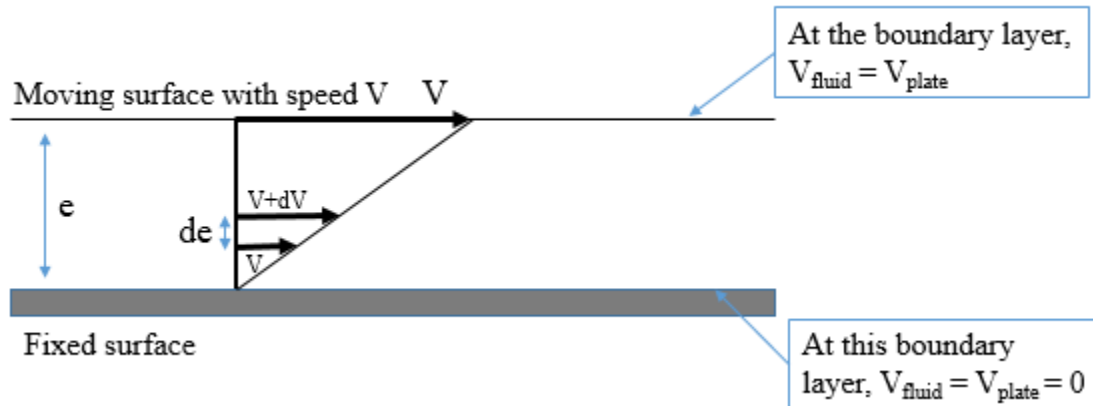


**Figure II.19.** Shear motion between two parallel planes [111].

The dynamic viscosity,  $\eta$ , of the fluid, is the ratio of tangential shear stress to shear rate:  $\eta = \sigma/\dot{\gamma}$ . It is generally expressed in Pa.s.

In the case of liquids, the fluid is defined as Newtonian when the linear behavior described by Newton is observed, and it is defined as non-Newtonian when it follows a non-linear behavior. Newtonian liquids present constant dynamic viscosity values versus shear rate, shear stress and time ( $\sigma = \eta \cdot \dot{\gamma}$ ) (Figure II.21 b)). Many common existing fluids are not Newtonian. Based on the evolution of dynamic viscosity as a function of shear rate, we can distinguish three main types of rheological behavior (Figure II.20):

*Shear-thinning behavior* (pseudoplastic fluid): the dynamic viscosity of the fluid decreases when the shear rate increases. This is the case with most polymers, for example. This behavior can be described by Ostwald de Waele model or power law:  $\sigma = \eta \cdot \dot{\gamma}^n$  where  $n < 1$ .

*Shear-thickening behavior* (dilatant fluid): in this case, the fluid becomes more viscous when the shear rate increases. It is an uncommon behavior:  $\sigma = \eta \cdot \dot{\gamma}^n$  where  $n > 1$ .

*Threshold stress (or plastic) behavior*: the fluid only flows above a certain threshold stress  $\sigma_0$ . This is the case with toothpaste and oil paint, for example. Beyond this constraint, the fluid can behave in a Newtonian way (one then defines its behavior by a Bingham's law,  $n=1$  in the following

equation) or in a non-Newtonian way with rheofluidification or rheosolidification (behavior described by Herschel-Bulkley's law given by the following equation):  $\sigma = \sigma_0 + \eta \cdot \dot{\gamma}^n$

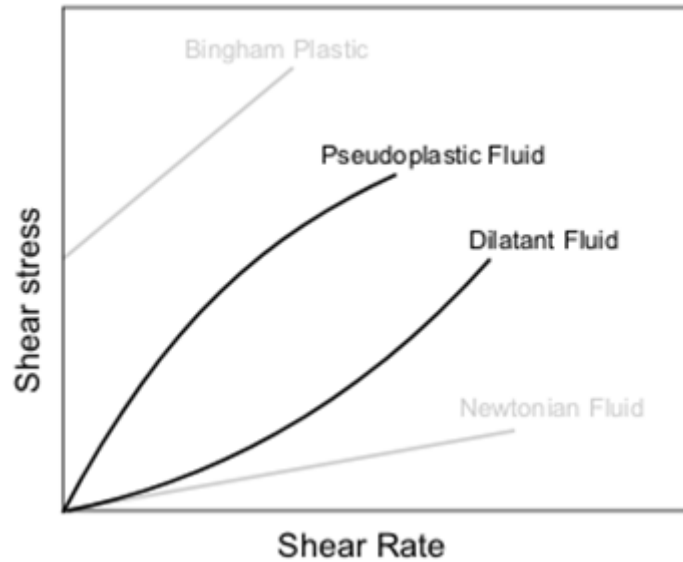


**Figure II.20.** Rheograms characteristic of different rheological behaviors [112].

Non-Newtonian fluids may be classified according to time as time-dependent or time-independent. In the case of non-Newtonian fluids that are time-dependent, dynamic viscosity depends on the shear rate and the time during which it is applied,  $\eta(t, \dot{\gamma})$ . According to this criterion, the fluid may be thixotropic or rheopectric, Figure II.21 a). The viscosity of thixotropic fluids decreases overtime for a constant shear rate, and then after the stress is removed, the initial value is gradually recovered. On the other hand, the viscosity of rheopectric fluids increases overtime for a constant shear rate, and then after the removal of the stress, the initial value is gradually recovered [110]. For non-Newtonian fluids that are time-independent, dynamic viscosity depends only on the shear rate, so not on time also,  $\eta(\dot{\gamma})$ . Given this condition, the fluid may be pseudoplastic or dilatant, Figure II.21 b).

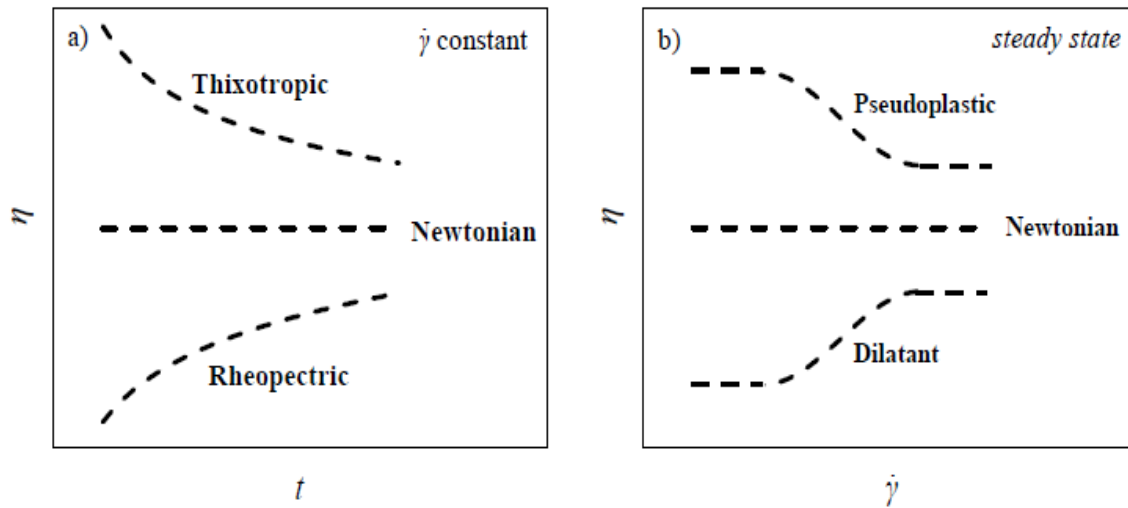


**Figure II.21.** Behaviors of Newtonian and non-Newtonian fluids: dynamic viscosity as a function of time (a) and shear rate (b) [79].

### II.3.2.2.2. Dynamic viscosity

Viscosity characterizes the ability of a fluid to flow [113]. The knowledge of viscosity is fundamental for all applications involving the transport of fluids because the pumping power and pressure drop depends on it. The addition of nanoparticles can increase and improve the thermal conductivity of the nanofluid, but this can also lead to an unfavorable increase in dynamic viscosity. Thus, these two properties are closely correlated and must be mastered to exploit this type of fluid in heat exchangers.

In general, as for all nanofluids [114], the viscosity of graphene nanofluids is influenced by several factors such as temperature, dispersion state, morphology, shear rate, volume concentration and viscosity of the base fluid, as shown in Figure II.22.

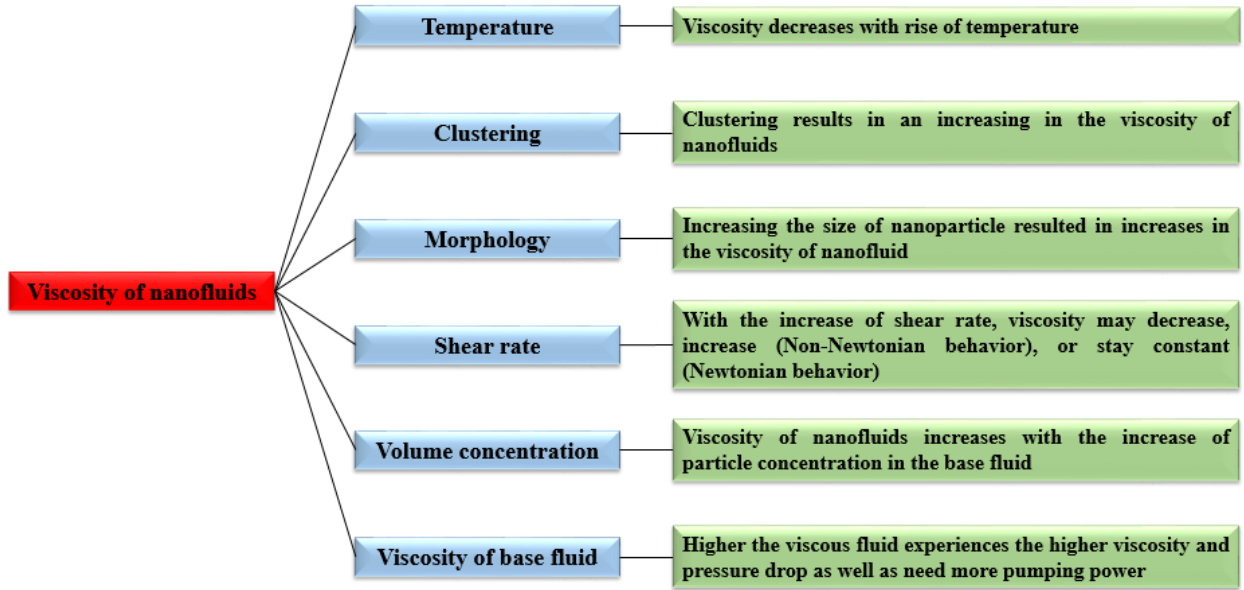


Figure II.22. Parameters that affect the viscosity of nanofluids [2].

### II.3.2.2.3. Theoretical models

Several theoretical or empirical models have been used or developed to predict the viscosity evolution of nanofluids under certain conditions, as reported in [114]. The most existing viscosity models are for nanofluids based on spherical nanoparticles, and few of them for rod-like nanoparticles. In this section, we only report the last models associated with graphene-based nanofluids.

Researchers have used the Andrade equation (Eq. II.1) to understand the relationship between the viscosity of nanofluids and the temperature. This equation is defined as follows:

$$\eta = A. e^{\frac{B}{T}} \quad \text{Eq.II.1}$$

where A and B are constants, and T is the absolute temperature (K) [115,116]. A correlation was postulated by Wand *et al.* [117] to estimate the apparent viscosity of graphene (GNP) nanofluids based on water as a function of nanoparticle mass fraction ( $\varphi$ ) and fluid temperature T (K), using a multiple steps regression analysis, as follows (Eq.II.2). This equation is valid for  $0.2 < \varphi < 1$  wt.% and  $278.15 < T < 298.15$  K.

$$\eta = 0.004 \cdot (1 - \varphi)^{-77.5} \cdot e^{\frac{1652}{T}} \quad (R^2=0.99) \quad \text{Eq.II.2}$$

On the other hand, the Vogel-Fulcher-Tammann (VFT) equation [118,119], also known as the Vogel-Fulcher-Tammann-Hesse equation, is one of the most widely used models to describe the temperature dependence of viscosity:

$$\eta = \eta_0 \cdot e^{\frac{A \cdot T_0}{T - T_0}} \quad \text{Eq.II.3}$$

where  $\eta_0$ , A, and  $T_0$  are fitting parameters.

Recently, the dynamic viscosity values of graphene nanofluids have been well modelled using Vallejo et al.'s equation [77], which includes, in the same expression, the dependence of the viscosity on the concentration and the temperature:

$$\eta = \eta_0 \cdot e^{\frac{A \cdot T_0}{T - T_0} + B \cdot \frac{C}{T}} \cdot \varphi - D \cdot \varphi^2 \quad \text{Eq.II.4}$$

where B, C, and D are a fitting parameters;  $\varphi$  is the volume fraction; and  $\eta_0$ , A, and  $T_0$  are the fitted parameters for the corresponding base fluid obtained previously from the VFT equation, Eq.II.3.

#### II.3.2.2.4. Previous experimental work

Experimental studies carried out on rheological behavior and dynamic viscosity of nanofluids, based on graphene, are more limited compared to those relating to the thermal conductivity of these same suspensions. In addition, most of the work performed on dynamic viscosity concern spherical nanoparticle-based nanofluids. As with thermal conductivity, several factors can influence the rheological behavior and the dynamic viscosity of nanofluids, as shown in Figure II.22. Available literature shows that nanofluids can exhibit two rheological behaviors, Newtonian or non-Newtonian, depending on nanoparticle shape, size or concentration [114,120].

For example, graphene nanosheets with a size of few layers (about 15-50 nm) were dispersed in glycerol by Moghaddam *et al.* [121]. They prepared nanofluids in the weight concentration range 0.0025-0.02% and measured their viscosity in the temperature range 20-60°C. In addition to the

non-Newtonian behavior, the authors found with the loading of 2% graphene nanosheets a viscosity enhancement of glycerol by 401.49% at 20°C and shear rate equal to 6.32 s<sup>-1</sup>.

In another work, Sarsam *et al.* [122] investigated 0.1 wt.% of graphene nanoplatelets (GNP) nanofluids based on water using different surfactants like sodium dodecyl sulfate (SDS), sodium dodecyl benzene sulfonate (SDBS), gum arabic (GA), and cetyl trimethylammonium bromide (CTAB). At shear rates from 20 to 200 s<sup>-1</sup> and in the temperature range 25-55°C, the authors found that the nanofluids with all surfactants are Newtonian except GA, a non-Newtonian behavior was observed for (0.5-1) GA-GNPs nanofluid. In the case of pristine GNPs nanofluids, a non-Newtonian behavior was obtained, except at 35°C it was Newtonian. In addition, nearly the lowest viscosity (7.4% higher than water) and the highest stability were for the (1-1) SDBS-GNPs nanofluid. Based on the viscosity average values, the nanofluids can be sequenced as (1-1) CTAB-GNPs < (1-1) SDS-GNPs < (1-1) SDBS-GNPs < pristine GNPs << (0.5-1) GA-GNPs.

Graphene nanoplatelets (GNP), with a diameter of 15 µm and about 5-10 nm of thickness, were dispersed in a mixture of deionized water:ethylene glycol (70:30 volume ratio) by Selvam *et al.* [123] using an amount of 0.75 vol.% of sodium deoxycholate (SDC) as a surfactant. The authors studied the viscosity of nanofluids in a range of volume concentration 0.1-0.5% between 30 and 50°C. The results showed an increase in the viscosity ratio ( $\mu_{nf}/\mu_{bf}$ ) from 1.06 and 1.13 to 1.16 and 1.39 at the nanoparticle loading 0.1 vol.% and 0.5 vol.%, respectively.

On the other hand, Wang *et al.* [124] studied the single-layer graphene nanofluids based on water that contain a special dispersant. The viscosity measurements showed a decreasing with the temperature rise from 5 to 25°C, and an increase with the increase of graphene concentration from 0.2 to 1 wt.%. The viscosity increment ratio between the nanofluids and water ranges from 1.24 to 2.35, in addition to the observed shear thinning effect and non-Newtonian behavior.

More studies on dynamic viscosity and rheological behavior of graphene-based nanofluids are presented in the following table:

**Table II.4.** A detailed summary of researches on rheology and dynamic viscosity of graphene-based nanofluids.

Type of nanoparticle	Type of treatment	Base fluid	Surfactant	Size of nanoparticles	Concentration range	Temperature range	Key results/remarks	Rheology	Reference
Single layer graphene (GNP)	N/A	Water	Special dispersant	1-12 $\mu\text{m}$ (diameter), 0.55-1.2 nm (thickness), 500-1200 $\text{m}^2/\text{g}$ (SSA)	0.2-1 wt.%	5-25°C	Viscosity decrease with rising temperature and viscosity increase with nanoparticle mass content. Viscosity increment ratio between water and GNP nanofluids ranges from 1.24 to 2.35	Non-Newtonian behavior and shear thinning effect	Wang <i>et al.</i> [124]
Graphene nanoplatelets GNP	Stable dispersions were prepared by non-covalent functionalization approach. The nanofluids were prepared by the two step method	Deionized water + ethylene glycol (70:30 volume ratio)	SDC (0.75 vol.%)	5-10 nm (thickness), 15 $\mu\text{m}$ (diameter)	0.1-0.5 vol.%	30-50°C	The viscosity ratio $\mu_{nf}/\mu_{bf}$ increases from 1.06 to 1.16 at 0.1 vol.% and from 1.13 to 1.39 at 0.5 vol.%	N/A	Selvam <i>et al.</i> [123]
Graphene nanoplatelets GNP	Nanofluids prepared via the two-step method	Water	SDBS, SDS, CTAB, GA	2 $\mu\text{m}$ (lateral size), 2 nm (thickness), 300 $\text{m}^2/\text{g}$ (specific surface area)	0.1 wt.%	25-55°C	The (1-1) SDBS-GNPs sample showed nearly the lowest viscosity (7.4% higher than distilled water) and the highest stability. Based on the viscosity average values, the nanofluids can be sequenced as (1-1) CTAB-GNPs < (1-1) SDS-GNPs < (1-1) SDBS-GNPs < pristine GNPs << (0.5-1) GA-GNPs	Newtonian behavior for nanofluids with surfactant (all except GA). Non-Newtonian behavior for pristine GNPs nanofluids except at 35°C the behavior was Newtonian. Non-Newtonian behavior for (0.5-1) GA-GNPs nanofluid (shear rates 20-200 $\text{s}^{-1}$ )	Sarsam <i>et al.</i> [122]
Graphene nanosheets	Graphene nanosheets were produced from burning magnesium metal in dry ice	Glycerol	N/A	15-50 nm (size of few layers)	0.0025-0.02 wt.%	20-60°C	Viscosity enhancement of glycerol of 401.49% was obtained by loading of 2% graphene nanosheets at 20°C and at shear rate of 6.32 $\text{s}^{-1}$	Non-Newtonian behavior	Moghaddam <i>et al.</i> [121]
Graphene GE	Graphite oxide (GO) was synthesized using Hummers' method	Ionic liquid	N/A	N/A	0.03 wt.%	25-75°C	The viscosity of nanofluids was found lower than that of the base fluid and decreases from 217.4 to	N/A	Wang <i>et al.</i> [125]

## Chapter II - General information on graphene nanofluids

							40.6 cp as the temperature increases from 25°C to 75°C		
Graphene nanoplatelets GNP	N/A	Distilled water	N/A	< 2 $\mu\text{m}$ (diameter), 2 nm (thickness), 300, 500, 750 $\text{m}^2/\text{g}$ (specific surface area)	0.025-0.1 wt. %	20-60°C	The authors found an improvement in the viscosity of nanofluids by 44% comparing to the base fluid for the highest concentration.	Newtonian and non-Newtonian behavior (for high concentrations)	Mehrali <i>et al.</i> [94]
Graphene nanoplatelets GNP	Nanofluids were prepared using a two-step technique	Kerosene	Oleylamine	300, 500, 750 $\text{m}^2/\text{g}$ (specific surface area)	0.005-0.2 wt. %	20-70°C	Viscosity increase by 8% was found at room temperature for 750 SSA, 0.2 wt. % kerosene-GNP nanofluid	N/A	Agarwal <i>et al.</i> [126]
Graphene nanosheets	Nanofluids were prepared through two-steps method	Hydrogenated oil	N/A	0.06-0.1 $\mu\text{m}$ (X-Y dimensions), 0.002-0.005 $\mu\text{m}$ (Z dimension)	25-100 ppm	30-50°C	Viscosity and shear stress increasing up to 33% was obtained at 30°C for the highest nanoparticle concentration	Shear thinning behavior at very low shear rates, and slight shear thickening behavior at a higher shear rate	Chai <i>et al.</i> [127]
Graphene nanosheets (alkaline graphene oxide)	Graphene nanosheets were prepared by CVD method, and the two-step method was used in the preparation of the nanofluids	Deionized water	N/A	N/A	0.05-0.1 wt. %	N/A	Viscosity increasing by 11.97% was determined for 0.1% weight fraction of graphene in water	N/A	Ghozatloo <i>et al.</i> [128]
Graphene nanoplatelets GNP	N/A	Distilled water	N/A	750 $\text{m}^2/\text{g}$ (specific surface area)	0.025-0.1 wt. %	20-60°C	Viscosity increase with increasing concentration and with decreasing temperature	Newtonian behavior	Iranmanesh <i>et al.</i> [129]
Graphene nanoplatelets GNP	The nanofluids were prepared using the two-step method	Distilled water	N/A	2 $\mu\text{m}$ (diameter), 2 nm (thickness), 300, 500, 750 $\text{m}^2/\text{g}$ (specific surface area)	0.025-0.1 wt. %	20-60°C	The authors found that the viscosity of nanofluids decreases at higher temperatures by 4-44% compared with DW at a high shear rate of 500 $\text{s}^{-1}$	N/A	Mehrali <i>et al.</i> [130]

Graphene nanoplatelets GNP	The GNP nanofluid was prepared by using the two-step method	Distilled water	N/A	2 μm (diameter), 2 nm (thickness), 500 m <sup>2</sup> /g (specific surface area)	0.025-0.1 wt.%	20-60°C	The viscosity of nanofluids decreased between 9% and 38% with the rise of temperature at a shear rate of 500 s <sup>-1</sup>	N/A	Sadeghinezhad <i>et al.</i> [131]
----------------------------	---	-----------------	-----	--	----------------	---------	--	-----	-----------------------------------

As mentioned before, the viscosity is directly related to the pressure drop of a fluid, which in turn is mainly influenced by the pumping power needed to circulate the fluid. The pumping power is a principal concern because of its economic implications [132]. Consequently, this property must be accurately evaluated in function of concentration and temperature and can give some information about the stability and dispersion state of nanofluids.

### II.3.2.3. Isobaric heat capacity

Thermal conductivity and dynamic viscosity are the most studied thermophysical properties of nanofluids. The isobaric heat capacity of nanofluids is more rarely investigated, especially experimentally.

The isobaric heat capacity denoted  $C_p$  (J.kg<sup>-1</sup>.K<sup>-1</sup>), is defined by the amount of energy to be supplied by heat exchange to raise the temperature of the mass unit of a substance. This quantity is incorporated in the energy equation and then needs to be rigorously determined. The addition of graphene nanoparticles generally translates into a relative decrease in the isobaric heat of the nanofluid due to the lower isobaric heat of graphene compared to that of the base fluid.

Most of the studies in the literature use one of the two models defined by the equations II.5 [133] and II.6 [134] for determining the isobaric heat of the nanofluids. The first model is based on the mixing law of a homogeneous suspension, while the model in equation II.6 is based on the assumption of thermal equilibrium between particles and base fluid [135].

$$C_{p,nf} = \varphi_v \cdot C_{p,np} + (1 - \varphi_v) \cdot C_{p,bf} \quad \text{Eq.II.5}$$

$$C_{p,nf} = \frac{\varphi_v \cdot \rho_{np} \cdot C_{p,np} + (1 - \varphi_v) \cdot \rho_{bf} \cdot C_{p,bf}}{\varphi_v \cdot \rho_{np} + (1 - \varphi_v) \cdot \rho_{bf}} \quad \text{Eq.II.6}$$

However, it was demonstrated in the subsequent literature that the conversion from volume fraction to a mass fraction in Eq. II.5 was more correct and more consistent with the experimental data [136–138]. It was frequently used to predict the isobaric heat capacity of nanofluids, even those based on graphene [96,139].

Most publications have shown that temperature has a significant effect on the isobaric heat capacity of nanofluids. An increase and a decrease in  $C_p$  of nanofluids were found in the literature while increasing the temperature [140]. Also, an analysis of the isobaric heat capacity of nanofluids showed that this property decreases with increasing nanoparticle's volume fraction since solids generally have a lower isobaric heat capacity than liquids [141,142].

For example, Amiri *et al.* [101] investigated experimentally water-based highly crumpled few-layer graphene (HCFLG) nanofluids where the nanoparticles were mixed with Gum Arabic by a ratio of 0.5:1. With increasing the nanoparticle concentration in the base fluid, the measurements showed a drop in the isobaric heat capacity. The drop was observed of 0.1-0.5% for a weight content of 0.001-0.01 wt.%. The isobaric heat capacity of HCFLG nanofluids was lower than that of the base fluid due to the lower isobaric heat capacity of the nanoparticles loaded in water.

On the other hand, Amiri *et al.* [100] studied also the case of monolayer graphene nanoparticles (SGr) dispersed in distilled water with different weight concentrations between 0.005% and 0.01%. Measurements of isobaric heat capacity of all samples, base fluid and nanofluids, showed that the addition of SGr in water decreases insignificantly its isobaric heat capacity, which is related to that the nanoparticles have a  $C_p$  lower than that of the base fluid. In particular, the average drop in the isobaric heat capacity of nanofluids was found of 0.1%-0.5% as compared with water.

In addition, graphene nanoplatelets nanofluids based on a water-ethylene glycol mixture were prepared by Selvam *et al.* [143]. Isobaric heat capacity of the nanofluids in the concentration range 0-0.45 vol.% was measured between 30 and 50°C. The authors found that the  $C_p$  of the nanofluids decreased with the nanoparticle loading and the rate of this decrease was around 8% for the highest concentration at 30°C. Experimental values of this property were calculated also using Eq. II.6. A comparison between the measured and the calculated values showed that the experimental results are lower than the predicted values. The authors explained that the reason for this difference is that base fluid and nanoparticles are not in thermal equilibrium due to a thermal diffusivity enhancement [136].

The conclusion from the literature review is that further studies are needed to properly determine the temperature and volume concentration dependencies on nanofluid isobaric heat capacities.

### II.3.2.4. Density

The density of nanofluids, which is the mass ( $m$ ) of the sample divided by its volume ( $V$ ) ( $\rho = m/V$ ), is directly related with the pressure loss, Reynolds number, friction factor, and Nusselt number. It is proportional to the density fraction of the particles and increases with the addition of nanoparticles. Usually, it is considered as a function of pressure and temperature. With the increase of temperature, the density of most liquids decreases (with some exceptions, like water between 273.15 and 277.15 K). Changes in density due to pressure or temperature change, influence the heat transfer, whether natural or forced convection mechanisms [144]. Thus, properties derived from density such as the isothermal compressibility or the isobaric thermal expansion can be obtained from volumetric behavior data [145].

In the literature, and the absence of experimental results, the density of nanofluids is often calculated from the mixture law (Eq.II.7) in which, as with specific heat, the nanofluid is assumed to be homogeneous [133,146].

$$\rho_{nf} = \varphi_v \cdot \rho_{np} + (1 - \varphi_v) \cdot \rho_{bf} \quad \text{Eq.II.7}$$

Some recent works about this property with graphene nanofluids are presented in the following. Amiri *et al.* [101] investigated experimentally the density of water-based highly crumpled few-layer graphene (HCFLG) nanofluids where the nanoparticles were mixed with Gum Arabic by a ratio of 0.5:1. They obtained that the density decreases with the increase of the temperature, and grows with the nanoparticle loading. For example, with the rise of temperature from 20 to 50°C, the density of the base fluid and HCFLG based nanofluids at weight content of 0.01% decreases by 1.01% and 0.99%, respectively.

On the other hand, Amiri *et al.* [100] focused on water-based monolayer graphene nanoparticles (SGr) nanofluids with different weight concentrations between 0.005% and 0.01%. Density measurements of all the samples were done as a function of temperature and concentration. The results showed a decreasing of density values of with the temperature rise and the density increases

with nanoparticle loading. The decrease was about 1.01% and 0.96% for the highest nanofluid concentration when the temperature increases from 20 to 50°C.

In addition, a functionalized graphene nanoplatelets were dispersed in a commercial industrial antifreeze Havoline® XLC Premixed 50/50 by Vallejo *et al.* [139] using SDBS as a surfactant. The density of the nanofluids in the concentration range 0.25-1 wt.% was measured experimentally between 293.15 and 343.15 K. The results showed an increase in density values by 0.37-0.58% in the case of the highest concentration, and a decreasing by about 0.26-0.28% with the temperature rise from 293.15 to 323.15 K. A comparison between the experimental density values with results obtained using equation Eq. II.7 showed a good agreement. As expected and generally reported, the density of graphene nanofluids decreases with temperature and increase with graphene content.

### II.3.2.5. Surface tension

Surface tension is the tendency of liquid molecules to “stick” together at the surface [148]. It is a force that exists at any interface between two different media (between a solid or liquid and gas) [147]. Surface tension is expressed in N/m. It is very important, especially in industrial processes. The higher the surface tension, the better the adhesion of the applied substance to the material will be. As recently pointed by Estellé *et al.* [149], the surface tension of nanofluids plays an important role in many configurations and heat transfer processes. It was indicated also in this paper that, in most cases, a surface tension decrease leads to an increase in heat transfer properties. Concerning thermal applications, this property controls the formation and growth of bubbles, and thus plays an important role in systems involving boiling and condensation. It also plays an important role in microchannels. Thermal applications involving the effect of surface tension are described in Table II.5.

**Table II.5.** Thermal configurations and applications involving the influence of surface tension [149].

Type of heat and mass transfer application	Principal equations governing heat and mass transfer depending on surface tension	Parameter involving the surface tension	Surface tension influence
Boiling heat transfer	$Nu = \frac{h \cdot L}{k} = f \left[ \frac{\rho \cdot g \cdot (\rho_l - \rho_v) \cdot L^3}{\mu^2}; Bo = \frac{g \cdot (\rho_l - \rho_v) \cdot L^2}{\gamma}; Pr = \frac{\mu \cdot c_p}{k}; Ja = \frac{\Delta T \cdot c_p}{h_{fg}} \right]$ <p>Where Nusselt (Nu), Bond (Bo), Prandl (Pr) and Jacob (Ja) numbers depend on thermal conductivity (k), isobaric heat capacity (c<sub>p</sub>), excess temperature (ΔT), the characteristic length (L), density (ρ), surface tension (γ), viscosity</p>	Bond number (Bo) and heat transfer coefficient (h) [150]	Bo ↑ and h ↑ if ST ↓

## Chapter II - General information on graphene nanofluids

( $\mu$ ), latent heat of vaporization ( $h_{fg}$ ) and acceleration due to gravity ( $g$ ).  
Subscripts stand for vapor (v) and liquid (l).

Nucleate pool boiling, Critical heat flux	$q'' = \mu_l \cdot h_{fg} \cdot \left( \frac{g \cdot (\rho_l - \rho_v)}{\gamma} \right)^{1/2} \cdot \left( \frac{c_{p,l} \cdot \Delta T}{C_{s,f} \cdot h_{fg} \cdot Pr_l^n} \right)^3$	Critical heat flux for nucleate boiling ( $q''$ ) [151,152]	$q'' \uparrow$ if ST $\downarrow$
	Where n exponent and $C_{s,f}$ coefficient depend on the solid-liquid combination.		
	$q''_{max} = C \cdot h_{fg} \cdot \rho_v \cdot \left( \frac{\gamma \cdot g \cdot (\rho_l - \rho_v)}{\rho_v^2} \right)^{1/4}$		
	Where C is a constant depending on the geometry of the heated surface.		
External flow convection	Low velocity: $\frac{q''_{max}}{\rho_v \cdot h_{fg} \cdot V} = \frac{1}{\pi} \cdot \left( 1 + \left( \frac{4}{We_D} \right)^{1/3} \right)$	Weber number (We) and critical heat flux for external convection boiling ( $q''$ ) [153]	$We \uparrow$ and $q'' \downarrow$ if ST $\downarrow$
	High velocity: $\frac{q''_{max}}{\rho_v \cdot h_{fg} \cdot V} = \frac{(\rho_l / \rho_v)^{3/4}}{169 \cdot \pi} + \frac{(\rho_l / \rho_v)^{1/2}}{19.2 \cdot \pi \cdot We^{1/3}}$		
	Where $We = (\rho_v \cdot V^2 \cdot D) / \gamma$ is the Weber number, V is the velocity of the liquid and D is the diameter.		
Flow boiling in Microchannels	$Ca = \frac{\mu \cdot V}{\gamma}; K_2 = \left( \frac{q''}{h_{fg}} \right)^2 \cdot \frac{D}{\rho_v \cdot \gamma}$	capillary (Ca) Kandlikar number ( $K_2$ ) [154]	$Ca \uparrow$ if ST $\downarrow$
Heat pipes	$We_{critical} = \frac{\rho_v \cdot v^2 \cdot z}{2 \cdot \pi \cdot \sigma} = 10^{-1.163} \cdot N_{vi}^{-0.744} \cdot \left( \frac{\lambda_c}{d_1} \right)^{-0.509} \cdot \left( \frac{D_h}{d_2} \right)^{0.276}$	Weber number (We) [155]	$We \uparrow$ if ST $\downarrow$
	Where z is a dimension characterizing the vapor liquid surface, v is the vapor velocity, $N_{vi}$ is the dimensionless viscosity number, $d_1$ is the mesh wire spacing, $\lambda_c$ is the critical wavelength, $d_2$ is the thickness of the wire and $D_h$ is the equivalent diameter of the vapor space.		
Thermosiphons	$Ku = \frac{q_{co}}{(\Delta h_{lv} \cdot \rho_v^{0.5} \cdot (\sigma \cdot g \cdot (\rho_l - \rho_v)^{0.25}))}$	Kutateladze number (Ku) and maximum heat flux ( $q_{co}$ ) [156]	$Ku \uparrow, q_{co} \downarrow$ if ST $\downarrow$

The techniques generally used for measuring the surface tension of nanofluids, like for usual fluids, are shown in Figure II.23 [157].

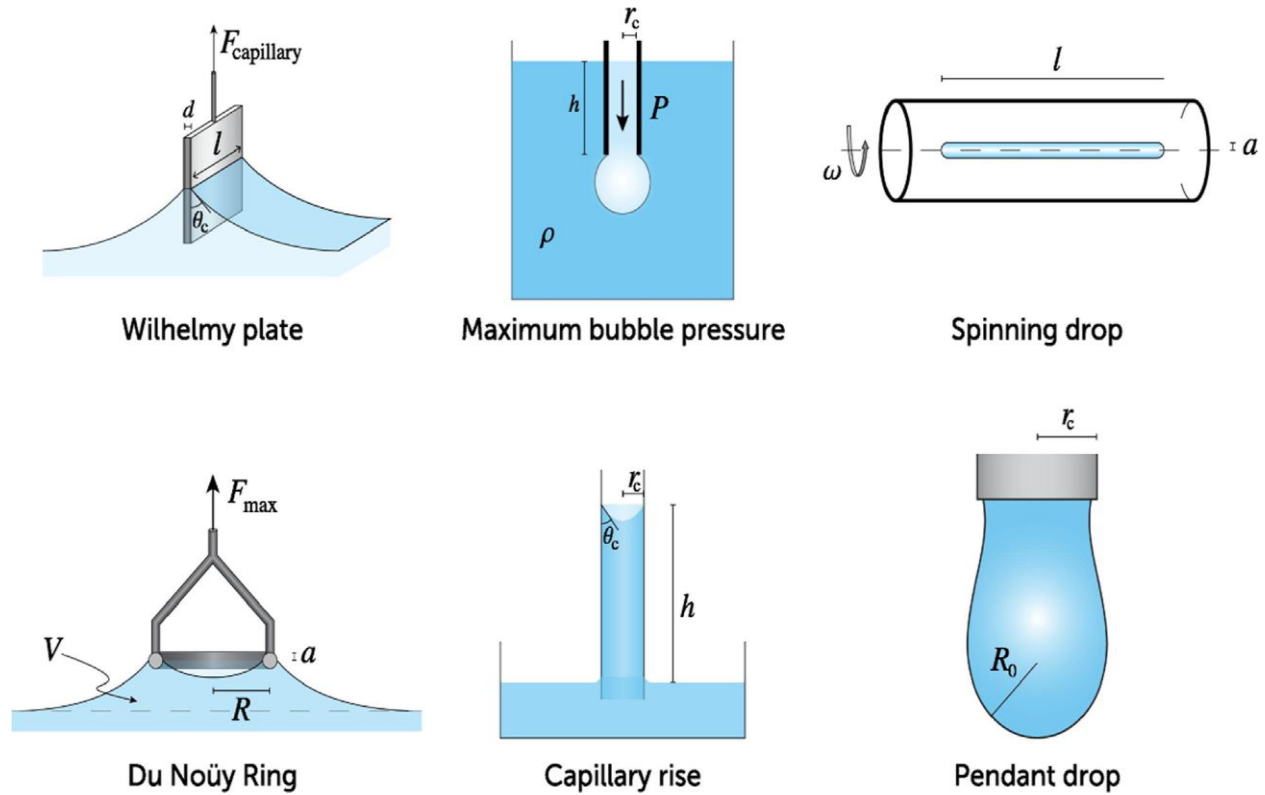


**Figure II.23.** Main techniques generally used for surface tension measurement of liquids and nanofluids, an excerpt from [149,157].

As for other thermophysical properties, ST of nanofluids is affected by various parameters such as surfactants, temperature, base fluid, nanoparticles nature, size, shape and volume fraction (Figure II.24). It generally decreases accordingly with the increase of surfactant concentration and temperature. Nevertheless, there have been some conflicting results on the volume fraction and surfactant effect and their coupled effect on the ST of nanofluids [158].

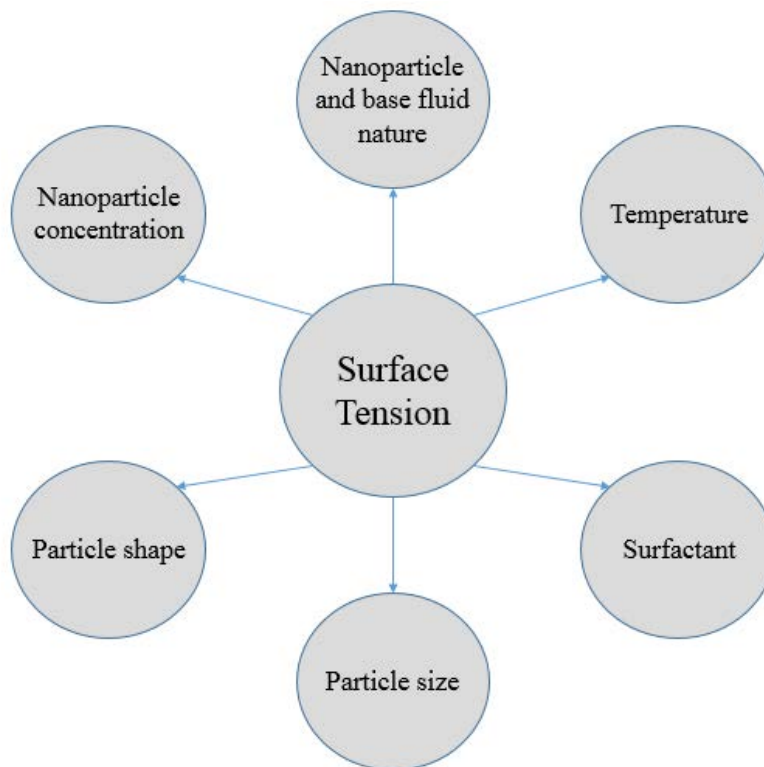


**Figure II.24.** Parameters that affect the surface tension of nanofluids [149].

Many researchers have focused on the investigation of thermophysical properties of nanofluids as thermal conductivity and rheology, but few of them paid attention to the surface tension of nanofluids [159]. Unfortunately, it is well-known that ideal pristine graphene is hydrophobic, so it tends to agglomerate in the presence of common solvents and particularly in the most widely used thermal medium which is water [160–162]. For this reason, the researchers try to decrease the hydrophobicity of this kind of nanoparticles by chemical treatments as covalent and non-covalent functionalization to render the material hydrophilic and even water-soluble.

In the literature, few data of surface tension of graphene-based nanofluids are available. The first study related to the surface tension of graphene-based nanofluid was reported by Zheng [163]. Authors worked on water-based graphene oxide nanofluids and obtained an increasing trend in ST with the increase of nanoparticle concentration, with a maximum enhancement of about 3% (in comparison to water) for the highest concentration, 0.1 wt.%. The results also showed a decreasing in ST with the rise of temperature from 293.15 to 333.15 K and with reducing the nanoparticle size, noting that by the presence of nanoparticles, the reduction rate of ST with temperature was

lowered. Later, the ST of reduced graphene oxide (rGO)/water nanofluids were studied by Kamatchi *et al.* [164] without using any surfactant considering the nanoparticle concentration (0.01, 0.1 and 0.3 g/l) and the temperature effect (in the range 308.15-348.15 K). The results showed a decrease in ST values with the rise of temperature and an increase with the nanoparticle loading. This increase was attributed to the displacement and accumulation of rGO nanosheets at the liquid-gas interface which increases the surface energy. On the other hand, Ahammed *et al.* [165] recently investigated graphene nanofluids based on water. The authors dispersed commercial graphene (with layers 1-5 nm thickness) in water with the use of 5% of sodium dodecylbenzene sulfonate (SDBS) as a surfactant to obtain nanofluids in the volume concentration range 0.05-0.15 %. The ST measurements were done at temperatures between 10 and 90 °C. The results showed a decrease in ST of nanofluids with nanoparticle concentration and with the temperature rise (3.3% for each 10 °C). These findings were explained by the reduction of the molecular attraction between nanoparticles and fluid molecules, as graphene is hydrophobic, by the enhancement of the absorption of nanoparticles at liquid-gas interface, respectively. Lastly, Cabaleiro *et al.* [160] focused on the effect of graphene functionalization and nanoparticle loading on surface tension of graphene aqueous nanofluids. They worked with GO and two different rGO at different nanoparticle volume fractions between 0.0005% and 0.1%. The ST measurements were done at room temperature. The results showed a decreasing in ST with the increase of graphene content with a maximum reduction of about 3% for the highest concentration. However, the chemical reduction had no clear effect on ST of nanofluids.

So from all these investigations on the surface tension of different graphene-based nanofluids, one can notice that this property doesn't change in the same way with the addition of graphene nanoparticles into the fluid and also depends on surfactant presence. That is why a full analysis of the effect of graphene on the surface tension of the fluids is needed, due to its involvement in some heat transfer processes.

### **II.3.3- Heat transfer performance**

Nanofluids seem attractive if we consider their remarkable thermal properties alone. However, one important point needs to be discussed in view of their industrial applications. The addition of nanoparticles can improve the thermal performance of the nanofluid, but this can lead to an unfavorable increase in hydrodynamic properties as shown in previous sections.

Generally speaking, two approaches (qualitative and quantitative) are used in the literature to assess the real gains from the use of nanofluids.

### II.3.3.1. Qualitative approach

It is based on an analysis of the thermophysical properties of the nanofluid and makes it possible, at first sight, and without performing an experiment, to evaluate the limits of the use of nanofluids according to the flow regime [166,167]. However, this approach does not take into account the real flow condition that could lead to possible rearrangement of flowing nanoparticles, change in stability, ....

#### a) *Laminar regime*

As mentioned earlier, the addition of nanoparticles leads to an increase in thermal conductivity and dynamic viscosity. Beyond the relations previously described, this change with nanoparticle content can be simply modelled at first sight by a linear evolution of the relative thermal conductivity (Eq.II.8) and the relative dynamic viscosity (Eq.II.9) as a function of the volume fraction of nanoparticles [166–168]. These empirical models are valid regardless of the shape, size and dispersion state of the nanoparticles in the base fluid [166,167].

$$\frac{k_{nf}}{k_{bf}} \approx 1 + C_k \phi_v \quad \text{Eq.II.8}$$

$$\frac{\eta_{nf}}{\eta_{bf}} \approx 1 + C_\eta \phi_v \quad \text{Eq.II.9}$$

where  $C_k$  and  $C_\eta$  are respectively the coefficient of thermal conductivity improvement and the coefficient of the dynamic viscosity improvement of the nanofluid.

According to the results of the literature, under steady-state laminar flow conditions, the use of nanofluids is favorable if the condition of Eq.II.10 is verified [166,167]:

$$\frac{C_\eta}{C_k} < 4 \quad \text{Eq.II.10}$$

**b) Turbulent regime**

In turbulent operation, the rate of heat transfer depends not only on the thermal conductivity and dynamic viscosity but also on the isobaric heat capacity and density of the fluid [169]. In order to evaluate the benefits of using nanofluids in turbulent conditions, a factor of merit (FOM) was used, called the Mouromsteff number, defined by Dittus–Boelter equation [170] (Eq.II.11) for base fluids [171,172] and Pak and Cho equation [173] (Eq.II.12) for nanofluids [171,174].

$$Mo_{bf} = \frac{\rho^{0.8} k^{0.6} C_p^{0.4}}{\eta^{0.4}} \quad \text{Eq.II.11}$$

$$Mo_{nf} = \frac{\rho^{0.8} k^{0.5} C_p^{0.5}}{\eta^{0.3}} \quad \text{Eq.II.12}$$

The nanofluid is considered advantageous compared to the base fluid if Eq.II.13 is verified [167,175].

$$\frac{Mo_{nf}}{Mo_{bf}} > 1 \quad \text{Eq.II.13}$$

This first approach does not allow a real evaluation of the benefits provided by nanofluids, but it can be used as a preliminary step to predict experimental conditions and particle concentrations that would tend towards a favorable energy balance [175].

### II.3.3.2. Quantitative approach

This approach, which is used in most cases, makes it possible to evaluate, under real flow conditions, the thermal properties (coefficient of convective exchange) and hydrodynamics (pressure losses) in a fluidic loop, especially in a heat exchanger.

Heat exchangers can be classified according to different criteria. Some of the most known classifications are based on the transfer contact type (direct or indirect contact), the heat transfer mechanism (single-phase convection or two-phase convection [condensers, evaporators]), the arrangement of the flows (co-current, counter-current or cross-flow), the phase of the fluids involved (liquid-liquid, gas-liquid or gas-gas) or the arrangement of the passages (single passage

or multiple passages) [176]. Depending on their construction characteristics, they can be classified into tubular, plate, extended surface and regenerators, as shown in Figure II.25.

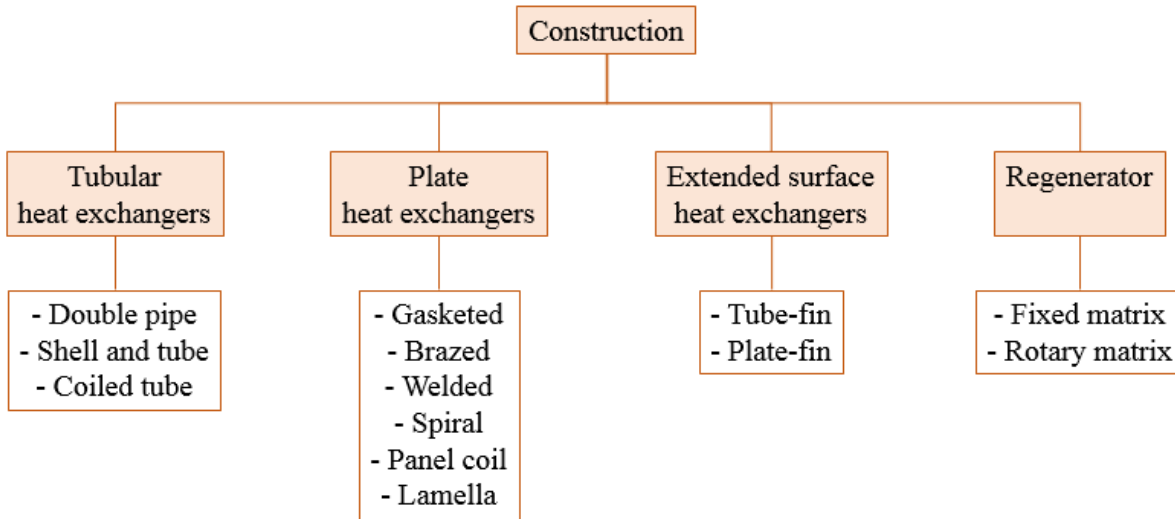


**Figure II.25.** Classification of heat exchangers according to their construction characteristics [79,176].

Double tube heat exchangers (also known as concentric tube/pipe, double pipe, pipe-in-pipe or tube-in-tube heat exchangers) are the simplest type but are commonly used in a variety of industries [177]. Their efficiency is not as high as that of other types of exchangers, but their instrumentation, ease of use and study makes them suitable for experimental evaluation in the area of research.

The heat transfer occurring between a fluid and the surface over which it flows, by convection, is quantitatively characterized by the convective heat transfer coefficient ( $h$ ) [178]. This coefficient is related to the difference between the temperature of the fluid and the temperature of the surface or wall ( $T_f - T_w$ ), the heat power ( $\dot{Q}$ ), and the surface ( $A$ ) (or heat flux,  $\dot{Q}/A$ ) [178,179] according to the expression  $\dot{Q} = h A.(T_f - T_w)$ . The convective heat transfer coefficient depends on the temperature, flow characteristics and thermophysical properties of the fluid [178].

In a heat exchanger, the pressure drop ( $\Delta P$ ) is defined as the difference between the inlet pressure and the outlet pressure of a fluid. The drop is proportional to the required pumping power, and is

a consequence of the fluid friction through the path of the flow, among other possible causes [180]. It is directly related to the size, economic costs, heat transfer, and morphology of the heat exchanger as well as the properties of the fluid [180].

Convection heat transfer coefficient and pressure drop for a fluid that flows in a heat exchanger are suitable for comparing the thermal behavior of different samples. These parameters are not fully exportable to other applications because of their dependence on dimensional and geometrical characteristics. Thus, dimensionless analysis becomes appropriate to show a larger general point of view and find correlations to predict the sample behavior in any condition, for example, those for water of Gnielinski [181], Dittus-Boelter [182] or Petukhov [183].

The most known dimensionless numbers used in heat transfer are presented in Table II.6.

**Table II.6.** Heat transfer dimensionless numbers and the corresponding equations [79].

Dimensionless number	Equation	Definition of involved parameters
Reynolds number (Re)	$Re = \frac{\text{Inertial forces}}{\text{Viscous forces}} = \frac{m \cdot a}{\eta \cdot \frac{v}{L} \cdot A} = \frac{\rho \cdot v \cdot L}{\eta}$	m = mass; a = acceleration; $\eta$ = dynamic viscosity; v = velocity; L = characteristic length; A = area; $\rho$ = density
Nusselt number (Nu)	$Nu = \frac{\text{Convective heat transfer}}{\text{Conductive heat transfer}} = \frac{h}{\frac{k}{L}} = \frac{h \cdot L}{k}$	h = convection coefficient; L = characteristic length; k = thermal conductivity
Prandtl number (Pr)	$Pr = \frac{\text{Viscous diffusion rate}}{\text{Thermal diffusion rate}} = \frac{\frac{\eta}{\rho}}{\frac{k}{\rho \cdot C_p}} = \frac{C_p \cdot \eta}{k}$	$\eta$ = dynamic viscosity; $\rho$ = density; k = thermal conductivity; $C_p$ = isobaric specific heat capacity
Peclet number (Pe)	$Pe = \frac{\text{Advective heat rate}}{\text{Diffusive heat rate}} = \frac{L \cdot v}{\frac{k}{C_p \cdot \rho}} = \frac{L \cdot v}{k} \cdot \frac{C_p \cdot \rho}{1}$ Re.Pr	L = characteristic length; v = velocity; k = thermal conductivity; $C_p$ = isobaric specific heat capacity; $\rho$ = density

For example, Yarmand *et al.* [184] investigated graphene nanoplatelets-silver hybrid nanofluids based on distilled water with weight concentrations up to 0.1%. The results showed an improvement in heat transfer. A maximum enhancement of 32.7% was found in Nusselt number for the highest concentration at a Reynolds number of 17500 compared to the base fluid.

On the other hand, graphene nanoplatelet aqueous nanofluids were studied by Mehrali *et al.* [130]. The prepared nanofluids were in the range of concentration 0.025-0.1% in weight. The authors found that the convective heat transfer coefficient of the nanofluids is higher than the distilled

water by around 83-200%. Also, the heat transfer coefficient of nanofluids increased with the increase of specific surface area and flow rate. However, an increase in the pressure drop was obtained simultaneously in the range of 0.06-14.7%.

Finally, Zubir *et al.* [185] worked on 0.05wt.% of reduced graphene oxide-based nanofluid, where the nanoparticles were synthesized using a reduction process of chemically exfoliated graphene oxide with the use of Tannic Acid as reductant. The authors found an enhancement in thermal conductivity as well as in the convective heat transfer coefficient, and enhancement of 144% in Nusselt number was obtained.

So all these experimental works have shown that graphene-based nanofluids used in different heat exchangers show a good thermal performance, which means that the use of graphene nanofluids in the domain of heat transfer is very useful and help to make an energy transition.

## **II.4- Conclusion**

In this chapter, we have first given a general description of graphene-based nanofluids, from the synthesis and characterization of graphene to the structure and stability evaluation of these nanofluids. A bibliographical synthesis of their thermophysical properties and their thermal and hydrodynamic performances was then carried out. Thus, we showed through an analysis of previous works that the results strongly depend on many parameters such as graphene structure and quality, and highlighted the factors that influence the thermal, rheological and hydrodynamic properties of these materials.

Consequently, it is necessary to rigorously evaluate the thermophysical properties of graphene-based nanofluids in order to study and better understand their flow behavior and thermal properties in view of possible application in thermal systems.

This step requires first the production of graphene with high structural quality and its dispersion in the base fluid. How is it achieved is the aim of the next chapter. In addition, the various experimental devices and methods used to characterize the graphene nanosheets and the thermophysical properties of graphene nanofluids (thermal conductivity, dynamic viscosity, specific heat capacity, density, surface tension) are also presented.

## II.5- References

1. R.L. Vander Wal, S.D. Mozes, V. Pushkarev, Nanocarbon nanofluids: morphology and nanostructure comparisons, *Nanotechnology*, 20 (2009) 105702.
2. Arshad, A.; Jabbal, M.; Yan, Y.; Reay, D. A review on graphene based nanofluids: Preparation, characterization and applications. *Journal of Molecular Liquids* **2019**, 279, 444–484, doi:10.1016/j.molliq.2019.01.153.
3. Gupta, M.; Singh, V.; Kumar, R.; Said, Z. A review on thermophysical properties of nanofluids and heat transfer applications. *Renewable and Sustainable Energy Reviews* **2017**, 74, 638–670, doi:10.1016/j.rser.2017.02.073.
4. Suganthi, K.S.; Rajan, K.S. Metal oxide nanofluids: Review of formulation, thermo-physical properties, mechanisms, and heat transfer performance. *Renewable and Sustainable Energy Reviews* **2017**, 76, 226–255, doi:10.1016/j.rser.2017.03.043.
5. Tawfik, M.M. Experimental studies of nanofluid thermal conductivity enhancement and applications: A review. *Renewable and Sustainable Energy Reviews* **2017**, 75, 1239–1253, doi:10.1016/j.rser.2016.11.111.
6. Choi, T.J.; Subedi, B.; Ham, H.J.; Park, M.S.; Jang, S.P. A review of the internal forced convective heat transfer characteristics of nanofluids: Experimental features, mechanisms and thermal performance criteria. *Journal of Mechanical Science and Technology* **2018**, 32, 3491–3505, doi:10.1007/s12206-018-0701-z.
7. Elochukwu, C.U. Electrochemically reduced Water: A Crucial Nutrient for Life. *International journal of Horticulture, Agriculture and Food science* **2018**, 2, 28–31, doi:10.22161/ijhaf.2.1.3.
8. J.M. Chesworth, T. Stuchbury, J.R. Scaife, An introduction to agricultural biochemistry, Springer Science & Business Media, 2012.
9. Ludwig, R. Water: From Clusters to the Bulk. *Angewandte Chemie International Edition* **2001**, 40, 1808–1827, doi:10.1002/1521-3773(20010518)40:10<1808::AID-ANIE1808>3.0.CO;2-1.
10. ASHRAE Handbook Fundamentals, Physical Properties of Secondary Coolants, Atlanta, (2009).
11. E.W. Lemmon, M.L. Huber, M.O. McLinden, REFPROP - Reference Fluid Thermodynamic and Transport Properties, Version 8.0, in, NIST Standard Reference Database 23, 2002.
12. Cortright, R.D.; Sanchez-Castillo, M.; Dumesic, J.A. Conversion of biomass to 1,2-propanediol by selective catalytic hydrogenation of lactic acid over silica-supported copper. *Applied Catalysis B: Environmental* **2002**, 39, 353–359, doi:10.1016/S0926-3373(02)00121-2.
13. European Commission, Proposal for a Directive of the European Parliament and of the Council on the promotion of the use of energy from renewable sources (recast) COM/2016/0767 final/2 - 2016/0382 (COD), in, Brussels, 2016.
14. Bang, I.C.; Heung Chang, S. Boiling heat transfer performance and phenomena of Al<sub>2</sub>O<sub>3</sub>-water nano-fluids from a plain surface in a pool. *International Journal of Heat and Mass Transfer* **2005**, 48, 2407–2419, doi:10.1016/j.ijheatmasstransfer.2004.12.047.
15. Berrada, N.; Hamze, S.; Desforges, A.; Ghanbaja, J.; Gleize, J.; Maré, T.; Vigolo, B.; Estellé, P. Surface tension of functionalized MWCNT-based nanofluids in water and

- commercial propylene-glycol mixture. *Journal of Molecular Liquids* **2019**, *293*, 111473, doi:10.1016/j.molliq.2019.111473.
16. Geim, A.K.; Novoselov, K.S. The rise of graphene. In *Nanoscience and Technology*; Co-Published with Macmillan Publishers Ltd, UK, 2009; pp. 11–19 ISBN 978-981-4282-68-0.
  17. Gómez-Navarro, C.; Burghard, M.; Kern, K. Elastic Properties of Chemically Derived Single Graphene Sheets. *Nano Letters* **2008**, *8*, 2045–2049, doi:10.1021/nl801384y.
  18. Balandin, A.A.; Ghosh, S.; Bao, W.; Calizo, I.; Teweldebrhan, D.; Miao, F.; Lau, C.N. Superior Thermal Conductivity of Single-Layer Graphene. *Nano Letters* **2008**, *8*, 902–907, doi:10.1021/nl0731872.
  19. Stoller, M.D.; Park, S.; Zhu, Y.; An, J.; Ruoff, R.S. Graphene-Based Ultracapacitors. *Nano Letters* **2008**, *8*, 3498–3502, doi:10.1021/nl802558y.
  20. Bunch, J.S.; Verbridge, S.S.; Alden, J.S.; van der Zande, A.M.; Parpia, J.M.; Craighead, H.G.; McEuen, P.L. Impermeable Atomic Membranes from Graphene Sheets. *Nano Letters* **2008**, *8*, 2458–2462, doi:10.1021/nl801457b.
  21. Bolotin, K.I.; Sikes, K.J.; Jiang, Z.; Klima, M.; Fudenberg, G.; Hone, J.; Kim, P.; Stormer, H.L. Ultrahigh electron mobility in suspended graphene. *Solid State Communications* **2008**, *146*, 351–355, doi:10.1016/j.ssc.2008.02.024.
  22. Bourourou M. Conception des bioélectrodes enzymatiques à base de nanomatériaux dans des piles à combustible et des capteurs, Université de Grenoble, 2015.
  23. Agromayor, R.; Cabaleiro, D.; Pardinias, A.; Vallejo, J.; Fernandez-Seara, J.; Lugo, L. Heat Transfer Performance of Functionalized Graphene Nanoplatelet Aqueous Nanofluids. *Materials* **2016**, *9*, 455, doi:10.3390/ma9060455.
  24. Papageorgiou, D.G.; Kinloch, I.A.; Young, R.J. Mechanical properties of graphene and graphene-based nanocomposites. *Progress in Materials Science* **2017**, *90*, 75–127, doi:10.1016/j.pmatsci.2017.07.004.
  25. Zhang, T.; Xue, Q.; Zhang, S.; Dong, M. Theoretical approaches to graphene and graphene-based materials. *Nano Today* **2012**, *7*, 180–200, doi:10.1016/j.nantod.2012.04.006.
  26. Phitsini Suvarnaphaet; Suejit Pechprasarn Graphene-Based Materials for Biosensors: A Review. *Sensors* **2017**, *17*, 2161, doi:10.3390/s17102161.
  27. Hummers, W.S.; Offeman, R.E. Preparation of Graphitic Oxide. *Journal of the American Chemical Society* **1958**, *80*, 1339–1339, doi:10.1021/ja01539a017.
  28. Ozhukil Valappil, M.; K. Pillai, V.; Alwarappan, S. Spotlighting graphene quantum dots and beyond: Synthesis, properties and sensing applications. *Applied Materials Today* **2017**, *9*, 350–371, doi:10.1016/j.apmt.2017.09.002.
  29. Wick, P.; Louw-Gaume, A.E.; Kucki, M.; Krug, H.F.; Kostarelos, K.; Fadeel, B.; Dawson, K.A.; Salvati, A.; Vázquez, E.; Ballerini, L.; et al. Classification Framework for Graphene-Based Materials. *Angewandte Chemie International Edition* **2014**, *53*, 7714–7718, doi:10.1002/anie.201403335.
  30. HAAR S. Supramolecular approaches to graphene: generation of functional hybrid assemblies, Université de Strasbourg, 2015.
  31. Vaari, J.; Lahtinen, J.; Hautojärvi, P. The adsorption and decomposition of acetylene on clean and K-covered Co(0001). *Catalysis Letters* **1997**, *44*, 43–49, doi:10.1023/A:1018972924563.
  32. Ueta, H.; Saida, M.; Nakai, C.; Yamada, Y.; Sasaki, M.; Yamamoto, S. Highly oriented monolayer graphite formation on Pt(111) by a supersonic methane beam. *Surface Science* **2004**, *560*, 183–190, doi:10.1016/j.susc.2004.04.039.

33. Eizenberg, M.; Blakely, J.M. Carbon monolayer phase condensation on Ni(111). *Surface Science* **1979**, *82*, 228–236, doi:10.1016/0039-6028(79)90330-3.
34. Li, X.; Cai, W.; An, J.; Kim, S.; Nah, J.; Yang, D.; Piner, R.; Velamakanni, A.; Jung, I.; Tutuc, E.; et al. Large-Area Synthesis of High-Quality and Uniform Graphene Films on Copper Foils. *Science* **2009**, *324*, 1312–1314, doi:10.1126/science.1171245.
35. Hernandez, Y.; Nicolosi, V.; Lotya, M.; Blighe, F.M.; Sun, Z.; De, S.; McGovern, I.T.; Holland, B.; Byrne, M.; Gun'Ko, Y.K.; et al. High-yield production of graphene by liquid-phase exfoliation of graphite. *Nature Nanotechnology* **2008**, *3*, 563–568, doi:10.1038/nnano.2008.215.
36. Ciesielski, A.; Samori, P. Grapheneviasonication assisted liquid-phase exfoliation. *Chem. Soc. Rev.* **2014**, *43*, 381–398, doi:10.1039/C3CS60217F.
37. Hamilton, C.E.; Lomeda, J.R.; Sun, Z.; Tour, J.M.; Barron, A.R. High-Yield Organic Dispersions of Unfunctionalized Graphene. *Nano Letters* **2009**, *9*, 3460–3462, doi:10.1021/nl9016623.
38. Economopoulos, S.P.; Rotas, G.; Miyata, Y.; Shinohara, H.; Tagmatarchis, N. Exfoliation and Chemical Modification Using Microwave Irradiation Affording Highly Functionalized Graphene. *ACS Nano* **2010**, *4*, 7499–7507, doi:10.1021/nn101735e.
39. Khan, U.; May, P.; O'Neill, A.; Coleman, J.N. Development of stiff, strong, yet tough composites by the addition of solvent exfoliated graphene to polyurethane. *Carbon* **2010**, *48*, 4035–4041, doi:10.1016/j.carbon.2010.07.008.
40. Khan, U.; O'Neill, A.; Lotya, M.; De, S.; Coleman, J.N. High-Concentration Solvent Exfoliation of Graphene. *Small* **2010**, *6*, 864–871, doi:10.1002/sml.200902066.
41. Lotya, M.; King, P.J.; Khan, U.; De, S.; Coleman, J.N. High-Concentration, Surfactant-Stabilized Graphene Dispersions. *ACS Nano* **2010**, *4*, 3155–3162, doi:10.1021/nn1005304.
42. Lotya, M.; Hernandez, Y.; King, P.J.; Smith, R.J.; Nicolosi, V.; Karlsson, L.S.; Blighe, F.M.; De, S.; Wang, Z.; McGovern, I.T.; et al. Liquid Phase Production of Graphene by Exfoliation of Graphite in Surfactant/Water Solutions. *Journal of the American Chemical Society* **2009**, *131*, 3611–3620, doi:10.1021/ja807449u.
43. Smith, R.J.; Lotya, M.; Coleman, J.N. The importance of repulsive potential barriers for the dispersion of graphene using surfactants. *New Journal of Physics* **2010**, *12*, 125008, doi:10.1088/1367-2630/12/12/125008.
44. Bepete, G.; Anglaret, E.; Ortolani, L.; Morandi, V.; Huang, K.; Pénicaud, A.; Drummond, C. Surfactant-free single-layer graphene in water. *Nature Chemistry* **2017**, *9*, 347–352, doi:10.1038/nchem.2669.
45. Liu, N.; Luo, F.; Wu, H.; Liu, Y.; Zhang, C.; Chen, J. One-Step Ionic-Liquid-Assisted Electrochemical Synthesis of Ionic-Liquid-Functionalized Graphene Sheets Directly from Graphite: Ionic-Liquid-Assisted Electrochemical Synthesis of Graphene. *Advanced Functional Materials* **2008**, *18*, 1518–1525, doi:10.1002/adfm.200700797.
46. El Achaby M. Nanocomposites graphène-polymère thermoplastique: Fabrication et étude des propriétés structurales, thermiques, rhéologiques et mécaniques, Université Mohammed V-AGDAL, 2012.
47. Stankovich, S.; Dikin, D.A.; Piner, R.D.; Kohlhaas, K.A.; Kleinhammes, A.; Jia, Y.; Wu, Y.; Nguyen, S.T.; Ruoff, R.S. Synthesis of graphene-based nanosheets via chemical reduction of exfoliated graphite oxide. *Carbon* **2007**, *45*, 1558–1565, doi:10.1016/j.carbon.2007.02.034.

48. Lomeda, J.R.; Doyle, C.D.; Kosynkin, D.V.; Hwang, W.-F.; Tour, J.M. Diazonium Functionalization of Surfactant-Wrapped Chemically Converted Graphene Sheets. *Journal of the American Chemical Society* **2008**, *130*, 16201–16206, doi:10.1021/ja806499w.
49. Wang, H.; Robinson, J.T.; Li, X.; Dai, H. Solvothermal Reduction of Chemically Exfoliated Graphene Sheets. *Journal of the American Chemical Society* **2009**, *131*, 9910–9911, doi:10.1021/ja904251p.
50. Stankovich, S.; Dikin, D.A.; Dommett, G.H.B.; Kohlhaas, K.M.; Zimney, E.J.; Stach, E.A.; Piner, R.D.; Nguyen, S.T.; Ruoff, R.S. Graphene-based composite materials. *Nature* **2006**, *442*, 282–286, doi:10.1038/nature04969.
51. Si, Y.; Samulski, E.T. Synthesis of Water Soluble Graphene. *Nano Letters* **2008**, *8*, 1679–1682, doi:10.1021/nl080604h.
52. Wang, G.; Yang, J.; Park, J.; Gou, X.; Wang, B.; Liu, H.; Yao, J. Facile Synthesis and Characterization of Graphene Nanosheets. *The Journal of Physical Chemistry C* **2008**, *112*, 8192–8195, doi:10.1021/jp710931h.
53. Williams, G.; Seger, B.; Kamat, P.V. TiO<sub>2</sub> -Graphene Nanocomposites. UV-Assisted Photocatalytic Reduction of Graphene Oxide. *ACS Nano* **2008**, *2*, 1487–1491, doi:10.1021/nl800251f.
54. Chen, W.; Yan, L.; Bangal, P.R. Chemical Reduction of Graphene Oxide to Graphene by Sulfur-Containing Compounds. *The Journal of Physical Chemistry C* **2010**, *114*, 19885–19890, doi:10.1021/jp107131v.
55. Fernández-Merino, M.J.; Guardia, L.; Paredes, J.I.; Villar-Rodil, S.; Solís-Fernández, P.; Martínez-Alonso, A.; Tascón, J.M.D. Vitamin C Is an Ideal Substitute for Hydrazine in the Reduction of Graphene Oxide Suspensions. *The Journal of Physical Chemistry C* **2010**, *114*, 6426–6432, doi:10.1021/jp100603h.
56. Fan, Z.-J.; Kai, W.; Yan, J.; Wei, T.; Zhi, L.-J.; Feng, J.; Ren, Y.; Song, L.-P.; Wei, F. Facile Synthesis of Graphene Nanosheets via Fe Reduction of Exfoliated Graphite Oxide. *ACS Nano* **2011**, *5*, 191–198, doi:10.1021/nl102339t.
57. Fan, X.; Peng, W.; Li, Y.; Li, X.; Wang, S.; Zhang, G.; Zhang, F. Deoxygenation of Exfoliated Graphite Oxide under Alkaline Conditions: A Green Route to Graphene Preparation. *Advanced Materials* **2008**, *20*, 4490–4493, doi:10.1002/adma.200801306.
58. Tour, J.M. Top-Down versus Bottom-Up Fabrication of Graphene-Based Electronics. *Chemistry of Materials* **2014**, *26*, 163–171, doi:10.1021/cm402179h.
59. Raccichini, R.; Varzi, A.; Passerini, S.; Scrosati, B. The role of graphene for electrochemical energy storage. *Nature Materials* **2015**, *14*, 271–279, doi:10.1038/nmat4170.
60. N. Berrada De l'interêt du dichlore pour une élimination hautement sélective des impuretés métalliques et carbonées des nanotubes de carbone, Université de Lorraine, 2019.
61. Titus, D.; James Jebaseelan Samuel, E.; Roopan, S.M. Nanoparticle characterization techniques. In *Green Synthesis, Characterization and Applications of Nanoparticles*; Elsevier, 2019; pp. 303–319 ISBN 978-0-08-102579-6.
62. N'DIAYE J. A. Synthèse et application du graphène en tant que mousse absorbante de contaminants en milieu aqueux et ainsi qu'électrode pour la détection électrochimique du peroxyde d'hydrogène, Université de Québec à Montréal, 2016.
63. Reza Sadrolhosseini, A.; Adzir Mahdi, M.; Alizadeh, F.; Abdul Rashid, S. Laser Ablation Technique for Synthesis of Metal Nanoparticle in Liquid. In *Laser Technology and its Applications*; Ma, Y., Ed.; IntechOpen, 2019 ISBN 978-1-78984-917-2.

64. S. Mukherjee, S. Paria, Preparation and stability of nanofluids-a review, *IOSR-JMCE*, 9 (2013) 63-69.
65. Yang, L.; Hu, Y. Toward TiO<sub>2</sub> Nanofluids—Part 1: Preparation and Properties. *Nanoscale Research Letters* **2017**, 12, doi:10.1186/s11671-017-2184-8.
66. Khodja M. Les fluides de forage: Etude des performances et considérations environnementales, INSA Toulouse, 2008.
67. Li, X.; Zhu, D.; Wang, X. Evaluation on dispersion behavior of the aqueous copper nano-suspensions. *Journal of Colloid and Interface Science* **2007**, 310, 456–463, doi:10.1016/j.jcis.2007.02.067.
68. Wei, X.; Wang, L. Synthesis and thermal conductivity of microfluidic copper nanofluids. *Particuology* **2010**, 8, 262–271, doi:10.1016/j.partic.2010.03.001.
69. Teissier A. Synthèse de matériaux à base de pentoxyde de niobium et de nanotubes de carbone pour la limitation optique dans l'infrarouge, Université de Strasbourg, 2009.
70. Halelfadl S. Caractérisation des propriétés thermo-physiques et d'échanges de chaleur des nanofluides à base de nanotubes de carbone, INSA Rennes, 2014.
71. Natarajan, E.; Sathish, R. Role of nanofluids in solar water heater. *Int J Adv Manuf Technol* **2009**, doi:10.1007/s00170-008-1876-8.
72. Wu D., Zhu H., Wang L., Liua L., Critical issues in nanofluids preparation, characterization and thermal conductivity, *Curr. Nanosci.*, 5 (2009) 103–112.
73. M.J. Kass, The End of the Road for Gas-Powered Automobiles?, *Nat. Resour. Environ.*, 32 (2018) 53-54.
74. B. Voigtländer, Scanning Probe Microscopy. Atomic Force Microscopy and Scanning Tunneling Microscopy, Springer, Berlin, Germany, 2016.
75. S.U.S. Choi, J.A. Eastman, Enhancing thermal conductivity of fluids with nanoparticles, International Mechanical Engineering Congress and Exhibition, Argonne National Lab, USA 1995, pp. 99–105.
76. Zoundi, Z. CO<sub>2</sub> emissions, renewable energy and the Environmental Kuznets Curve, a panel cointegration approach. *Renewable and Sustainable Energy Reviews* **2017**, 72, 1067–1075, doi:10.1016/j.rser.2016.10.018.
77. Vallejo, J.P.; Gómez-Barreiro, S.; Cabaleiro, D.; Gracia-Fernández, C.; Fernández-Seara, J.; Lugo, L. Flow behaviour of suspensions of functionalized graphene nanoplatelets in propylene glycol–water mixtures. *International Communications in Heat and Mass Transfer* **2018**, 91, 150–157, doi:10.1016/j.icheatmasstransfer.2017.12.001.
78. Timofeeva, E.V.; Yu, W.; France, D.M.; Singh, D.; Routbort, J.L. Nanofluids for heat transfer: an engineering approach. *Nanoscale Res Lett* **2011**, 6, 182, doi:10.1186/1556-276X-6-182.
79. Vallejo J. P. Design, characterization and heat transfer performance evaluation of carbon-based nanofluids for renewable energy applications, Universida de Vigo, 2019.
80. Phuoc, T.X.; Massoudi, M.; Chen, R.-H. Viscosity and thermal conductivity of nanofluids containing multi-walled carbon nanotubes stabilized by chitosan. *International Journal of Thermal Sciences* **2011**, 50, 12–18, doi:10.1016/j.ijthermalsci.2010.09.008.
81. A. Bejan, A.D. Kraus, Heat transfer handbook, John Wiley & Sons, Hoboken, NJ, USA, 2003.
82. R. Davis, The effective thermal conductivity of a composite material with spherical inclusions, *Int. J. Thermophys.* 7 (3) (1986) 609–620.

83. Subramanian, K.R.V.; Rao, T.N.; Balakrishnan, A. *Nanofluids and their engineering applications*; 2020; ISBN 978-0-429-46822-3.
84. Hamilton, R.L.; Crosser, O.K. Thermal Conductivity of Heterogeneous Two-Component Systems. *Ind. Eng. Chem. Fund.* **1962**, *1*, 187–191, doi:10.1021/i160003a005.
85. Hasselman, D.P.H.; Johnson, L.F. Effective Thermal Conductivity of Composites with Interfacial Thermal Barrier Resistance. *Journal of Composite Materials* **1987**, *21*, 508–515, doi:10.1177/002199838702100602.
86. Nan, C.-W.; Birringer, R.; Clarke, D.R.; Gleiter, H. Effective thermal conductivity of particulate composites with interfacial thermal resistance. *Journal of Applied Physics* **1997**, *81*, 6692–6699, doi:10.1063/1.365209.
87. Wang, Z.; Wu, Z.; Han, F.; Wadsö, L.; Sundén, B. Experimental comparative evaluation of a graphene nanofluid coolant in miniature plate heat exchanger. *International Journal of Thermal Sciences* **2018**, *130*, 148–156, doi:10.1016/j.ijthermalsci.2018.04.021.
88. O. Wiener, Der Abhandlungen der Mathematisch-Physischen Klasse der Konigl, Sachsischen Gesellschaft der Wissenschaften 32 (1912) 509–604.
89. Yu, W.; Xie, H.; Wang, X.; Wang, X. Significant thermal conductivity enhancement for nanofluids containing graphene nanosheets. *Physics Letters A* **2011**, *375*, 1323–1328, doi:10.1016/j.physleta.2011.01.040.
90. khosrojerdi, S.; Vakili, M.; Yahyaei, M.; Kalhor, K. Thermal conductivity modeling of graphene nanoplatelets/deionized water nanofluid by MLP neural network and theoretical modeling using experimental results. *International Communications in Heat and Mass Transfer* **2016**, *74*, 11–17, doi:10.1016/j.icheatmasstransfer.2016.03.010.
91. Kole, M.; Dey, T.K. Investigation of thermal conductivity, viscosity, and electrical conductivity of graphene based nanofluids. *Journal of Applied Physics* **2013**, *113*, 084307, doi:10.1063/1.4793581.
92. Hadadian, M.; Goharshadi, E.K.; Youssefi, A. Electrical conductivity, thermal conductivity, and rheological properties of graphene oxide-based nanofluids. *J Nanopart Res* **2014**, *16*, 2788, doi:10.1007/s11051-014-2788-1.
93. Kamatchi, R.; Venkatachalapathy, S.; Abhinaya Srinivas, B. Synthesis, stability, transport properties, and surface wettability of reduced graphene oxide/water nanofluids. *International Journal of Thermal Sciences* **2015**, *97*, 17–25, doi:10.1016/j.ijthermalsci.2015.06.011.
94. Mehrali, M.; Sadeghinezhad, E.; Latibari, S.; Kazi, S.; Mehrali, M.; Zubir, M.N.B.M.; Metselaar, H.S. Investigation of thermal conductivity and rheological properties of nanofluids containing graphene nanoplatelets. *Nanoscale Res Lett* **2014**, *9*, 15, doi:10.1186/1556-276X-9-15.
95. J.C. Maxwell, *A Treatise on Electricity and Magnetism*, Clarendon Press (1881).
96. Vallejo, J.P.; Pérez-Tavernier, J.; Cabaleiro, D.; Fernández-Seara, J.; Lugo, L. Potential heat transfer enhancement of functionalized graphene nanoplatelet dispersions in a propylene glycol-water mixture. Thermophysical profile. *The Journal of Chemical Thermodynamics* **2018**, *123*, 174–184, doi:10.1016/j.jct.2018.04.007.
97. Wang, J.; Carson, J.K.; North, M.F.; Cleland, D.J. A new approach to modelling the effective thermal conductivity of heterogeneous materials. *International Journal of Heat and Mass Transfer* **2006**, *49*, 3075–3083, doi:10.1016/j.ijheatmasstransfer.2006.02.007.
98. Cabaleiro, D.; Nimo, J.; Pastoriza-Gallego, M.J.; Piñeiro, M.M.; Legido, J.L.; Lugo, L. Thermal conductivity of dry anatase and rutile nano-powders and ethylene and propylene

- glycol-based TiO<sub>2</sub> nanofluids. *The Journal of Chemical Thermodynamics* **2015**, *83*, 67–76, doi:10.1016/j.jct.2014.12.001.
99. Sun, Z.; Pöller, S.; Huang, X.; Guschin, D.; Taetz, C.; Ebbinghaus, P.; Masa, J.; Erbe, A.; Kilzer, A.; Schuhmann, W.; et al. High-yield exfoliation of graphite in acrylate polymers: A stable few-layer graphene nanofluid with enhanced thermal conductivity. *Carbon* **2013**, *64*, 288–294, doi:10.1016/j.carbon.2013.07.063.
  100. Amiri, A.; Shanbedi, M.; Rafieerad, A.R.; Rashidi, M.M.; Zaharinie, T.; Zubir, M.N.M.; Kazi, S.N.; Chew, B.T. Functionalization and exfoliation of graphite into mono layer graphene for improved heat dissipation. *Journal of the Taiwan Institute of Chemical Engineers* **2017**, *71*, 480–493, doi:10.1016/j.jtice.2016.12.009.
  101. Amiri, A.; Ahmadi, G.; Shanbedi, M.; Etemadi, M.; Mohd Zubir, M.N.; Chew, B.T.; Kazi, S.N. Heat transfer enhancement of water-based highly crumpled few-layer graphene nanofluids. *RSC Adv.* **2016**, *6*, 105508–105527, doi:10.1039/C6RA22365F.
  102. Cabaleiro, D.; Colla, L.; Barison, S.; Lugo, L.; Fedele, L.; Bobbo, S. Heat Transfer Capability of (Ethylene Glycol + Water)-Based Nanofluids Containing Graphene Nanoplatelets: Design and Thermophysical Profile. *Nanoscale Res Lett* **2017**, *12*, 53, doi:10.1186/s11671-016-1806-x.
  103. Mehrali, M.; Sadeghinezhad, E.; Rosen, M.A.; Akhiani, A.R.; Tahan Latibari, S.; Mehrali, M.; Metselaar, H.S.C. Heat transfer and entropy generation for laminar forced convection flow of graphene nanoplatelets nanofluids in a horizontal tube. *International Communications in Heat and Mass Transfer* **2015**, *66*, 23–31, doi:10.1016/j.icheatmasstransfer.2015.05.007.
  104. Amiri, A.; Sadri, R.; Shanbedi, M.; Ahmadi, G.; Chew, B.T.; Kazi, S.N.; Dahari, M. Performance dependence of thermosyphon on the functionalization approaches: An experimental study on thermo-physical properties of graphene nanoplatelet-based water nanofluids. *Energy Conversion and Management* **2015**, *92*, 322–330, doi:10.1016/j.enconman.2014.12.051.
  105. Park, S.S.; Kim, N.J. Influence of the oxidation treatment and the average particle diameter of graphene for thermal conductivity enhancement. *Journal of Industrial and Engineering Chemistry* **2014**, *20*, 1911–1915, doi:10.1016/j.jiec.2013.09.011.
  106. Jyothirmayee Aravind, S.S.; Ramaprabhu, S. Surfactant free graphene nanosheets based nanofluids by in-situ reduction of alkaline graphite oxide suspensions. *Journal of Applied Physics* **2011**, *110*, 124326, doi:10.1063/1.3671613.
  107. Ghozatloo, A.; Shariaty-Niasar, M.; Rashidi, A.M. Preparation of nanofluids from functionalized Graphene by new alkaline method and study on the thermal conductivity and stability. *International Communications in Heat and Mass Transfer* **2013**, *42*, 89–94, doi:10.1016/j.icheatmasstransfer.2012.12.007.
  108. Lee, G.-J.; Rhee, C.K. Enhanced thermal conductivity of nanofluids containing graphene nanoplatelets prepared by ultrasound irradiation. *J Mater Sci* **2014**, *49*, 1506–1511, doi:10.1007/s10853-013-7831-6.
  109. Le Ba, T.; Mahian, O.; Wongwises, S.; Szilágyi, I.M. Review on the recent progress in the preparation and stability of graphene-based nanofluids. *J Therm Anal Calorim* **2020**, doi:10.1007/s10973-020-09365-9.
  110. H.A. Barnes, J.F. Hutton, K. Walters, An introduction to rheology, Elsevier B.V., Amsterdam, Netherlands, 1989.

111. Coussot P., Grossiord J. L., Comprendre la rhéologie de la circulation du sang à la prise du béton, EDP Science, 2001.
112. <http://ssaft.com/Blog/dotclear/index.php?post/2009/12/01/Have-fun-with-non-newtonian-fluid>.
113. Groupe français de rhéologie; Grossiord, J.-L.; Ponton, A.; Léger, L. *La mesure en rhéologie des avancées récentes aux perspectives*; EDP Sciences: Les Ulis, 2013; ISBN 978-2-7598-0623-2.
114. Murshed, S.M.S.; Estellé, P. A state of the art review on viscosity of nanofluids. *Renewable and Sustainable Energy Reviews* **2017**, *76*, 1134–1152, doi:10.1016/j.rser.2017.03.113.
115. E.N.C. Andrade, Theory of viscosity of liquid Phil. Mag., 17 (1934), pp. 497-511.
116. Lakshmi, R.; Athithan, S.K. An empirical model for the viscosity buildup of hydroxy terminated polybutadiene based solid propellant slurry. *Polym. Compos.* **1999**, *20*, 346–356, doi:10.1002/pc.10361.
117. Wang, Y.; Al-Saaidi, H.A.I.; Kong, M.; Alvarado, J.L. Thermophysical performance of graphene based aqueous nanofluids. *International Journal of Heat and Mass Transfer* **2018**, *119*, 408–417, doi:10.1016/j.ijheatmasstransfer.2017.11.019.
118. Fulcher, G.S. Analysis of recent measurements of the viscosity of glasses. *J American Ceramic Society* **1925**, *8*, 339–355, doi:10.1111/j.1151-2916.1925.tb16731.x.
119. Vogel, H. The law of the relation between the viscosity of liquids and the temperature. *Phys. Z* 1921, *22*, 645–646.
120. Cabaleiro, D.; Estellé, P.; Navas, H.; Desforges, A.; Vigolo, B. Dynamic Viscosity and Surface Tension of Stable Graphene Oxide and Reduced Graphene Oxide Aqueous Nanofluids. *J nanofluids* **2018**, *7*, 1081–1088, doi:10.1166/jon.2018.1539.
121. Moghaddam, M.B.; Goharshadi, E.K.; Entezari, M.H.; Nancarrow, P. Preparation, characterization, and rheological properties of graphene–glycerol nanofluids. *Chemical Engineering Journal* **2013**, *231*, 365–372, doi:10.1016/j.cej.2013.07.006.
122. Sarsam, W.S.; Amiri, A.; Kazi, S.N.; Badarudin, A. Stability and thermophysical properties of non-covalently functionalized graphene nanoplatelets nanofluids. *Energy Conversion and Management* **2016**, *116*, 101–111, doi:10.1016/j.enconman.2016.02.082.
123. Selvam, C.; Mohan Lal, D.; Harish, S. Enhanced heat transfer performance of an automobile radiator with graphene based suspensions. *Applied Thermal Engineering* **2017**, *123*, 50–60, doi:10.1016/j.applthermaleng.2017.05.076.
124. Wang, Y.; Al-Saaidi, H.A.I.; Kong, M.; Alvarado, J.L. Thermophysical performance of graphene based aqueous nanofluids. *International Journal of Heat and Mass Transfer* **2018**, *119*, 408–417, doi:10.1016/j.ijheatmasstransfer.2017.11.019.
125. Wang, F.; Han, L.; Zhang, Z.; Fang, X.; Shi, J.; Ma, W. Surfactant-free ionic liquid-based nanofluids with remarkable thermal conductivity enhancement at very low loading of graphene. *Nanoscale Res Lett* **2012**, *7*, 314, doi:10.1186/1556-276X-7-314.
126. Agarwal, D.K.; Vaidyanathan, A.; Sunil Kumar, S. Experimental investigation on thermal performance of kerosene–graphene nanofluid. *Experimental Thermal and Fluid Science* **2016**, *71*, 126–137, doi:10.1016/j.expthermflusci.2015.10.028.
127. Chai, Y.H.; Yusup, S.; Chok, V.S.; Irawan, S.; Singh, J.S.D.B. Thermophysical properties of graphene nanosheets – Hydrogenated oil based nanofluid for drilling fluid improvements. *Applied Thermal Engineering* **2017**, *122*, 794–805, doi:10.1016/j.applthermaleng.2017.05.012.

128. Ghozatloo, A.; Rashidi, A.; Shariaty-Niassar, M. Convective heat transfer enhancement of graphene nanofluids in shell and tube heat exchanger. *Experimental Thermal and Fluid Science* **2014**, *53*, 136–141, doi:10.1016/j.expthermflusci.2013.11.018.
129. Iranmanesh, S.; Ong, H.C.; Ang, B.C.; Sadeghinezhad, E.; Esmaeilzadeh, A.; Mehrali, M. Thermal performance enhancement of an evacuated tube solar collector using graphene nanoplatelets nanofluid. *Journal of Cleaner Production* **2017**, *162*, 121–129, doi:10.1016/j.jclepro.2017.05.175.
130. Mehrali, M.; Sadeghinezhad, E.; Rosen, M.A.; Tahan Latibari, S.; Mehrali, M.; Metselaar, H.S.C.; Kazi, S.N. Effect of specific surface area on convective heat transfer of graphene nanoplatelet aqueous nanofluids. *Experimental Thermal and Fluid Science* **2015**, *68*, 100–108, doi:10.1016/j.expthermflusci.2015.03.012.
131. Sadeghinezhad, E.; Togun, H.; Mehrali, M.; Sadeghi Nejad, P.; Tahan Latibari, S.; Abdulrazzaq, T.; Kazi, S.N.; Metselaar, H.S.C. An experimental and numerical investigation of heat transfer enhancement for graphene nanoplatelets nanofluids in turbulent flow conditions. *International Journal of Heat and Mass Transfer* **2015**, *81*, 41–51, doi:10.1016/j.ijheatmasstransfer.2014.10.006.
132. Ilyas, S.U.; Pendyala, R.; Narahari, M.; Susin, L. Stability, rheology and thermal analysis of functionalized alumina- thermal oil-based nanofluids for advanced cooling systems. *Energy Conversion and Management* **2017**, *142*, 215–229, doi:10.1016/j.enconman.2017.01.079.
133. Pak, B.C.; Cho, Y.I. Hydrodynamic and heat transfer study of dispersed fluids with submicron metallic oxide particles. *Experimental Heat Transfer* **1998**, *11*, 151–170, doi:10.1080/08916159808946559.
134. Xuan, Y.; Roetzel, W. Conceptions for heat transfer correlation of nanofluids. *International Journal of Heat and Mass Transfer* **2000**, *43*, 3701–3707, doi:10.1016/S0017-9310(99)00369-5.
135. O’Hanley, H.; Buongiorno, J.; McKrell, T.; Hu, L. Measurement and Model Validation of Nanofluid Specific Heat Capacity with Differential Scanning Calorimetry. *Advances in Mechanical Engineering* **2012**, *4*, 181079, doi:10.1155/2012/181079.
136. Vajjha, R.S.; Das, D.K. Specific Heat Measurement of Three Nanofluids and Development of New Correlations. *Journal of Heat Transfer* **2009**, *131*, 071601, doi:10.1115/1.3090813.
137. Zhou, S.-Q.; Ni, R. Measurement of the specific heat capacity of water-based Al<sub>2</sub>O<sub>3</sub> nanofluid. *Appl. Phys. Lett.* **2008**, *92*, 093123, doi:10.1063/1.2890431.
138. Bergman, T.L. Effect of reduced specific heats of nanofluids on single phase, laminar internal forced convection. *International Journal of Heat and Mass Transfer* **2009**, *52*, 1240–1244, doi:10.1016/j.ijheatmasstransfer.2008.08.019.
139. Vallejo, J.P.; Álvarez-Regueiro, E.; Cabaleiro, D.; Fernández-Seara, J.; Fernández, J.; Lugo, L. Functionalized graphene nanoplatelet nanofluids based on a commercial industrial antifreeze for the thermal performance enhancement of wind turbines. *Applied Thermal Engineering* **2019**, *152*, 113–125, doi:10.1016/j.applthermaleng.2019.02.046.
140. Shahrul, I.M.; Mahbubul, I.M.; Khaleduzzaman, S.S.; Saidur, R.; Sabri, M.F.M. A comparative review on the specific heat of nanofluids for energy perspective. *Renewable and Sustainable Energy Reviews* **2014**, *38*, 88–98, doi:10.1016/j.rser.2014.05.081.
141. Chandrasekar, M.; Suresh, S.; Senthilkumar, T. Mechanisms proposed through experimental investigations on thermophysical properties and forced convective heat

- transfer characteristics of various nanofluids – A review. *Renewable and Sustainable Energy Reviews* **2012**, *16*, 3917–3938, doi:10.1016/j.rser.2012.03.013.
142. Susan Mousavi, N.S.; Kumar, S. Effective heat capacity of ferrofluids – Analytical approach. *International Journal of Thermal Sciences* **2014**, *84*, 267–274, doi:10.1016/j.ijthermalsci.2014.05.012.
  143. Selvam, C.; Mohan Lal, D.; Harish, S. Thermal conductivity and specific heat capacity of water–ethylene glycol mixture-based nanofluids with graphene nanoplatelets. *J Therm Anal Calorim* **2017**, *129*, 947–955, doi:10.1007/s10973-017-6276-6.
  144. M. Kaviany, Principles of convective heat transfer, Springer Science & Business Media, Ann Arbor, MI, USA, 2013.
  145. Gaciño, F.M.; Regueira, T.; Bolotov, A.V.; Sharipov, A.; Lugo, L.; Comuñas, M.J.P.; Fernández, J. Volumetric behaviour of six ionic liquids from T = (278 to 398) K and up to 120 MPa. *The Journal of Chemical Thermodynamics* **2016**, *93*, 24–33, doi:10.1016/j.jct.2015.09.013.
  146. Ferrouillat, S.; Bontemps, A.; Ribeiro, J.-P.; Gruss, J.-A.; Soriano, O. Hydraulic and heat transfer study of SiO<sub>2</sub>/water nanofluids in horizontal tubes with imposed wall temperature boundary conditions. *International Journal of Heat and Fluid Flow* **2011**, *32*, 424–439, doi:10.1016/j.ijheatfluidflow.2011.01.003.
  147. <http://tensionsuperficielle.free.fr/tension-superficielle/>.
  148. Hanrahan, G. Aqueous Chemistry. In *Key Concepts in Environmental Chemistry*; Elsevier, 2012; pp. 73–106 ISBN 978-0-12-374993-2.
  149. Estellé, P.; Cabaleiro, D.; Żyła, G.; Lugo, L.; Murshed, S.M.S. Current trends in surface tension and wetting behavior of nanofluids. *Renewable and Sustainable Energy Reviews* **2018**, *94*, 931–944, doi:10.1016/j.rser.2018.07.006.
  150. Incropera FP, DeWitt DP, Bergman TL, Lavine AS. Introduction to heat transfer. sixth ed. New York: John Wiley; 2007.
  151. Kutateladze SS. On the transition to film boiling under natural convection. *Kotloturbostroenie* 1948;3:10.
  152. Zuber N, Tribus M, Westwater JW. The hydrodynamic crisis in pool boiling of saturated and subcooled liquids. In: Paper 27 International Dev. in Heat Transfer, ASME, New York; 1961.
  153. Lienhard, J.H.; Eichhorn, R. Peak boiling heat flux on cylinders in a cross flow. *International Journal of Heat and Mass Transfer* **1976**, *19*, 1135–1142, doi:10.1016/0017-9310(76)90146-0.
  154. Kandlikar, S.G. Heat Transfer Mechanisms During Flow Boiling in Microchannels. *Journal of Heat Transfer* **2004**, *126*, 8–16, doi:10.1115/1.1643090.
  155. Kim, B.H.; Peterson, G.P. Analysis of the critical Weber number at the onset of liquid entrainment in capillary-driven heat pipes. *International Journal of Heat and Mass Transfer* **1995**, *38*, 1427–1442, doi:10.1016/0017-9310(94)00249-U.
  156. Terdtoon P. et al. Investigation of effect of inclination angle on heat transfer characteristics of closed two-phase thermosyphons, Paper B9P, in: Proceedings of the Seventh International Heat Pipe Conference, Minsk, May; 1990.
  157. Drelich J, Fang C, White CL. Measurement of interfacial tension in fluid-fluid systems, *Enc Surf Coll Sci*. second ed. Boca Raton: CRC Press; 2006.
  158. Khaleduzzaman, S.S.; Mahbulbul, I.M.; Shahrul, I.M.; Saidur, R. Effect of particle concentration, temperature and surfactant on surface tension of nanofluids. *International*

- Communications in Heat and Mass Transfer* **2013**, *49*, 110–114, doi:10.1016/j.icheatmasstransfer.2013.10.010.
159. Wanic, M.; Cabaleiro, D.; Hamze, S.; Fal, J.; Estellé, P.; Żyła, G. Surface tension of ethylene glycol-based nanofluids containing various types of nitrides: An experimental study. *J Therm Anal Calorim* **2020**, *139*, 799–806, doi:10.1007/s10973-019-08512-1.
  160. Cabaleiro, D.; Estellé, P.; Navas, H.; Desforges, A.; Vigolo, B. Dynamic Viscosity and Surface Tension of Stable Graphene Oxide and Reduced Graphene Oxide Aqueous Nanofluids. *J nanofluids* **2018**, *7*, 1081–1088, doi:10.1166/jon.2018.1539.
  161. Kim, E.J.; Desforges, A.; Speyer, L.; Ghanbaja, J.; Gleize, J.; Estellé, P.; Vigolo, B. Graphene for Water-Based Nanofluid Preparation: Effect of Chemical Modifications on Dispersion and Stability. *J nanofluids* **2017**, *6*, 603–613, doi:10.1166/jon.2017.1353.
  162. Cong, H.-P.; Chen, J.-F.; Yu, S.-H. Graphene-based macroscopic assemblies and architectures: an emerging material system. *Chem. Soc. Rev.* **2014**, *43*, 7295–7325, doi:10.1039/C4CS00181H.
  163. Zheng, Z.Z. Experimental Investigation on Surface Tension of Water-Based Graphene Oxide Nanofluids. *AMR* **2014**, *1082*, 297–301, doi:10.4028/www.scientific.net/AMR.1082.297.
  164. Kamatchi, R.; Venkatachalapathy, S.; Abhinaya Srinivas, B. Synthesis, stability, transport properties, and surface wettability of reduced graphene oxide/water nanofluids. *International Journal of Thermal Sciences* **2015**, *97*, 17–25, doi:10.1016/j.ijthermalsci.2015.06.011.
  165. Ahammed, N.; Asirvatham, L.G.; Wongwises, S. Effect of volume concentration and temperature on viscosity and surface tension of graphene–water nanofluid for heat transfer applications. *J Therm Anal Calorim* **2016**, *123*, 1399–1409, doi:10.1007/s10973-015-5034-x.
  166. Prasher, R.; Song, D.; Wang, J.; Phelan, P. Measurements of nanofluid viscosity and its implications for thermal applications. *Appl. Phys. Lett.* **2006**, *89*, 133108, doi:10.1063/1.2356113.
  167. Timofeeva, E.V.; Routbort, J.L.; Singh, D. Particle shape effects on thermophysical properties of alumina nanofluids. *Journal of Applied Physics* **2009**, *106*, 014304, doi:10.1063/1.3155999.
  168. Chen, L.; Xie, H.; Li, Y.; Yu, W. Nanofluids containing carbon nanotubes treated by mechanochemical reaction. *Thermochimica Acta* **2008**, *477*, 21–24, doi:10.1016/j.tca.2008.08.001.
  169. Bergles A.E., Bar-Cohen A., Direct Liquid Cooling of Microelectronic Components, Advances in Thermal Modeling of Electronic Components and Systems, 2 (1990), eds., ASME Press, New York, NY.
  170. Dittus, F.W.; Boelter, L.M.K. Heat transfer in automobile radiators of the tubular type. *International Communications in Heat and Mass Transfer* **1985**, *12*, 3–22, doi:10.1016/0735-1933(85)90003-X.
  171. Vajjha, R.S.; Das, D.K. A review and analysis on influence of temperature and concentration of nanofluids on thermophysical properties, heat transfer and pumping power. *International Journal of Heat and Mass Transfer* **2012**, *55*, 4063–4078, doi:10.1016/j.ijheatmasstransfer.2012.03.048.
  172. Saylor, J.R.; Bar-Cohen, A.; Lee Tien-Yu; Simon, T.W.; Tong Wei; Wu Pey-Shey Fluid selection and property effects in single- and two-phase immersion cooling (of electronic

- components). *IEEE Trans. Comp., Hybrids, Manufact. Technol.* **1988**, *11*, 557–565, doi:10.1109/33.16697.
173. American Society of Heating, Refrigerating and Air-conditioning Engineers, ASHRAE Handbook Fundamentals, Atlanta, GA, 2009.
174. Cabaleiro, D.; Colla, L.; Agresti, F.; Lugo, L.; Fedele, L. Transport properties and heat transfer coefficients of ZnO/(ethylene glycol + water) nanofluids. *International Journal of Heat and Mass Transfer* **2015**, *89*, 433–443, doi:10.1016/j.ijheatmasstransfer.2015.05.067.
175. Halelfadl, S.; Maré, T.; Estellé, P. Efficiency of carbon nanotubes water based nanofluids as coolants. *Experimental Thermal and Fluid Science* **2014**, *53*, 104–110, doi:10.1016/j.expthermflusci.2013.11.010.
176. K. Thulukkanam, Heat exchanger design handbook, CRC Press, Boca Raton, FL, USA, 2013.
177. Ranjith; Shaji, K. Numerical Analysis on a Double Pipe Heat Exchanger with Twisted Tape Induced Swirl Flow on Both Sides. *Procedia Technology* **2016**, *24*, 436–443, doi:10.1016/j.protcy.2016.05.060.
178. B. Zohuri, N. Fathi, Thermal-hydraulic analysis of nuclear reactors, Springer, New York, NY, USA, 2015.
179. Fundamentals of thermal-fluid science, Content Technologies Inc., Moore Park, CA, USA, 2013.
180. R.K. Shah, D.P. Sekulic, Fundamentals of heat exchanger design, John Wiley & Sons, Hoboken, NJ, USA, 2003.
181. V. Gnielinski, G1 Heat transfer in pipe flow, in: VDI Heat Atlas, Springer, 2010, pp. 691-700.
182. F. Dittus, L. Boelter, University of California publications on engineering, University of California publications in Engineering, 2 (1930) 371.
183. B. Petukhov, Heat transfer and friction in turbulent pipe flow with variable physical properties, *Adv. heat transfer*, 6 (1970) 503-564.
184. Yarmand, H.; Gharekhani, S.; Ahmadi, G.; Shirazi, S.F.S.; Baradaran, S.; Montazer, E.; Zubir, M.N.M.; Alehashem, M.S.; Kazi, S.N.; Dahari, M. Graphene nanoplatelets–silver hybrid nanofluids for enhanced heat transfer. *Energy Conversion and Management* **2015**, *100*, 419–428, doi:10.1016/j.enconman.2015.05.023.
185. Zubir, M.N.M.; Badarudin, A.; Kazi, S.N.; Huang, N.M.; Misran, M.; Sadeghinezhad, E.; Mehrali, M.; Syuhada, N.I.; Gharekhani, S. Experimental investigation on the use of reduced graphene oxide and its hybrid complexes in improving closed conduit turbulent forced convective heat transfer. *Experimental Thermal and Fluid Science* **2015**, *66*, 290–303, doi:10.1016/j.expthermflusci.2015.03.022.

# Chapter III- Materials and experimental methods

III.1- Introduction.....	84
III.2- Presentation of the nanofluids used.....	84
III.3- Graphene synthesis.....	86
III.4- Graphene characterization.....	88
III.5- Nanofluid preparation.....	89
III.6- Nanofluid stability.....	92
III.7- Thermophysical properties of nanofluids: measurement techniques, experimental protocol and validation.....	93
III.7.1- Thermal conductivity.....	93
III.7.2- Isobaric heat capacity.....	97
III.7.3- Dynamic viscosity.....	98
III.7.4- Density.....	102
III.7.5- Surface tension .....	105
III.8- Conclusion.....	106
III.9- References.....	107

### III.1- Introduction

In this chapter, we present the materials used for the preparation of the graphene-based nanofluids and in particular the method for few-layer graphene production. A detailed description of the nanofluid preparation method and stability analysis is realized. Then, the various systems and protocols, as well as their validations, used for the experimental characterization of the thermo-physical properties of base fluids and nanofluids - thermal conductivity, isobaric heat capacity, dynamic viscosity, density and surface tension - are fully described.

### III.2- Presentation of the nanofluids used

The proposal process of the nanofluid production and characterization can be summarized by the methodology diagram shown in Figure III.1, which is followed in our work. In the next sections, each step and the corresponding equipment and methods are described. This diagram also highlights the partnership of this study and the tasks of each group that contributed to the development of this research work.

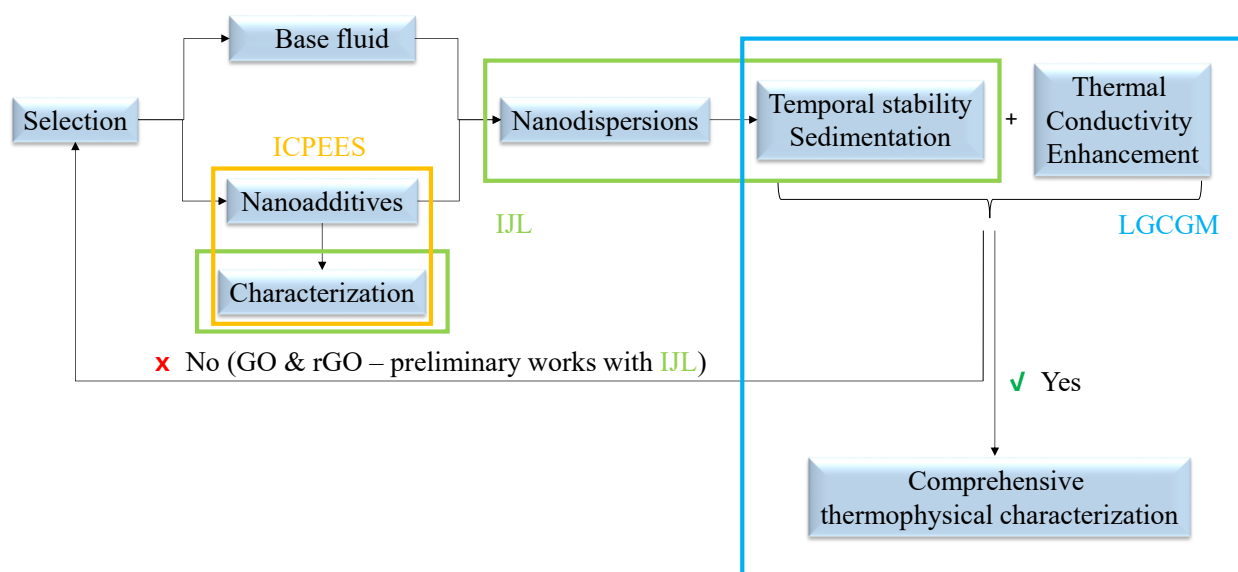


Figure III.1. Diagram of the experimental procedure.

As shown in Figure III.1, graphene production was performed at ICPEES (Strasbourg) while the graphene was characterized at IJL (Nancy) where the nanofluids were also produced. Finally, the full characterization of the base fluids and nanofluids was performed in our laboratory, namely LGCGM.

Graphite powder, i.e. TIMCAL TIMREX® SFG6 Primary Synthetic Graphite (Timcal Inc., USA), was used for comparison with the as produced FLG for Raman spectroscopy. Tyfocor® LS (Figure III.2), a commercial heat transfer fluid, pink colored, which is a mixture of propylene glycol:water (40:60) wt.% [1], was gently provided by Viessmann S.A. and used as a solvent for nanofluid preparation [2] (additional information about this fluid can be found in the appendix). It is referred to Tyfocor in the following (figures and text). This fluid was selected, as it is a ready-to-use industrial material containing corrosion and ageing inhibitors [3]. This fluid, up to now, was only previously used as thermal fluid in a solar collector absorber plate with microchannels [1,4].



**Figure III.2.** Photo of the used commercial base fluid Tyfocor® LS.

Nonionic surfactant Triton X-100 (Acros Organics, France), Gum Arabic (Acros Organics, France), and P123 (Sigma Aldrich, France) have been chosen for their good thermal stability and good ability to disperse carbon nanomaterials [5,6] (Table III.1) (Figure III.3). Additional information about the selection of these nanofluids can be found in chapter IV [3].

**Table III.1.** Name and formula of the three used surfactants for nanofluid preparation.

Surfactant name	Chemical formula
Triton X-100	$C_8H_{17}C_6H_4(OC_2H_4)_{9-10}OH$
Gum Arabic	Natural polysaccharides and glycoproteins
Pluronic® P-123	$HO(CH_2CH_2O)_{20}(CH_2CH(CH_3)O)_{70}(CH_2CH_2O)_{20}H$



**Figure III.3.** Photos of the three used surfactants: (a) Pluronic® P-123 (semi-solid, cloudy), (b) Gum Arabic (powder, white), and (c) Triton X-100 (liquid, colorless).

### III.3- Graphene synthesis

Compared to the Hummers' method [7], graphene of better structural quality was produced by a bulk synthesis of graphenic materials from mechanical exfoliation of graphite or expanded graphite [8] assisted by sonication (see method "c" in chapter II.3.1.1.1 and Figure II.12). By comparison to the methods that use organic solvents [9], aqueous media were advantageously easier to handle and non-toxic. A high ability to assist graphene exfoliation has been shown by surfactants such as polycyclic aromatic hydrocarbons due to strong  $\pi$ - $\pi$  interactions [10,11]. Here, expanded graphite aqueous exfoliation in a whole green process is assisted by biosourced surfactants such as tannic acid. So few-layer graphene nanosheets were synthesized by a mechanical exfoliation method assisted by tannic acid (Figure III.4). Tannic acid, which is a phenolic acid ( $C_{76}H_{52}O_{46}$ ), has two positive roles: i) inducing  $\pi$ - $\pi$  interactions between its  $C_6$  rings and those of the graphene surface, thereby promoting the intercalation of tannic acid between the graphene sheets, and ii) facilitating the dispersion of graphene nanosheets in water by means to

the OH groups to which the acid tannic belongs (see Figure III.4). Such a green procedure can be very suitable for the preparation of nanofluids requiring relatively high amount of nanomaterials.

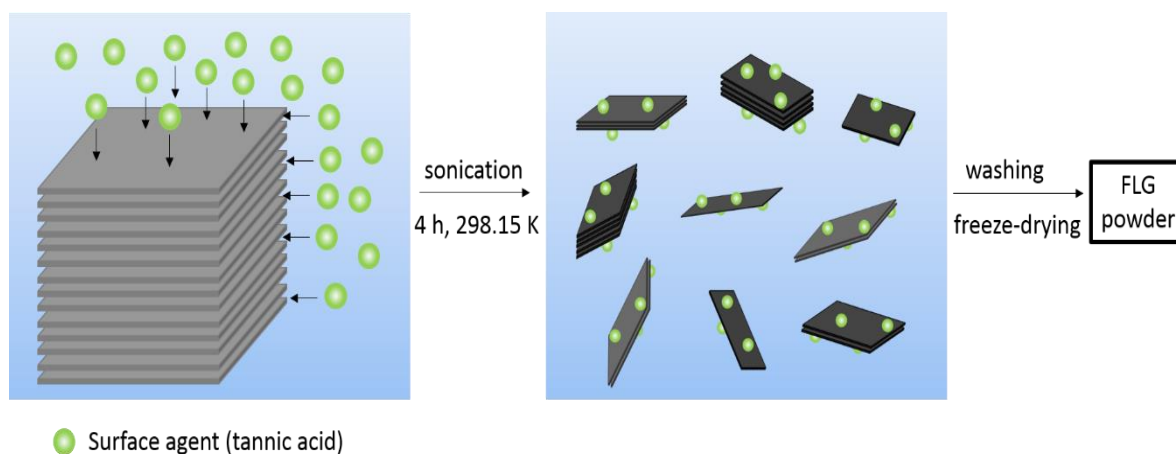


**Figure III.4.** Schematic of the liquid phase exfoliation process [3].

As also reported in [3], 200 mg of tannic acid (Sigma-Aldrich, France) was dissolved in 400 mL of deionized water, then 400 mg of expanded graphite (provided by Mersen, France) was added to the beaker in which a sonication probe (Branson Ultrasonics™ Sonicator 400W) was immersed. Sonication (80 W, 50 kHz, continuous mode) was performed during 4 hours at 298.15 K. The prepared pre-dispersed FLG was washed with deionized water before freeze-drying. Typically, 250 mL of the pre-dispersed solution was placed in a vacuum filtration device and filtered through a membrane with a porosity of 0.45  $\mu\text{m}$  (Merck Millipore, Germany) and washed five times with 250 mL of deionized water. After freeze-drying of the obtained FLG powder, it was used for characterization and preparation of the nanofluids (Figure III.5) as explained in the following. The FLG produced for each batch is around 300 mg, which means that the production yield is around 80 %.



**Figure III.5.** Samples of FLG being freeze-dried.

### **III.4- Graphene characterization**

#### *Scanning electron microscopy and Transmission electron microscopy*

Scanning electron microscopy (SEM) analysis was performed using an XL30 S-FEG apparatus (Philips, Netherland). Transmission electron microscopy (TEM) and high-resolution TEM (HRTEM) observations were carried out using a JEM-ARM 200F apparatus (JEOL, Japan) at a low accelerating voltage (80 kV) to avoid possible electron beam damage (Figure III.6). The observations were done by Dr. J. Ghanbaja at the IJL microscopy platform CC3M (Centre de compétences en Microscopies, Microsondes et Métallographie), Nancy. For SEM and TEM observations, the FLG powder was dispersed in ethanol and deposited in the dedicated sample holder. Holey carbon grids (200 mesh size) were used to improve the image contrast for this all-carbon nanomaterial. Approximately 30 images were taken at different locations for each sample to ensure a statistical observation of the samples. Fast Fourier Transform (FFT) and Inverse FFT (IFFT) were calculated on selected areas of the FLG images using Digital micrograph software.

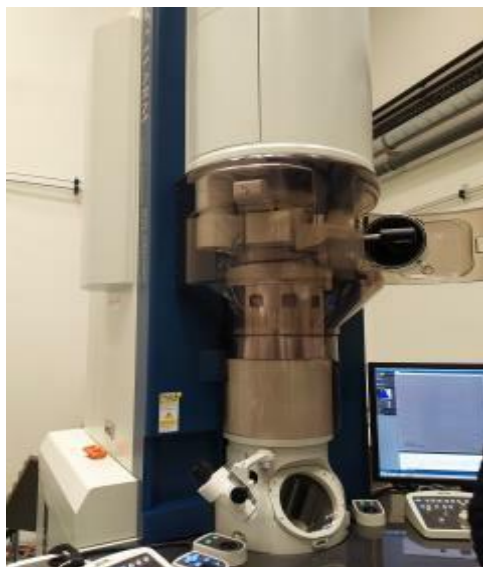


**Figure III.6.** TEM machine JEM-ARM 200F at the IJL.

### *Raman spectroscopy*

For Raman spectroscopy analysis, a LabRAM HR 800 micro-Raman spectrometer was used. A red light at  $\lambda = 632.8$  nm is the incident wavelength. These experiments were performed in collaboration with Dr. J. Gleize at the LCP-A2MC, Laboratoire de Chimie et Physique – Approche Multi-échelles des milieux Complexes, Université de Lorraine, Metz. For the analysis, the FLG was gently dispersed in ethanol using a sonication bath and deposited on a glass slide. For each sample, at least 5 spectra were recorded. For data analysis, a baseline was first subtracted and the height of band D was divided by the height of band G to calculate the  $I_D/I_G$  intensity ratio.

## **III.5- Nanofluid preparation**

As it is fully explained in [3], the base fluids corresponding to each surfactant at 1 wt.% were prepared by adding the desired amount of surfactant to Tyfocor (Figure III.7). An FLG based nanofluid preparation at 0.5 wt.% of FLG concentration was first prepared from the two-step method by adding the desired amount of FLG powder to the base fluid (the procedure is the same for each surfactant). The FLG/surfactant/Tyfocor mixture was dispersed thanks to a probe sonicator (Bioblock Scientific Vibra cell 75042, 125 W with a pulse mode 2 s ON / 1 s OFF) for 5x15 min controlling also the sample's temperature to avoid overheating effects. This concentrated nanofluid was then diluted with Tyfocor to obtain different nanofluid samples with lower FLG

weight concentrations: 0.25, 0.1 and 0.05% respectively (Table III.2) (Figure III.8). So for all samples, the ratio amount of surfactant/amount of FLG is 2. The diluted samples were also sonicated following the same procedure. For each surfactant (Triton X-100, Gum Arabic or Pluronic® P-123), the procedure described before was also used. Figure III.7 shows that the presence of surfactant does not modify the visual aspect of Tyfocor that is pink.

**Table III.2.** FLG and surfactant concentration for the FLG based nanofluids prepared with Tyfocor as a solvent.

<b>Nanofluid</b>	<b>Surfactant</b>	<b>FLG concentration (wt.%)</b>	<b>Surfactant concentration (wt.%)</b>
0.5wt%FLG+Tyfocor+1wt%TrX	Triton X-100	0.5	1
0.25wt%FLG+Tyfocor+0.5wt%TrX	Triton X-100	0.25	0.5
0.1wt%FLG+Tyfocor+0.2wt%TrX	Triton X-100	0.1	0.2
0.05wt%FLG+Tyfocor+0.1wt%TrX	Triton X-100	0.05	0.1
0.5wt%FLG+Tyfocor+1wt%GA	Gum Arabic	0.5	1
0.25wt%FLG+Tyfocor+0.5wt%GA	Gum Arabic	0.25	0.5
0.1wt%FLG+Tyfocor+0.2wt%GA	Gum Arabic	0.1	0.2
0.05wt%FLG+Tyfocor+0.1wt%GA	Gum Arabic	0.05	0.1
0.5wt%FLG+Tyfocor+1wt%P123	Pluronic® P-123	0.5	1
0.25wt%FLG+Tyfocor+0.5wt%P123	Pluronic® P-123	0.25	0.5
0.1wt%FLG+Tyfocor+0.2wt%P123	Pluronic® P-123	0.1	0.2
0.05wt%FLG+Tyfocor+0.1wt%P123	Pluronic® P-123	0.05	0.1

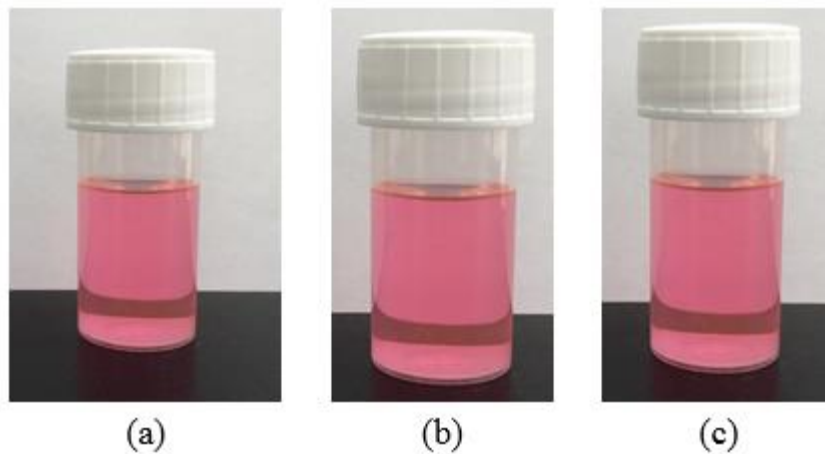
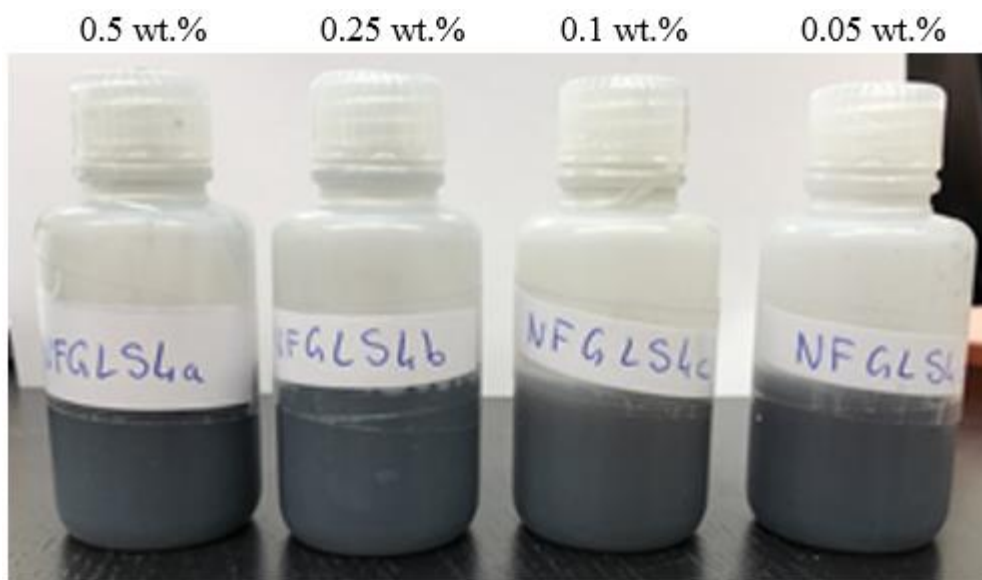
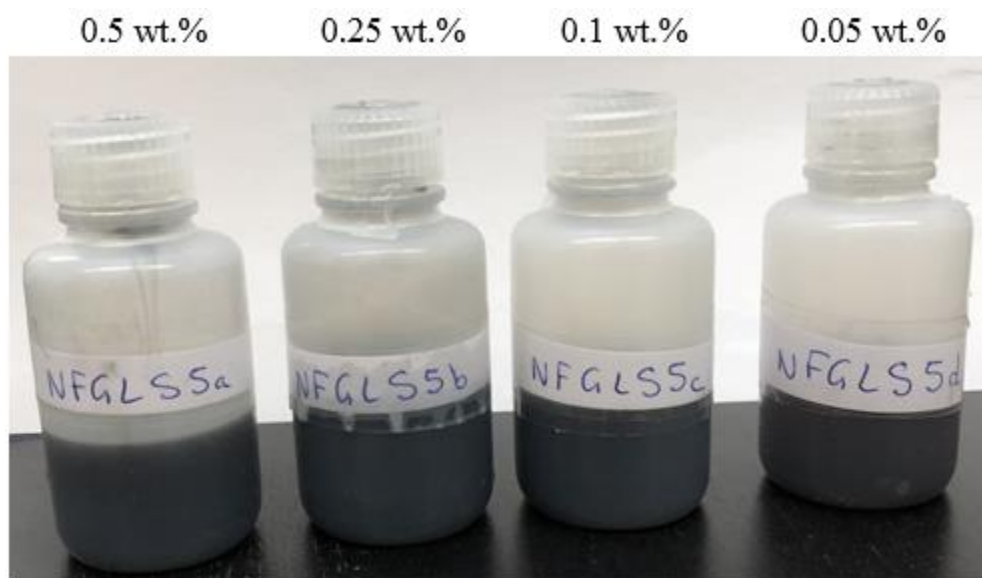


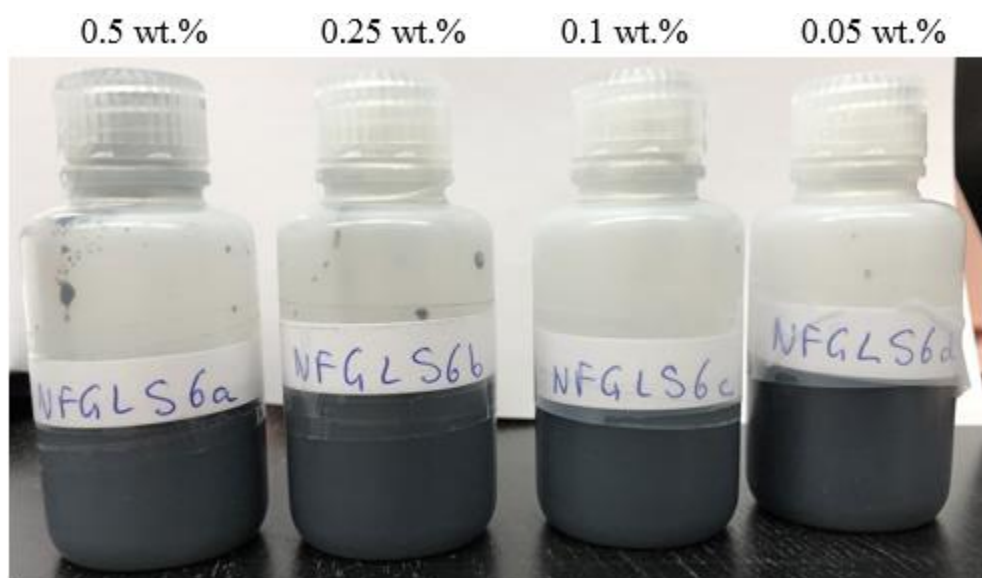
**Figure III.7.** Photos of Tyfocor<sup>®</sup> LS with the highest surfactant concentration, 1 wt.% of Triton X-100 (a), Pluronic<sup>®</sup> P-123 (b), and Gum Arabic (c).



(a)



(b)



(c)

**Figure III.8.** Photos of prepared nanofluids with Triton X-100 (a), Pluronic® P-123 (b), and Gum Arabic (c) described above.

### III.6- Nanofluid stability

As explained in [3], and in absence of the techniques described in the previous chapter for stability analysis, a Turbiscan Classic MA2000 apparatus (Formulacion, France) using a pulsed near-

infrared light source ( $\lambda = 850$  nm) was used to perform multiple light scattering measurements to follow the stability of nanofluids against sedimentation. These experiments were performed in collaboration with Dr. F. Michaux at the LIbio, Laboratoire d'Ingénierie des Biomolécules, Université de Lorraine, Nancy. Two synchronous detectors measured the transmitted and backscattered light upon the height of the sample by several upward sweeps (every 40  $\mu\text{m}$ ) all along a cylindrical glass cell until the top of the sample (5-7 cm). In the case of the nanofluids dispersions, only the intensity of the transmitted light was monitored upon the sample height as no backscattered light was detected due to light absorption by the black particles. And only the nanofluids with the two lowest FLG concentrations were analyzed. For nanofluids with high FLG concentration, the transmission of the light was too low to obtain reliable measurements. The intensities transmitted throughout the sample height were then recorded over time. The scans were recorded for five days after the dispersion of the particles ( $t_0$ ). The first scan recorded at  $t_0$  was deleted for subsequent scans to show the evolution of the system over time using the Turbisoft software. Then, the relative percentage of the transmitted intensity ( $\Delta\text{BS}$ ) upon the height of the sample was reported and its evolution over time was also visualized using this software. A phenomenon of sedimentation is then characterized by an increase of the transmitted light at the top of the sample over time until all particles settle. Then, the transmitted signal remains constant. The rate of sedimentation was calculated considering that the height of the sediment at 5 days (longest time) corresponded to the final sedimentation state. The Turbiscan measurements were performed at room temperature.

## **III.7- Thermo-physical properties of nanofluids: measurement techniques, experimental protocol and validation**

### **III.7.1- Thermal conductivity**

It has been proven that the transient hot-wire (THW) method is one of the most accurate and fast ways of determining the fluid thermal conductivity [12]. A THW-L2 device (Thermtest Inc., Canada) (Figure III.9) was used to evaluate the thermal conductivity of both the base fluids and nanofluids using the transient short hot-wire method according to the ASTM D7896 standard. It has been designed to perform thermal conductivity measurements of liquids between 0.01 and 2  $\text{W}\cdot\text{m}^{-1}\cdot\text{K}^{-1}$  and with a wide viscosity range (0.1-10000 mPa.s) under short measurement time to

avoid natural convection that causes problems for the measurement. This guarantees very precise measurements with excellent reproducibility.

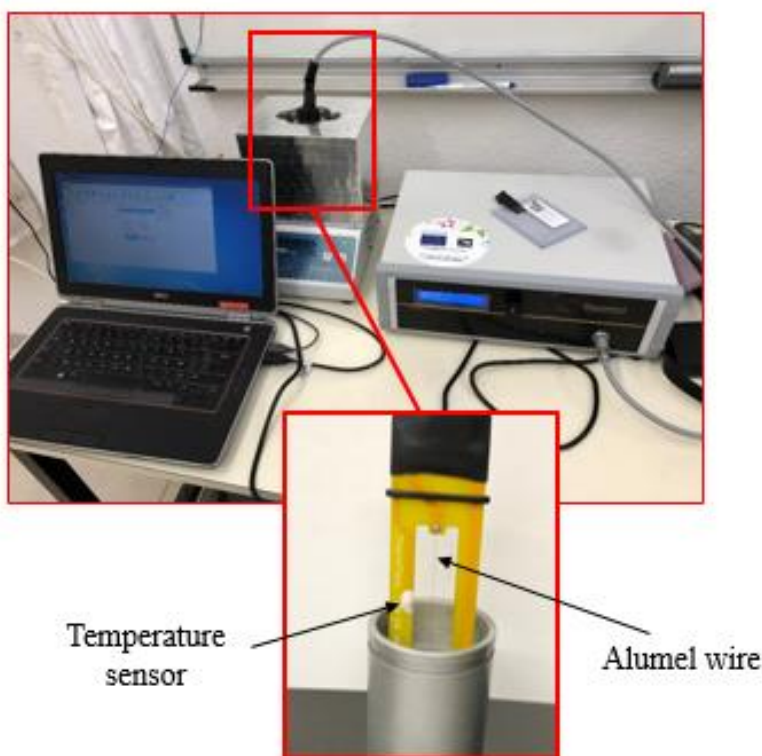


**Figure III.9.** The used thermal conductivity machine THW-L2 and its accessories.

The THW sensor consists of thin heating alumel wire, 60 mm long, and about 0.1 mm in diameter which is fully inserted into the sample to be tested. Measurements can be performed with this instrument in the temperature range 263.15-373.15 K, and a small volume of 20 mL is only required. First, the container is filled with the tested sample. After that, the probe is inserted into the sample. Finally, the container is placed in a dry bath. Then, the thermal conductivity measurements start once the required temperature of the sample is achieved and stabilized. This procedure is similar to the ones used in [13,14] with different base fluids and nanofluids. A power supply varying in the range 90-110 mW was applied here to the samples with a measurement time of 1.5 s to achieve a temperature rise of 1.2 K for the evaluation of thermal conductivity. This value was classically calculated in the linear region of the temperature increase with time in a logarithm scale. In the measurement performing, the sensor wire is heated with a constant current source ( $q$ ) and the temperature increase is recorded by monitoring the change in the electrical

resistance of the wire. The slope ( $a$ ) of the temperature rise curve as a function of the logarithm of time is used in the calculation of the thermal conductivity ( $k$ ). For liquid samples with high thermal conductivity, the lower the slope. For liquid samples with low thermal conductivity, the steeper the slope (see Figure III.10). The device and its software display a thermal conductivity value based on this equation:

$$k = \frac{q}{4\pi a} \quad \text{Eq. III.1}$$

Where  $k$  is the thermal conductivity in  $\text{W}\cdot\text{m}^{-1}\cdot\text{K}^{-1}$ ;  $q$  is the heating power in  $\text{W}\cdot\text{m}^{-1}$ ;  $a$  is the slope in the linear region from the plot of temperature rise vs. logarithm of time (see Figure III.10).

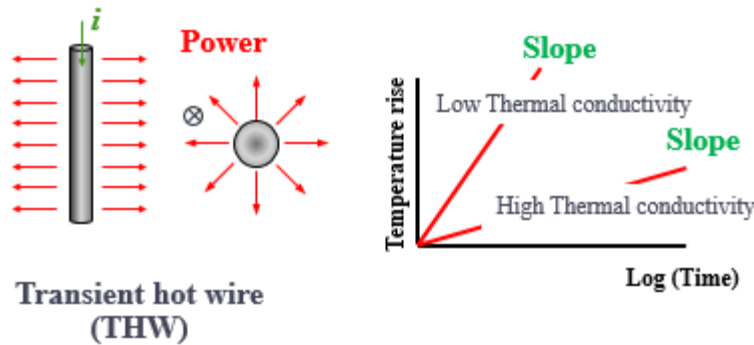


**Figure III.10.** Schematic representing the principle of the thermal conductivity determination.

At the end of each measurement, all the accessories used (probe and container) were carefully washed and cleaned two times, the first one with distilled water, and the other one with acetone or ethanol. The manufacturer indicated that the experimental uncertainty of the measurements made with this device was 5 %. Before measurements, the temperature probe and the sensor wire have been calibrated with distilled water (DIUF, CAS 1132-18-5, Fisher Chemical,  $0.599 \text{ W}\cdot\text{m}^{-1}\cdot\text{K}^{-1}$  at 293.15 K) [15]. Once the device was calibrated, the thermal conductivity of distilled water (DW) was measured between 278.15 and 333.15 K, as shown in Figure III.11, to assess the experimental uncertainty of the device. A comparison of these data with reference values [16] shows a really good agreement, with an average absolute deviation (AAD) around 1 %, as evidenced by Figure III.11. For all tests, thermal conductivity value consists of an average of at least 6 measurements with intervals of 5 min. Additionally, thermal conductivity measurements for Tyfocor fluid were carried out in the temperature range 283.15-323.15 K and compared with the data provided by the manufacturer [2] (see Figure III.12). An AAD of approximately 6% was found, which may be due

to the type of device used and the conditions of measurements not specified by the manufacturer. On the other hand, the thermal conductivity of water/ethylene glycol mixture with a ratio of 50:50 in volume was compared to ASHRAE data by [13]. An AAD < 1.5% was found between 263.15 and 293.15 K [17]. All base fluids and nanofluids were measured between 283.15 and 323.15 K. Each day, before to start measurements, a verification of the thermal conductivity of distilled water is performed. In case of deviation higher than 1%, the device is newly calibrated. The THW-L2 Meter can operate as an autonomous system using the integrated results display of the facade screen or as a benchtop system controlled, by the THW-L2 software.

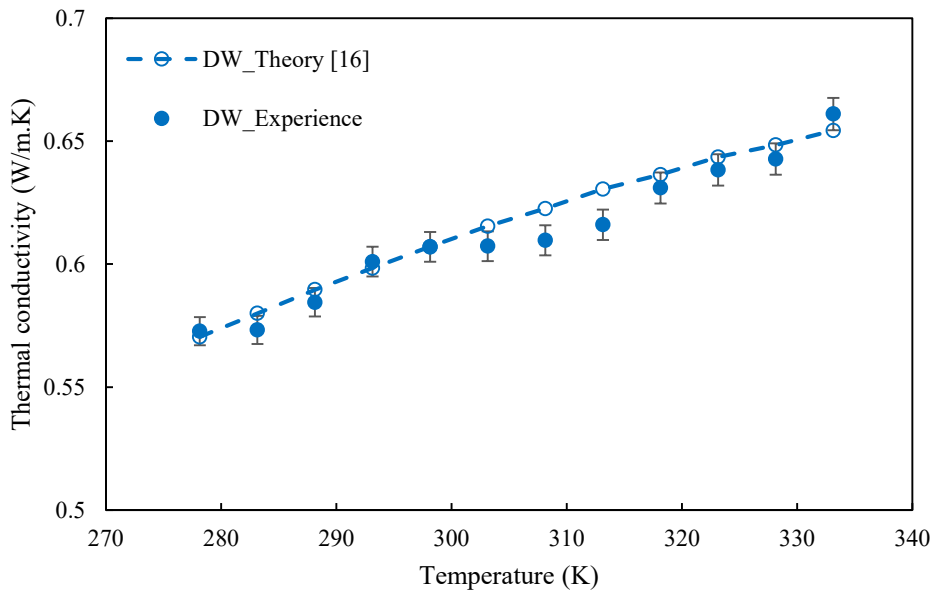


**Figure III.11.** Comparison between the experimental thermal conductivity of DW and the theoretical values from [16]. Error bars indicate average absolute of 1% deviation between experiments and reference values in the temperature range between 278.15 and 333.15 K [3].

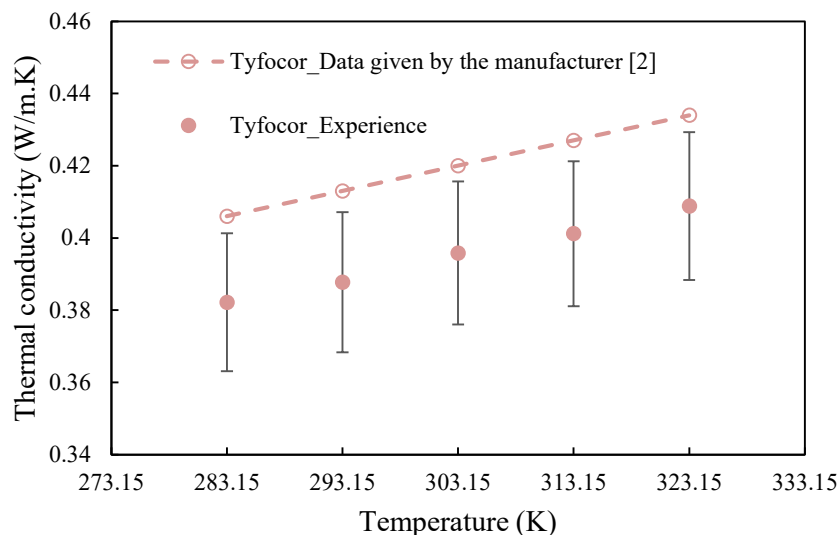


**Figure III.12.** Comparison between the experimental thermal conductivity of Tyfocor and the data given by the manufacturer [2]. Error bars indicate the uncertainty of measurements reported by the manufacturer of the device, 5%.

### III.7.2- Isobaric heat capacity

Measurements of isobaric heat capacities,  $C_p$ , of FLG, surfactants, Tyfocor® LS, and the highest concentration of base fluids and nanofluids, were conducted at 283.15 K, 303.15 K and 323.15 K with a Differential Scanning Calorimeter DSC-Q2000 (TA Instruments, New Castle, USA), which measures the difference between the amounts of heat that they need to be supplied to a reference and the studied sample to obtain in both cells the same temperature conditions (Figure III.13).



**Figure III.13.** Differential Scanning Calorimeter DSC-Q2000 apparatus.

For  $C_p$  measurement, a method known as quasi-isothermal Temperature-Modulated Differential Scanning Calorimetry (TMDSC) was used, in which sample temperature is sinusoidally varied around nominal temperature without a low-temperature amplitude and a long period [18–20]. Samples were hermetically encapsulated into Tzero aluminium pans, which can withstand pressures up to 4 bar, and weighed before and after performing the tests to verify that no change in mass occurred during the experiments and to validate the measurement [20]. The results of Tyfocor® LS were compared with the values given by the manufacturer [2], and the absolute average deviation obtained at the three temperatures was equal to 2%, which is lower than the experimental uncertainty of the device (3%) [20] (see Figure III.14).

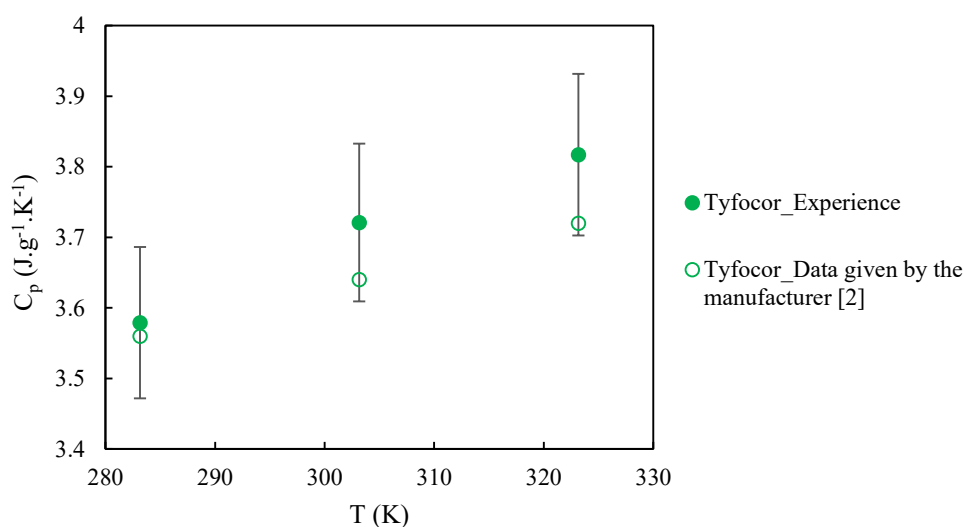


**Figure III.14.** Comparison between the isobaric heat capacity of Tyfocor® LS determined experimentally and that given by the manufacturer [2]. The error bars here correspond to the uncertainty of the device, 3%.

### III.7.3- Dynamic viscosity

A Malvern Kinexus Pro stress-controlled rheometer from Malvern Instruments Ltd. (Malvern, United Kingdom) working with a cone-plate geometry suitable for the study of low-viscosity colloidal dispersions was used to carry out the dynamic viscosity measurements (Figure III.15).

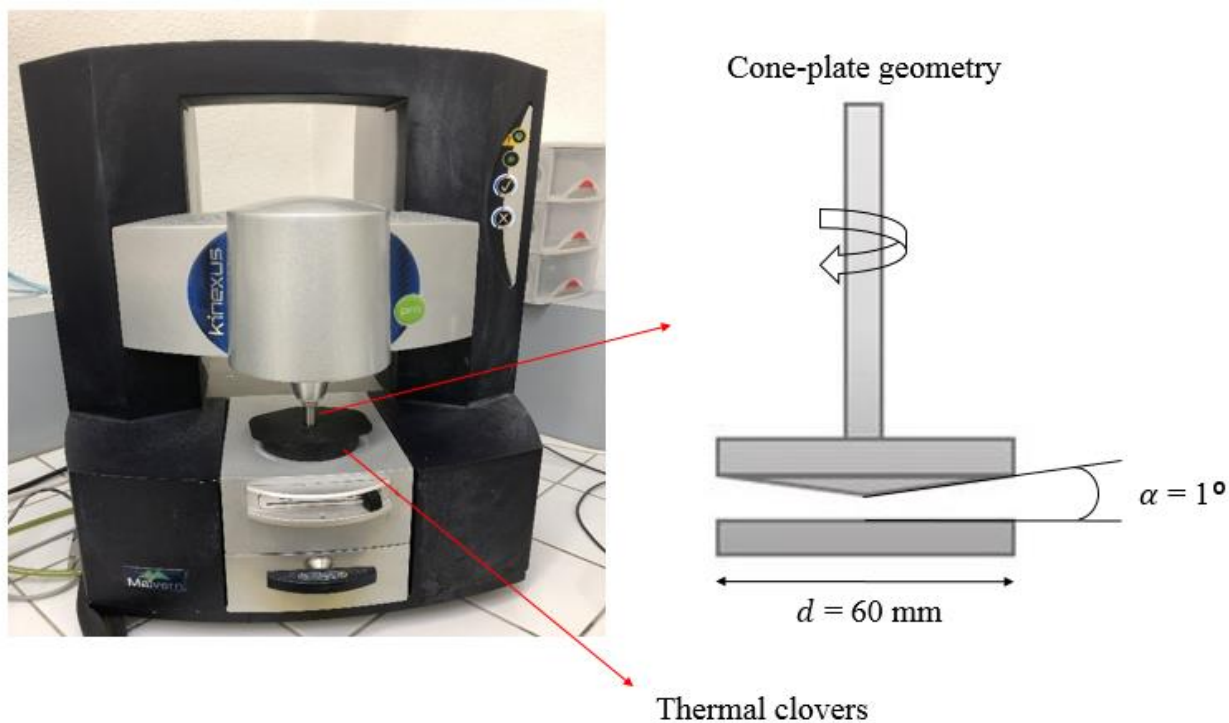


**Figure III.15.** Rheometer Malvern Kinexus Pro and schematic of the cone-plate geometry used.

The cone has an angle of  $1^\circ$  and a diameter of 60 mm. The gap between the plate and the cone is 0.03 mm. The measurements were performed in the temperature range 283.15-323.15 K with an interval of 10 K. A Peltier temperature control device placed below the lower surface was used to control the temperature, with a precision of  $\pm 0.01$  K. To ensure constant temperature within the sample gap during experiments, a thermal covers were used. This geometry needs an optimal volume of  $1 \text{ cm}^3$ . Using a syringe-type automatic pipette, each volume of the tested sample has been taken from its container and transferred to the lower plate, ensuring that no air bubbles are trapped in the sample. Thus, the cone is moved to obtain the required sampling gap. The excess sample is finally removed. A stabilization time of 5 min has waited before experiments.

Tests were performed in three ways:

1. Without shearing (shear rate equal to  $0 \text{ s}^{-1}$ ) and with increasing the temperature from 283.15 to 323.15 K to see the effect of temperature alone. The sample stays at constant temperature 10 minutes before ramping the temperature to the next value (+5 min stabilization time).

2. In a steady state regime at shear stresses corresponding to shear rates between 10 and 1000  $\text{s}^{-1}$ , to determine the rheological behavior of the sample at a constant temperature. Stress-controlled measurements were carried out by imposing a logarithmic stress ramp under steady-state conditions with a maximum step duration of 180 s. The shear rate was measured once a steady-state flow was reached and maintained for 10 s. The applicability of the shear stress range has been preliminarily evaluated to ensure steady-state flow at low shear stress, and to avoid flow instability and the ejection of the sample at high shear stress, especially for suspensions with low particle mass concentration. The final value of the shear stress ramp may vary depending on the tested suspension and has been set to achieve a shear rate of 1000  $\text{s}^{-1}$  for each nanosuspension [21].
3. At single shear rate equal to 500  $\text{s}^{-1}$  (a shear rate higher than 200  $\text{s}^{-1}$  within Newtonian region as it will be explained later in chapter IV) with ramping of temperature starting by 283.15 K with the use of the same sample until finishing all the imposed temperatures. The sample stays at constant temperature 5 minutes before ramping the temperature to the next value (+5 min stabilization time).

It should be mentioned that for each measurement a new sample was used and that the plate and the cone were cleaned using acetone at the end of each one.

The estimated uncertainty of the dynamic viscosities measured with this device within the studied shear rate range is less than 4% with water [21]. A Newtonian behavior was found at all temperatures for Tyfocor. As an example, Figure III.16 shows the evolution of dynamic viscosity of Tyfocor with the shear rate at 283.15 K, 303.15 K and 323.15 K. A comparison between the experimental viscosities of Tyfocor fluid with the data given by the manufacturer [2] was done between 273.15 and 373.15 K, and an AAD by about 5% was obtained (see Figure III.17). Additional details about the measuring procedure and this experimental device can be found in Halelfadl *et al.* [22]. The experiments were performed at least in two replicates for each nanofluid without significant difference in values and flow curves obtained.

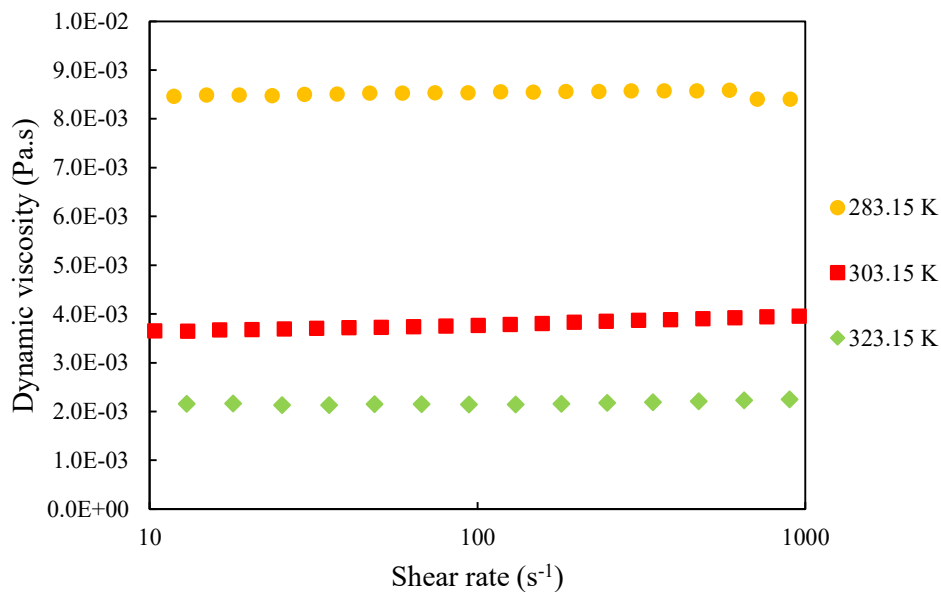


**Figure III.16.** Rheological behavior of Tyfocor® LS at 283.15, 303.15 and 323.15 K.

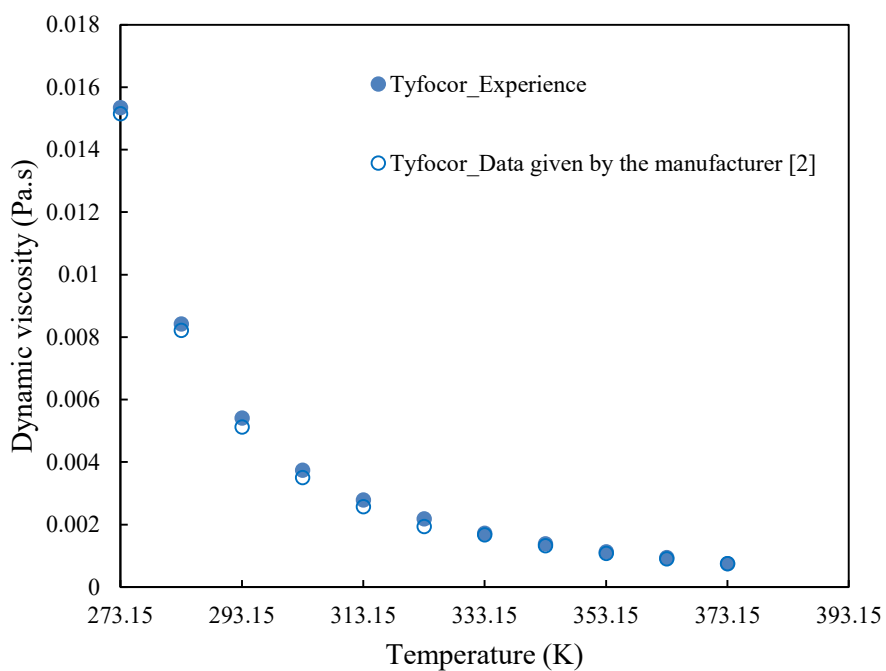


**Figure III.17.** Comparison between the experimental dynamic viscosity of Tyfocor® LS and the data given by the manufacturer [2].

### III.7.4- Density

#### *Density of FLG*

Density of graphene nanoparticles was measured at ambient temperature using a pycnometer ULTRAPYC 1200e (Quantachrome Instruments, Anton Paar, USA) (Figure III.18). This instrument measures the true volume of solid materials by employing Archimedes' principle of fluid (gas) displacement and the technique of gas expansion (Boyle's law). Ideally, a gas is used as a displacing fluid since it penetrates the finest pores assuring maximum accuracy. For this reason, helium is recommended since its small atomic dimensions assure penetration into crevices and pores approaching 0.2 nm in diameter. For the measurements, a micro cell (4.5 cm<sup>3</sup> of volume) was used, the place where we put the nanoparticles. Then the mass of the sample is weighed and inputted in the device with the target pressure (19 psig) for the density of the powder to be calculated. Verification of the accuracy of the pycnometer was done before starting measurements using two small balls (1.0725 cm<sup>3</sup> each one). An absolute average deviation (AAD) between the volume obtained with the instrument and their real volume (2.145 cm<sup>3</sup>) was found equal to 0.66%. Before analysis, the sample was automatically conditioned to remove contaminants and trapped air by a pulse mode suitable for powders. Many runs between 30 and 60 were performed for the same sample as the density decreases each time until obtaining a stable value. The measurement was duplicated without any relevant difference. At the end of each measurement, the cell was cleaned with distilled water and acetone respectively.

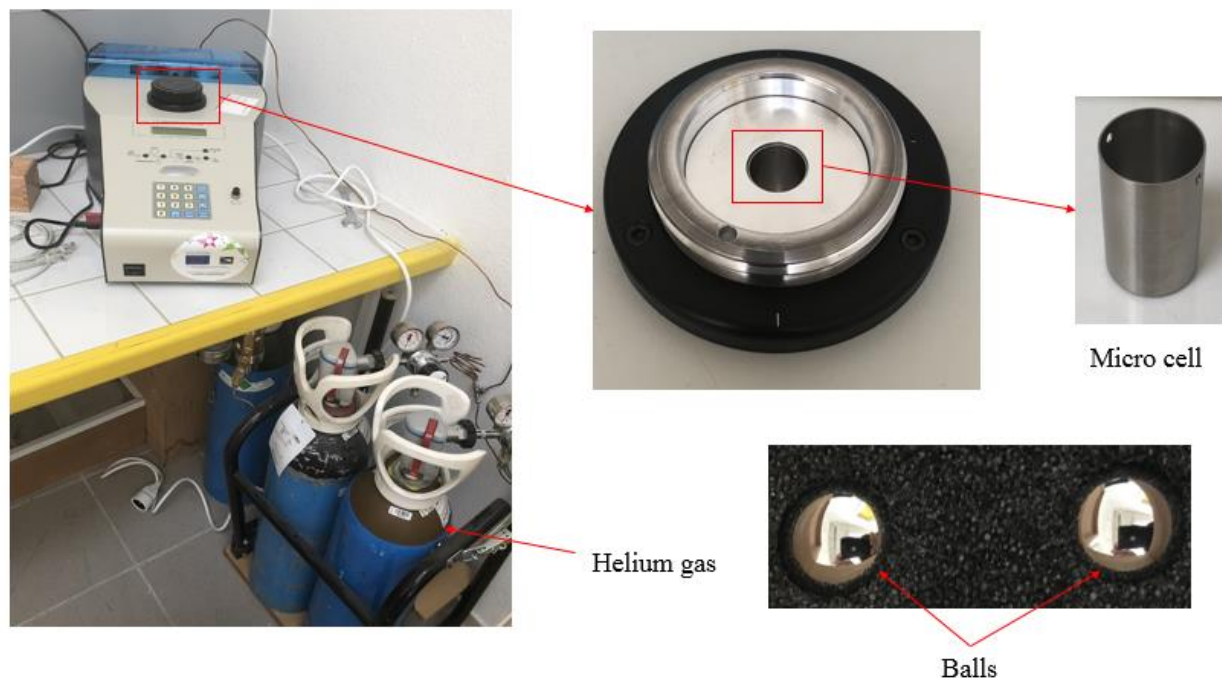


**Figure III.18.** Pycnometer ULTRAPYC 1200e and its accessories.

*Density of base fluids and nanofluids*

A density meter DMA 501 (Anton Paar, Austria) was used to perform density measurements of Tyfocor® LS, liquid Triton X-100, the surfactant and Tyfocor® LS mixtures used as base fluids and the corresponding FLG based nanofluids (Figure III.19).



**Figure III.19.** Density meter DMA 501.

This device can only perform density measurements for liquid samples. It is based on the oscillating U-tube technique and allows measurements at temperatures between 288.15 and 313.15 K. 2 mL of each sample were withdrawn in a syringe and then released into the U-tube until it was filled. At the end of each sample measurement, careful rinsing with both ethanol and acetone was performed. Before starting measurements of each series of samples, the density meter was carefully checked by measuring the density of air and distilled water at 293.15 K. The AAD between the experimental density results of distilled water and literature data [23] at 293.15 K were found less or equal to 0.02%. Also, experimental densities obtained in this work for Tyfocor® LS show an AAD of 0.13% in comparison to available manufacturer data [2] (see Figure III.20). The estimated uncertainty of the density measurements is less than  $0.001 \text{ g.cm}^{-3}$ .

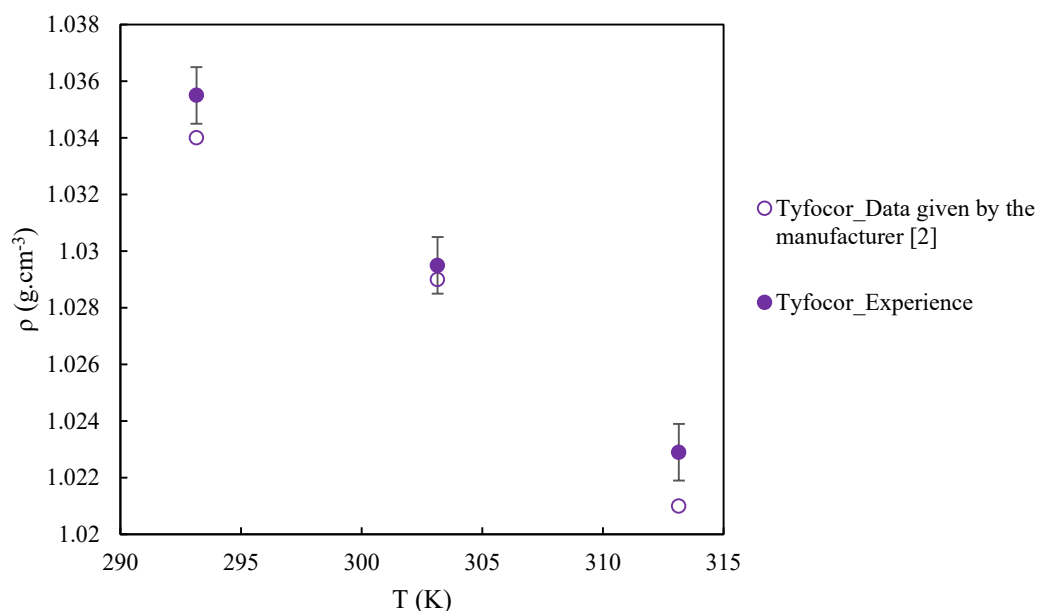


**Figure III.20.** Comparison between the experimental density of Tyfocor® LS and the data given by the manufacturer [2]. Error bars here correspond to the uncertainty of density measurements,  $0.001 \text{ g.cm}^{-3}$ .

### **III.7.5- Surface tension**

Surface tension measurements between the air and both the base fluids and nanofluids were performed using a Drop Shape Analyzer DSA-30 from KRÜSS GmbH (Hamburg, Germany) based on the pendant drop technique in the temperature range 283.15-323.15 K (Figure III.21). Typically, as reported previously [24,25], a 15-gauge needle with an outer diameter of 1.835 mm was used to produce drops, at controlled flow rate and volume within a temperature chamber. A Peltier system was used to regulate the temperature in the chamber which was monitored by a PT100 probe. The instrument digitally records and analyses the shape of the sample drops formed at the tip of a syringe just at the moment when the drop detaches from the top of the needle. Then, in the configuration of the pendant drop, ST of a sample was determined from its density and the image analysis of the drop shape produced at the end of the needle, by an equilibrium of internal and external forces acting on the drop and based on the Young-Laplace equation, as shown in Figure III.21.b. Each sample was measured three times, each time with a new drop, with obtaining similar values. Before starting the measurement, the needle stays in the chamber around 10 minutes to ensure that the sample reaches the imposed temperature. After the measurement, the drop was reentered into the needle to drop it outside the chamber with one or two other (on a paper), to not modify the chamber's humidity, and keep doing all the measurements in the same conditions. Then, the needle is entered again into the chamber, and the measurement is repeated ten minutes later with a new drop. For each drop, the ST value is an average of at least 10 measurements. ST of distilled water was measured between 283.15 and 333.15 K [1]. An absolute average deviation AAD between reference data and experimental data was obtained in this temperature range equal to 1.08% [23].

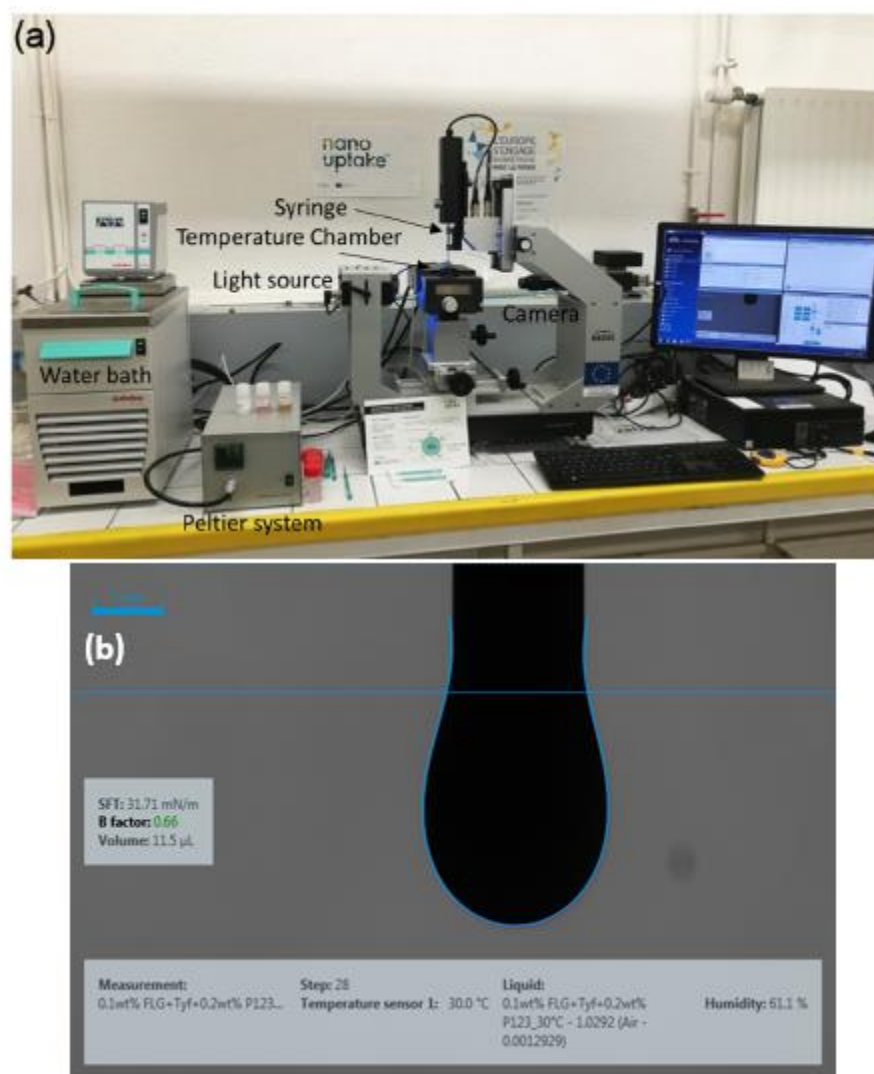


**Figure III.21.** (a) Experimental equipment for surface tension measurements [24], and (b) example of a pendant drop image of the nanofluid 0.1wt.% FLG+Tyfocor+0.2wt.% P123 at 303.15 K.

### III.8- Conclusion

We have presented in this chapter the materials used for producing the graphene-based nanofluids, as well as the production method for few-layer graphene and nanofluids. Then, all experimental devices and procedures used for graphene characterization, for stability evaluation and thermo-physical properties measurements of nanofluids have been fully described. The results of this wide experimental campaign are described in the next chapter.

**Acknowledgements:** Part of the experimental work performed in this study was made possible thanks to the European Union through the European Regional Development Fund (ERDF), the Ministry of Higher Education and Research, the French region of Brittany and Rennes Métropole that supported the purchase of thermal conductivity, density, and surface tension experimental devices. EU COST through the STMS grant ref. COST-STSM-CA15119- 45590 allowed the density and isobaric heat capacity measurements of materials to be performed by Samah Hamze in Universidade de Vigo.

### III.9- References

1. Berrada, N.; Hamze, S.; Desforges, A.; Ghanbaja, J.; Gleize, J.; Maré, T.; Vigolo, B.; Estellé, P. Surface tension of functionalized MWCNT-based nanofluids in water and commercial propylene-glycol mixture. *Journal of Molecular Liquids* **2019**, *293*, 111473, doi:10.1016/j.molliq.2019.111473.
2. Tyfocor LS technical information, available at <https://tyfo.de/en/produkt/Tyfocor-ls/> (n.d.).
3. Hamze, S.; Berrada, N.; Cabaleiro, D.; Desforges, A.; Ghanbaja, J.; Gleize, J.; Bégin, D.; Michaux, F.; Maré, T.; Vigolo, B.; et al. Few-Layer Graphene-Based Nanofluids with Enhanced Thermal Conductivity. *Nanomaterials* **2020**, *10*, 1258, doi:10.3390/nano10071258.
4. Oyinlola, M.A.; Shire, G.S.F.; Moss, R.W. Thermal analysis of a solar collector absorber plate with microchannels. *Experimental Thermal and Fluid Science* **2015**, *67*, 102–109, doi:10.1016/j.expthermflusci.2014.10.014.
5. Borode, A.O.; Ahmed, N.A.; Olubambi, P.A. Surfactant-aided dispersion of carbon nanomaterials in aqueous solution. *Physics of Fluids* **2019**, *31*, 071301, doi:10.1063/1.5105380.
6. Guardia, L.; Fernández-Merino, M.J.; Paredes, J.I.; Solís-Fernández, P.; Villar-Rodil, S.; Martínez-Alonso, A.; Tascón, J.M.D. High-throughput production of pristine graphene in an aqueous dispersion assisted by non-ionic surfactants. *Carbon* **2011**, *49*, 1653–1662, doi:10.1016/j.carbon.2010.12.049.
7. Hummers, W.S.; Offeman, R.E. Preparation of Graphitic Oxide. *Journal of the American Chemical Society* **1958**, *80*, 1339–1339, doi:10.1021/ja01539a017.
8. Kairi, M.I.; Dayou, S.; Kairi, N.I.; Bakar, S.A.; Vigolo, B.; Mohamed, A.R. Toward high production of graphene flakes – a review on recent developments in their synthesis methods and scalability. *J. Mater. Chem. A* **2018**, *6*, 15010–15026, doi:10.1039/C8TA04255A.
9. Hernandez, Y.; Nicolosi, V.; Lotya, M.; Blighe, F.M.; Sun, Z.; De, S.; McGovern, I.T.; Holland, B.; Byrne, M.; Gun'Ko, Y.K.; et al. High-yield production of graphene by liquid-phase exfoliation of graphite. *Nature Nanotechnology* **2008**, *3*, 563–568, doi:10.1038/nnano.2008.215.
10. Ershova, O.V.; Lillestolen, T.C.; Bichoutskaia, E. Study of polycyclic aromatic hydrocarbons adsorbed on graphene using density functional theory with empirical dispersion correction. *Phys. Chem. Chem. Phys.* **2010**, *12*, 6483, doi:10.1039/c000370k.

11. Schmaltz, B.; Weil, T.; Müllen, K. Polyphenylene-Based Materials: Control of the Electronic Function by Molecular and Supramolecular Complexity. *Adv. Mater.* **2009**, *21*, 1067–1078, doi:10.1002/adma.200802016.
12. Murshed, S.M.S.; Leong, K.C.; Yang, C. Enhanced thermal conductivity of TiO<sub>2</sub>-water based nanofluids. *International Journal of Thermal Sciences* **2005**, *44*, 367–373, doi:10.1016/j.ijthermalsci.2004.12.005.
13. Banisharif, A.; Aghajani, M.; Van Vaerenbergh, S.; Estellé, P.; Rashidi, A. Thermophysical properties of water ethylene glycol (WEG) mixture-based Fe<sub>3</sub>O<sub>4</sub> nanofluids at low concentration and temperature. *Journal of Molecular Liquids* **2020**, *302*, 112606, doi:10.1016/j.molliq.2020.112606.
14. Zeroual, S.; Estellé, P.; Cabaleiro, D.; Vigolo, B.; Emo, M.; Halim, W.; Ouaskit, S. Ethylene glycol based silver nanoparticles synthesized by polyol process: Characterization and thermophysical profile. *Journal of Molecular Liquids* **2020**, *310*, 113229, doi:10.1016/j.molliq.2020.113229.
15. Zeroual, S.; Estellé, P.; Cabaleiro, D.; Vigolo, B.; Emo, M.; Halim, W.; Ouaskit, S. Ethylene glycol based silver nanoparticles synthesized by polyol process: Characterization and thermophysical profile. *Journal of Molecular Liquids* **2020**, *310*, 113229, doi:10.1016/j.molliq.2020.113229.
16. Sengers, J.V.; Watson, J.T.R. Improved International Formulations for the Viscosity and Thermal Conductivity of Water Substance. *Journal of Physical and Chemical Reference Data* **1986**, *15*, 1291–1314, doi:10.1063/1.555763.
17. American Society of Heating, R. and A.-C.E. *ASHRAE handbook: heating, ventilating, and air-conditioning applications*; ASHRAE: Atlanta, Ga., 2012; ISBN 978-1-62198-036-0.
18. Żyła, G.; Vallejo, J.P.; Lugo, L. Isobaric heat capacity and density of ethylene glycol based nanofluids containing various nitride nanoparticle types: An experimental study. *Journal of Molecular Liquids* **2018**, *261*, 530–539, doi:10.1016/j.molliq.2018.04.012.
19. Xu, S.X.; Li, Y.; Feng, Y.P. Study of temperature profile and specific heat capacity in temperature modulated DSC with a low sample heat diffusivity. *Thermochimica Acta* **2000**, *360*, 131–140, doi:10.1016/S0040-6031(00)00564-5.
20. Cabaleiro, D.; Gracia-Fernández, C.; Legido, J.L.; Lugo, L. Specific heat of metal oxide nanofluids at high concentrations for heat transfer. *International Journal of Heat and Mass Transfer* **2015**, *88*, 872–879, doi:10.1016/j.ijheatmasstransfer.2015.04.107.
21. Halelfadl, S.; Estellé, P.; Aladag, B.; Doner, N.; Maré, T. Viscosity of carbon nanotubes water-based nanofluids: Influence of concentration and temperature. *International Journal of Thermal Sciences* **2013**, *71*, 111–117, doi:10.1016/j.ijthermalsci.2013.04.013.
22. Halelfadl, S.; Estellé, P.; Aladag, B.; Doner, N.; Maré, T. Viscosity of carbon nanotubes water-based nanofluids: Influence of concentration and temperature. *International Journal of Thermal Sciences* **2013**, *71*, 111–117, doi:10.1016/j.ijthermalsci.2013.04.013.
23. Vargaftik, N.B.; Volkov, B.N.; Voljak, L.D. International Tables of the Surface Tension of Water. *Journal of Physical and Chemical Reference Data* **1983**, *12*, 817–820, doi:10.1063/1.555688.
24. Gómez-Villarejo, R.; Aguilar, T.; Hamze, S.; Estellé, P.; Navas, J. Experimental analysis of water-based nanofluids using boron nitride nanotubes with improved thermal properties. *Journal of Molecular Liquids* **2019**, *277*, 93–103, doi:10.1016/j.molliq.2018.12.093.

25. Cabaleiro, D.; Estellé, P.; Navas, H.; Desforges, A.; Vigolo, B. Dynamic Viscosity and Surface Tension of Stable Graphene Oxide and Reduced Graphene Oxide Aqueous Nanofluids. *j nanofluids* **2018**, 7, 1081–1088, doi:10.1166/jon.2018.1539.



# **Chapter IV- Characterization of FLG based nanofluids and their thermophysical properties: results and discussion**

IV.1- Introduction.....	112
IV.2- Few-Layer Graphene-Based Nanofluids with Enhanced Thermal Conductivity.....	114
IV.3- Isobaric heat capacity.....	136
IV.4- Volumetric properties and surface tension of few-layer graphene nanofluids based on a commercial heat transfer fluid.....	144
IV.5- Shear flow behavior and dynamic viscosity of few-layer graphene nanofluids based on propylene glycol-water mixture.....	163
IV.6- Conclusion.....	176

## **IV.1- Introduction**

As reported in Chapter II from numerous examples, the addition of the graphene considerably modifies the thermo-physical properties of the base fluid. Indeed, the insertion of graphene nanosheets in the base fluid improves the thermal conductivity of the nanofluid but can also lead to an unfavorable increase in dynamic viscosity and relatively modify the density, the isobaric heat capacity and the surface tension of this fluid. In the absence of reliable relationships and models to theoretically predict the evolution of these properties, it is therefore necessary to consider an experimental characterization with nanofluids in order to better control the solution used.

This chapter presents the comprehensive description and the analysis of the experimental characterization of the graphene (FLG) and the graphene-based nanofluids studied. The results include stability of nanofluids (at rest and under shear) and thermophysical properties evaluation (thermal conductivity, isobaric heat capacity, density, surface tension, and dynamic viscosity) following the experimental procedures described in the previous chapter. An analysis of the results is rigorously developed to study the influence of FLG volume fraction, temperature, surfactant type and concentration on the thermo-physical properties of FLG based nanofluids thus evaluated. The results are also compared and discussed with respect to some existing models described in Chapter II, by proposing improvements and interpretations based on the trends obtained. Most of the presented results and discussion have been published in peer-reviewed international scientific Journals with the following references and compose this chapter.

- S. Hamze *et al.*, “Few-Layer Graphene-Based Nanofluids with Enhanced Thermal Conductivity,” *Nanomaterials*, vol. 10, no. 7, p. 1258, Jun. 2020, doi: 10.3390/nano10071258. Open Access
- S. Hamze *et al.*, “Volumetric Properties and Surface Tension of Few-Layer Graphene Nanofluids Based on a Commercial Heat Transfer Fluid,” *Energies*, vol. 13, no. 13, p. 3462, Jul. 2020, doi: 10.3390/en13133462. Open Access
- S. Hamze *et al.*, “Shear flow behavior and dynamic viscosity of few-layer graphene nanofluids based on propylene glycol-water mixture,” *Journal of Molecular Liquids*, vol. 316, p. 113875, Oct. 2020, doi: 10.1016/j.molliq.2020.113875. Open Access

The first paper presents the synthesis of FLG and their characterization, the nanofluids stability, and the thermal conductivity results of the FLG-based nanofluids. The volumetric properties (density and isobaric thermal expansivity) and the surface tension of the studied nanofluids are presented in the second paper. Finally, the last paper includes the rheological behavior results and the dynamic viscosity of the graphene nanofluids. The study of the isobaric heat capacity of nanofluids is presented independently after the first paper.

A general presentation of the main results and conclusions is finally proposed at the end of the chapter.

## **IV.2- Few-Layer Graphene-Based Nanofluids with Enhanced Thermal Conductivity**



Article

# Few-Layer Graphene-Based Nanofluids with Enhanced Thermal Conductivity

Samah Hamze <sup>1</sup>, Nawal Berrada <sup>2</sup>, David Cabaleiro <sup>1,3</sup>, Alexandre Desforges <sup>2</sup>, Jaafar Ghanbaja <sup>2</sup>, Jérôme Gleize <sup>4</sup>, Dominique Bégin <sup>5</sup>, Florentin Michaux <sup>6</sup>, Thierry Maré <sup>1</sup>, Brigitte Vigolo <sup>2</sup> and Patrice Estellé <sup>1,\*</sup>

<sup>1</sup> Laboratoire de Génie Civil et Génie Mécanique, Université de Rennes, F-35000 Rennes, France; samah.hamze@univ-rennes1.fr (S.H.); dacabaleiro@uvigo.es (D.C.); thierry.mare@univ-rennes1.fr (T.M.)

<sup>2</sup> Institut Jean Lamour UMR7198, CNRS, Université de Lorraine, F-54000 Nancy, France; nawal.berrada@univ-lorraine.fr (N.B.); alexandre.desforges@univ-lorraine.fr (A.D.); jaafar.ghanbaja@univ-lorraine.fr (J.G.); brigitte.vigolo@univ-lorraine.fr (B.V.)

<sup>3</sup> Dpto. Física Aplicada, Facultad de Ciencias, Universidade de Vigo, 36310 Vigo, Spain

<sup>4</sup> Laboratoire de Chimie et Physique Approche Multi-échelles des Milieux Complexes, Université de Lorraine F-57000 Metz, France; jerome.gleize@univ-lorraine.fr

<sup>5</sup> Institut de Chimie et Procédés pour l'Energie, l'Environnement et la Santé (ICPEES) CNRS-University of Strasbourg, 25, rue Becquerel, 67087 Strasbourg CEDEX, France; dominique.begin@unistra.fr

<sup>6</sup> Laboratoire d'Ingénierie des Biomolécules, Université de Lorraine, 2, avenue de la Forêt de Haye, 54500 Vandoeuvre-lès-Nancy, France; florentin.michaux@univ-lorraine.fr

\* Correspondence: patrice.estelle@univ-rennes1.fr; Tel.: +33-022-323-4200

Received: 8 June 2020; Accepted: 25 June 2020; Published: 28 June 2020

**Abstract:** High-quality graphene is an especially promising carbon nanomaterial for developing nanofluids for enhancing heat transfer in fluid circulation systems. We report a complete study on few layer graphene (FLG) based nanofluids, including FLG synthesis, FLG-based nanofluid preparation, and their thermal conductivity. The FLG sample is synthesized by an original mechanical exfoliation method. The morphological and structural characterization are investigated by both scanning and transmission electron microscopy and Raman spectroscopy. The chosen two-step method involves the use of three nonionic surfactants (Triton X-100, Pluronic® P123, and Gum Arabic), a commercial mixture of water and propylene glycol and a mass content in FLG from 0.05 to 0.5%. The thermal conductivity measurements of the three FLG-based nanofluid series are carried out in the temperature range 283.15–323.15 K by the transient hot-wire method. From a modeling analysis of the nanofluid thermal conductivity behavior, it is finally shown that synergetic effects of FLG nanosheet size and thermal resistance at the FLG interface both have significant impact on the evidenced thermal conductivity enhancement.

**Keywords:** few-layer graphene; propylene-glycol/water; nanofluids; thermal conductivity; temperature effect; concentration influence; theoretical prediction

## 1. Introduction

The growth in energy consumption pushes us to make an energy transition to low carbon generation and design more efficient utilization approaches, which requires a research effort focused on the development of innovative, intelligent, durable, and effective solutions [1]. Heat transfer plays an important role in many industrial processes, such as electronic and thermoelectric devices, refrigerators, heat exchangers, solar energy systems, heating and cooling of buildings, among others [2–5]. In such applications, the low inherent thermal conductivity of most conventional thermal media can become the main limitation in improving performances and reducing energy consumption

[6]. Because solids have intrinsic thermal properties higher than conventional heat transfer fluids, like water, ethylene glycol, and engine oil; it was proposed to disperse millimetric and micrometric solid particles within standard fluids to enhance their thermal properties. The idea of “nanofluids” appeared in 1995 by Choi et al. [7], who introduced the use of nanosized particles, which makes the solutions more stable than when bigger particles are used because of the size effect and the Brownian motion of the nanoparticles in the fluid [8]. Nanoparticles do not only stay suspended much longer in the base fluid than micron-sized suspensions [9]; as compared with microparticles, their surface to volume ratio of nanoparticles is much higher (~1000 times) [6]. This, in turn, allows for obtaining much better thermal properties in the case of nanofluids rather than colloidal suspensions of microparticles or the base fluids alone. Over the last decades, many scholars focused on the investigation of nanometric particle suspensions [10–18]. The key issues in nanofluid research are to prepare stable solutions and increase the thermal conductivity of the liquid, without a significant increase in viscosity that could penalize pumping power [19].

Many factors have been reported to affect the thermal conductivity of a nanofluid, such as temperature [20,21], particle size [22,23], particle shape [24], concentration of nanoparticles [25], and addition and type of surfactant [26,27]. For that, the researchers studied different types of nanofluids based on various thermal fluids and containing a wide selection of nanoparticles, such as metal oxides [28–32], metallic nanoparticles [33,34], or carbon nanomaterials [35–41]. Since 2004, when Novoselov et al. [42] first isolated graphene, this material has been proposed for many interesting applications, owing to its excellent physical, chemical, and mechanical features [10]. The researchers investigated many nanofluids based on graphene, as this carbon allotrope exhibits high intrinsic thermal properties, with thermal conductivities of several order higher than other types of nanomaterials [43]. For example, Gupta et al. [44] compared different water based nanofluids that differed by the nanoparticle type, and showed that their graphene based nanofluids had the highest thermal conductivity enhancement, with a maximum value equal to 27% at 0.2 vol.%. Gao et al. [45] obtained an increase of the thermal conductivity of their graphene nanofluids based on ethylene glycol, ethylene glycol:water (1:1), and water, by 4.6, 18, and 6.8%, respectively (in all three cases with a 0.15 wt.% content of graphene). On the other hand, functionalized graphene nanosheets were dispersed by Vallejo et al. [46] in a mixture of propylene glycol:water (30:70) wt.%. The thermal conductivity results showed an enhancement about 16% at the maximum weight concentration 1%. In addition, Seong et al. [35] prepared 0.1 wt.% of graphene water-based nanofluids (7 nm of thickness and size about 40 nm) where sodium dodecyl sulfate (SDS) and sodium dodecyl benzene sulphonate (SDBS) were added separately as surfactants. The investigated graphene:surfactant ratios were 1:3, 1:2, 1:1, 2:1, 2:1, and 3:1. Their measurements have shown that the thermal conductivity decreased with increasing the amount of surfactant in the sample. In addition, the authors found that, with 1:3 and 1:2 of graphene:surfactant, nanofluids with SDS had a lower conductivity than with SDBS, while, with the graphene:surfactant ratios lower than 1:1, SDS showed a thermal conductivity greater than for SDBS, and a maximum improvement was achieved in the case of the graphene:SDS ratio of 2:1. Bahaya et al. [38] focused on the graphene nanosheets (diameter 5  $\mu\text{m}$  and thickness 3 nm) dispersed in water with the addition of gelatin to prevent the sedimentation. The authors prepared their nanofluids with nanoparticle concentrations up to 0.014% in volume. A maximum relative thermal conductivity equal to 1.43 was obtained at the higher concentration. Graphene based nanofluids can also differ in terms of treatment applied to graphene and it is generally admitted that the thermophysical properties depend on these treatments and dispersion methods. While previous studies mainly focused on graphene oxide (GO), reduced GO (rGO), or functionalized graphene, only few studies have been reported about the use of few layer graphene to produce and characterize nanofluids.

Sun et al. studied the exfoliation of pristine graphite into few layer graphene (FLG) while using acrylate polymer solutions in low boiling point alcohols [47]. The authors proved the effectiveness of acrylate polymers to exfoliate a few layers graphene and obtain stable suspensions in both ethanol and isopropanol. Thermal conductivity measurements at different temperatures from 283.15 to 333.15 K showed a quasi-constant enhancement (around 25%) for low nanofluid volume concentration of

0.055% in ethanol. Amiri et al. investigated a water based highly crumpled few layer graphene (HFLG) nanofluids where the nanoparticles were mixed with Gum Arabic (GA) by a GA:HFLG ratio of 0.5:1 [48]. With increasing the weight concentration of the nanofluid from 0 to 0.01%, an enhancement of 42.5% was obtained at 323.15 K. In addition, the authors found that the thermal conductivity increased by 8.6, 20.8, 23.8, and 21.9% for deionized water and nanofluids concentrations 0.001, 0.005, and 0.01 wt.%, respectively, with temperature increasing from 283.15 to 323.15 K. Amiri et al. focused on mono-layer graphene nanoparticles dispersed in water with different weight contents between 0.005 and 0.01% [49]. They found an increase in thermal conductivity values with increasing temperature from 283.15 to 323.15 K. The results showed an enhancement in the thermal conductivity of nanofluids by more than 25% for different temperatures and weight fraction of 0.01%. Alawi et al. recently presented a new method to prepare covalent-functionalized FLG based on a thermal treatment using pentaethylene glycol [50,51]. Water-based nanofluids containing various concentrations of functionalized FLG (0.025–0.1 wt.%) were characterized in terms of temporal stability and thermo-physical properties. A maximum enhancement in the thermal conductivity of 31% was observed at 323.15 K for the highest nanoparticle concentration (0.1 wt.%).

We report, in this study, the preparation and the comprehensive characterization of FLG prepared from an ecofriendly mechanical exfoliation method presented here for the first time as a contribution of graphene-based nanofluid development for heat transfer applications, and the use of FLG in particular that still remains weakly investigated. The as-produced high-quality FLG is used for the production of graphene based-nanofluids prepared with a commercial heat transfer fluid, namely Tyfocor® LS, which is a mixture of propylene glycol:water (40:60) wt.% [52]. These nanofluids were produced when considering Triton X-100, Pluronic® P-123, and Gum Arabic as surfactants. The stability at rest of the nanofluids was analyzed by Turbiscan and their thermal conductivity was measured and analyzed with regard to the kind of the used surfactant, temperature (283.15–323.15 K), and concentration of graphene (0.05, 0.1, 0.25, and 0.5 wt.%). Finally, the thermal conductivity of the FLG-based nanofluids was analyzed with relevant models while taking the influence of several parameters, such as the average length, interfacial thermal resistance, thickness, or flatness ratio of FLG, into consideration in order to provide a further insight that could help to understand the reasons behind the thermal conductivity enhancements in such prepared graphene-based nanofluids.

## 2. Materials and Methods

### 2.1. Materials

FLG was synthesized by a mechanical exfoliation method that was assisted by tannic acid. Typically, 200 mg of tannic acid (Sigma–Aldrich, Lyon, France) was dissolved in 400 mL of deionized water, and then 400 mg of expanded graphite (provided by Mersen, Courbevoie, France) was added in the beaker in which a sonication probe (Branson Ultrasonics™ Sonicator 400W) was plunged. Sonication (80 W, 50 kHz, continuous mode) was performed for 4 hours at 298.15 K.

The prepared FLG pre-dispersed in the aqueous tannic solution was washed with DW before freeze-drying. Typically, 250 mL of the FLG solution was placed in a vacuum filtration set-up and then filtered on a membrane of 0.45 µm porosity (Merck Millipore, Darmstadt, Germany) and washed five times with 250 mL of DW. After freeze-drying, the obtained FLG powder was ready for analysis and nanofluid preparation. The FLG graphene produced for each batch and following this method is around 300 mg, which means that the production yield is around 80%.

Graphite powder, namely TIMCAL TIMREX® SFG6 Primary Synthetic Graphite (Timcal Inc., Westlake, OH, USA), was used for comparison with the as produced FLG for Raman spectroscopy. A commercial water-propylene glycol-based heat transfer fluid, namely Tyfocor® LS (referred to Tyfocor in the following figures and text) was gently provided by Viessmann S.A. and it was used for nanofluid preparation. Tyfocor® LS consists in a mixture of propylene glycol:water with 40:60 wt.% [52]. This heat transfer fluid was selected, as it is a ready-to-use industrial material containing corrosion and ageing inhibitors. Nonionic surfactants such as Triton X-100 (Sigma Aldrich,

Germany), Pluronic® P123 (Sigma Aldrich, Saint-Quentin Fallavier, France), and Gum Arabic (Acros Organics, Illkirch, France) have been selected for the nanofluid preparation, because they have been reported to have good ability to disperse carbon nanomaterials [53,54]. Actually, the use of surfactants is an effective approach for efficiently unbundling nanoparticles and ensuring nanofluid stability without altering the pristine graphene structure [55]. Ionic surfactants have proven effective to provide good dispersibility of carbon-based nanoparticles in water. However, those ionic surfactants may lead to the formation of foam inside thermal facilities, which, in turn, may reduce the effective surface of heat transfer and, consequently, thermal performance. Unlike some ionic surfactants, non-ionic surfactant, such as Gum Arabic, do not create foam when agitated [53]. Among the surfactants containing non-ionic block copolymers, Triton X series (Triton X-100 or Triton X-405, for instance) [56–58] or Gum Arabic (GA) [57,59–61] have been the most common when preparing surfactant-aid graphene nanofluids. Moreover, as compared with other surfactants (SDS, CTAC, or PVP), Triton X-100 surfactant aqueous solutions seem to be more effective to enhance the thermal performance of pulsating heat pipes, for example [62]. Pluronic® P-123 was proven to be an effective surfactant to prepare graphene dispersions in water, methanol, ethanol, 1-hexano, or ethylene glycol (in comparison with equivalent graphene:surfactant ratios of SDS, CTAB, or Triton-X). In addition, such non-ionic surfactant is biodegradable and economical and does not lead to any foam formation, which makes it an interesting alternative to design graphene nanofluids [63].

For each surfactant, nanofluids with 0.5 wt.% of FLG were first prepared from the two-step method by adding the desired amount of surfactant to Tyfocor® LS, respectively 1 wt.%, and then introducing the right amount of FLG powder within this mixture. Afterwards, the nanofluid sample with 0.5 wt.% in FLG was sonicated while using a probe sonicator (Bioblock Scientific Vibra cell 75042, 125 W with a pulse mode 2 s ON/1 s OFF) for  $5 \times 15$  min. controlling also the temperature of the sample to avoid overheating effects. This nanofluid was then diluted with Tyfocor to obtain nanofluid samples with lower FLG concentrations: 0.25, 0.1, and 0.05 wt.%. These samples were also sonicated following the same procedure after dilution. Consequently, the ratio of surfactant/FLG was similar and equal to 2 for the three prepared nanofluid series. A similar procedure was used for each surfactant (Triton X-100, Pluronic® P123 or Gum Arabic).

## 2.2. Characterization Techniques

Scanning electron microscopy (SEM) analysis was carried out using a XL30 S-FEG apparatus. Transmission electron microscopy (TEM) and high-resolution TEM (HRTEM) observations were performed using a JEM-ARM 200F apparatus at a low accelerating voltage (80 kV) to avoid possible damaging by the electron beam. Holey carbon grids (200 mesh size) were used, so that the image contrast could be improved for this all-carbon nanomaterial. Approximately 30 images were taken at different areas for each sample to guarantee statistically representative observations. Fast Fourier Transform (FFT) and Inverse FFT (IFFT) were calculated on the selected area of FLG images by using Digital micrograph software.

A LabRAM HR 800 micro-Raman spectrometer was used for Raman spectroscopy analysis. The incident wavelength was a red light at  $\lambda = 632.8$  nm. For the analysis, the FLG was gently dispersed in ethanol by means of a sonication bath and then deposited on a glass slide. At least five spectra were recorded for each sample. For data analysis, a baseline was first subtracted and the height of the D band was divided by that of the G band to calculate the  $I_D/I_G$  intensity ratio.

In an original way, nanofluids stability against sedimentation was followed by multiple light scattering measurements using a Turbiscan Classic MA2000 apparatus (Formulation, Toulouse, France) using a pulsed near infrared light source ( $\lambda = 850$  nm). Two synchronous detectors measured transmitted and backscattered light upon sample height by several scans by up movements (every 40  $\mu\text{m}$ ) all along a glass cylindrical cell until the top of the sample (5–7 cm). In the case of nanofluid dispersions, only the transmitted light intensity has been followed upon sample height, since no backscattered light has been detected due to black particles light absorption. Additionally, only the nanofluids with the two lowest FLG concentrations were analyzed. For the high FLG concentration nanofluids, the light transmission was too low to obtain reliable measurements. Transmitted

intensities all along the sample height have then been recorded upon time. Scans have been recorded during five days after particles dispersion ( $t_0$ ). The first scan recorded at  $t_0$  has been removed to the followings in order to highlight the system evolution upon time using Turbisoft software (version 1.2.2, FormulAction, Toulouse, France). Subsequently, the relative percentage of transmitted intensity ( $\Delta BS$ ) upon sample height has been reported and its evolution upon time has also been visualized while using this software. A sedimentation phenomenon is then characterized by an increase of the transmitted light at the top of the sample upon time until every particle settles. The transmitted signal then remains constant. The sedimentation rate was calculated by considering that the height of the sediment at five days (longest time) corresponded to the final sedimentation state. The Turbiscan measurements have been performed at room temperature.

The density of FLG was measured at ambient temperature while using a Quantachrome gas pycnometer Ultrapyc 1200e (Quantachrome Instruments, Anton Paar, USA) working with helium under a pulse mode suitable for powders. Before starting measurements, the device was calibrated to an accuracy of  $\pm 0.002 \text{ cm}^3$  using two standard steel spheres ( $1.0725 \text{ cm}^3$  each one). An absolute average deviation (AAD) of 0.66% was found between the volume measurements with the instrument and their real volume ( $2.145 \text{ cm}^3$ ). For the measurements of FLG density, a micro cell of  $4.5 \text{ cm}^3$  was used and the FLG sample was carefully weighted with a precision balance. A true density value of  $1.82 \pm 0.02 \text{ g/cm}^3$  was finally obtained. This value will be considered later in order to evaluate the thermal conductivity of FLG and the FLG volume fraction used in thermal conductivity models for nanofluids.

The thermal conductivity of the dry FLG nanopowder was obtained by means of a Direct Thermal Conductivity-meter DTC-25 (TA instruments, New Castle) working with the guarded heat flow meter technique according to the Standard Test Method proposed in the ASTM E1530 [64]. This device is suitable for studying thermal conductivities from  $0.1$  to  $20 \text{ W}\cdot\text{m}^{-1}\cdot\text{K}^{-1}$  at an ambient temperature. A manual press B13142 Graseby Specac (Specac Ltd., Orpington, U.K.) was used to compact the dry nanopowder and create a disk  $50 \text{ mm}$  in diameter. Thermal conductivity results with this device have an experimental accuracy of 6% and repeatability of 2%. Additional details regarding this instrument or the followed experimental procedure can be found in [65].

The thermal conductivity of both base fluids and nanofluids was evaluated with a THW-L2 device (Thermtest Inc., Richibucto Road, NB, Canada) using the transient short hot-wire method according to the ASTM D7896 standard. This device has been designed to measure the thermal conductivity of liquids in the range  $0.01$ - $2 \text{ W}\cdot\text{m}^{-1}\cdot\text{K}^{-1}$  under short time of measurement to avoid convection. The full description of the experimental set-up has been previously reported in [66,67] and a similar experimental procedure has been followed. A power supply varying between  $90$  and  $110 \text{ mW}$ , to reach a temperature rise of  $1.2 \text{ K}$ , has been applied here to samples with a time measurement of  $1.5 \text{ s}$  for thermal conductivity evaluation. This value has been classically calculated in the linear region of the temperature enhancement versus time in logarithm scale. The temperature probe and the wire of the sensor have been calibrated with DW (DIUF, CAS 1132-18-5, Fisher Chemical,  $0.599 \text{ W}\cdot\text{m}^{-1}\cdot\text{K}^{-1}$  at  $293.15 \text{ K}$ ) before measurements [67]. Once the device calibrated, the thermal conductivity of deionized water has been measured in the temperature range  $278.15$ - $333.15 \text{ K}$ , as shown in Figure 1, in order to evaluate the experimental uncertainty of the device. These data have been compared to reference values [56]. A really good agreement was achieved, with an average absolute deviation (AAD) around 1%, as evidenced by Figure 1. As for DW, thermal conductivity values of base fluids and nanofluids presented in the following consist in an average of at least six measurements with  $5 \text{ min.}$  between each test for each tested temperature. A total of 25 different samples, including pure Tyfocor® LS, base fluids (three Tyfocor+surfactant series containing 0.1, 0.2, 0.5 and 1 wt.% concentrations of either Triton-X100, Triton X-100, Pluronic® P-123, Gum Arabic), and nanofluids (three FLG+Tyfocor+surfactant series containing 0.05, 0.1, 0.25, and 0.5 wt.% loadings of FLG) have been tested. This leads to at least 750 data points.

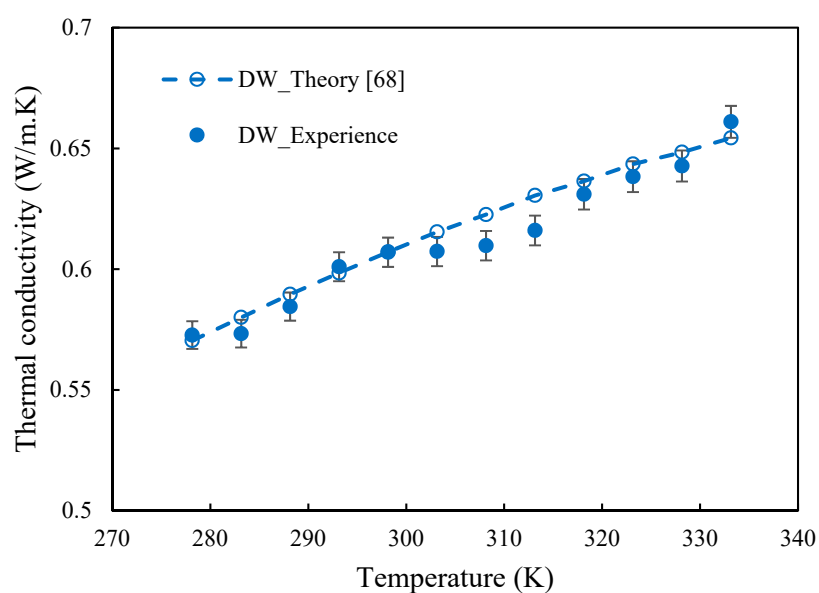
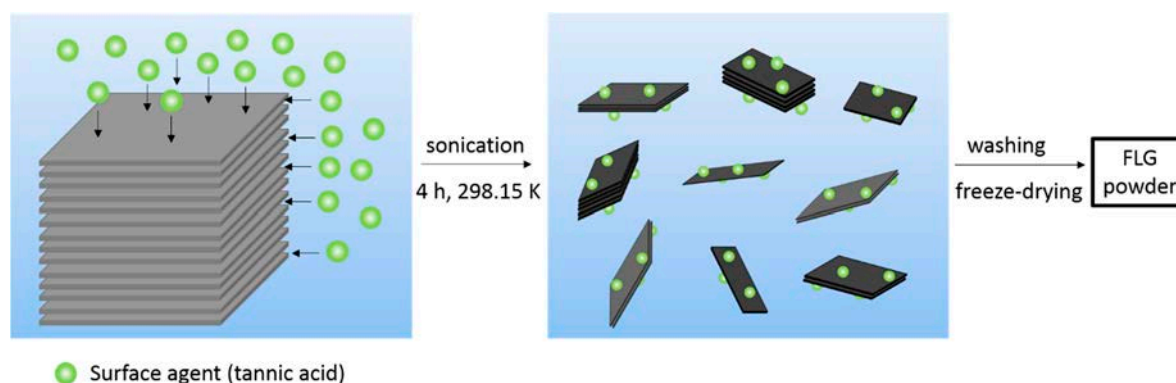


**Figure 1.** Comparison between the experimental thermal conductivity of DW and reference values extracted from [68]. Error bars indicate average absolute deviation between experiments and reference values in the temperature range 278.15–333.15 K.

### 3. Results and Discussion

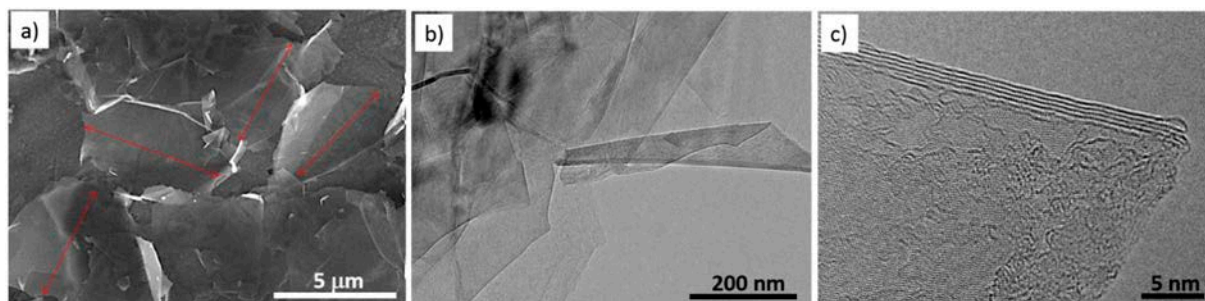
#### 3.1. Few-layer Graphene Synthesis and Characterization

When compared to the Hummers' method [69], bulk synthesis of graphenic materials from mechanical exfoliation of graphite or expanded graphite [70] assisted by sonication produced graphene with better structural quality. Aqueous media were advantageously non-toxic and easier to handle as compared to the methods using organic solvents [71]. Surfactants, such as polycyclic aromatic hydrocarbons, have shown high ability to assist graphene exfoliation due to strong  $\pi$ - $\pi$  interactions [72,73]. For the first time in the literature, here we propose assisting aqueous exfoliation of expanded graphite by biosourced surfactants, such as tannic acid, in a whole green process. Tannic acid, a phenolic acid ( $C_{76}H_{52}O_{46}$ ), has the double positive role of i) inducing  $\pi$ - $\pi$  interactions between its  $C_6$  rings and those of the graphene surface assisting that way tannic acid intercalation between graphene sheets together with ii) facilitating graphene nanosheet dispersion in water thanks to the OH groups that acid tannic belongs (see Figure 2). Such a green procedure can be very suitable to nanofluid preparation requiring a relatively high amount of nanomaterials.



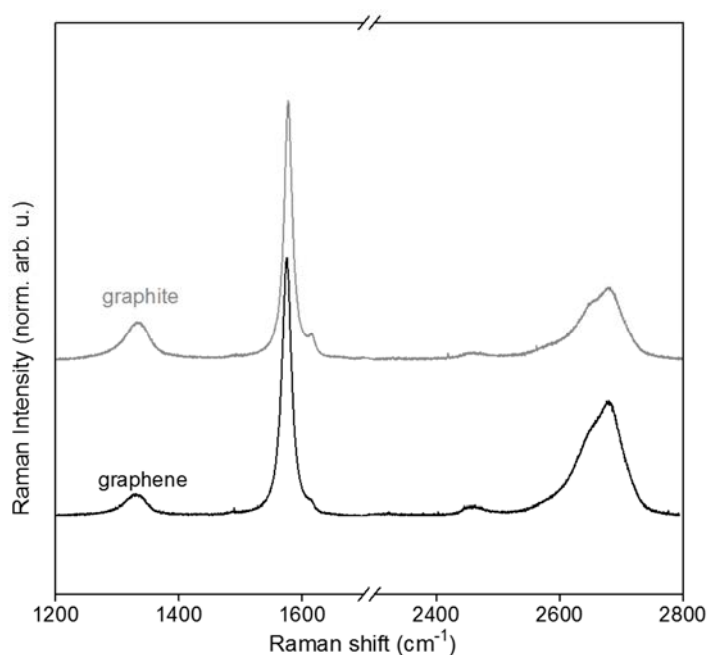
**Figure 2.** Schematic of the mechanical exfoliation method in aqueous medium assisted with tannic acid.

Figure 3 shows the SEM and TEM images of the synthesized graphenic material. SEM (Figure 3a) and TEM low magnification observation images (Figure 3b) both show that the prepared material is under the form of very thin sheets of about 3–5 layers with a thickness typically between 1 and 2 nm (typical image shown in Figure 3c), meaning that the used exfoliation method preferentially produced FLG [74]. The mean lateral size of the FLG sheets was found around 5  $\mu\text{m}$  on average, as evidenced in Figure 3a.



**Figure 3.** Scanning electron microscopy (SEM) (a), Transmission electron microscopy (TEM) (b), and (c) images of the synthesized few-layer graphene (FLG).

HRTEM and Raman spectroscopy are commonly used as complementary techniques to finely probe the structural quality of nanostructured carbon materials. Figure 4 shows a typical spectra of high-quality graphite (SFG6) and the FLG used in this study. The most intense peak is the G band that originates from the  $\text{sp}^2$  bonded carbon atoms of the hexagonal lattice of a graphitic structure, and it is well visible around  $1580\text{ cm}^{-1}$  [75]. The D band, around  $1350\text{ cm}^{-1}$ , is related to  $\text{sp}^3$  defects present in the  $\text{sp}^2$  carbon atom network [76].  $I_D/I_G$  is relatively low for both samples and the  $I_D/I_G$  of graphite is higher than that of FLG, meaning that this latter was of high structural quality. The 2D band, around  $2700\text{ cm}^{-1}$ , of higher intensity for FLG is in agreement with the few layer nature of the used graphenic material (Figure 3c). In agreement with Raman spectroscopy, HRTEM, FFT, and IFFT images (Figure 5a–c, respectively) have shown the used FLG has an excellent structural quality with its well noticeable honeycomb carbon atom network [77].



**Figure 4.** Raman spectra of FSG6 “graphite” and produced few layer “graphene” FLG.

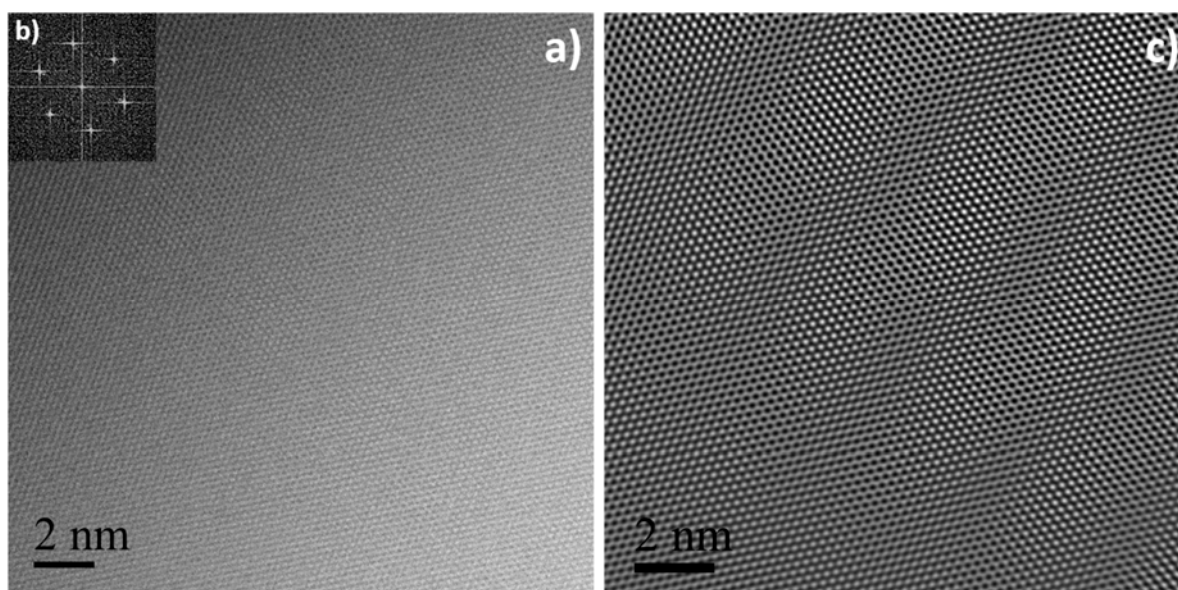


**Figure 5.** High-resolution TEM (HRTEM) image of FLG (a), corresponding Fast Fourier Transform (FFT) (b), and Inverse FFT (IFFT) (c).

### 3.2. Stability at Rest of the Prepared FLG-based Nanofluids

Static stability of the FLG-based nanofluids was followed over time by both visual observations and Turbiscan analysis. Turbiscan allowed for measuring sedimentation evolution within the FLG based nanofluids that were prepared with Triton X-100 and Pluronic® P123 (Figure 6b). In the case of these two nanofluid series, the sedimentation behavior was not modified by the FLG concentration. Complete sedimentation was more rapid for Triton X-100 than for Pluronic® P123. Sedimentation of the FLG nanoparticles was completed after one day with Triton X-100 while with Pluronic® P123, sedimentation of FLG was reached three days after the nanofluid preparation (Figure 6b). Unfortunately, a reliable analysis was not possible with Gum Arabic, while this nanofluid was visually observed more stable than the two others. It should be finally mentioned that the thermal conductivity values of nanofluids reported thereafter are obtained after sample preparation. Their dispersion state is stable for the whole measurement run period. Indeed, if a sedimentation was occurring during the measurements, a decrease of the thermal conductivity would be detected during the experiment, as has been observed for unstable GO-based nanofluids [78].

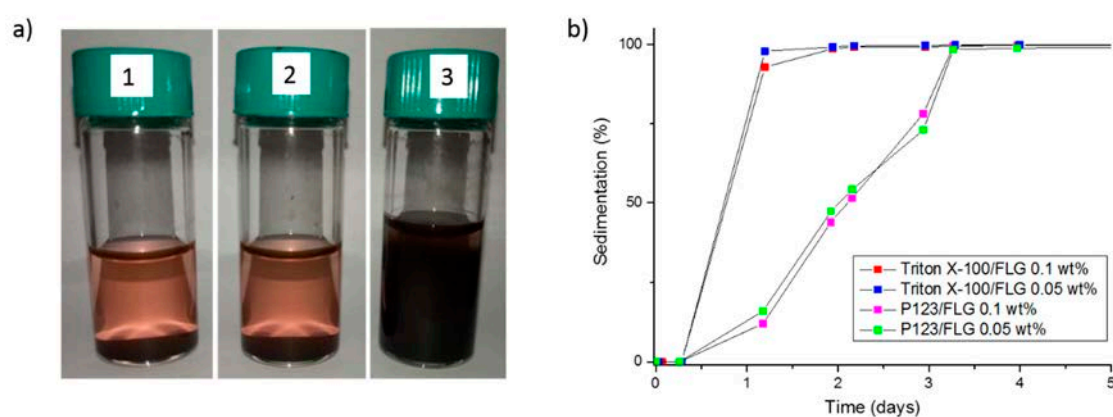


**Figure 6.** (a) Photos of FLG based nanofluids with 0.1 wt.% of FLG and (1) Triton X-100, (2) Pluronic® P123, and (3) Gum Arabic as surfactant six days after their preparation. (b) Sedimentation level from

Turbiscan for FLG based nanofluids with Triton X-100 and Pluronic® P123 for 0.05 and 0.1 wt.% of FLG.

### 3.3. Thermal Conductivity of FLG and Nanofluids

According to the parallel cylinder model of porous media [79], the “apparent” thermal conductivity of the FLG nanosheets, denoted  $k_{app}$ , was estimated as the ratio between the values directly measured by the thermal conductivity-meter  $k$  and the apparent volume fraction of FLG nanosheets  $\phi$  in the studied disk by the following Equation (1):

$$k_{app} = \frac{k}{\phi} \quad (1)$$

The apparent volume fraction of FLG,  $\phi$ , in the compacted disk was calculated from the ratio between the apparent density of the FLG nanosheets in the disk (ratio between the FLG mass used to produce the disk and the theoretical volume of the disk) and the experimental density of the FLG powder, determined previously from gas pycnometry. An apparent thermal conductivity of  $\sim 12.0 \text{ W}\cdot\text{m}^{-1}\cdot\text{K}^{-1}$  was obtained with compacted volume fractions of  $\sim 0.33\text{--}0.34$ . These values are higher than the effective thermal conductivities of  $1.37$  or  $10.7 \text{ W}\cdot\text{m}^{-1}\cdot\text{K}^{-1}$  measured by Vallejo et al. [46,80] for other graphene samples. Such a difference might be attributed to the less aggressiveness exfoliation process that was used in this study (aqueous medium assisted with tannic acid).

Thermal conductivity of the prepared FLG nanofluids with different weight concentrations (0.05–0.5%) were measured between 283.15 and 323.15 K in the presence of Triton X-100, Pluronic® P123 and Gum Arabic as surfactants. The results are presented in the following by first discussing the effect of the surfactant addition alone on the thermal conductivity of Tyfocor® LS. Subsequently, the effect of the surfactant, temperature, and nanoparticle content on the thermal conductivity of the FLG-based nanofluids are analyzed. Finally, thermal conductivity enhancement of FLG-based nanofluids are compared to some theoretical models in an attempt to explain the observed behavior.

As expected, an enhancement of thermal conductivity of Tyfocor® LS and base fluids was observed with the temperature rise. For the base fluids, this enhancement did not vary with the concentration of surfactant and, over the 40 K temperature domain, the thermal conductivity of the base fluids with Triton X-100, Pluronic® P123, and Gum Arabic increased by 6.4, 7, and 6.3%, respectively. The thermal conductivity of Tyfocor® LS alone and the ratio between the base fluids of the three series (Tyfocor® LS + Triton X-100, Tyfocor® LS + Pluronic® P123 and Tyfocor® LS + Gum Arabic) where the concentration of surfactant was varied between 0.1 and 1% in mass is shown in Figure 7. In all cases, deviations between thermal conductivities of Tyfocor® LS with surfactant and Tyfocor® LS only remained within the 2%. Taking the experimental uncertainty into account, the presence of surfactant (whatever the concentration used) did not significantly impact the thermal conductivity of Tyfocor® LS over the tested temperature range of 283.15–323.15 K.

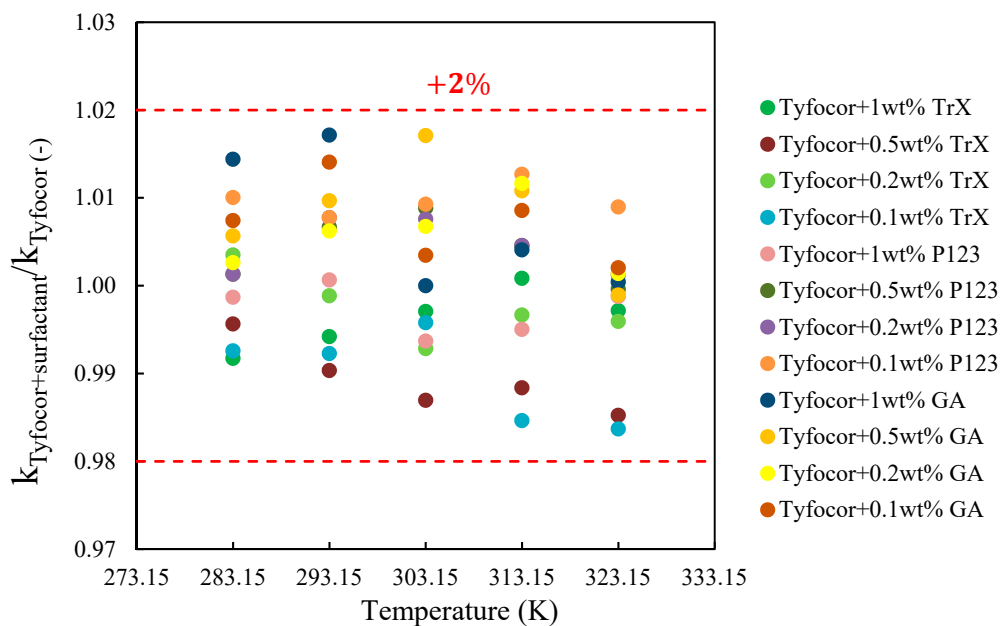
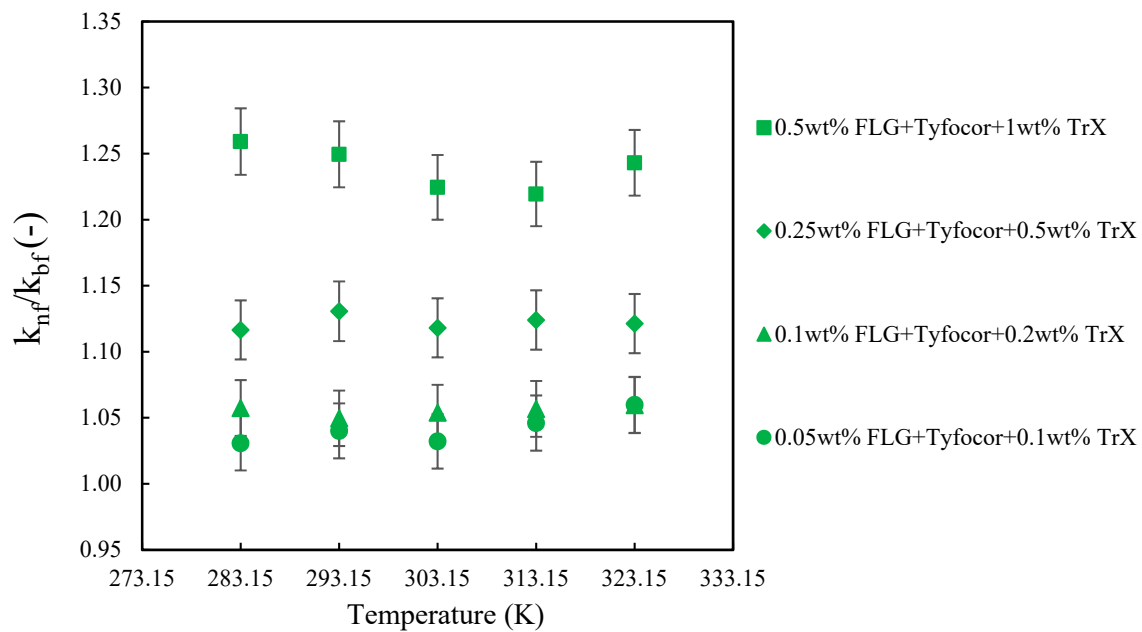
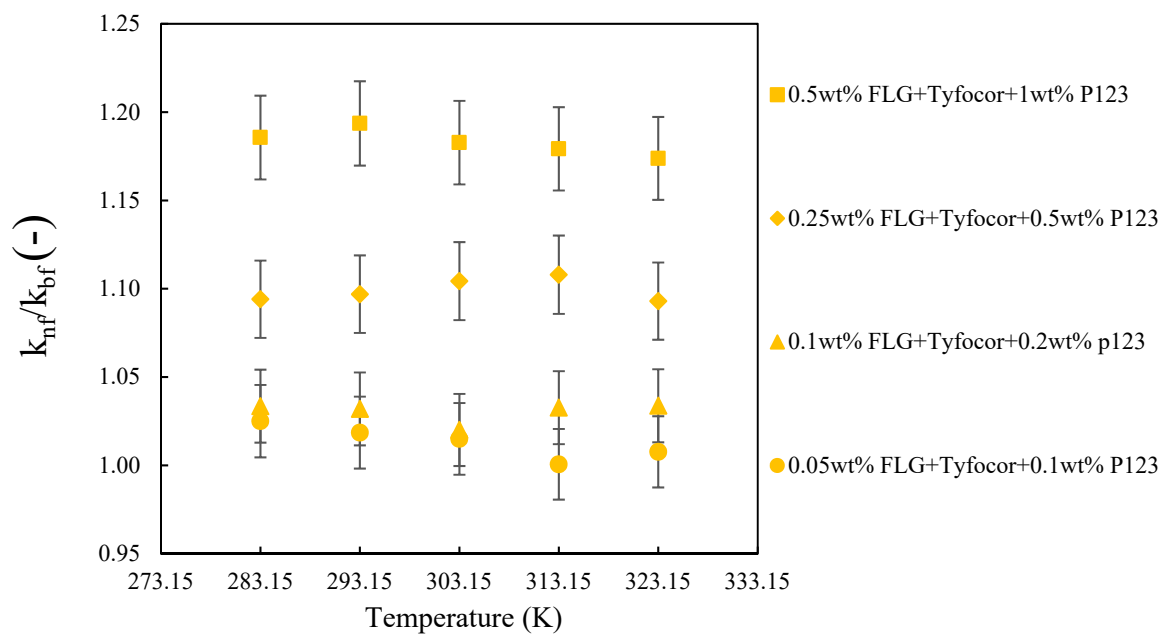


**Figure 7.** Thermal conductivity of Tyfocor® LS alone and the base fluids with the three different surfactants used: Triton X-100 (TrX), Pluronic® P-123 (P123), Gum Arabic (GA) for the given surfactant concentration between 283.15 and 323.15 K.

Like for the base fluids, the thermal conductivity of the prepared nanofluids was observed here to increase with both temperature and FLG concentration in agreement with the literature. Figure 8 presents the thermal conductivity ratio for the three series of nanofluids as function of temperature and FLG content. The results show that the thermal conductivity of the base fluids and those of the nanofluids increased with temperature and the relative thermal conductivity of all nanofluids was quasi-constant with the variation of the temperature, within the experimental uncertainty. A similar trend has been previously reported in other works [81–83]. It is widely known that the concentration of the nanoparticles plays an important role in improving the thermal conductivity and then heat transfer of nanofluids. As already mentioned, the studied concentration of FLG nanosheets varies between 0.05 and 0.5% in mass. Figure 8 shows that the thermal conductivity of nanofluids increased with FLG content. For the FLG concentration of 0.05, 0.1, 0.25, and 0.5 wt.%, the nanofluid thermal conductivity increases by 4.2, 5.5, 12.2, and 23.9%, respectively, as compared to the corresponding base fluids when using Triton X-100 as a surfactant. The thermal conductivity enhancements are 1.3, 3.0, 9.9, and 18.3% in the case of Pluronic® P-123. Finally, the observed increases in conductivity reach 2.1, 4.0, 10.5, and 21.5% with Gum Arabic. Due to the slight change of thermal conductivity enhancement with temperature, the previous values corresponded to the average of the results in the studied temperature range. A weak dependence in the type of the used surfactant with regards of thermal conductivity enhancement was also observed. One can notice that the enhancement presently reported for the higher FLG concentration is better than the values obtained by Agromayor et al. [82], who reported an enhancement of 12% at the mass concentration of 1% of graphene in water at 313.15 K, or by Cabaleiro et al. [81] who showed an enhancement up to 5% for 0.5 wt.% of sulfonic acid-functionalized graphene oxide nanoplatelets in ethylene glycol:water mixture at (10:90) wt.% at 323.15 K.



(a)



(b)

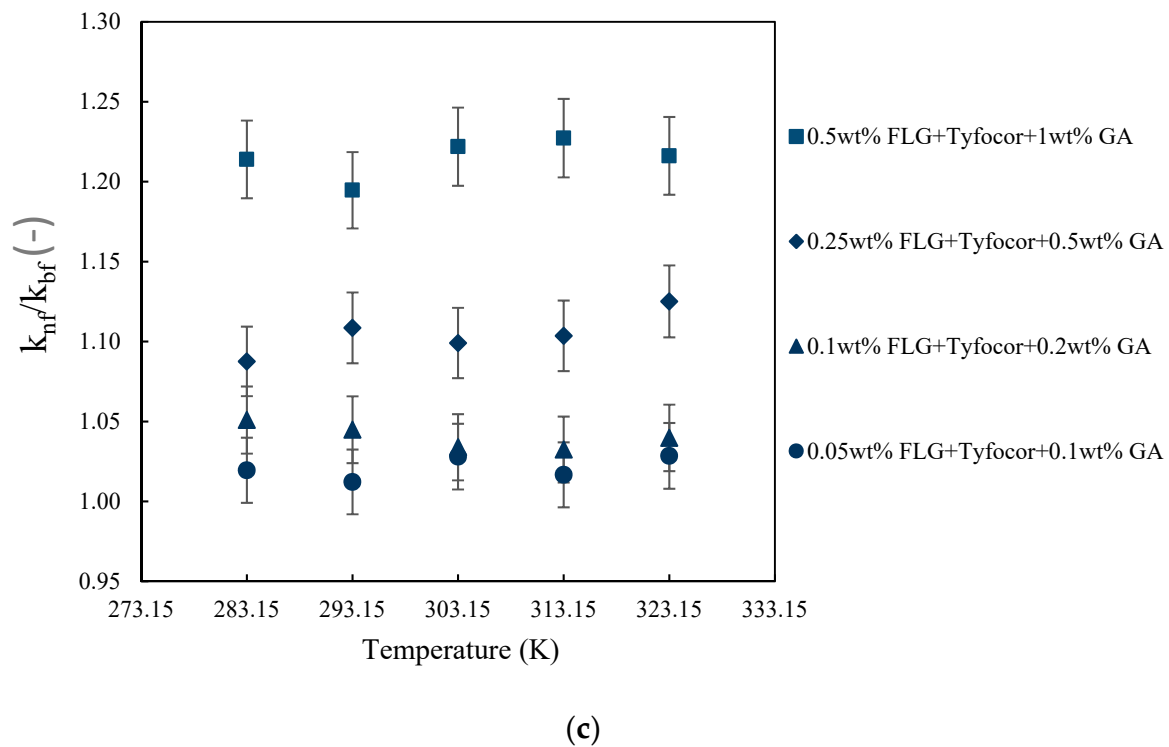


**Figure 8.** Thermal conductivity ratio of the FLG-based nanofluids with TrX (a), P123 (b), and Gum Arabic (GA) (c), as surfactant as function of FLG concentration and temperature between 283.15 and 323.15 K. Error bars indicate 2%.

Figure 9 highlights the thermal conductivity ratio of FLG nanofluids at 293.15 K as a function of the volume fraction of FLG. A linear increase in the thermal conductivity ratio with a slight difference in the slope for each used surfactant was observed. In this figure, as well as in the following models, the volume fraction of FLG, denoted  $\varphi$  and given by Equation (2), was obtained from the FLG mass concentrations  $\varphi_m$ , the density of each base fluid was evaluated from mixing rule using the density of each compound at 293.15 K and the density of FLG  $\rho_{np}$  measured earlier, as in Equation (2).

$$\varphi = \frac{\varphi_m \frac{\rho_{bf}}{\rho_{np}}}{\left(1 - \varphi_m \left(1 - \frac{\rho_{bf}}{\rho_{np}}\right)\right)} \quad (2)$$

Some models, presented in the following and that were previously used with graphene-based nanofluids or composites, are considered to analyze the observed thermal conductivity behaviors as the FLG content increases.

First, the upper Wiener bound or Parallel model [80] defined by Equation (3), was considered. In this equation,  $k_{nf}$  and  $k_{bf}$  correspond to the thermal conductivity of the nanofluid and base fluid, respectively, while  $k_{np}$  is here the apparent thermal conductivity of the FLG, which is taken at  $12 \text{ W m}^{-1}\cdot\text{K}^{-1}$ , as evaluated earlier from the guarded heat flow meter technique.

$$k_{nf} = k_{np}\varphi + (1 - \varphi)k_{bf} \quad (3)$$

Nan et al. [84] developed a thermal conductivity model for two-phase materials composed of dispersed particles in a liquid medium while taking the effect of interfacial resistance based on multiple scattering theory and the effective medium theory (EMT) model of Maxwell into account. Such a model also integrates the thermal conductivity along transverse and longitudinal axes of the particles. This model was previously used for the comparison purpose of the thermal conductivity of carbon-based nanofluids [85]. In the presence of graphene nanosheets, e.g., particles with large length and low thickness, it is admitted that the aspect ratio is quite high. By considering the fact that the

thermal conductivity along transverse and longitudinal axes of the FLG nanosheets is much larger than that of the thermal conductivity of the base fluid, the model of Nan et al. [84] takes the form of Equation (4), as proposed by [86]:

$$k_{nf} = k_{bf} \left( \frac{1 + \frac{2\varphi \left( \frac{k_{np}}{k_{bf}} \right)}{3}}{1 - \frac{\varphi}{3}} \right) \quad (4)$$

In this equation,  $k_{np}$  is the thermal conductivity of the FLG along the inplane direction, which depends on the graphene thickness and, consequently, the number of layers. This dependence of  $k_{np}$  with graphene thickness  $t$  was modeled by molecular dynamic simulations in [87] and expressed by Equation (5) as followed:

$$k_{np} = 4058 \times \left( \frac{t}{3.4 \times 10^{-10}} \right)^{-1/2} \quad (5)$$

Based on the average thickness of 1.5 nm from TEM characterization, this leads to a thermal conductivity of the FLG along in plane direction of around  $1930 \text{ W}\cdot\text{m}^{-1}\cdot\text{K}^{-1}$ . Thus, by considering the significant thermal resistance effect at the interface between graphene and base fluid, the effective thermal conductivity of the FLG  $k_{np}^{eff}$  can be written, as follows, Equation (6) [86].

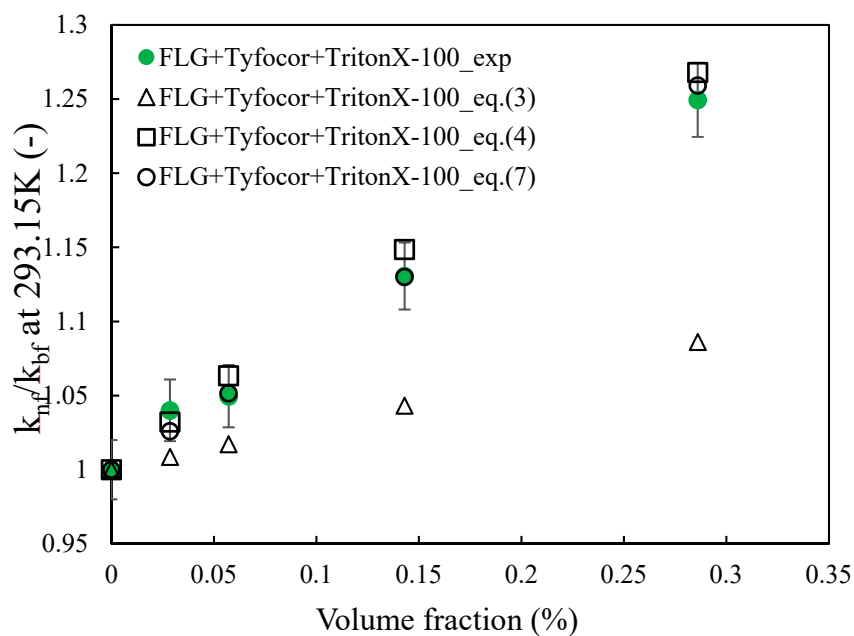
$$k_{np}^{eff} = \frac{k_{np}}{1 + \frac{2R_K k_{np}}{L}} \quad (6)$$

where  $L$  is the average length of graphene taken here is  $5 \mu\text{m}$ , as shown earlier from TEM, and  $R_K$  the interfacial thermal resistance. It is assumed here that  $R_K$  corresponds to the geometric average (60%/40%) of the interfacial resistance between the graphene nanosheets and water, it was fixed at  $4.5 \text{ m}^2\cdot\text{K}\cdot\text{W}^{-1}$  considering the number of layers [88] and the interfacial resistance between the graphene nanosheets and propylene glycol is assumed to be close to that ethylene glycol  $2.2 \text{ m}^2\cdot\text{K}\cdot\text{W}^{-1}$  [89]. This leads to a value of  $R_K$  of  $3.58 \text{ m}^2\cdot\text{K}\cdot\text{W}^{-1}$  for the used solvent (water and propylene glycol mixture). Consequently, from Equation (6), the obtained effective thermal conductivity is of around  $67 \text{ W}\cdot\text{m}^{-1}\cdot\text{K}^{-1}$ . This shows the influence of the interfacial thermal resistance, as this value is lower than the value given by Equation (5). This value is also far below the interfacial thermal resistance found from Equation (5) ( $1930 \text{ W}\cdot\text{m}^{-1}\cdot\text{K}^{-1}$ ) without considering the interfacial resistance between the FLG nanosheets and the base fluid, meaning that, for these nanosized platelets, the exposed surfaced within the fluid has great importance on the nanofluid behavior.

Finally, in addition to the thickness and interfacial thermal resistance dependence, the flatness ratio effect of graphene, denoted  $\eta$ , was also considered by Chu et al. [86] to take that contribution into account. Normally, thin nanosheets, like graphene, cannot be perfectly flat thermal platelets within the fluid in which they are dispersed, it is admitted that they rather adopt folded and corrugated shapes. Such a folded and wrinkled structure of FLG in solution reduces the effective length of the graphene nanosheets. This effect was shown to induce loss in the intrinsic thermal conductivity of graphene, which, consequently, may reduce thermal conductivity enhancements of graphene-based nanofluids. Chu et al. [86] proposed the following expression for thermal conductivity, which was used in [45] with graphene nanoplatelet nanofluids.

$$k_{nf} = k_{bf} \left( \frac{3 + \frac{2\eta^2\varphi}{\left[ k_{bf} \left( \frac{2R_K}{L} + 13.4\sqrt{t} \right) \right]}}{3 - \eta\varphi} \right) \quad (7)$$

The comparison between the observed experimental thermal conductivity enhancement of the prepared FLG-based nanofluids at 293.15 K and theoretical models of Equations (3), (4), and (7) are presented in Figure 9. Equation (3) was not able to predict the evolution of thermal conductivity whatever the surfactant used. This result could be explained by the low thermal conductivity value used in this model. However, good agreement was observed for all nanofluid series with the model described by Equation (7). This correlation was obtained with only one adjustable parameter, namely the flatness ratio effect of graphene,  $\eta$  previously introduced, while the other values were used as defined before. The values of  $\eta$  are 0.75, 0.88 and 0.77 with TritonX-100, Pluronic® P-123 and Gum Arabic, respectively. With these flatness ratios, the AAD (%) between data from the experiments and the models are 0.35, 0.11, and 0.21, respectively. The reported values of  $\eta$  are also in good agreement with the values previously reported with FLG [45,86–89]. This put into evidence the importance of the flatness ratio in addition to graphene nanosheet dimensions and thermal resistance at graphene interface in the thermal conductivity enhancement of graphene-based nanofluids. A relatively good agreement was also achieved with Equation (4), but with higher AAD of 4.11, 0.9, and 3.5%, with TritonX-100, Pluronic® P-123, and Gum Arabic as surfactants, respectively.



(a)

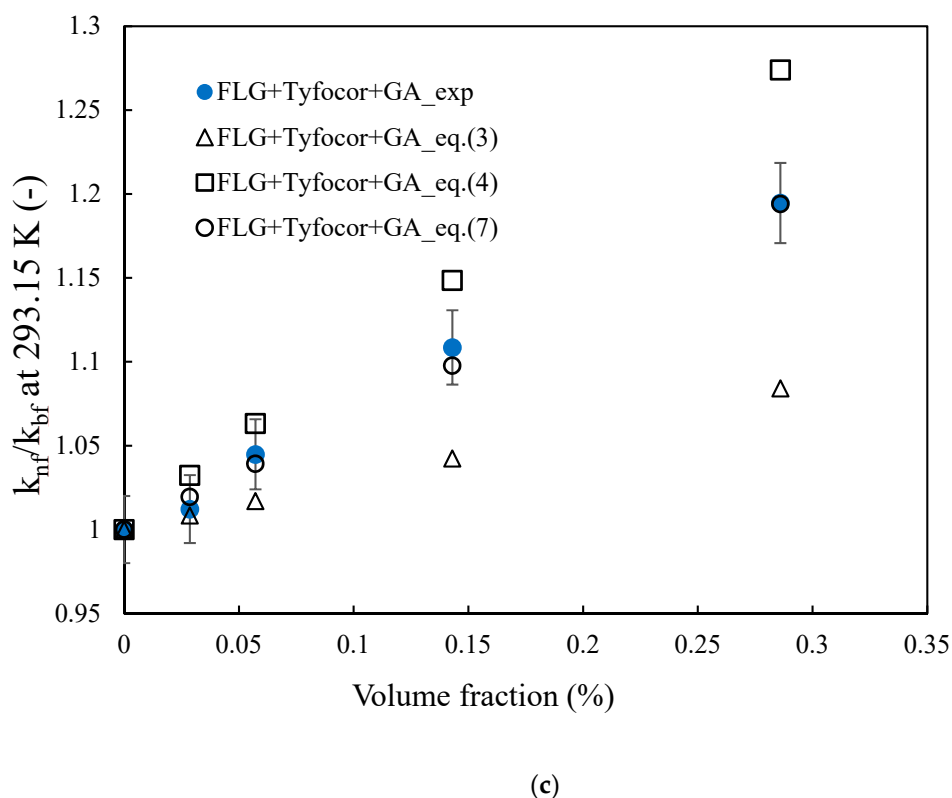
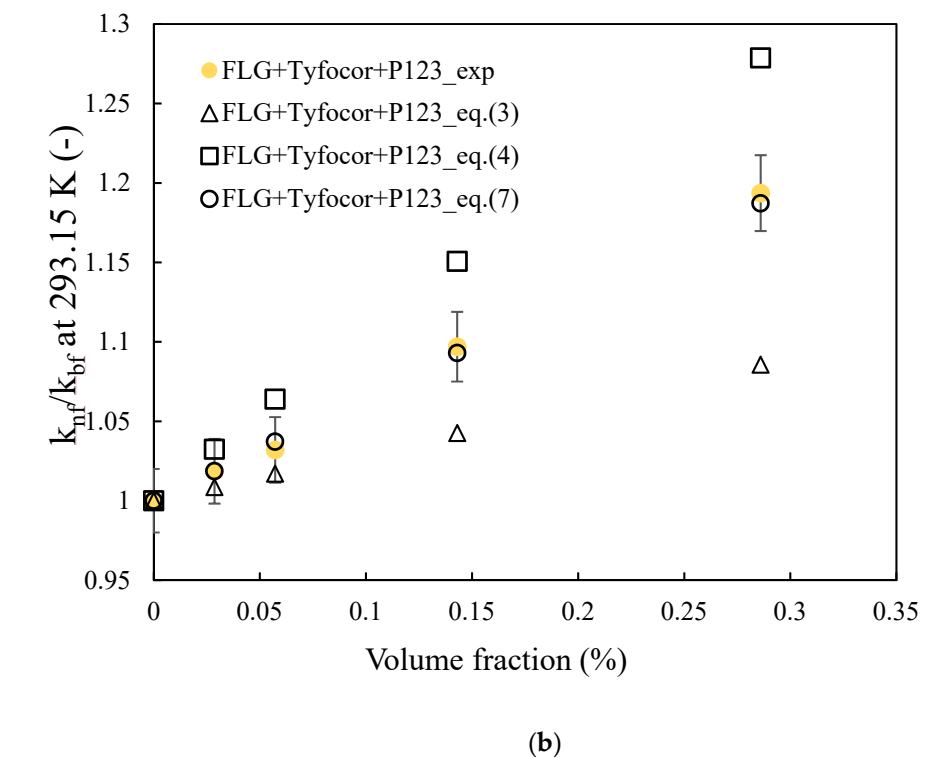


**Figure 9.** Thermal conductivity ratio of the FLG-based nanofluids over that of the corresponding base fluid at 293.15 K with TritonX-100 (a), Pluronic® P-123 (P123) (b), and Gum Arabic (GA) (c)—Comparison between experimental data and theoretical models from Equations (3), (4), and (7).

#### 4. Conclusions

Few-layer graphene (FLG) was produced following a mechanical exfoliation method that was assisted by tannic acid and then characterized by SEM, TEM, Raman spectroscopy demonstrating the

excellent structural quality of the FLG nanosheets, and the efficiency of the exfoliation process. The density and the apparent thermal conductivity of these FLGs were also evaluated. The FLG nanosheets were used to develop nanofluids when considering a commercial heat transfer fluid based on a mixture of water and propylene glycol and different nonionic surfactants. The stability and the thermal conductivity of the produced nanofluids were experimentally characterized by multiple light scattering measurements and the transient short hot-wire method. The thermal conductivity studied was performed in the temperature range 283.15–323.15 K varying the mass content in FLG from 0.05 to 0.5%. The thermal conductivity of the prepared nanofluids was compared to several relevant models and it was shown the enhancement in thermal conductivity of graphene-based nanofluids is governed by combined effects, such as FLG size, thermal resistance at FLG interface, thickness, and their flatness ratio. Such reported thermal conductivity enhancement is promising in view of possible thermal applications.

**Author Contributions:** Conceptualization, B.V. and P.E.; FLG preparation, D.B.; nanofluid preparation and FLG characterization, N.B., B.V., A.D. and D.B.; T.M., J.G. (Jaafar Ghanbaja); Raman: J.G. (Jérôme Gleize); stability analysis, F.M.; methodology, B.V. and P.E.; formal analysis, S.H., D.C., B.V. and P.E.; investigation, S.H., D.C., B.V. and P.E.; writing—original draft preparation, S.H., D.C., B.V. and P.E.; writing—review and editing, S.H., D.C., B.V. and P.E.; supervision, B.V., T.M. and P.E. All authors have read and agreed to the published version of the manuscript.

**Funding:** P.E. acknowledges the European Union through the European Regional Development Fund (ERDF), the Ministry of Higher Education and Research, the French region of Brittany and Rennes Métropole for the financial support of thermal conductivity and density experimental devices. D.C. is recipient of a postdoctoral fellowship from Xunta de Galicia (Spain). This investigation is a contribution to the COST (European Cooperation in Science and Technology) Action CA15119: Overcoming Barriers to Nanofluids Market Uptake (NanoUptake).

**Acknowledgments:** B.V. and J.G. (Jérôme Gleize) would like to thank Pascal Franchetti for his valuable assistance for Raman spectroscopy.

**Conflicts of Interest:** The authors declare no conflict of interest.

## Nomenclature

ABS	Transmitted intensity
AAD	absolute average deviation [%]
DW	Deionized Water
$\eta$	flatness ratio effect of graphene
FFT	Fast Fourier Transform
GA	Gum Arabic
HFLG	highly crumpled few layer graphene
HRTEM	high-resolution transmission electron microscopy
FLG	few layer graphene
IFFT	Inverse FFT
L	Average length of graphene
PG	Propylene glycol
P123	Pluronic® P123
$\rho$	Density
$R_K$	Interfacial thermal resistance
SEM	scanning electron microscopy
St. Dev.	standard deviation
TEM	transmission electron microscopy
T	temperature [K]
t	graphene thickness
$t_0$	particles dispersion
TrX	Triton X-100
$\varphi_m$	mass fraction

$\varphi$	apparent mass fraction
$\phi$	volume fraction
Subscripts/superscripts	
<i>eff</i>	effective
<i>nf</i>	nanofluid
<i>np</i>	nanoparticles
<i>bf</i>	base fluid

## References

- Nižetić, S.; Djilali, N.; Papadopoulos, A.; Rodrigues, J.J.P.C. Smart technologies for promotion of energy efficiency, utilization of sustainable resources and waste management. *Journal of Cleaner Production* **2019**, *231*, 565–591, doi:10.1016/j.jclepro.2019.04.397.
- Riffat, S.B.; Ma, X. Thermoelectrics: a review of present and potential applications. *Applied Thermal Engineering* **2003**, *23*, 913–935, doi:10.1016/S1359-4311(03)00012-7.
- Park, S.; Kang, H.; Yoon, H.J. Structure–thermopower relationships in molecular thermoelectrics. *J. Mater. Chem. A* **2019**, *7*, 14419–14446, doi:10.1039/C9TA03358K.
- Wang, H.; Yu, C. Organic Thermoelectrics: Materials Preparation, Performance Optimization, and Device Integration. *Joule* **2019**, *3*, 53–80, doi:10.1016/j.joule.2018.10.012.
- Hajatzadeh Pordanjani, A.; Aghakhani, S.; Afrand, M.; Mahmoudi, B.; Mahian, O.; Wongwises, S. An updated review on application of nanofluids in heat exchangers for saving energy. *Energy Conversion and Management* **2019**, *198*, 111886, doi:10.1016/j.enconman.2019.111886.
- Tawfik, M.M. Experimental studies of nanofluid thermal conductivity enhancement and applications: A review. *Renewable and Sustainable Energy Reviews* **2017**, *75*, 1239–1253, doi:10.1016/j.rser.2016.11.111.
- Choi, S.U.S.; Eastman, J.A. *Enhancing Thermal Conductivity of Fluids with Nanoparticles*, International Mechanical Engineering Congress and Exhibition; Argonne National Lab: Lemont, IL, USA, 1995; pp. 99–105.
- Haddad, Z.; Abid, C.; Oztop, H.F.; Mataoui, A. A review on how the researchers prepare their nanofluids. *International Journal of Thermal Sciences* **2014**, *76*, 168–189, doi:10.1016/j.ijthermalsci.2013.08.010.
- Puliti, G.; Paolucci, S.; Sen, M. Nanofluids and Their Properties. *Appl. Mech. Rev* **2011**, *64*, doi:10.1115/1.4005492.
- Bahiraei, M.; Heshmatian, S. Graphene family nanofluids: A critical review and future research directions. *Energy Conversion and Management* **2019**, *196*, 1222–1256, doi:10.1016/j.enconman.2019.06.076.
- Bellos, E.; Tzivanidis, C. Investigation of a nanofluid-based concentrating thermal photovoltaic with a parabolic reflector. *Energy Conversion and Management* **2019**, *180*, 171–182, doi:10.1016/j.enconman.2018.11.008.
- Yen, P.-H.; Wang, J.-C. Power generation and electric charge density with temperature effect of alumina nanofluids using dimensional analysis. *Energy Conversion and Management* **2019**, *186*, 546–555, doi:10.1016/j.enconman.2019.03.005.
- Nazari, S.; Safarzadeh, H.; Bahiraei, M. Experimental and analytical investigations of productivity, energy and exergy efficiency of a single slope solar still enhanced with thermoelectric channel and nanofluid. *Renewable Energy* **2019**, *135*, 729–744, doi:10.1016/j.renene.2018.12.059.
- Karimipour, A.; Bagherzadeh, S.A.; Goodarzi, M.; Alnaqi, A.A.; Bahiraei, M.; Safaei, M.R.; Shadloo, M.S. Synthesized CuFe<sub>2</sub>O<sub>4</sub>/SiO<sub>2</sub> nanocomposites added to water/EG: Evaluation of the thermophysical properties beside sensitivity analysis & EANN. *International Journal of Heat and Mass Transfer* **2018**, *127*, 1169–1179, doi:10.1016/j.ijheatmasstransfer.2018.08.112.
- Safaei, M.R.; Ranjbarzadeh, R.; Hajizadeh, A.; Bahiraei, M.; Afrand, M.; Karimipour, A. Effects of cobalt ferrite coated with silica nanocomposite on the thermal conductivity of an antifreeze: New nanofluid for refrigeration condensers. *International Journal of Refrigeration* **2019**, *102*, 86–95, doi:10.1016/j.ijrefrig.2018.12.007.
- Sardarabadi, H.; Zeinali Heris, S.; Ahmadpour, A.; Passandideh-Fard, M. Experimental investigation of a novel type of two-phase closed thermosyphon filled with functionalized carbon nanotubes/water nanofluids for electronic cooling application. *Energy Conversion and Management* **2019**, *188*, 321–332, doi:10.1016/j.enconman.2019.03.070.

17. Qi, C.; Liu, M.; Tang, J. Influence of triangle tube structure with twisted tape on the thermo-hydraulic performance of nanofluids in heat-exchange system based on thermal and exergy efficiency. *Energy Conversion and Management* **2019**, *192*, 243–268, doi:10.1016/j.enconman.2019.04.047.
18. Bahiraei, M.; Ahmadi, A.A. Thermohydraulic performance analysis of a spiral heat exchanger operated with water–alumina nanofluid: Effects of geometry and adding nanoparticles. *Energy Conversion and Management* **2018**, *170*, 62–72, doi:10.1016/j.enconman.2018.05.061.
19. Murshed, S.M.S.; Estelle, P. A state of the art review on viscosity of nanofluids. *Renew. Sust. Energ. Rev.* **2017**, *76*, 1134–1152, doi:10.1016/j.rser.2017.03.113.
20. Afrand, M.; Hemmat Esfe, M.; Abedini, E.; Teimouri, H. Predicting the effects of magnesium oxide nanoparticles and temperature on the thermal conductivity of water using artificial neural network and experimental data. *Physica E: Low-dimensional Systems and Nanostructures* **2017**, *87*, 242–247, doi:10.1016/j.physe.2016.10.020.
21. Hemmat Esfe, M.; Hajmohammad, M.H. Thermal conductivity and viscosity optimization of nanodiamond-Co<sub>3</sub>O<sub>4</sub>/EG (40:60) aqueous nanofluid using NSGA-II coupled with RSM. *Journal of Molecular Liquids* **2017**, *238*, 545–552, doi:10.1016/j.molliq.2017.04.056.
22. Li, C.H.; Peterson, G.P. The effect of particle size on the effective thermal conductivity of Al<sub>2</sub>O<sub>3</sub>-water nanofluids. *Journal of Applied Physics* **2007**, *101*, 044312, doi:10.1063/1.2436472.
23. Esfahani, M.R.; Languri, E.M.; Nunna, M.R. Effect of particle size and viscosity on thermal conductivity enhancement of graphene oxide nanofluid. *International Communications in Heat and Mass Transfer* **2016**, *76*, 308–315, doi:10.1016/j.icheatmasstransfer.2016.06.006.
24. Sarviya, R.M.; Fuskale, V. Review on Thermal Conductivity of Nanofluids. *Mater. Today-Proc.* **2017**, *4*, 4022–4031.
25. Esfahani, N.N.; Toghraie, D.; Afrand, M. A new correlation for predicting the thermal conductivity of ZnO–Ag (50%–50%)/water hybrid nanofluid: An experimental study. *Powder Technology* **2018**, *323*, 367–373, doi:10.1016/j.powtec.2017.10.025.
26. Xia, G.; Jiang, H.; Liu, R.; Zhai, Y. Effects of surfactant on the stability and thermal conductivity of Al<sub>2</sub>O<sub>3</sub>/de-ionized water nanofluids. *International Journal of Thermal Sciences* **2014**, *84*, 118–124, doi:10.1016/j.ijthermalsci.2014.05.004.
27. Estellé, P.; Halefadi, S.; Maré, T. Lignin as dispersant for water-based carbon nanotubes nanofluids: Impact on viscosity and thermal conductivity. *International Communications in Heat and Mass Transfer* **2014**, *57*, 8–12, doi:10.1016/j.icheatmasstransfer.2014.07.012.
28. Yasinskiy, A.; Navas, J.; Aguilar, T.; Alcántara, R.; Gallardo, J.J.; Sánchez-Coronilla, A.; Martín, E.I.; De Los Santos, D.; Fernández-Lorenzo, C. Dramatically enhanced thermal properties for TiO<sub>2</sub>-based nanofluids for being used as heat transfer fluids in concentrating solar power plants. *Renewable Energy* **2018**, *119*, 809–819, doi:10.1016/j.renene.2017.10.057.
29. Yiamsawas, T.; Dalkilic, A.S.; Mahian, O.; Wongwises, S. Measurement and Correlation of the Viscosity of Water-Based Al<sub>2</sub>O<sub>3</sub> and TiO<sub>2</sub> Nanofluids in High Temperatures and Comparisons with Literature Reports. *Journal of Dispersion Science and Technology* **2013**, *34*, 1697–1703, doi:10.1080/01932691.2013.764483.
30. Angayarkanni, S.A.; Philip, J. Review on thermal properties of nanofluids: Recent developments. *Advances in Colloid and Interface Science* **2015**, *225*, 146–176, doi:10.1016/j.cis.2015.08.014.
31. Lee, S.; Choi, S.U.-S.; Li, S.; Eastman, J.A. Measuring Thermal Conductivity of Fluids Containing Oxide Nanoparticles. *Journal of Heat Transfer* **1999**, *121*, 280–289, doi:10.1115/1.2825978.
32. Mahian, O.; Kianifar, A.; Heris, S.Z.; Wongwises, S. Natural convection of silica nanofluids in square and triangular enclosures: Theoretical and experimental study. *International Journal of Heat and Mass Transfer* **2016**, *99*, 792–804, doi:10.1016/j.ijheatmasstransfer.2016.03.045.
33. Gómez-Villarejo, R.; Martín, E.I.; Navas, J.; Sánchez-Coronilla, A.; Aguilar, T.; Gallardo, J.J.; Alcántara, R.; De los Santos, D.; Carrillo-Berdugo, I.; Fernández-Lorenzo, C. Ag-based nanofluidic system to enhance heat transfer fluids for concentrating solar power: Nano-level insights. *Applied Energy* **2017**, *194*, 19–29, doi:10.1016/j.apenergy.2017.03.003.
34. Navas, J.; Sánchez-Coronilla, A.; Martín, E.I.; Teruel, M.; Gallardo, J.J.; Aguilar, T.; Gómez-Villarejo, R.; Alcántara, R.; Fernández-Lorenzo, C.; Piñero, J.C.; et al. On the enhancement of heat transfer fluid for concentrating solar power using Cu and Ni nanofluids: An experimental and molecular dynamics study. *Nano Energy* **2016**, *27*, 213–224, doi:10.1016/j.nanoen.2016.07.004.

35. Seong, H.; Kim, G.; Jeon, J.; Jeong, H.; Noh, J.; Kim, Y.; Kim, H.; Huh, S. Experimental Study on Characteristics of Grinded Graphene Nanofluids with Surfactants. *Materials* **2018**, *11*, 950, doi:10.3390/ma11060950.
36. Naddaf, A.; Zeinali Heris, S. Experimental study on thermal conductivity and electrical conductivity of diesel oil-based nanofluids of graphene nanoplatelets and carbon nanotubes. *International Communications in Heat and Mass Transfer* **2018**, *95*, 116–122, doi:10.1016/j.icheatmasstransfer.2018.05.004.
37. Kamatchi, R.; Kannan, K.G. An aqua based reduced graphene oxide nanofluids for heat transfer applications: Synthesis, characterization, stability analysis, and thermophysical properties. *Int. J. Renew. Energy Res.* **2018**, *8*, 313–319.
38. Bahaya, B.; Johnson, D.W.; Yavuzturk, C.C. On the Effect of Graphene Nanoplatelets on Water–Graphene Nanofluid Thermal Conductivity, Viscosity, and Heat Transfer Under Laminar External Flow Conditions. *Journal of Heat Transfer* **2018**, *140*, 064501, doi:10.1115/1.4038835.
39. Hussien, A.A.; Abdullah, M.Z.; Yusop, N.M.; Al-Nimr, M.A.; Atieh, M.A.; Mehrali, M. Experiment on forced convective heat transfer enhancement using MWCNTs/GNPs hybrid nanofluid and mini-tube. *International Journal of Heat and Mass Transfer* **2017**, *115*, 1121–1131, doi:10.1016/j.ijheatmasstransfer.2017.08.120.
40. Manasrah, A.D.; Al-Mubaiyedh, U.A.; Lau, T.; Ben-Mansour, R.; Al-Marri, M.J.; Almanassra, I.W.; Abdala, A.; Atieh, M.A. Heat transfer enhancement of nanofluids using iron nanoparticles decorated carbon nanotubes. *Applied Thermal Engineering* **2016**, *107*, 1008–1018, doi:10.1016/j.applthermaleng.2016.07.026.
41. Etefaghi, E.; Ghobadian, B.; Rashidi, A.; Najafi, G.; Khoshtaghaza, M.H.; Pourhashem, S. Preparation and investigation of the heat transfer properties of a novel nanofluid based on graphene quantum dots. *Energy Conversion and Management* **2017**, *153*, 215–223, doi:10.1016/j.enconman.2017.10.010.
42. Novoselov, K.S. Electric Field Effect in Atomically Thin Carbon Films. *Science* **2004**, *306*, 666–669, doi:10.1126/science.1102896.
43. Balandin, A.A.; Ghosh, S.; Bao, W.; Calizo, I.; Teweldebrhan, D.; Miao, F.; Lau, C.N. Superior thermal conductivity of single-layer graphene. *Nano Lett.* **2008**, *8*, 902–907, doi:10.1021/nl0731872.
44. Sen Gupta, S.; Manoj Siva, V.; Krishnan, S.; Sreeprasad, T.S.; Singh, P.K.; Pradeep, T.; Das, S.K. Thermal conductivity enhancement of nanofluids containing graphene nanosheets. *Journal of Applied Physics* **2011**, *110*, 084302, doi:10.1063/1.3650456.
45. Gao, Y.; Wang, H.; Sasmito, A.P.; Mujumdar, A.S. Measurement and modeling of thermal conductivity of graphene nanoplatelet water and ethylene glycol base nanofluids. *International Journal of Heat and Mass Transfer* **2018**, *123*, 97–109, doi:10.1016/j.ijheatmasstransfer.2018.02.089.
46. Vallejo, J.P.; Pérez-Tavernier, J.; Cabaleiro, D.; Fernández-Seara, J.; Lugo, L. Potential heat transfer enhancement of functionalized graphene nanoplatelet dispersions in a propylene glycol-water mixture. Thermophysical profile. *The Journal of Chemical Thermodynamics* **2018**, *123*, 174–184, doi:10.1016/j.jct.2018.04.007.
47. Sun, Z.; Pöller, S.; Huang, X.; Guschin, D.; Taetz, C.; Ebbinghaus, P.; Masa, J.; Erbe, A.; Kilzer, A.; Schuhmann, W.; et al. High-yield exfoliation of graphite in acrylate polymers: A stable few-layer graphene nanofluid with enhanced thermal conductivity. *Carbon* **2013**, *64*, 288–294, doi:10.1016/j.carbon.2013.07.063.
48. Amiri, A.; Ahmadi, G.; Shanbedi, M.; Etemadi, M.; Zubir, M.N.M.; Chew, B.T.; Kazi, S.N. Heat transfer enhancement of water-based highly crumpled few-layer graphene nanofluids. *RSC Adv.* **2016**, *6*, 105508–105527, doi:10.1039/C6RA22365F.
49. Amiri, A.; Shanbedi, M.; Rafieerad, A.R.; Rashidi, M.M.; Zaharinie, T.; Zubir, M.N.M.; Kazi, S.N.; Chew, B.T. Functionalization and exfoliation of graphite into mono layer graphene for improved heat dissipation. *Journal of the Taiwan Institute of Chemical Engineers* **2017**, *71*, 480–493, doi:10.1016/j.jtice.2016.12.009.
50. Alawi, O.A.; Sidik, N.A.C.; Kazi, S.N.; Najafi, G. Graphene nanoplatelets and few-layer graphene studies in thermo-physical properties and particle characterization. *J Therm Anal Calorim* **2019**, *135*, 1081–1093, doi:10.1007/s10973-018-7585-0.
51. Alawi, O.A.; Mallah, A.R.; Kazi, S.N.; Sidik, N.A.C.; Najafi, G. Thermophysical properties and stability of carbon nanostructures and metallic oxides nanofluids. *J Therm Anal Calorim* **2019**, *135*, 1545–1562, doi:10.1007/s10973-018-7713-x.
52. Berrada, N.; Hamze, S.; Desforges, A.; Ghanbaja, J.; Gleize, J.; Maré, T.; Vigolo, B.; Estellé, P. Surface tension of functionalized MWCNT-based nanofluids in water and commercial propylene-glycol mixture. *Journal of Molecular Liquids* **2019**, *293*, 111473, doi:10.1016/j.molliq.2019.111473.

53. Borode, A.O.; Ahmed, N.A.; Olubambi, P.A. Surfactant-aided dispersion of carbon nanomaterials in aqueous solution. *Physics of Fluids* **2019**, *31*, 071301, doi:10.1063/1.5105380.
54. Guardia, L.; Fernández-Merino, M.J.; Paredes, J.I.; Solís-Fernández, P.; Villar-Rodil, S.; Martínez-Alonso, A.; Tascón, J.M.D. High-throughput production of pristine graphene in an aqueous dispersion assisted by non-ionic surfactants. *Carbon* **2011**, *49*, 1653–1662, doi:10.1016/j.carbon.2010.12.049.
55. Rasheed, A.K.; Khalid, M.; Rashmi, W.; Gupta, T.C.S.M.; Chan, A. Graphene based nanofluids and nanolubricants – Review of recent developments. *Renewable and Sustainable Energy Reviews* **2016**, *63*, 346–362, doi:10.1016/j.rser.2016.04.072.
56. Keklikcioglu Cakmak, N. The impact of surfactants on the stability and thermal conductivity of graphene oxide de-ionized water nanofluids. *J Therm Anal Calorim* **2020**, *139*, 1895–1902, doi:10.1007/s10973-019-09096-6.
57. Mehrali, M.; Sadeghinezhad, E.; Tahan Latibari, S.; Mehrali, M.; Togun, H.; Zubir, M.N.M.; Kazi, S.N.; Metselaar, H.S.C. Preparation, characterization, viscosity, and thermal conductivity of nitrogen-doped graphene aqueous nanofluids. *J Mater Sci* **2014**, *49*, 7156–7171, doi:10.1007/s10853-014-8424-8.
58. Qamar, S.; Yasin, S.; Ramzan, N.; Iqbal, T.; Akhtar, M.N. Preparation of stable dispersion of graphene using copolymers: dispersity and aromaticity analysis. *Soft Materials* **2019**, *17*, 190–202, doi:10.1080/1539445X.2019.1583673.
59. Akbari, A.; Alavi Fazel, S.A.; Maghsoodi, S.; Shahbazi Kootenaei, A. Thermo-physical and stability properties of raw and functionalization of graphene nanoplatelets-based aqueous nanofluids. *Journal of Dispersion Science and Technology* **2019**, *40*, 17–24, doi:10.1080/01932691.2018.1462713.
60. Sarsam, W.S.; Amiri, A.; Kazi, S.N.; Badarudin, A. Stability and thermophysical properties of non-covalently functionalized graphene nanoplatelets nanofluids. *Energy Conversion and Management* **2016**, *116*, 101–111, doi:10.1016/j.enconman.2016.02.082.
61. Azizi, M.; Hosseini, M.; Zafarnak, S.; Shanbedi, M.; Amiri, A. Experimental Analysis of Thermal Performance in a Two-Phase Closed Thermosiphon Using Graphene/Water Nanofluid. *Ind. Eng. Chem. Res.* **2013**, *52*, 10015–10021, doi:10.1021/ie401543n.
62. Xu, Y.; Xue, Y.; Qi, H.; Cai, W. Experimental study on heat transfer performance of pulsating heat pipes with hybrid working fluids. *International Journal of Heat and Mass Transfer* **2020**, *157*, 119727, doi:10.1016/j.ijheatmasstransfer.2020.119727.
63. Shazali, S.S.; Amiri, A.; Mohd Zubir, M.N.; Rozali, S.; Zabri, M.Z.; Mohd Sabri, M.F.; Soleymaniha, M. Investigation of the thermophysical properties and stability performance of non-covalently functionalized graphene nanoplatelets with Pluronic P-123 in different solvents. *Materials Chemistry and Physics* **2018**, *206*, 94–102, doi:10.1016/j.matchemphys.2017.12.008.
64. E37 Committee *Test Method for Evaluating the Resistance to Thermal Transmission of Materials by the Guarded Heat Flow Meter Technique*; ASTM International: West Conshohocken, PA, USA, 2019.
65. Cabaleiro, D.; Nimo, J.; Pastoriza-Gallego, M.J.; Piñeiro, M.M.; Legido, J.L.; Lugo, L. Thermal conductivity of dry anatase and rutile nano-powders and ethylene and propylene glycol-based TiO<sub>2</sub> nanofluids. *The Journal of Chemical Thermodynamics* **2015**, *83*, 67–76, doi:10.1016/j.jct.2014.12.001.
66. Banisharif, A.; Aghajani, M.; Van Vaerenbergh, S.; Estellé, P.; Rashidi, A. Thermophysical properties of water ethylene glycol (WEG) mixture-based Fe<sub>3</sub>O<sub>4</sub> nanofluids at low concentration and temperature. *Journal of Molecular Liquids* **2020**, *302*, 112606, doi:10.1016/j.molliq.2020.112606.
67. Zeroual, S.; Estellé, P.; Cabaleiro, D.; Vigolo, B.; Emo, M.; Halim, W.; Ouaskit, S. Ethylene glycol based silver nanoparticles synthesized by polyol process: Characterization and thermophysical profile. *Journal of Molecular Liquids* **2020**, *310*, 113229, doi:10.1016/j.molliq.2020.113229.
68. Sengers, J.; Watson, J. Improved International Formulations for the Viscosity and Thermal-Conductivity of Water Substance. *J. Phys. Chem. Ref. Data* **1986**, *15*, 1291–1314, doi:10.1063/1.555763.
69. Hummers, W.S.; Offeman, R.E. Preparation of Graphitic Oxide. *J. Am. Chem. Soc.* **1958**, *80*, 1339–1339, doi:10.1021/ja01539a017.
70. Kairi, M.I.; Dayou, S.; Kairi, N.I.; Abu Bakar, S.; Vigolo, B.; Mohamed, A.R. Toward high production of graphene flakes - a review on recent developments in their synthesis methods and scalability. *J. Mater. Chem. A* **2018**, *6*, 15010–15026, doi:10.1039/c8ta04255a.
71. Hernandez, Y.; Nicolosi, V.; Lotya, M.; Blighe, F.M.; Sun, Z.; De, S.; McGovern, I.T.; Holland, B.; Byrne, M.; Gun'Ko, Y.K.; et al. High-yield production of graphene by liquid-phase exfoliation of graphite. *Nat Nanotechnol* **2008**, *3*, 563–568, doi:10.1038/nnano.2008.215.

72. V. Ershova, O.; C. Lillestolen, T.; Bichoutskaia, E. Study of polycyclic aromatic hydrocarbons adsorbed on graphene using density functional theory with empirical dispersion correction. *Physical Chemistry Chemical Physics* **2010**, *12*, 6483–6491, doi:10.1039/C000370K.
73. Schmaltz, B.; Weil, T.; Müllen, K. Polyphenylene-Based Materials: Control of the Electronic Function by Molecular and Supramolecular Complexity. *Advanced Materials* **2009**, *21*, 1067–1078, doi:10.1002/adma.200802016.
74. Bianco, A.; Cheng, H.-M.; Enoki, T.; Gogotsi, Y.; Hurt, R.H.; Koratkar, N.; Kyotani, T.; Monthieux, M.; Park, C.R.; Tascon, J.M.D.; et al. All in the graphene family - A recommended nomenclature for two-dimensional carbon materials. *Carbon* **2013**, *65*, 1–6, doi:10.1016/j.carbon.2013.08.038.
75. Ferrari, A.C.; Meyer, J.C.; Scardaci, V.; Casiraghi, C.; Lazzeri, M.; Mauri, F.; Piscanec, S.; Jiang, D.; Novoselov, K.S.; Roth, S.; et al. Raman Spectrum of Graphene and Graphene Layers. *Phys. Rev. Lett.* **2006**, *97*, 187401, doi:10.1103/PhysRevLett.97.187401.
76. Tuinstra, F.; Koenig, J. Raman Spectrum of Graphite. *J. Chem. Phys.* **1970**, *53*, 1126-, doi:10.1063/1.1674108.
77. Allen, M.J.; Tung, V.C.; Kaner, R.B. Honeycomb Carbon: A Review of Graphene. *Chem. Rev.* **2010**, *110*, 132–145, doi:10.1021/cr900070d.
78. Navas, H.; Desforges, A.; Ghanbaja, J.; Vigolo, B.; Estellé, P. Long-term Stability of Graphene Based Nanofluids. *IJMERR* **2017**, *6*, 529–533, doi:10.18178/ijmerr.6.6.529-533.
79. Timofeeva, E.V.; Gavrilov, A.N.; McCloskey, J.M.; Tolmachev, Y.V.; Sprunt, S.; Lopatina, L.M.; Selinger, J.V. Thermal conductivity and particle agglomeration in alumina nanofluids: Experiment and theory. *Phys. Rev. E* **2007**, *76*, 061203, doi:10.1103/PhysRevE.76.061203.
80. Vallejo, J.P.; Álvarez-Regueiro, E.; Cabaleiro, D.; Fernández-Seara, J.; Fernández, J.; Lugo, L. Functionalized graphene nanoplatelet nanofluids based on a commercial industrial antifreeze for the thermal performance enhancement of wind turbines. *Applied Thermal Engineering* **2019**, *152*, 113–125, doi:10.1016/j.applthermaleng.2019.02.046.
81. Cabaleiro, D.; Colla, L.; Barison, S.; Lugo, L.; Fedele, L.; Bobbo, S. Heat Transfer Capability of (Ethylene Glycol + Water)-Based Nanofluids Containing Graphene Nanoplatelets: Design and Thermophysical Profile. *Nanoscale Res Lett* **2017**, *12*, 53, doi:10.1186/s11671-016-1806-x.
82. Agromayor, R.; Cabaleiro, D.; Pardiñas, Á.; Vallejo, J.; Fernández-Seara, J.; Lugo, L. Heat Transfer Performance of Functionalized Graphene Nanoplatelet Aqueous Nanofluids. *Materials* **2016**, *9*, 455, doi:10.3390/ma9060455.
83. R. Rodríguez-Laguna, M.; Castro-Alvarez, A.; Sledzinska, M.; Maire, J.; Costanzo, F.; Ensing, B.; Pruneda, M.; Ordejón, P.; Torres, C.M.S.; Gómez-Romero, P.; et al. Mechanisms behind the enhancement of thermal properties of graphene nanofluids. *Nanoscale* **2018**, *10*, 15402–15409, doi:10.1039/C8NR02762E.
84. Nan, C.-W.; Birringer, R.; Clarke, D.R.; Gleiter, H. Effective thermal conductivity of particulate composites with interfacial thermal resistance. *Journal of Applied Physics* **1997**, *81*, 6692–6699, doi:10.1063/1.365209.
85. Estellé, P.; Halelfadl, S.; Maré, T. Thermal conductivity of CNT water based nanofluids: Experimental trends and models overview. *Journal of Thermal Engineering* **2015**, *1*, 381, doi:10.18186/jte.92293.
86. Chu, K.; Li, W.; Tang, F. Flatness-dependent thermal conductivity of graphene-based composites. *Physics Letters A* **2013**, *377*, 910–914, doi:10.1016/j.physleta.2013.02.009.
87. Zhong, W.-R.; Zhang, M.-P.; Ai, B.-Q.; Zheng, D.-Q. Chirality and thickness-dependent thermal conductivity of few-layer graphene: A molecular dynamics study. *Appl. Phys. Lett.* **2011**, *98*, 113107, doi:10.1063/1.3567415.
88. Alexeev, D.; Chen, J.; Walther, J.H.; Giapis, K.P.; Angelikopoulos, P.; Koumoutsakos, P. Kapitza Resistance between Few-Layer Graphene and Water: Liquid Layering Effects. *Nano Lett.* **2015**, *15*, 5744–5749, doi:10.1021/acs.nanolett.5b03024.
89. Selvam, C.; Lal, D.M.; Harish, S. Thermal conductivity enhancement of ethylene glycol and water with graphene nanoplatelets. *Thermochimica Acta* **2016**, *642*, 32–38, doi:10.1016/j.tca.2016.09.002.



### **IV.3- Isobaric heat capacity**

Isobaric heat capacity,  $C_p$ , is an important parameter when it comes to heat exchange balances between fluids. In such balances the transferred or absorbed heat flow by a fluid is equal to the product of its isobaric heat capacity, its mass flow rate, and the difference between its inlet and outlet temperature in the control volume [1–5]. So the heat capacities of heat transfer fluids need to be increased. The significant increase is necessary not only to reduce the costs of liquid cooling and heating processes but also to bring clean energy generation technologies such as concentrating solar power (CSP) to price parity with conventional energy generation [6].

The isobaric heat capacity of FLG, surfactants, Tyfocor® LS, and the highest concentration of base fluids (1wt.%) and nanofluids (0.5wt.%), was measured at 283.15, 303.15, and 323.15 K respectively, according to the experimental procedure described earlier in chapter III.

#### **IV.3.1- Effect of temperature**

The obtained experimental values of isobaric heat capacity of FLG and the three used surfactants (Pluronic® P-123, Triton X-100 and Gum Arabic) at the tested temperatures are shown in Table IV.1.

**Table IV.1.** Experimental isobaric heat capacity results of FLG and the three different surfactants.

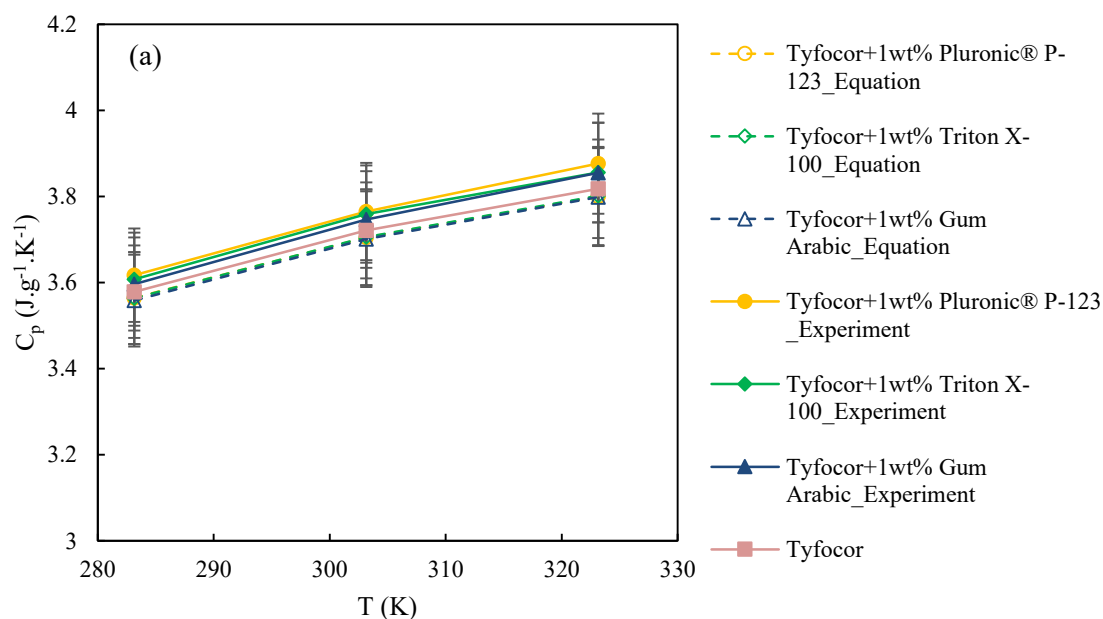
<b>T (K)</b>	<b><math>C_p</math> (J.g<sup>-1</sup>.K<sup>-1</sup>)</b>			
	<b>FLG</b>	<b>Pluronic® P-123</b>	<b>Triton X-100</b>	<b>Gum Arabic</b>
283.15	1.070	2.102	2.046	1.515
303.15	1.196	2.090	2.142	1.692
323.15	1.324	2.044	2.178	1.917

For these components, an increase in the isobaric heat capacity with the temperature rise from 283.15 to 323.15 K was found equal to 23.7%, 6.5% and 26.6% for FLG, Triton X-100 and Gum Arabic, respectively. With Pluronic® P-123 surfactant, the  $C_p$  decreases with the temperature of about 2.8%. It should be noted that a phase transition could happen during the measurements of this surfactant due to the temperature rise as it is in form of paste at ambient temperature and its

freezing point is about 305.15 K [7] (e.g. between the measurements at 303.15 and 323.15 K). This could explain the different trend of  $C_p$  value for this surfactant in comparison to other ones.

For solid particles, it is expected to obtain an increase in the isobaric heat capacity with the temperature rise [8]. In the literature, the isobaric heat capacity of other types of graphene nanosheets was previously measured. For example, Vallejo *et al.* [9] evaluated the  $C_p$  of functionalized graphene nanoplatelets, and found a values equal to 0.87, 0.905, 0.951, 0.989, 1.052 and 1.088  $J.g^{-1}.K^{-1}$  at 293.15, 303.15, 313.15, 323.15, 333.15 and 343.15 K, respectively. So an increase of about 25% was obtained with temperature rise in the tested range. We can remark that this graphene has a lower isobaric heat than that of FLG tested in the present study. In addition, another functionalized graphene nanoplatelets tested by Vallejo *et al.* [10] showed also a lower isobaric heat capacity than those of FLG. The obtained values were 0.688, 0.726, 0.764 and 0.8  $J.g^{-1}.K^{-1}$  at 293.15, 303.15, 313.15 and 323.15 K, respectively. So the enhancement rate of  $C_p$  in the tested temperature range was around 16%. In this two studies, the two different functionalized graphene samples are commercial and may present some defects due to their treatment, which could explain the reason of the higher  $C_p$  values presently obtained due to high quality of FLG.

In Figure IV.1, the isobaric heat capacity evolution of Tyfocor, tested base fluids and nanofluids is presented as a function of temperature. The error bars here correspond to the uncertainty of the device which was determined equal to  $\sim 3\%$  [3].



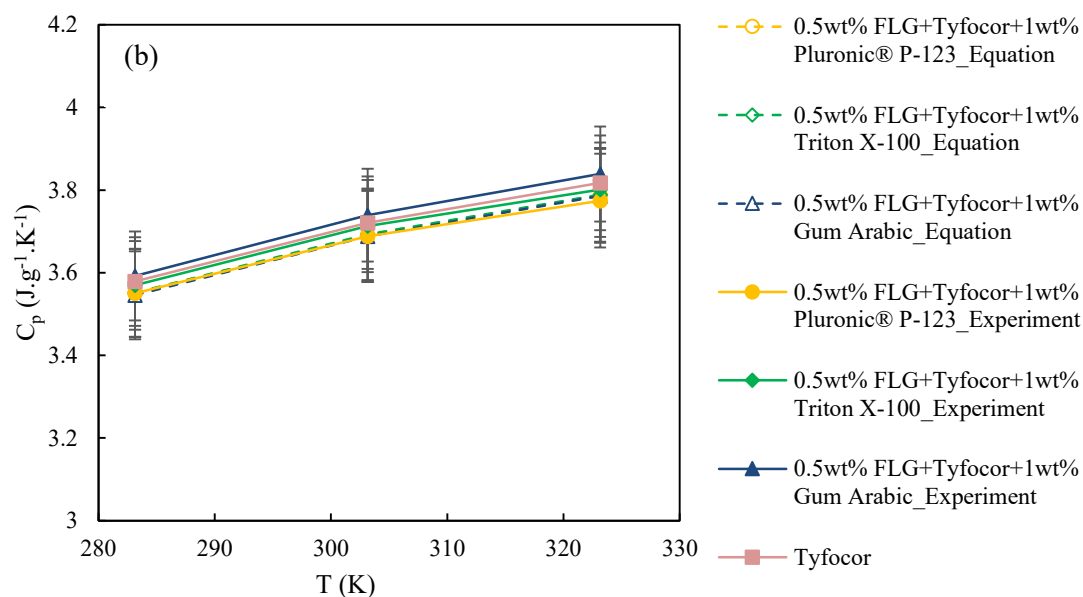


**Figure IV.1.** Isobaric heat capacity of base fluids (a) and nanofluids (b) as a function of temperature.

As mentioned before in chapter III (see Figure III.14), the measured values of isobaric heat capacity for Tyfocor® LS are in good agreement with the values given by the manufacturer [11]. It can be seen in Figure IV.1 that  $C_p$  of Tyfocor, base fluids and nanofluids increases with the rise of temperature from 283.15 to 323.15 K. The rate of this increase is  $\sim 7\%$  and it is approximately the same for all samples whatever the surfactant used. Also, the  $C_p$  of Tyfocor is higher than the values of FLG and the different surfactants.

For comparison purpose, Vallejo *et al.* [9] studied the effect of temperature on the  $C_p$  of functionalized graphene nanoplatelet nanofluids based on a commercial industrial antifreeze (Havoline® XLC Premixed 50/50 -solution of 50 vol.% of Havoline® XLC and 50 vol.% of water-) with weight concentrations up to 1%. An increase in the isobaric heat capacity up to 7.7% for base fluid and nanofluids was reported in the temperature range 293.15-343.15 K. In another study, Vallejo *et al.* [10] investigated a different functionalized graphene nanoplatelet nanofluids based on propylene glycol-water mixture with a mass ratio of (30:70)%. Here, the isobaric heat capacity of prepared nanofluids with concentrations from 0.25 to 1wt.% showed an increase lower than 2% for all samples with raising the temperature in the range 293.15-323.15 K.

### IV.3.2- Effect of surfactant and graphene concentration

Regarding the effect of surfactant and FLG concentration on the isobaric heat capacity of Tyfocor® LS, the experimental results showed that there is no significant change in the  $C_p$  after the addition of 1wt.% of each surfactant to Tyfocor® LS fluid (see Figure IV.1 (a)), and also the addition of 0.5wt.% of FLG to the base fluids (see Figure IV.1 (b)). So the  $C_p$  of Tyfocor® LS is not significantly modified with the presence of surfactant, nor with the addition of FLG.

On the other hand, the obtained experimental results were compared to the following well-known equation, the mixing rule (Eq.IV.1) presented earlier in chapter II, commonly used in nanofluid literature to predict the isobaric heat capacity of nanofluids from the  $C_p$  values and mass fractions,  $\varphi$ , of the different compounds. Note that here the presence of surfactant is clearly distinguished to the Tyfocor® LS.

$$C_{p,nf} = \varphi_{np} \cdot C_{p,np} + \varphi_{sft} \cdot C_{p,sft} + (1 - \varphi_{np} - \varphi_{sft}) \cdot C_{p,tyf} \quad \text{Eq.IV.1}$$

where  $nf$ ,  $np$ ,  $sft$ , and  $tyf$  subscripts stand for nanofluid, nanoparticles, surfactant, and Tyfocor® LS.  $\varphi$  is in wt.%.

A comparison between the experimental values and the  $C_p$  calculated using Eq.IV.1 shows that this equation can adequately describe the experimental results of base fluids and nanofluids in the temperature range 283.15-323.15 K with an absolute average deviation of 1.4% and 0.7% for the base fluids and nanofluids, respectively (see Figure IV.1).

After verifying the goodness of Eq.IV.1, the same equation was used to determine the isobaric heat capacity of the other concentrations of base fluids and nanofluids at 283.15, 303.15 and 323.15 K respectively. In addition, and because of the linear evolution of  $C_p$  with temperature (see Figure IV.1), the isobaric heat capacity of all samples (base fluids and nanofluids) at the two other temperatures, 293.15 and 313.15 K were extrapolated from the following simple linear equation (Eq.IV.2):

$$C_p = a_0 + a_1 T \quad \text{Eq.IV.2}$$

**Chapter IV - Characterization of FLG based nanofluids and their thermophysical properties: results and discussion**

where  $C_p$  is the isobaric heat in  $J.g^{-1}.K^{-1}$  and  $T$  is the temperature in K.  $a_i$ , the coefficients of each sample, and the respective standard deviation are gathered in Table IV.2.

**Table IV.2.** Fitting parameters  $a_i$  and standard deviations (St. Dev.) from Eq.IV.2 for the base fluids and nanofluids at different mass fractions.

	<b>Tyfocor® LS</b>	<b>Base fluids</b>				<b>Nanofluids</b>			
$\varphi_{m,ft}(\%)$	0	0.1	0.2	0.5	1.0	0.1	0.2	0.5	1.0
$\varphi_{m,np}(\%)$	0	0	0	0	0	0.05	0.1	0.25	0.5
<i>FLG nanofluids based on Tyfocor® LS and Triton X-100</i>									
$a_0/J.g^{-1}.K^{-1}$	1.896	1.895	1.894	1.892	1.861	1.894	1.892	1.886	1.939
$a_1/J.g^{-1}.K^{-2}$	0.006	0.006	0.006	0.006	0.006	0.006	0.006	0.006	0.006
St. Dev./ $J.g^{-1}.K^{-1}$	0.00940	0.00958	0.00977	0.01036	0.00850	0.00980	0.00998	0.01049	0.00967
Regression coefficient $R^2$	0.9878	0.9878	0.9878	0.9877	0.9839	0.9878	0.9878	0.9878	0.9812
<i>FLG nanofluids based on Tyfocor® LS and Pluronic® P-123</i>									
$a_0/J.g^{-1}.K^{-1}$	1.896	1.897	1.897	1.899	1.787	1.895	1.895	1.893	1.974
$a_1/J.g^{-1}.K^{-2}$	0.006	0.006	0.006	0.006	0.007	0.006	0.006	0.006	0.006
St. Dev./ $J.g^{-1}.K^{-1}$	0.00940	0.00992	0.01044	0.00697	0.00680	0.01014	0.01065	0.00697	0.00833
Regression coefficient $R^2$	0.9878	0.9878	0.9878	0.9877	0.9934	0.9878	0.9878	0.9878	0.9833
<i>FLG nanofluids based on Tyfocor® LS and Gum Arabic</i>									
$a_0/J.g^{-1}.K^{-1}$	1.896	1.893	1.890	1.880	1.774	1.891	1.887	1.873	1.853
$a_1/J.g^{-1}.K^{-2}$	0.006	0.006	0.006	0.006	0.007	0.006	0.006	0.006	0.006
St. Dev./ $J.g^{-1}.K^{-1}$	0.00940	0.00907	0.00878	0.00786	0.00923	0.00929	0.00898	0.00800	0.00977
Regression coefficient $R^2$	0.9878	0.9879	0.9879	0.9881	0.9917	0.9879	0.9880	0.9882	0.9881

So the experimental values of isobaric heat capacity and those determined using Eq.IV.1 and Eq.IV.2 of all samples, base fluids and nanofluids, and at all temperatures between 283.15 and 323.15 K are gathered in Table IV.3.

**Table IV.3.** Isobaric heat capacity values obtained experimentally (in **bold**), from Eq.IV.1 (in *italic*) and from Eq. IV.2 (in *italic and bold*) for the base fluids and nanofluids at different temperatures and mass fractions.

	Tyfocor® LS		Base fluids			Nanofluids			
$\varphi_{m,sft}$ (%)	0	0.1	0.2	0.5	1.0	0.1	0.2	0.5	1.0
$\varphi_{m,np}$ (%)	0	0	0	0	0	0.05	0.1	0.25	0.5
T(K)	C <sub>p</sub> (J.g <sup>-1</sup> .K <sup>-1</sup> )								
<i>FLG nanofluids based on Tyfocor® LS and Triton X-100</i>									
283.15	<b>3.579</b>	<i>3.577</i>	<i>3.576</i>	<i>3.571</i>	<b>3.607</b>	<i>3.576</i>	<i>3.573</i>	<i>3.565</i>	<b>3.569</b>
293.15	<b>3.655</b>	<i>3.654</i>	<i>3.653</i>	<i>3.651</i>	<b>3.678</b>	<i>3.653</i>	<i>3.651</i>	<i>3.644</i>	<b>3.639</b>
303.15	<b>3.721</b>	<i>3.719</i>	<i>3.718</i>	<i>3.713</i>	<b>3.759</b>	<i>3.718</i>	<i>3.715</i>	<i>3.707</i>	<b>3.713</b>
313.15	<b>3.775</b>	<i>3.774</i>	<i>3.773</i>	<i>3.771</i>	<b>3.802</b>	<i>3.773</i>	<i>3.771</i>	<i>3.764</i>	<b>3.755</b>
323.15	<b>3.817</b>	<i>3.816</i>	<i>3.814</i>	<i>3.809</i>	<b>3.856</b>	<i>3.815</i>	<i>3.812</i>	<i>3.803</i>	<b>3.801</b>
<i>FLG nanofluids based on Tyfocor® LS and Pluronic® P-123</i>									
283.15	<b>3.579</b>	<i>3.577</i>	<i>3.576</i>	<i>3.571</i>	<b>3.617</b>	<i>3.576</i>	<i>3.573</i>	<i>3.565</i>	<b>3.551</b>
293.15	<b>3.655</b>	<i>3.656</i>	<i>3.656</i>	<i>3.629</i>	<b>3.692</b>	<i>3.654</i>	<i>3.654</i>	<i>3.622</i>	<b>3.616</b>
303.15	<b>3.721</b>	<i>3.719</i>	<i>3.718</i>	<i>3.713</i>	<b>3.765</b>	<i>3.718</i>	<i>3.715</i>	<i>3.707</i>	<b>3.688</b>
313.15	<b>3.775</b>	<i>3.776</i>	<i>3.776</i>	<i>3.747</i>	<b>3.822</b>	<i>3.774</i>	<i>3.774</i>	<i>3.740</i>	<b>3.728</b>
323.15	<b>3.817</b>	<i>3.816</i>	<i>3.814</i>	<i>3.809</i>	<b>3.876</b>	<i>3.814</i>	<i>3.811</i>	<i>3.802</i>	<b>3.775</b>
<i>FLG nanofluids based on Tyfocor® LS and Gum Arabic</i>									
283.15	<b>3.579</b>	<i>3.577</i>	<i>3.574</i>	<i>3.568</i>	<b>3.596</b>	<i>3.575</i>	<i>3.572</i>	<i>3.562</i>	<b>3.592</b>
293.15	<b>3.655</b>	<i>3.652</i>	<i>3.648</i>	<i>3.639</i>	<b>3.679</b>	<i>3.650</i>	<i>3.646</i>	<i>3.632</i>	<b>3.671</b>
303.15	<b>3.721</b>	<i>3.719</i>	<i>3.717</i>	<i>3.711</i>	<b>3.746</b>	<i>3.718</i>	<i>3.714</i>	<i>3.705</i>	<b>3.739</b>
313.15	<b>3.775</b>	<i>3.772</i>	<i>3.768</i>	<i>3.759</i>	<b>3.809</b>	<i>3.770</i>	<i>3.766</i>	<i>3.752</i>	<b>3.795</b>
323.15	<b>3.817</b>	<i>3.816</i>	<i>3.814</i>	<i>3.808</i>	<b>3.855</b>	<i>3.814</i>	<i>3.811</i>	<i>3.802</i>	<b>3.839</b>

An analysis on the isobaric heat capacity data of nanofluids in Table IV.3 shows that this property slightly decreases with increasing nanoparticle's volume fraction since FLG have a lower isobaric heat capacity than Tyfocor. This agrees well with previous experimental [6,12–16] and theoretical results [17,18].

However, the change in C<sub>p</sub> for nanofluids with the FLG content is not significant at all because of the low content in FLG nanosheets and the large difference between C<sub>p</sub> of FLG and Tyfocor® LS. Similar results were also previously reported in the literature for graphene-based nanofluids. For example, Amiri *et al.* [19,20] studied a highly crumpled few-layer graphene (HCFLG)/water nanofluids using Gum Arabic as a surfactant and monolayer graphene nanoparticles (SGr)/water nanofluids with concentrations up to 0.01wt.%. A small drop of 0.1-0.5% in heat capacity of nanofluids with concentration decrease was reported. In addition, Vallejo *et al.* [9] showed a non-significant decrease in the C<sub>p</sub> of the studied functionalized graphene nanoplatelet nanofluids based on a commercial industrial antifreeze with the use of sodium dodecylbenzene sulfonate (SDBS) as

a surfactant, as the  $C_p$  only increases by 0.74% for the highest concentration, 1wt.% in comparison to base fluid.

In conclusion, the isobaric heat capacity of the studied FLG nanofluids based on Tyfocor® LS does not increase with FLG, whatever the FLG concentration. In addition, the isobaric heat capacity of nanofluids increases with temperature similarly to base fluid in the temperature range from 283.15 to 323.15 K.

### IV.3.3- References

1. Żyła, G.; Vallejo, J.P.; Lugo, L. Isobaric heat capacity and density of ethylene glycol based nanofluids containing various nitride nanoparticle types: An experimental study. *Journal of Molecular Liquids* **2018**, *261*, 530–539, doi:10.1016/j.molliq.2018.04.012.
2. Agromayor, R.; Cabaleiro, D.; Pardinas, A.; Vallejo, J.; Fernandez-Seara, J.; Lugo, L. Heat Transfer Performance of Functionalized Graphene Nanoplatelet Aqueous Nanofluids. *Materials* **2016**, *9*, 455, doi:10.3390/ma9060455.
3. Cabaleiro, D.; Gracia-Fernández, C.; Legido, J.L.; Lugo, L. Specific heat of metal oxide nanofluids at high concentrations for heat transfer. *International Journal of Heat and Mass Transfer* **2015**, *88*, 872–879, doi:10.1016/j.ijheatmasstransfer.2015.04.107.
4. Teng, T.-P.; Hung, Y.-H.; Teng, T.-C.; Chen, J.-H. Performance evaluation on an air-cooled heat exchanger for alumina nanofluid under laminar flow. *Nanoscale Res Lett* **2011**, *6*, 488, doi:10.1186/1556-276X-6-488.
5. Teng, T.-P.; Hung, Y.-H. Estimation and experimental study of the density and specific heat for alumina nanofluid. *Journal of Experimental Nanoscience* **2014**, *9*, 707–718, doi:10.1080/17458080.2012.696219.
6. Starace, A.K.; Gomez, J.C.; Wang, J.; Pradhan, S.; Glatzmaier, G.C. Nanofluid heat capacities. *Journal of Applied Physics* **2011**, *110*, 124323, doi:10.1063/1.3672685.
7. <http://candmz04.brenntag.ca/MSDS/Fr/00070113.pdf>.
8. Naef, R. Calculation of the Isobaric Heat Capacities of the Liquid and Solid Phase of Organic Compounds at and around 298.15 K Based on Their “True” Molecular Volume. *Molecules* **2019**, *24*, 1626, doi:10.3390/molecules24081626.
9. Vallejo, J.P.; Álvarez-Regueiro, E.; Cabaleiro, D.; Fernández-Seara, J.; Fernández, J.; Lugo, L. Functionalized graphene nanoplatelet nanofluids based on a commercial industrial antifreeze for the thermal performance enhancement of wind turbines. *Applied Thermal Engineering* **2019**, *152*, 113–125, doi:10.1016/j.applthermaleng.2019.02.046.
10. Vallejo, J.P.; Pérez-Tavernier, J.; Cabaleiro, D.; Fernández-Seara, J.; Lugo, L. Potential heat transfer enhancement of functionalized graphene nanoplatelet dispersions in a propylene glycol-water mixture. Thermophysical profile. *The Journal of Chemical Thermodynamics* **2018**, *123*, 174–184, doi:10.1016/j.jct.2018.04.007.
11. Tyfocor LS technical information, available at <https://tyfo.de/en/produkt/Tyfocor-ls/> (n.d.).
12. Chandrasekar, M.; Suresh, S.; Senthilkumar, T. Mechanisms proposed through experimental investigations on thermophysical properties and forced convective heat transfer

- characteristics of various nanofluids – A review. *Renewable and Sustainable Energy Reviews* **2012**, *16*, 3917–3938, doi:10.1016/j.rser.2012.03.013.
13. Fakoor Pakdaman, M.; Akhavan-Behabadi, M.A.; Razi, P. An experimental investigation on thermo-physical properties and overall performance of MWCNT/heat transfer oil nanofluid flow inside vertical helically coiled tubes. *Experimental Thermal and Fluid Science* **2012**, *40*, 103–111, doi:10.1016/j.expthermflusci.2012.02.005.
  14. Vajjha, R.S.; Das, D.K. Specific Heat Measurement of Three Nanofluids and Development of New Correlations. *Journal of Heat Transfer* **2009**, *131*, 071601, doi:10.1115/1.3090813.
  15. Pantzali, M.N.; Kanaris, A.G.; Antoniadis, K.D.; Mouza, A.A.; Paras, S.V. Effect of nanofluids on the performance of a miniature plate heat exchanger with modulated surface. *International Journal of Heat and Fluid Flow* **2009**, *30*, 691–699, doi:10.1016/j.ijheatfluidflow.2009.02.005.
  16. He, Q.; Wang, S.; Tong, M.; Liu, Y. Experimental study on thermophysical properties of nanofluids as phase-change material (PCM) in low temperature cool storage. *Energy Conversion and Management* **2012**, *64*, 199–205, doi:10.1016/j.enconman.2012.04.010.
  17. Pak, B.C.; Cho, Y.I. Hydrodynamic and heat transfer study of dispersed fluids with submicron metallic oxide particles. *Experimental Heat Transfer* **1998**, *11*, 151–170, doi:10.1080/08916159808946559.
  18. Xuan, Y.; Roetzel, W. Conceptions for heat transfer correlation of nanofluids. *International Journal of Heat and Mass Transfer* **2000**, *43*, 3701–3707, doi:10.1016/S0017-9310(99)00369-5.
  19. Amiri, A.; Shanbedi, M.; Rafieerad, A.R.; Rashidi, M.M.; Zaharinie, T.; Zubir, M.N.M.; Kazi, S.N.; Chew, B.T. Functionalization and exfoliation of graphite into mono layer graphene for improved heat dissipation. *Journal of the Taiwan Institute of Chemical Engineers* **2017**, *71*, 480–493, doi:10.1016/j.jtice.2016.12.009.
  20. Amiri, A.; Ahmadi, G.; Shanbedi, M.; Etemadi, M.; Mohd Zubir, M.N.; Chew, B.T.; Kazi, S.N. Heat transfer enhancement of water-based highly crumpled few-layer graphene nanofluids. *RSC Adv.* **2016**, *6*, 105508–105527, doi:10.1039/C6RA22365F.

#### **IV.4- Volumetric properties and surface tension of few-layer graphene nanofluids based on a commercial heat transfer fluid**

Article

# Volumetric Properties and Surface Tension of Few-Layer Graphene Nanofluids Based on a Commercial Heat Transfer Fluid

Samah Hamze <sup>1</sup>, David Cabaleiro <sup>1,2</sup>, Dominique Bégin <sup>3</sup>, Alexandre Desforges <sup>4</sup>, Thierry Maré <sup>1</sup>, Brigitte Vigolo <sup>4</sup>, Luis Lugo <sup>2</sup> and Patrice Estellé <sup>1,\*</sup>

- <sup>1</sup> Laboratoire de Génie Civil et Génie Mécanique, Université de Rennes, F-35000 Rennes, France; samah.hamze@univ-rennes1.fr (S.H.); dacabaleiro@uvigo.es (D.C.); thierry.mare@univ-rennes1.fr (T.M.)
- <sup>2</sup> Dpto. Física Aplicada, Facultad de Ciencias, Universidad de Vigo, E-36310 Vigo, Spain; luis.lugo@uvigo.es
- <sup>3</sup> Institut de Chimie et Procédés pour l’Energie, l’Environnement et la Santé (ICPEES) CNRS-University of Strasbourg, 25, rue Becquerel, F-67087 Strasbourg Cedex, France; dominique.begin@unistra.fr
- <sup>4</sup> Institut Jean Lamour UMR7198, Université de Lorraine, CNRS, F-54000 Nancy, France; alexandre.desforges@univ-lorraine.fr (A.D.); brigitte.vigolo@univ-lorraine.fr (B.V.)
- \* Correspondence: patrice.estelle@univ-rennes1.fr; Tel.: +33-0223-234-200

Received: 9 June 2020; Accepted: 2 July 2020; Published: 4 July 2020



**Abstract:** Volumetric properties such as density and isobaric thermal expansivity, and surface tension are of paramount importance for nanofluids to evaluate their ability to be used as efficient heat transfer fluids. In this work, the nanofluids are prepared by dispersing few-layer graphene in a commercial heat transfer fluid Tyfocor<sup>®</sup> LS (40:60 wt.% propylene-glycol/water) with the aid of three different nonionic surfactants: Triton X-100, Pluronic<sup>®</sup> P-123 and Gum Arabic. The density, isobaric thermal expansivity and surface tension of each of the base fluids and nanofluids are evaluated between 283.15 and 323.15 K. The influence of the mass content in few-layer graphene from 0.05 to 0.5% on these nanofluid properties was studied. The density behavior of the different proposed nanofluids is slightly affected by the presence of graphene, and its evolution is well predicted by the weight-average equation depending on the density of each component of the nanofluids. For all the analyzed samples, the isobaric thermal expansivity increases with temperature which can be explained by a weaker degree of cohesion within the fluids. The surface tension evolution of the graphene-based nanofluids is found to be sensitive to the used surfactant, its content and the few-layer graphene concentration.

**Keywords:** few-layer graphene; propylene-glycol/water; nanofluids; density; surface tension; isobaric thermal expansivity

## 1. Introduction

Nanofluids are suspensions of nanoparticles (1–100 nm in size) dispersed in base fluids commonly used in heat transfer processes [1]. These engineering materials are potentially attractive for many applications in the energy field including cooling engines and electronic circuits or increasing and recovering solar thermal energy [2]. In the last century, the enhancement of thermal performance has become a key issue in the energy field considering the rapid growth in energy consumption worldwide [3–5]. Interestingly, many studies have reported enhancement of thermal conductivity and heat transfer performance of nanofluids. The found key parameters are both the nature of nanoparticles and effect of the used base fluids, as given in some articles on this topic [2,6–14]. Carbon nanomaterials are of major interest in this field due to their excellent intrinsic thermal properties, which are superior to those of metallic or metal oxide nanoparticles; carbon nanomaterials such as carbon nanotubes (CNTs)

or graphene are consequently expected to be better thermal enhancers in nanofluid design [5,15]. In particular, graphene exhibits the best characteristics regarding its thermal conductivity spectrum amongst the carbon nanomaterials [5,15,16]. Graphene is a sheet of an atomic thickness only composed of carbon atoms which are hybridized  $sp^2$  and arranged in a honeycomb network. Thermophysical behavior of graphene-based nanofluids has been the topic of several investigations [17–19]. However, so far, analysis and evolution of the surface tension (ST) of graphene-based nanofluids, which is another important aspect to take into account in nanofluid behavior, has been overlooked [20].

When analyzing the performance of thermal systems, evolution of ST has a significant impact on the surface properties such as wettability [21,22]. Hence, together with the vaporization latent heat of the nanofluid and the difference between the density of the liquid and the vapor phase, nanofluid ST allows the description of condensation and boiling phenomena [23,24]. The ST study is especially a relevant parameter to study for graphene nanofluid since, as it is widely known, graphene is highly hydrophobic. Pristine graphene nanosheets have consequently high tendency to agglomerate in all common aqueous solvents and particularly those (often water or water/glycol-based compound mixtures) used as thermal medium [5,25,26]. Decrease in hydrophobicity or in other words improving affinity of graphene with water can be obtained by non-covalent or covalent functionalization of graphene surface. Such chemical treatments can be involved in ST evolution of graphene-based nanofluids. As shown in Table 1, studies about ST of graphene-based nanofluids are limited.

**Table 1.** Summary of previous surface tension studies on graphene nanofluids.

Reference	Nanoparticle		Base Fluid	Surfactant (np:sft Ratio)	Surface Tension Technique	Main Result with NP Loading
	Type	Concentration				
Ahamed et al. [27]	Graphene	0–0.15 vol.%	Water	SDBS (5 vol.%)	Bubble pressure method	ST↓
Cabaleiro et al. [5]	Graphene oxide and reduced graphene oxide	0–0.1 vol.%	Water	No surfactant	Pendant drop method	ST↓
Ilyas et al. [28]	Graphene nanoplatelets	0–0.25 wt.%	Saline aqueous media (NaCl)	SDS (1:1.5)	Pendant drop method	ST↓
Kamatchi et al. [29]	Reduced graphene oxide	0–0.3 g/l	Water	No surfactant	Bubble pressure method	ST↑
Liu et al. [30]	Graphene oxide	0–0.12 wt.%	Water	No surfactant	Oscillation droplet method	ST↑
Zheng et al. [31]	Graphene oxide	0–1 wt.%	Water	Not mentioned	Ring method	ST↑

In 2014, Zheng studied the ST of water/graphene oxide (GO)-based nanofluids [31] and reported that ST increases with the rising of nanoparticle content. A maximum enhancement of about 3% (with respect to that of water) was found for the highest GO weight content used 0.1 wt.%. The results have also shown that ST decreased when the nanoparticle size was reduced and when the temperature raised from 293.15 to 333.15 K. Later, Kamatchi et al. investigated the ST of reduced graphene oxide (rGO) dispersed in water with nanoparticle concentration from 0.01 to 0.3 g/L [29]. They also showed a decrease in ST when temperature increased from 308.15 to 348.15 K. Graphene–water nanofluids were also recently investigated by Ahmed et al. [27]. The concentration of nanoparticles was varied from 0.05 to 0.15 vol.% and the tested temperature range was 283.15–363.15 K. The nanofluids were prepared by dispersing a commercial graphene (with 1–5 nm of thickness) in water by using 5% of Sodium DodecylBenzene Sulfonate (SDBS) as surfactant. ST of these graphene-based nanofluids decreased with temperature (3.3% for each 10 K) and also with nanoparticle content. This behavior was related to the reduction of the attractive interactions between the fluid molecules and the nanoparticles by enhancing of nanoparticle absorption at liquid–gas interface since graphene is hydrophobic. Cabaleiro et al. [5] focused on the effect of graphene type (GO or rGO) and nanoparticle loading on ST of the prepared nanofluids with GO and two different reduction rates of rGO at different nanoparticle concentrations between 0.0005 and 0.1 vol.%. The measurements, performed at room temperature, showed that ST decreased with graphene loading. The maximum reduction in ST (about 3%) was obtained for the highest graphene volume fraction used. No significant effect of the chemical reduction of GO was

observed on ST behavior. The surface tension of graphene oxide nanofluids was measured at low temperature by the oscillation droplet method in an acoustic levitator by Liu et al. [30]. The ST of these nanofluids was reported to increase with mass concentration (in the range from 0.02 to 0.12%) and decrease with increasing temperature, with a strong effect of the subcooled temperature. Recently, Ilyas et al. [28] investigated temperature (298.15–338.15 K) and nanoparticle concentration (0–0.25 wt.%) effects on the surface tension of graphene nanoplatelets-based saline (NaCl) aqueous nanofluids using the pendant drop method. Samples were stabilized using anionic sodium dodecyl sulfate (SDS) at a nanoparticle:surfactant ratio of 1:1.5. Obtained results showed that the addition of nanoplatelets reduced the surface tension of the saline base fluid by 21% (modifications in ST were similar for the four analyzed graphene concentrations).

Some previous investigations on the density or volumetric behavior of graphene nanofluids are gathered in Table 2.

**Table 2.** Some volumetric behavior/density studies on graphene nanofluids.

Reference	Nanoparticle		Base Fluid	Surfactant	Measuring Technique	Main Result with NP Loading
	Type	Concentration				
Alawi et al. [32]	Pentaethylene glycol-(thermally)-treated graphene nanoplatelets	0–0.1 wt.%	Water	No surfactant	Vibrating U-tube	$\rho \uparrow$
Amiri et al. [33]	Amine-treated graphene quantum dots	0–0.02 wt.%	Water	No surfactant	Vibrating U-tube	$\rho \rightarrow$
Azizi et al. [34]	Functionalized few-layer graphene	0.025, 0.05, 0.1 wt.%	Water, ethylene glycol	PVA	Vibrating U-tube	$\rho \uparrow$
Cabaleiro et al. [16]	Functionalized graphene nanoplatelets	0.1, 0.25, 0.5 wt.%	Ethylene glycol: water (10:90)	No surfactant	Vibrating U-tube	$\rho \uparrow, \alpha_p \downarrow$
Ijam et al. [35]	Graphene oxide nanosheets	0–0.1 wt.%	Ethylene glycol: water (40:60)	No surfactant	Vibrating U-tube	$\rho \downarrow$
Karami et al. [36]	Carboxyl-functionalized graphene nanoplatelets	0.1, 0.2 wt.%	Water	No surfactant	Vibrating U-tube	$\rho \rightarrow \uparrow$
Sani et al. [37]	Functionalized graphene nanoplatelets	0.005, 0.05 wt.%	Havoline® XLC Premixed 50/50,	SDBS(0.125 wt.%)	Vibrating U-tube	$\rho \uparrow$
Vallejo et al. [38]	Functionalized graphene nanoplatelets	0.25–1 wt.%	Propylene glycol: water (30:70)	No surfactant	Vibrating U-tube	$\rho \uparrow, \alpha_p \downarrow$
Vallejo et al. [39]	Functionalized graphene nanoplatelets	0.25–1 wt.%	Havoline® XLC Premixed 50/50,	SDBS(0.125 wt.%)	Vibrating U-tube	$\rho \uparrow, \alpha_p \downarrow$
Yarmad et al. [40]	Functionalized graphene nanoplatelets	0–0.1 wt.%	Water	No surfactant	Vibrating U-tube	$\rho \uparrow$
Yarmand et al. [41]	Activate carbon/graphene hybrid	0.02, 0.04, 0.06 wt.%	Ethylene glycol	No surfactant	Vibrating U-tube	$\rho \uparrow$

Azizi et al. [34] studied the density of ethylene glycol-based and water-based nanofluids containing 0.025–0.1 wt.% of polyvinyl alcohol-functionalized few-layer graphene. Results in the temperature range from 293.15 to 323.15 K showed as density increased with nanoparticle loading and declines with temperature (~0.98% for the 0.1 wt.% aqueous nanofluid in the whole studied temperature range). Ijam et al. [35] investigated the density of graphene oxide nanosheet dispersions in an ethylene glycol:water mixture at 40:60 mixing ratio. In the analyzed nanoparticle (0.01–0.1 wt.%) and temperature (298.15–318.15 K) ranges density decreased with the addition of the nanoparticles, with maximum reductions 1–1.13% for the highest nanoparticle concentration. Vallejo et al. [39] and Sani et al. [37] investigated the volumetric behavior of polycarboxylate chemically modified graphene nanoplatelet dispersions based on a commercial coolant, Havoline® XLC Premixed 50/50. In both studies, a concentration of 0.125 wt.% of SDBS was used to improve nanofluid stability. Density measurements showed as density increased with nanoparticle concentration, up to 0.37–0.58% for the 1 wt.% in the temperature range from 293.15 to 343.15 K [39]. Yarmand et al. [40] analyzed the density of water-based nanofluids loaded with 0.02–0.1 wt.% of graphene nanoplatelets functionalized using nitric and sulfuric acid. In the studied temperature range (from 293.15 to 313.15 K) a maximum increase of 0.06% was observed for the 0.1 wt.% at 313.15 K.

Here, nanofluids were prepared with few-layer graphene (FLG). Tyfocor® LS, a commercial fluid which is a mixture of propylene-glycol/water (around 40:60 wt%) was used as base fluid [42,43] and three different surfactants (Triton X-100, Pluronic® P-123 and Gum Arabic) were used to help in the

dispersion and stabilization of FLG in the base fluid and to counterbalance hydrophobic attractive forces. The concentrations of nanoparticles in these nanofluids were 0.05, 0.1, 0.25 and 0.5 wt.%. The nanoparticle:surfactant ratio added was fixed to 1:2. Density, isobaric thermal expansivity and surface tension of all base fluids and nanofluids were evaluated between 283.15 and 323.15 K. These properties and their evolutions are finally discussed according to the temperature dependence, concentration and the used type of surfactant and the nanoparticle content. This will complete the thermal conductivity evaluation of these nanofluids recently performed in [44].

## 2. Materials and Methods

### 2.1. Nanofluid Preparation

As recently described in [44], FLG was synthesized by a mechanical exfoliation method. Typically, 400 mg of expanded graphite (provided by Mersen, France) was sonicated by using a Branson probe sonicator (80 W, 4 h, 298.15 K) in water in the presence of tannic acid (Sigma-Aldrich). The prepared FLG was thereafter washed typically 5 times with deionized water before being freeze-dried. The obtained FLG powder was added to different base fluids prepared by adding the chosen amount of surfactant to Tyfocor<sup>®</sup> LS used as solvent. Tyfocor<sup>®</sup> LS was kindly provided by Viessmann S.A. Three different nonionic surfactants were used: Triton X-100 (C<sub>8</sub>H<sub>17</sub>C<sub>6</sub>H<sub>4</sub>(OC<sub>2</sub>H<sub>4</sub>)<sub>9-10</sub>OH), Pluronic<sup>®</sup> P-123 -a linear triblock copolymer comprising poly(ethylene oxide) (PEO) and poly(propylene oxide) (PPO) alternating blocks such as PEO-PPO-PEO- and Gum Arabic (natural mixture of polysaccharides and glycoproteins). The nanofluid of the highest FLG concentration (0.5 wt.%) was first prepared by adding the desired amount of FLG powder in the surfactant+Tyfocor<sup>®</sup> LS-based fluid and dispersing the mixture with a Bioblock Scientific VibraCell 75,042 probe sonicator (125 W with a pulse mode 2 s ON/1 s OFF) by 5 runs of 15 min. This concentrated nanofluid was then diluted with Tyfocor<sup>®</sup> LS to obtain the nanofluids with different FLG concentrations of 0.05, 0.1 and 0.25 wt.%.

### 2.2. Characterization Techniques

An XL30 S-FEG apparatus (Philips, Netherlands) was used for scanning electron microscopy (SEM) observations. High-resolution transmission electron microscopy (HRTEM) investigations were performed thanks to a JEM-ARM 200F apparatus (JEOL, Japan) at 80 kV. For both SEM and TEM observations, the FLG powder was dispersed in ethanol and deposited in the dedicated sample holder. Holey carbon grids (200 mesh size) were used for TEM. For each sample, about 30 images were taken at different areas to guarantee a statistical description of the sample.

Density,  $\rho$ , of Tyfocor<sup>®</sup> LS, liquid Triton X-100, each surfactant+Tyfocor<sup>®</sup> LS mixture used as base fluids and the prepared FLG-based nanofluids were experimentally determined by means of a density meter DMA 501 (Anton Paar, Austria). The measurement principle is based on the oscillating U-tube technique. The density measurements were carried out in the temperature range from 288.15 to 313.15 K. 2 mL of each sample were withdrawn into a syringe and then released in the U-tube until the tube was completely full. Careful rinsing with ethanol and acetone was performed at the end of each measurement. Between each series of measurements, the densimeter was carefully checked by measuring air and distilled water densities at 293.15 K. The absolute average deviations (AAD) between the experimental results of distilled water at 293.15 K and literature data [45] were less or equal to 0.02%. The estimated uncertainty of the density determinations was lower than 1 kg.m<sup>-3</sup>. During density measurements with DMA500 densimeter, temperature was controlled within an accuracy of  $\pm 0.3$  K (repeatability of  $\pm 0.1$  K) using cascaded Peltier elements integrated in the U-tube vibrating cell.

A Drop Shape Analyzer DSA-30 from KRÜSS GmbH (Hamburg, Germany) was used to perform the ST measurements. Drops of samples were produced with a 15-gauge needle (outer diameter of 1.835 mm) controlling the flow rate and volume. The entire followed experimental procedure was described in detail in refs. [5,46]. With pendant drop technique, ST was determined from the density of each sample and the drop shape analysis suspended to the extremity of the needle, using

Young–Laplace equation. In the following, each reported ST value was calculated from the average of at least 10 measurements. ST of distilled water was measured in the 283.15–333.15 K temperature range [42]. The uncertainty with this equipment is low and an AAD of 1.1% was obtained between the experimental data of water and reference data in this temperature range [45]. Regarding surface tension experiments, samples were thermostated with a precision of  $\pm 0.2$  K by means of a TC40 environmental chamber in which temperature is regulated using a Peltier system and monitored by a PT100 probe. It should be also noted that a series of ST experiments at ambient temperature has been previously performed by varying the surfactant content to determine the adsorption phenomenon of these surfactants in Tyfocor<sup>®</sup> LS and the critical micelle concentration (CMC). This is useful for the discussion about the influence of surfactant and FLG content on the ST of nanofluids.

### 3. Results and Discussion

#### 3.1. FLG Nanosheets Characterization

Figure 1 shows images from both SEM and TEM observations of FLGs used in this work. They appear as nanosheets of around 5  $\mu\text{m}$  in lateral size (Figure 1a). From TEM observations at low magnification, very thin layers deposited on the holed TEM carbon grid are visible (Figure 1b). Their thickness, if of only a few layers of graphene, as it is observed in Figure 1c and its insert, are consistent with the graphene nomenclature [47]. The hexagonal lattice of the graphene layer well noticeable in high TEM magnification image is the sign of the high structural quality of the used FLGs (Figure 1d).

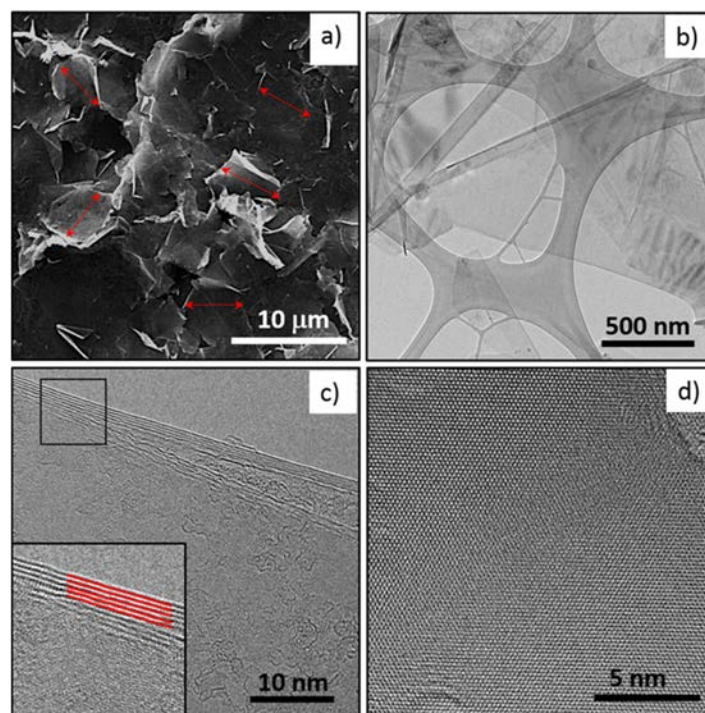


**Figure 1.** SEM and TEM observations of the used few-layer graphene (FLG). (a) SEM image, (b–d) TEM images at different magnifications.

#### 3.2. Density

Surface tension and isobaric thermal expansivities are related to the density of fluids. This is the reason why it is important to determine this property first determined. The densities of each of the base fluids and nanofluids were experimentally evaluated from 288.15 to 313.15 K in intervals of 5 K. First, the experimental densities for Tyfocor<sup>®</sup> LS showed an AAD of 0.13% in comparison to manufacturer data [46]. The experimental density values were correlated to Equation (1) [38,42,49] to obtain the density values for all samples below 288.15 and above 313.15 K.

$$\rho(T) = a_0 + a_1T + a_2T^2 \quad (1)$$

where  $\rho$  is the density in  $\text{kg}\cdot\text{m}^{-3}$  and  $T$  is the temperature in K. Densities at 283.15 and 323.15 K were calculated using this equation.  $a_i$  coefficients of each sample are gathered in Table 3 along with their respective standard deviation.

The experimental density values were correlated to Equation (1) [38,42,49] to obtain the density values for all samples below 288.15 and above 313.15 K.

$$\rho(T) = a_0 + a_1T + a_2T^2 \quad (1)$$

where  $\rho$  is the density in  $\text{kg}\cdot\text{m}^{-3}$  and  $T$  is the temperature in K. Densities at 283.15 and 323.15 K were calculated using this equation.  $a_i$  coefficients of each sample are gathered in Table 3 along with their respective standard deviation.

**Table 3.** Fitting parameters  $a_i$  and standard deviations (St. Dev.) from Equation (1) for the base fluids and nanofluids with Triton X-100, Pluronic® P-123, and Gum Arabic as surfactant for different mass fractions.

	Tyfocor® LS		Base Fluids			Nanofluids			
$\varphi_{m,sft}$ (%)	0	0.1	0.2	0.5	1.0	0.1	0.2	0.5	1.0
$\varphi_{m,np}$ (%)	0	0	0	0	0	0.05	0.1	0.25	0.5
<i>FLG nanofluids based on Tyfocor® LS and Triton X-100</i>									
$a_0/\text{kg}\cdot\text{m}^{-3}$	1043.8	1038.3	1038.4	1005.5	1005.7	991.41	1007.5	1021.4	987.16
$(a_1)/\text{kg}\cdot\text{m}^{-3}\cdot\text{K}^{-1}$	0.53736	0.57746	0.57689	0.79449	0.79449	0.87035	0.76469	0.67879	0.91615
$(10^3\cdot a_2)/\text{kg}\cdot\text{m}^{-3}\cdot\text{K}^{-2}$	-1.93	-2.00	-2.00	-2.36	-2.36	-2.46	-2.29	-2.14	-2.54
$(10^2\cdot\text{St. Dev.})/\text{kg}\cdot\text{m}^{-3}$	3.6	1.8	2.0	2.3	2.3	0.8	3.4	1.8	0.8
<i>FLG nanofluids based on Tyfocor® LS and Pluronic® P-123</i>									
$a_0/\text{kg}\cdot\text{m}^{-3}$	1043.8	1070	1012.5	1041.3	1044.1	1044.7	990.15	1008.8	1012.1
$(a_1)/\text{kg}\cdot\text{m}^{-3}\cdot\text{K}^{-1}$	0.53736	0.36499	0.74983	0.55741	0.54941	0.5107	0.87577	0.76411	0.75897
$(10^3\cdot a_2)/\text{kg}\cdot\text{m}^{-3}\cdot\text{K}^{-2}$	-1.93	-1.64	-2.29	-1.96	-1.96	-1.86	-2.46	-2.29	-2.29
$(10^2\cdot\text{St. Dev.})/\text{kg}\cdot\text{m}^{-3}$	3.7	1.8	1.8	2.1	1.9	1.9	0.9	2.2	2.1
<i>FLG nanofluids based on Tyfocor® LS and Gum Arabic</i>									
$a_0/\text{kg}\cdot\text{m}^{-3}$	1043.8	1037.1	1029.3	1022.8	1041.9	1013.3	988.12	977.14	1003.7
$(a_1)/\text{kg}\cdot\text{m}^{-3}\cdot\text{K}^{-1}$	0.53736	0.5826	0.64217	0.68855	0.57746	0.72345	0.89554	0.98172	0.8294
$(10^3\cdot a_2)/\text{kg}\cdot\text{m}^{-3}\cdot\text{K}^{-2}$	-1.93	-2.00	-2.11	-2.18	-2.00	-2.21	-2.50	-2.64	-2.39
$(10^2\cdot\text{St. Dev.})/\text{kg}\cdot\text{m}^{-3}$	3.7	1.1	2.1	1.5	1.8	2.7	0.4	0.9	3.2

Figure 2 shows the variation of the density of the nanofluids and base fluids measured and extrapolated with Equation (1) for the three surfactant series. The density of both base fluids and the corresponding nanofluids decreases by 2.4% between 283.15 and 323.15 K with a similar trend. Except for addition of 0.5 and 1 wt.% of Gum Arabic in Tyfocor® LS for which the density increases by 0.18 and 0.36%, respectively, addition of surfactant has no significant effect on the density evolution compared to Tyfocor® LS alone.

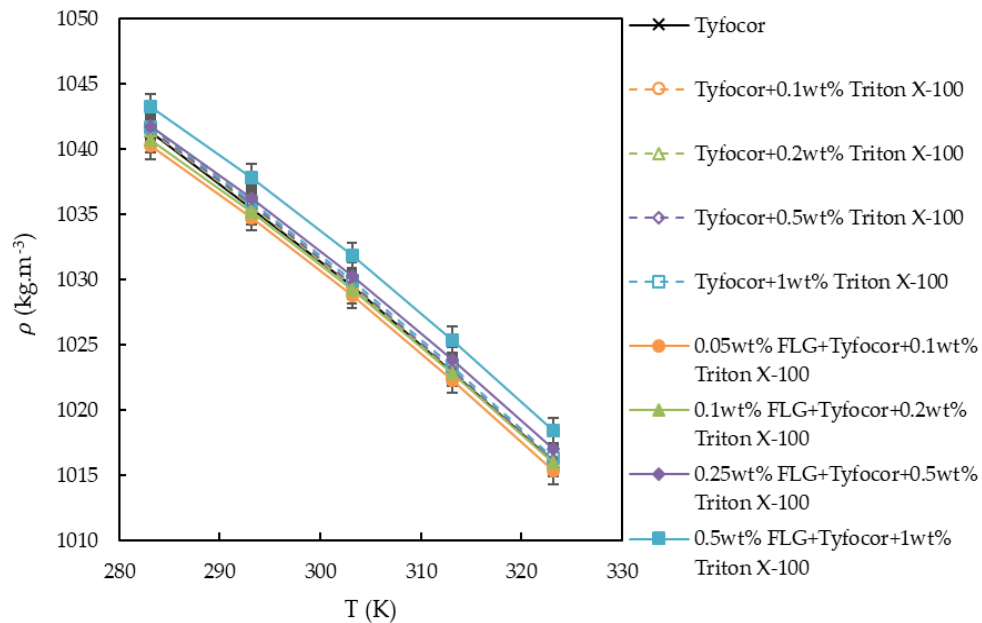
The effect that the addition of FLG has on the density of the base fluids (i.e., corresponding Tyfocor® LS–surfactant mixtures) is shown in Figure 3. The results show that the nanofluid density decreases slightly for the lowest FLG concentrations and increases for the highest FLG concentration studied. Results are similar for the three studied nanofluid sets, with average deviations of the density obtained at all temperatures for the four concentrations (0.05, 0.1, 0.25, and 0.5 wt.%) around  $-0.08$ ,  $-0.05$ ,  $0.05$ , and  $0.2\%$ , respectively. The decrease in density after adding a small amount of FLG to the base fluids could be explained by the existence of a negative excess volume, which represents a deviation from the ideal mixing volume. The FLG nanosheets (relatively big compared to the surrounding fluid molecules) may indeed impact the local organization of the base fluid molecules which are much more packed together than in the pure base fluid, resulting in the observed decrease in density [50,51]. A contractive volumetric behavior was also reported for aqueous nanofluids of CuO [52] or Al<sub>2</sub>O<sub>3</sub> [53], for ZnO suspensions in a mixture of ethylene glycol and water [54] or for polyethylene glycol (PEG)-based nanofluids of Fe<sub>3</sub>O<sub>4</sub> coated with oleic acid–PEG [55], for instance.

The results of both the base fluids and the nanofluids were compared with the values calculated the weight-average equation, Equation (2) [56]:

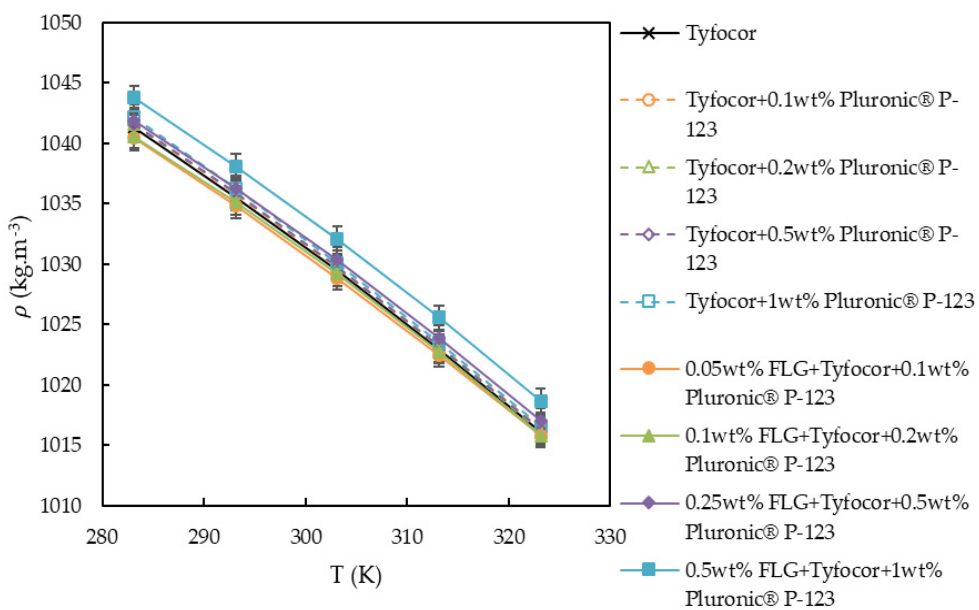
$$\frac{1}{\rho_{nf}} = \frac{\varphi_{m,np}}{\rho_{np}} + \frac{\varphi_{m,sft}}{\rho_{sft}} + \frac{1 - \varphi_{m,np} - \varphi_{m,sft}}{\rho_{bf}} \quad (2)$$

where  $\rho$  is the density,  $\varphi_m$  is the mass fraction and  $nf$ ,  $np$ ,  $sft$  and  $bf$  are subscripts for the nanofluid, the nanoparticles (e.g., FLG), the used surfactant and the corresponding base fluid, respectively. Density of Triton X-100 was also measured as this surfactant is under a liquid form in the studied temperature range, while the density values of Pluronic® P-123 and Gum Arabic at ambient temperature were  $1040 \text{ kg}\cdot\text{m}^{-3}$  and  $1400 \text{ kg}\cdot\text{m}^{-3}$ , respectively, as taken from the literature [57,58]. The density of FLG powder measured at ambient temperature using a gas pycnometer AccPyc 1330 (micromeritics) was determined to be  $1820 \text{ kg}\cdot\text{m}^{-3}$ . Density of Pluronic® P-123, Gum Arabic and FLG nanoparticles is assumed to not depend on the temperature in the studied range.

7 of 19

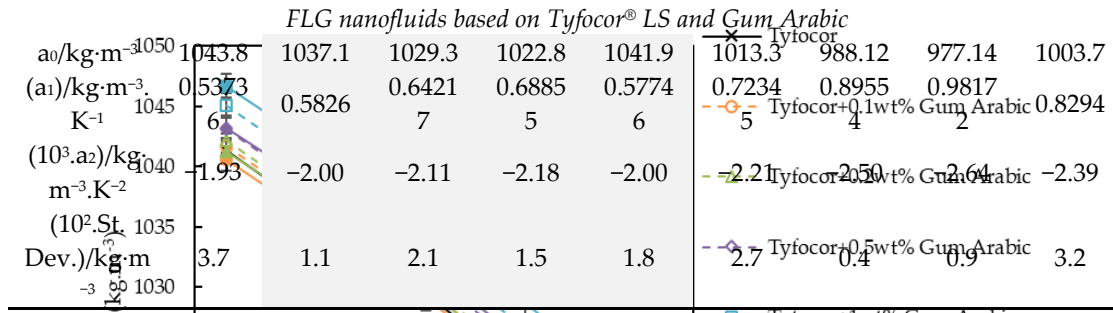


(a)



(b)

Figure 2. Cont.



The effect that the addition of FLG has on the density of the base fluids (i.e., corresponding Tyfocor® LS-surfactant mixtures) is shown in Figure 3. The results show that the nanofluid density decreases slightly for the lowest FLG concentrations and increases for the highest FLG concentration studied. Results are similar for the three studied nanofluid sets, with average deviations of the density obtained at all temperatures for the four concentrations (0.05, 0.1, 0.25, and 0.5 wt.%) around -0.08, -0.05, 0.05, and 0.2%, respectively. The decrease in density after adding a small amount of FLG to the base fluids could be explained by the existence of a negative excess volume, which represents a deviation from the ideal mixing volume. The FLG nanosheets (relatively big compared to the surrounding fluid molecules) may indeed impact the local organization of the base fluid molecules which are much more packed together than in the pure base fluid, resulting in the observed decrease in density [50,51]. A contractive volumetric behavior was also reported for aqueous nanofluids of CuO [52] or Al<sub>2</sub>O<sub>3</sub> [53] for ZnO suspensions in a mixture of ethylene glycol and water [54] or for polyethylene glycol (PEG)-based nanofluids of PEG-coated with citric acid-PEG [55], for instance.

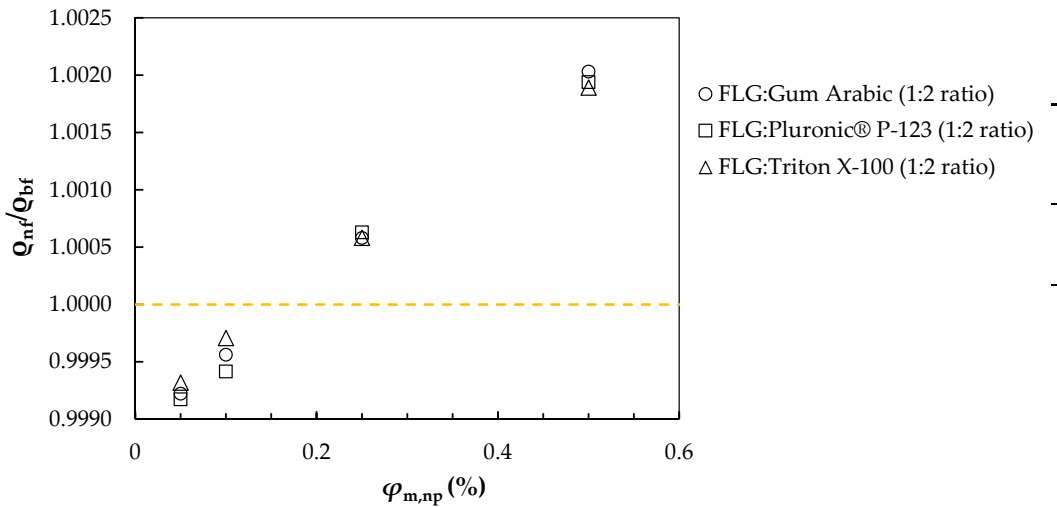


Figure 3. Relative density of nanofluids, which is defined as the ratio of the nanofluid density to the corresponding base fluids density (Tyfocor® LS-surfactant mixtures) as a function of FLG mass concentration at 303.15 K. By comparing the densities calculated using Equation (2) with the experimental values for the samples (base fluids and nanofluids), an AAD of 0.02%, 0.009% and 0.01% was obtained for the samples prepared with Triton X-100, Pluronic® P-123, and Gum Arabic, respectively, leading to a good agreement. Since the densities of the FLG nanoparticles and the three surfactants are higher than the density of the Tyfocor® LS according to Equation (2), this difference is observed for both surfactant and FLG (except FLG). This surfactant and the corresponding fluid respectively. Density of Triton X-100 was also measured as this surfactant is under a 0.05 and 0.1 wt. concentration of FLG, however, while deviations for values of 0.05 and 0.1 wt. concentrations are in the range which temperature was 1010 kg·m<sup>-3</sup> and 1400 kg·m<sup>-3</sup>, respectively, as taken from the literature [57,58]. The are slightly lower or close to the uncertainty of the experimental device (0.1%).

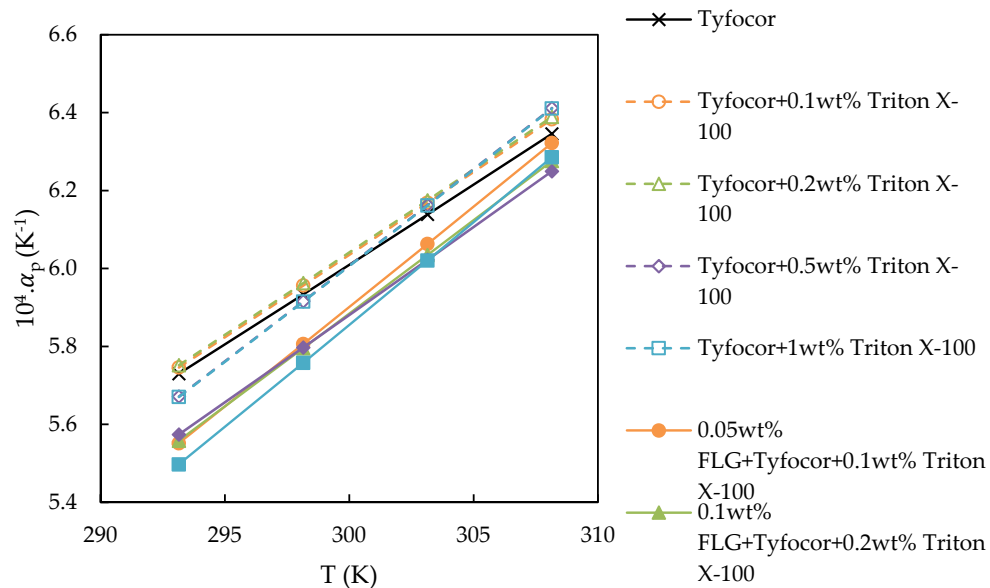
samples prepared with Triton X-100, Pluronic P-123, and Gum Arabic, respectively, leading to a good agreement. Since the densities of the FLG nanoparticles and the three surfactants are higher than the density of the Tyfocor® LS, according to Equation (2), this property should increase with both surfactant and FLG concentration. This behavior does not agree with the slight volumetric contraction experimentally observed for the two lowest nanoparticle concentrations (0.05 and 0.1 wt. %) of FLG). However, maximum deviations for these two concentrations are in the 0.06 to 0.10% range which are slightly lower or closer to the uncertainty of the experimental device (0.1%).

### 3.3. Isobaric Thermal Expansivity

From the data gathered in Table 3, the effects of temperature, nature and concentration of the surfactant, as well as FLG mass concentration on the isobaric thermal expansivity,  $\alpha_p$  [38,54,59] is evaluated according to the following equation, Equation (3):

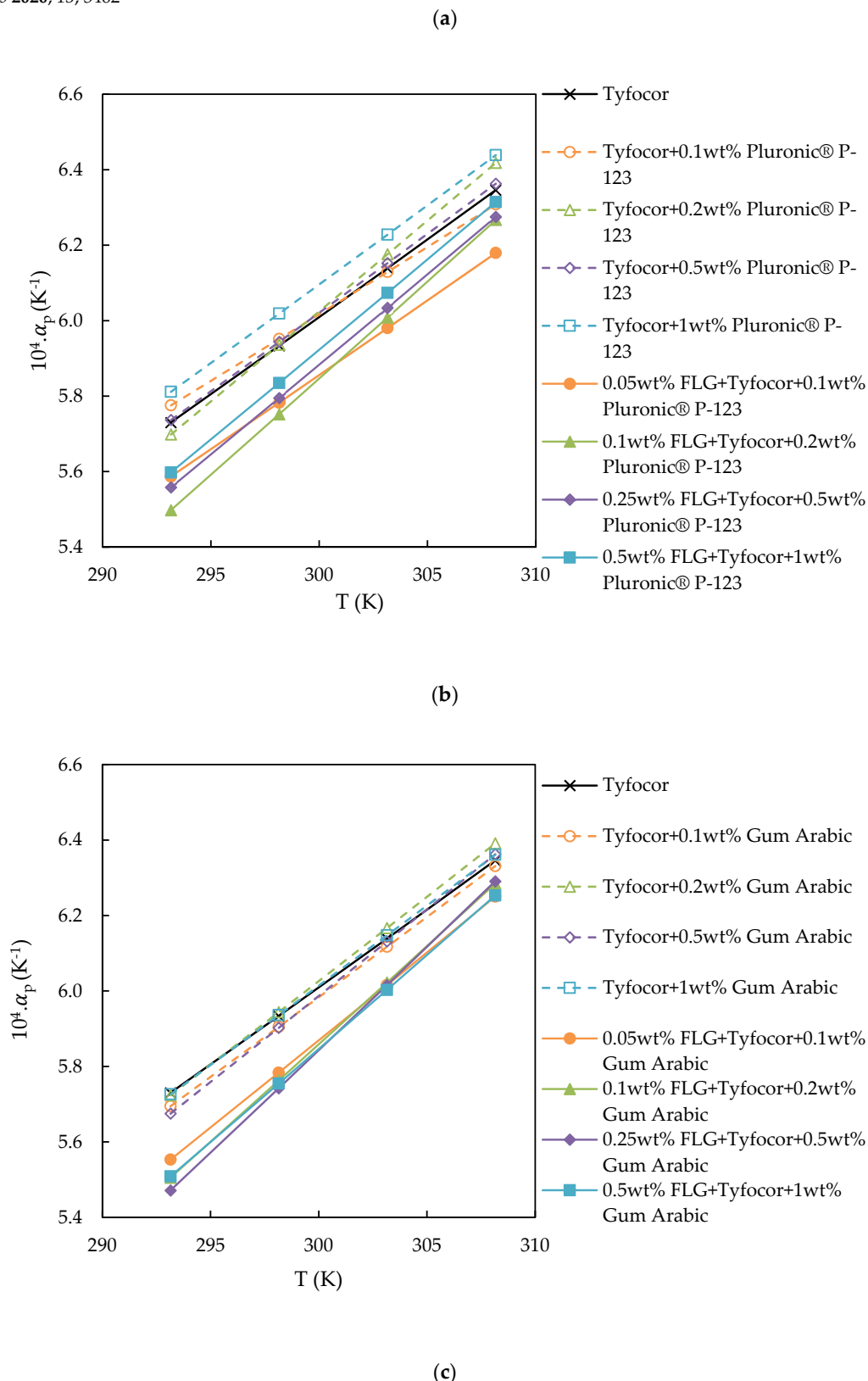
$$\alpha_p = 1 - \frac{1}{\rho} \left( \frac{\partial \rho}{\partial T} \right)_p \quad (3)$$

Figure 4 shows that  $\alpha_p$  increases when the temperature rises. In the case of Tyfocor® LS alone, this increase is about 11% across the 293.15–308.15 K temperature interval. The results also show that the addition of surfactant to Tyfocor® LS has no effect on their isobaric thermal expansivity with no significant difference between the three used surfactants, except a slight increase, about 1.4% for the highest weight concentration of Pluronic® P123 (1 wt. %). In contrast to the base fluids, a decrease in  $\alpha_p$  of all the used base fluids was observed in the presence of FLG; the reduction rate decreases from 2.9 to 1.8% in the case of Triton X-100, from 3.4 to 1.9% for nanofluids with Pluronic® P-123 and from 3.4 to 1.4% in the case of Gum Arabic, without any significant difference between the four FLG concentrations.



(a)

Figure 4. Cont.



**Figure 4.** Variation of the isobaric thermal expansivity,  $\alpha_p$ , as a function of temperature of both base fluids and nanofluids series prepared with (a) Triton X-100, (b) Pluronic® P-123 and (c) Gum Arabic.

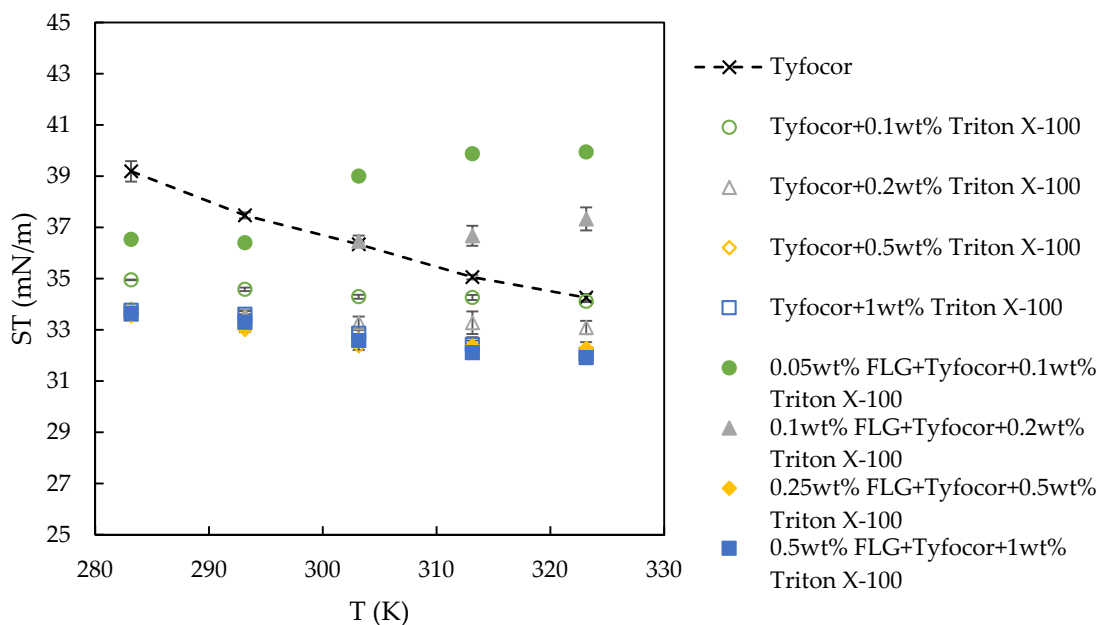
The increase of  $\alpha_p$  of nanofluids with temperature may be the indication that nanostructured fluids undergo a minor degree of cohesion when compared to base fluids. This behavior agrees with the work reported by Vallejo et al. [38], although with a lower increase in  $\alpha_p$  with the temperature for their functionalized graphene nanoplatelets (fGnP)/propylene glycol:water (PG:W) (30:70) wt.%

the work reported by Vallejo et al. [38], although with a lower increase in  $\alpha_p$  with the temperature for their functionalized graphene nanoplatelets (fGnP)/propylene glycol:water (PG:W) (30:70) wt.% nanofluids between 303.15 and 313.15 K, and a decrease in  $\alpha_p$  with increasing fGnP content were observed. In the literature, the dependence of  $\alpha_p$  with the addition of nanoparticles showed dissimilar results. Cabaleiro et al. [60] investigated ethylene glycol-based nanofluids containing two different nanocrystalline structures of titanium dioxide. They observed that  $\alpha_p$  of these nanofluids exhibited similar values to those of the corresponding base fluid with only a small decrease in  $\alpha_p$  reported for the nanofluids at different temperature and pressure conditions. In addition, Cabaleiro et al. [54] showed a continuous decrease in  $\alpha_p$  that reached 18% with the increasing content of ZnO nanoparticles in ethylene glycol and water mixture up to 10 wt.% at various temperatures and pressures. On the contrary, a significant increase in the isobaric thermal expansivity was reported by Nayak et al. [62,63] of water to 27.2% with respect to the base fluid in the case of water-based CuO, TiO<sub>2</sub>, Al<sub>2</sub>O<sub>3</sub> and SiO<sub>2</sub> nanofluids. They obtained  $\alpha_p$  values thanks to an experimental setup that measured the bulk variation with temperature in a glass flask with a calibrated stem. Further studies on this property are required to clarify the role of each parameter and its precise impact on isobaric thermal expansivity of the nanofluids, especially those based on propylene glycol–water mixtures such as commercial Tyfocor® LS.

3.4. Surface Tension

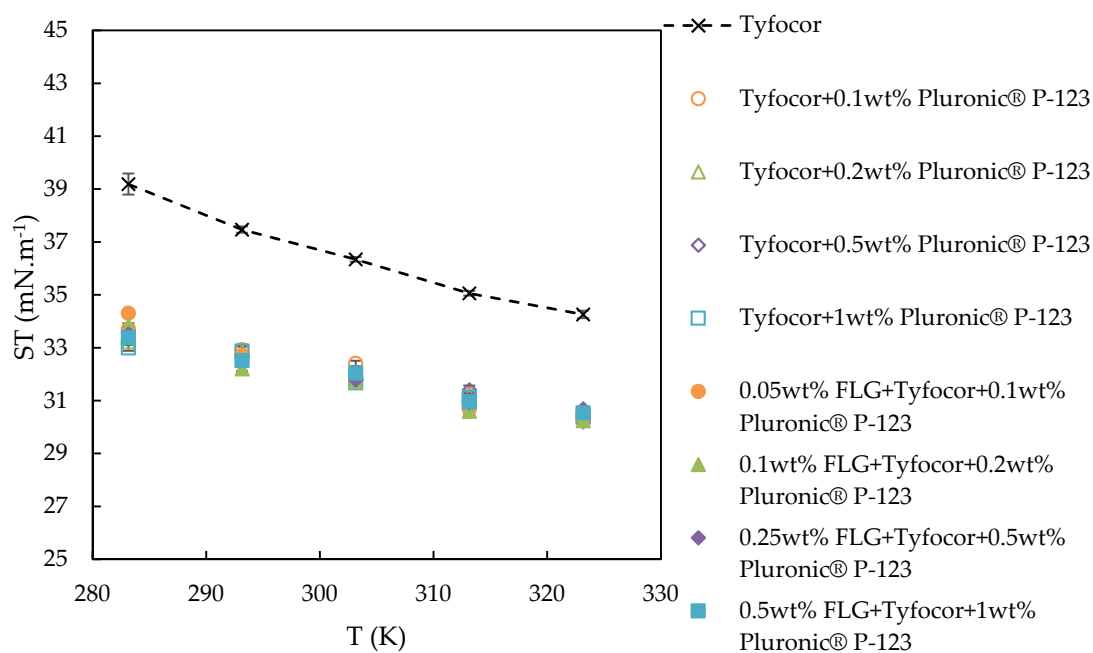
3.4. Surface Tension

Fluid ST is an important property to be investigated since it plays an important role in many heat transfer and fluid flow processes. It has been extensively studied by Estellé et al. [23]. In this work, the surface tension of the base fluids and nanofluids at the concentrations of 0.1, 0.2, 0.5, 1, and 2 wt.% of the nanofluids Tyfocor® LS based on the nanofluids concentrations, Fig. 5. The surface tension of the base fluid Tyfocor® LS was experimentally determined in the temperature range of 283.15–323.15 K and the values were also experimentally determined in the temperature range of 293.15 and 313.15 K and were also experimentally determined (if both the temperature and height between 293.15 and 313.15 K) and calculated using Eq. (1). The standard deviation and the average value of the ST error bars were determined from the standard deviation to the average value of ST.

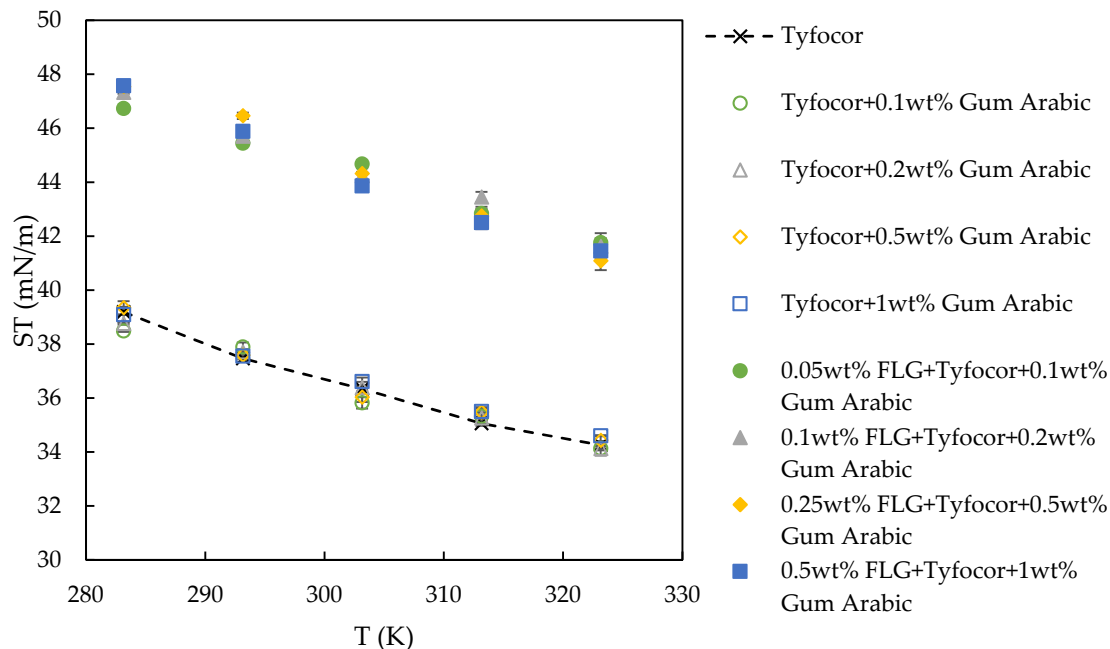


(a)

Figure 5. Cont.



(b)



(c)

**Figure 5.** Evolution of surface tension (ST) of the FLG nanofluids prepared with (a) Triton X-100, (b) Pluronic® P-123 and (c) Gum Arabic as a function of temperature. Dashed lines are drawn to guide the eyes.

The results about ST are presented and discussed below considering the effect of surfactant, temperature and nanoparticle addition. Before that, in order to clearly distinguish in the following the

effect of surfactant and the FLG presence on the ST evolution of FLG-based nanofluids, the variation of ST of each base fluid with surfactant content was measured to possibly evaluate the adsorption phenomenon of these surfactants in Tyfocor<sup>®</sup> LS. The addition of a surfactant into a liquid generally reduces the interfacial tension since the presence of the surfactant leads to adsorption at gas–liquid interface, and the rate of reduction depends on the surfactant type and concentration in the solution. It is well admitted that the CMC of a surfactant within a liquid can be determined at the inflexion point of the decreasing value and the plateau of ST with the increase in surfactant content. The surface tension of some samples may continue slightly decreasing even beyond the CMC, as reported by Radulovic et al. [64] for Triton X-100 aqueous solutions. The CMC of surfactants in Tyfocor<sup>®</sup> LS experimentally determined in this work at ambient temperature was found around 0.01 and 0.2 wt.% for Pluronic<sup>®</sup> P-123 and for Triton X-100, respectively. No significant change was noticed for Gum Arabic in the range 0.1–1 wt.% as shown in Figure 5c as the ST of base fluid is similar to that of Tyfocor<sup>®</sup> LS whatever the Gum Arabic content.

The effect of the addition of Triton X-100 to Tyfocor<sup>®</sup> LS is illustrated in Figure 5a, it induces a reduction of ST for the corresponding base fluids. With the lowest surfactant content, 0.1 wt.%, ST is reduced by 10.8% at 283.15 K and 0.4% at 323.15 K. For the higher Triton X-100 concentrations, the reduction rates become 13.9 and 5.5% on average at 283.15 and 323.15 K, respectively. This evidences the effect of temperature on ST of this base fluid, below and above the CMC. Pluronic<sup>®</sup> P-123 addition to the Tyfocor<sup>®</sup> LS decreases the ST by 14.8 to 11.4% with increasing temperature from 283.15 to 323.15 K, without any significant rate difference between the concentrations. The CMC is here achieved regardless of the surfactant content and can explain this result.

Figure 5 shows a decrease in ST for both base fluids and nanofluids with rising temperature, as expected [23,42], for the three surfactants Triton X-100, Pluronic<sup>®</sup> P-123 and Gum Arabic, respectively. The reduction rate of ST for Tyfocor<sup>®</sup> LS alone in the tested temperature range is equal to 12.6%.

For the samples prepared with Gum Arabic, ST of base fluids decreases following the same trend as that of Tyfocor<sup>®</sup> LS (Figure 5c) whatever the Gum Arabic content. In the case of the samples containing Pluronic<sup>®</sup> P-123, the ST reduction rate was lowered by the presence of surfactant, at a rate of 9.4% between 283.15 and 323.15 K. However, no significant change was noticed with the surfactant content, as this content is always higher than CMC. In case of Triton X-100 samples (Figure 5a), ST decreases with temperature with a different trend from that observed for Tyfocor<sup>®</sup> LS. The reduction rate of ST with temperature also depends on surfactant content. This rate was equal to 2.0% in the case of the two base fluids with the lowest surfactant concentrations. For the base fluids with the two highest concentrations of surfactant (above the CMC), the decreasing rate is around 4.8%.

As shown in Figure 5a–c, the effect of addition of FLG nanoparticles on nanofluids' ST depends on the nature and concentration of the surfactant used. FLG addition on ST for the samples prepared with Pluronic<sup>®</sup> P-123 (Figure 5b) has no significant effect on the ST measured values in the whole FLG concentration range from 0.05 to 0.5 wt.%. ST behavior is here rather governed by the presence of Pluronic<sup>®</sup> P-123 than by the presence of FLG. Actually, in that case, while surfactant molecules adsorb to the FLG, the content of surfactant, higher than CMC is too high for the change in equilibrium and the modification of ST by the presence of the FLG nanoparticles in the medium. The findings are different when Gum Arabic is used as surfactant (Figure 5c) since the ST values increase after adding the FLGs. It seems here that adsorption of the Gum Arabic (GA) to graphene promotes the attraction between the graphene and base fluid molecules that reduces the intermolecular spacing, leading to the increase in the surface tension. The observed ST evolution is independent on the temperature and FLG concentration, an increase around 21.5% in ST is here reported whatever the FLG content.

For the nanofluids prepared with Triton X-100 (Figure 5a), the ST evolution is more complex. An increase in ST of 4.9% (with respect to the corresponding base fluid) was observed for the lowest mass loading of FLG, 0.05 wt.%, at 283.15 and 293.15 K. In absolute value, ST of this nanofluid is still lower than that of Tyfocor<sup>®</sup> LS alone, which can be explained by the reduced amount of surfactant molecules adsorbed at the liquid–gas interface competing with Triton X-100 adsorption onto solid–liquid interface,

e.g., the FLG surface. By increasing FLG concentration within the nanofluids, a decrease in ST is observed and the ST reaches the values of the corresponding base fluids. The ST behavior is governed by the presence of surfactant and not only by that of the nanoparticle concentration in this domain, as the CMC is reached. For these nanofluids, a decrease in ST is obtained when the temperature is increased, except, surprisingly for the two lowest FLG concentrations. Such an unexpected trend is difficult to explain based on our current knowledge. Finally, when a decrease in ST of nanofluids is observed with the presence of nanoparticles and the increase of temperature, this could lead to an increase in heat flux in real systems [23,46] which is of practical interest in energy applications.

#### 4. Conclusions

Few-layer graphene (FLG) produced following a mechanical exfoliation method was used to develop nanofluids considering a commercial heat transfer fluid based on a mixture of water and propylene glycol and different nonionic surfactants. These nanofluids were experimentally characterized in terms of density and surface tension in a wide temperature range varying the mass content in FLG from 0.05 to 0.5%. Overall, it is observed that the density of the prepared nanofluids decreases with temperature and slightly increases with FLG content in comparison to base fluids. The density evolution of the FLG-based nanofluids with temperature and FLG concentration is well predicted by the weight-average equation for density considering the densities of all components. From the experimental density results, the effects of temperature, nature and concentration of the surfactant, as well as FLG mass concentration on the isobaric thermal expansivity were also evaluated. It was shown that the isobaric thermal expansivity, which increases with temperature, was similar for all base fluids without any distinct effect of the used surfactant. In contrast to the base fluids, a decrease in this property was noticed in the presence of FLG with all the used base fluids. The surface tension of the different nanofluids was more sensitive to the type of surfactant and its content in relation with their CMC. Consequently, this property could evolve differently following the surfactant used and the FLG content. The surface tension of base fluids could decrease or remain unchanged following the surfactant, and the addition of FLG can induce an increase or may not strongly modify the surface tension. To complete the characterization of these nanofluids, the next step concerns the evaluation of their flow properties.

**Author Contributions:** “Conceptualization, B.V. and P.E.; FLG preparation, D.B.; Nanofluid preparation and FLG characterization, B.V., A.D. and D.B.; Investigation: S.H., D.C. and P.E.; data curation, S.H., D.C. and P.E.; writing—original draft preparation, S.H., D.C. and P.E.; writing—review and editing, S.H., D.C., P.E., B.V. and L.L.; supervision, B.V., L.L., T.M. and P.E.; project administration, P.E.; All authors have read and agreed to the published version of the manuscript”.

**Funding:** P.E. acknowledges the European Union through the European Regional Development Fund (ERDF), the Ministry of Higher Education and Research, the French region of Brittany and Rennes Métropole for the financial support of surface tension experimental device. S.H. acknowledges EU COST for the STMS grant ref. COST-STSM-CA15119- 45590. D.C. is recipient of a postdoctoral fellowship from Xunta de Galicia (Spain). This investigation is a contribution to the COST (European Cooperation in Science and Technology) Action CA15119: Overcoming Barriers to Nanofluids Market Uptake (NanoUptake). This work was also partially supported by the Ministerio de Economía y Competitividad (Spain) and FEDER program through ENE2017-86425-C2-1-R project.

**Acknowledgments:** B.V. would like to thank Dr. Jaafar Ghanbaja and the microscopy platform (CC3M) at the Institut Jean Lamour for TEM and SEM observations.

**Conflicts of Interest:** The authors declare no conflict of interest.

#### Nomenclature

CNTs	carbon nanotubes
ST	surface tension ( $\text{mN}\cdot\text{m}^{-1}$ )
GO	graphene oxide
rGO	reduced graphene oxide

SDBS	sodium dodecylbenzene sulfonate
FLG	few-layer graphene
GA	gum arabic
PEO	poly(ethylene oxide)
PPO	poly(propylene oxide)
SEM	scanning electron microscopy
HRTEM	high-resolution transmission electron microscopy
TEM	transmission electron microscopy
$\rho$	density ( $\text{kg}\cdot\text{m}^{-3}$ )
AAD	absolute average deviation (%)
T	temperature (K)
$a_i$	fitting parameters
St. Dev.	standard deviation
CMC	critical micelle concentration
PEG	polyethylene glycol
$\varphi_m$	mass fraction
$\alpha_p$	isobaric thermal expansivity ( $\text{K}^{-1}$ )
fGnP	functionalized graphene nanoplatelets
PG	propylene glycol
W	water
Subscripts	
$nf$	nanofluid
$np$	nanoparticles
$sft$	surfactant
$bf$	Base fluid
Symbols	
↑	increase
→	stable or constant
↓	decrease

## References

- Choi, S.U.S.; Eastman, J.A. *Enhancing Thermal Conductivity of Fluids with Nanoparticles*, International Mechanical Engineering Congress and Exhibition; Argonne National Lab: Argonne, IL, USA, 1995; pp. 99–105.
- Żyła, G.; Fal, J.; Estellé, P. Thermophysical and dielectric profiles of ethylene glycol based titanium nitride (TiN-EG) nanofluids with various size of particles. *Int. J. Heat Mass Transf.* **2017**, *113*, 1189–1199. [[CrossRef](#)]
- Godson, L.; Raja, B.; Mohan Lal, D.; Wongwises, S. Enhancement of heat transfer using nanofluids—An overview. *Renew. Sustain. Energy Rev.* **2010**, *14*, 629–641. [[CrossRef](#)]
- Wen, D.; Lin, G.; Vafaei, S.; Zhang, K. Review of nanofluids for heat transfer applications. *Particuology* **2009**, *7*, 141–150. [[CrossRef](#)]
- Cabaleiro, D.; Estellé, P.; Navas, H.; Desforges, A.; Vigolo, B. Dynamic Viscosity and Surface Tension of Stable Graphene Oxide and Reduced Graphene Oxide Aqueous Nanofluids. *J. Nanofluids* **2018**, *7*, 1081–1088. [[CrossRef](#)]
- Kakaç, S.; Pramuanjaroenkij, A. Review of convective heat transfer enhancement with nanofluids. *Int. J. Heat Mass Transf.* **2009**, *52*, 3187–3196. [[CrossRef](#)]
- Ramesh, G.; Prabhu, N.K. Review of thermo-physical properties, wetting and heat transfer characteristics of nanofluids and their applicability in industrial quench heat treatment. *Nanoscale Res. Lett.* **2011**, *6*, 334. [[CrossRef](#)]
- Kleinstreuer, C.; Feng, Y. Experimental and theoretical studies of nanofluid thermal conductivity enhancement: A review. *Nanoscale Res. Lett.* **2011**, *6*, 229. [[CrossRef](#)]
- Eggers, J.R.; Kabelac, S. Nanofluids revisited. *Appl. Therm. Eng.* **2016**, *106*, 1114–1126. [[CrossRef](#)]
- Azmi, W.H.; Sharma, K.V.; Mamat, R.; Najafi, G.; Mohamad, M.S. The enhancement of effective thermal conductivity and effective dynamic viscosity of nanofluids—A review. *Renew. Sustain. Energy Rev.* **2016**, *53*, 1046–1058. [[CrossRef](#)]

11. Timofeeva, E.V.; Yu, W.; France, D.M.; Singh, D.; Routbort, J.L. Nanofluids for heat transfer: An engineering approach. *Nanoscale Res. Lett.* **2011**, *6*, 182. [[CrossRef](#)]
12. Sarkar, J.; Ghosh, P.; Adil, A. A review on hybrid nanofluids: Recent research, development and applications. *Renew. Sustain. Energy Rev.* **2015**, *43*, 164–177. [[CrossRef](#)]
13. Minea, A.A. Challenges in hybrid nanofluids behavior in turbulent flow: Recent research and numerical comparison. *Renew. Sustain. Energy Rev.* **2017**, *71*, 426–434. [[CrossRef](#)]
14. Sundar, L.S.; Sharma, K.V.; Singh, M.K.; Sousa, A.C.M. Hybrid nanofluids preparation, thermal properties, heat transfer and friction factor—A review. *Renew. Sustain. Energy Rev.* **2017**, *68*, 185–198. [[CrossRef](#)]
15. Balandin, A.A. Thermal properties of graphene and nanostructured carbon materials. *Nat. Mater.* **2011**, *10*, 569–581. [[CrossRef](#)]
16. Cabaleiro, D.; Colla, L.; Barison, S.; Lugo, L.; Fedele, L.; Bobbo, S. Heat Transfer Capability of (Ethylene Glycol + Water)-Based Nanofluids Containing Graphene Nanoplatelets: Design and Thermophysical Profile. *Nanoscale Res. Lett.* **2017**, *12*, 53. [[CrossRef](#)]
17. Rasheed, A.K.; Khalid, M.; Rashmi, W.; Gupta, T.C.S.M.; Chan, A. Graphene based nanofluids and nanolubricants—Review of recent developments. *Renew. Sustain. Energy Rev.* **2016**, *63*, 346–362. [[CrossRef](#)]
18. Sadeghinezhad, E.; Mehrali, M.; Saidur, R.; Mehrali, M.; Tahan Latibari, S.; Akhiani, A.R.; Metselaar, H.S.C. A comprehensive review on graphene nanofluids: Recent research, development and applications. *Energy Convers. Manag.* **2016**, *111*, 466–487. [[CrossRef](#)]
19. Arshad, A.; Jabbal, M.; Yan, Y.; Reay, D. A review on graphene based nanofluids: Preparation, characterization and applications. *J. Mol. Liq.* **2019**, *279*, 444–484. [[CrossRef](#)]
20. Wanic, M.; Cabaleiro, D.; Hamze, S.; Fal, J.; Estellé, P.; Żyła, G. Surface tension of ethylene glycol-based nanofluids containing various types of nitrides: An experimental study. *J. Therm. Anal. Calorim.* **2020**, *139*, 799–806. [[CrossRef](#)]
21. Moffat, J.R.; Sefiane, K.; Shanahan, M.E.R. Effect of TiO<sub>2</sub> Nanoparticles on Contact Line Stick–Slip Behavior of Volatile Drops. *J. Phys. Chem. B* **2009**, *113*, 8860–8866. [[CrossRef](#)]
22. Askounis, A.; Sefiane, K.; Koutsos, V.; Shanahan, M.E.R. Effect of particle geometry on triple line motion of nano-fluid drops and deposit nano-structuring. *Adv. Colloid Interface Sci.* **2015**, *222*, 44–57. [[CrossRef](#)] [[PubMed](#)]
23. Estellé, P.; Cabaleiro, D.; Żyła, G.; Lugo, L.; Murshed, S.M.S. Current trends in surface tension and wetting behavior of nanofluids. *Renew. Sustain. Energy Rev.* **2018**, *94*, 931–944. [[CrossRef](#)]
24. Incropera, F.P.; DeWitt, D.P.; Bergman, T.L.; Lavine, A.S. *Introduction to Heat Transfer*, 6th ed.; John Wiley: New York, NY, USA, 2007.
25. Kim, E.J.; Desforges, A.; Speyer, L.; Ghanbaja, J.; Gleize, J.; Estellé, P.; Vigolo, B. Graphene for Water-Based Nanofluid Preparation: Effect of Chemical Modifications on Dispersion and Stability. *J. Nanofluids* **2017**, *6*, 603–613. [[CrossRef](#)]
26. Cong, H.-P.; Chen, J.-F.; Yu, S.-H. Graphene-based macroscopic assemblies and architectures: An emerging material system. *Chem. Soc. Rev.* **2014**, *43*, 7295–7325. [[CrossRef](#)]
27. Ahammed, N.; Asirvatham, L.G.; Wongwises, S. Effect of volume concentration and temperature on viscosity and surface tension of graphene–water nanofluid for heat transfer applications. *J. Therm. Anal. Calorim.* **2016**, *123*, 1399–1409. [[CrossRef](#)]
28. Ilyas, S.U.; Ridha, S.; Abdul Kareem, F.A. Dispersion stability and surface tension of SDS-Stabilized saline nanofluids with graphene nanoplatelets. *Colloids Surf. Physicochem. Eng. Asp.* **2020**, *592*, 124584. [[CrossRef](#)]
29. Kamatchi, R.; Venkatachalapathy, S.; Abhinaya Srinivas, B. Synthesis, stability, transport properties, and surface wettability of reduced graphene oxide/water nanofluids. *Int. J. Therm. Sci.* **2015**, *97*, 17–25. [[CrossRef](#)]
30. Liu, Y.; Chen, B.; Wang, D.; Jiang, N.; Tan, J.; Fu, J.; Wu, B.; Hu, Y.; Guo, Z. Surface tension of supercooled graphene oxide nanofluids measured with acoustic levitation. *J. Therm. Anal. Calorim.* **2020**. [[CrossRef](#)]
31. Zheng, Z.Z. Experimental Investigation on Surface Tension of Water-Based Graphene Oxide Nanofluids. *Adv. Mater. Res.* **2014**, *1082*, 297–301. [[CrossRef](#)]
32. Alawi, O.A.; Mallah, A.R.; Kazi, S.N.; Sidik, N.A.C.; Najafi, G. Thermophysical properties and stability of carbon nanostructures and metallic oxides nanofluids: Experimental approach. *J. Therm. Anal. Calorim.* **2019**, *135*, 1545–1562. [[CrossRef](#)]
33. Amiri, A.; Shanbedi, M.; Dashti, H. Thermophysical and rheological properties of water-based graphene quantum dots nanofluids. *J. Taiwan Inst. Chem. Eng.* **2017**, *76*, 132–140. [[CrossRef](#)]

34. Azizi, M.; Honarvar, B. Investigation of thermophysical properties of nanofluids containing poly(vinyl alcohol)-functionalized graphene. *J. Therm. Anal. Calorim.* **2018**, *133*, 1259–1269. [CrossRef]
35. Ijam, A.; Saidur, R.; Ganesan, P.; Moradi Golsheikh, A. Stability, thermo-physical properties, and electrical conductivity of graphene oxide-deionized water/ethylene glycol based nanofluid. *Int. J. Heat Mass Transf.* **2015**, *87*, 92–103. [CrossRef]
36. Karami, H.; Papari-Zare, S.; Shanbedi, M.; Eshghi, H.; Dashtbozorg, A.; Akbari, A.; Mohammadian, E.; Heidari, M.; Sahin, A.Z.; Teng, C.B. The thermophysical properties and the stability of nanofluids containing carboxyl-functionalized graphene nano-platelets and multi-walled carbon nanotubes. *Int. Commun. Heat Mass Transf.* **2019**, *108*, 104302. [CrossRef]
37. Sani, E.; Vallejo, J.P.; Cabaleiro, D.; Lugo, L. Functionalized graphene nanoplatelet-nanofluids for solar thermal collectors. *Sol. Energy Mater. Sol. Cells* **2018**, *185*, 205–209. [CrossRef]
38. Vallejo, J.P.; Pérez-Tavernier, J.; Cabaleiro, D.; Fernández-Seara, J.; Lugo, L. Potential heat transfer enhancement of functionalized graphene nanoplatelet dispersions in a propylene glycol-water mixture. Thermophysical profile. *J. Chem. Thermodyn.* **2018**, *123*, 174–184. [CrossRef]
39. Vallejo, J.P.; Álvarez-Regueiro, E.; Cabaleiro, D.; Fernández-Seara, J.; Fernández, J.; Lugo, L. Functionalized graphene nanoplatelet nanofluids based on a commercial industrial antifreeze for the thermal performance enhancement of wind turbines. *Appl. Therm. Eng.* **2019**, *152*, 113–125. [CrossRef]
40. Yarmand, H.; Gharekhani, S.; Shirazi, S.F.S.; Amiri, A.; Alehashem, M.S.; Dahari, M.; Kazi, S.N. Experimental investigation of thermo-physical properties, convective heat transfer and pressure drop of functionalized graphene nanoplatelets aqueous nanofluid in a square heated pipe. *Energy Convers. Manag.* **2016**, *114*, 38–49. [CrossRef]
41. Yarmand, H.; Gharekhani, S.; Shirazi, S.F.S.; Amiri, A.; Montazer, E.; Arzani, H.K.; Sadri, R.; Dahari, M.; Kazi, S.N. Nanofluid based on activated hybrid of biomass carbon/graphene oxide: Synthesis, thermo-physical and electrical properties. *Int. Commun. Heat Mass Transf.* **2016**, *72*, 10–15. [CrossRef]
42. Berrada, N.; Hamze, S.; Desforges, A.; Ghanbaja, J.; Gleize, J.; Maré, T.; Vigolo, B.; Estellé, P. Surface tension of functionalized MWCNT-based nanofluids in water and commercial propylene-glycol mixture. *J. Mol. Liq.* **2019**, *293*, 111473. [CrossRef]
43. Oyinola, M.A.; Shire, G.S.F.; Moss, R.W. Thermal analysis of a solar collector absorber plate with microchannels. *Exp. Therm. Fluid Sci.* **2015**, *67*, 102–109. [CrossRef]
44. Hamze, S.; Berrada, N.; Cabaleiro, D.; Desforges, A.; Ghanbaja, J.; Gleize, J.; Bégin, D.; Michaux, F.; Maré, T.; Vigolo, B.; et al. Few-layer graphene-based nanofluids with enhanced thermal conductivity. *Nanomaterials* **2020**, *10*, 1258. [CrossRef] [PubMed]
45. Vargaftik, N.B.; Volkov, B.N.; Voljak, L.D. International Tables of the Surface Tension of Water. *J. Phys. Chem. Ref. Data* **1983**, *12*, 817–820. [CrossRef]
46. Gómez-Villarejo, R.; Aguilar, T.; Hamze, S.; Estellé, P.; Navas, J. Experimental analysis of water-based nanofluids using boron nitride nanotubes with improved thermal properties. *J. Mol. Liq.* **2019**, *277*, 93–103. [CrossRef]
47. Bianco, A.; Cheng, H.-M.; Enoki, T.; Gogotsi, Y.; Hurt, R.H.; Koratkar, N.; Kyotani, T.; Monthieux, M.; Park, C.R.; Tascon, J.M.D.; et al. All in the graphene family—A recommended nomenclature for two-dimensional carbon materials. *Carbon* **2013**, *65*, 1–6. [CrossRef]
48. Available online: <https://tyfo.de/en/produkt/tyfocor-ls> (accessed on 9 June 2020).
49. Cabaleiro, D.; Pastoriza-Gallego, M.J.; Piñeiro, M.M.; Legido, J.L.; Lugo, L. Thermophysical properties of (diphenyl ether+biphenyl) mixtures for their use as heat transfer fluids. *J. Chem. Thermodyn.* **2012**, *50*, 80–88. [CrossRef]
50. Available online: <https://chemistry.stackexchange.com/questions/45079/does-adding-mass-to-a-liquid-not-water-increase-the-volume> (accessed on 9 June 2020).
51. Available online: <https://www.carolina.com/teacher-resources/interactive/chemistry-lost-volume-demonstration/tr10785.tr> (accessed on 9 June 2020).
52. Pastoriza-Gallego, M.J.; Casanova, C.; Legido, J.L.; Piñeiro, M.M. CuO in water nanofluid: Influence of particle size and polydispersity on volumetric behaviour and viscosity. *Fluid Phase Equilibria* **2011**, *300*, 188–196. [CrossRef]

53. Pastoriza-Gallego, M.J.; Casanova, C.; Páramo, R.; Barbés, B.; Legido, J.L.; Piñeiro, M.M. A study on stability and thermophysical properties (density and viscosity) of Al<sub>2</sub>O<sub>3</sub> in water nanofluid. *J. Appl. Phys.* **2009**, *106*, 064301. [CrossRef]
54. Cabaleiro, D.; Pastoriza-Gallego, M.J.; Piñeiro, M.M.; Lugo, L. Characterization and measurements of thermal conductivity, density and rheological properties of zinc oxide nanoparticles dispersed in (ethane-1,2-diol+water) mixture. *J. Chem. Thermodyn.* **2013**, *58*, 405–415. [CrossRef]
55. Zafarani-Moattar, M.T.; Majdan-Cegincara, R. Stability, rheological, magnetorheological and volumetric characterizations of polymer based magnetic nanofluids. *Colloid Polym. Sci.* **2013**, *291*, 1977–1987. [CrossRef]
56. Marcos, M.A.; Cabaleiro, D.; Hamze, S.; Fedele, L.; Bobbo, S.; Estellé, P.; Lugo, L. NePCM Based on Silver Dispersions in Poly(Ethylene Glycol) as a Stable Solution for Thermal Storage. *Nanomaterials* **2019**, *10*, 19. [CrossRef] [PubMed]
57. Available online: <http://candmz04.brenntag.ca/MSDS/Fr/00070113.pdf> (accessed on 9 June 2020).
58. Available online: [http://www.merckmillipore.com/FR/fr/product/Gum-arabic,MDA\\_CHEM-104228](http://www.merckmillipore.com/FR/fr/product/Gum-arabic,MDA_CHEM-104228) (accessed on 9 June 2020).
59. Cabaleiro, D.; Segovia, J.J.; Martín, M.C.; Lugo, L. Isobaric heat capacity at high pressure, density, and viscosity of (diphenyl ether + biphenyl) mixtures. *J. Chem. Thermodyn.* **2016**, *93*, 86–94. [CrossRef]
60. Cabaleiro, D.; Pastoriza-Gallego, M.J.; Gracia-Fernández, C.; Piñeiro, M.M.; Lugo, L. Rheological and volumetric properties of TiO<sub>2</sub>-ethylene glycol nanofluids. *Nanoscale Res. Lett.* **2013**, *8*, 286. [CrossRef] [PubMed]
61. Korolovych, V.F.; Bulavin, L.A.; Prylutsky, Y.I.; Khrapaty, S.V.; Tsierkezos, N.G.; Ritter, U. Influence of Single-Walled Carbon Nanotubes on Thermal Expansion of Water. *Int. J. Thermophys.* **2014**, *35*, 19–31. [CrossRef]
62. Nayak, A.K.; Singh, R.K.; Kulkarni, P.P. Measurement of volumetric thermal expansion coefficient of various nanofluids. *Tech. Phys. Lett.* **2010**, *36*, 696–698. [CrossRef]
63. Nayak, A.K.; Singh, R.K.; Kulkarni, P.P. Thermal expansion characteristics of Al<sub>2</sub>O<sub>3</sub> nanofluids: More to understand than understood. *Appl. Phys. Lett.* **2009**, *94*, 094102. [CrossRef]
64. Radulovic, J.; Sefiane, K.; Shanahan, M.E.R. On the effect of pH on spreading of surfactant solutions on hydrophobic surfaces. *J. Colloid Interface Sci.* **2009**, *332*, 497–504. [CrossRef]



© 2020 by the authors. Licensee MDPI, Basel, Switzerland. This article is an open access article distributed under the terms and conditions of the Creative Commons Attribution (CC BY) license (<http://creativecommons.org/licenses/by/4.0/>).

**IV.5- Shear flow behavior and dynamic viscosity of few-layer graphene nanofluids based on propylene glycol-water mixture**



# Shear flow behavior and dynamic viscosity of few-layer graphene nanofluids based on propylene glycol-water mixture

Samah Hamze<sup>a</sup>, David Cabaleiro<sup>a,b</sup>, Thierry Maré<sup>a</sup>, Brigitte Vigolo<sup>c</sup>, Patrice Estellé<sup>a,\*</sup>

<sup>a</sup> Université de Rennes, LGCGM, F-35000 Rennes, France

<sup>b</sup> Dpto. Física Aplicada, Faculdade de Ciências, E-36310, Universidade de Vigo, Vigo, Spain

<sup>c</sup> Université de Lorraine, CNRS, Institut Jean Lamour UMR7198, F-54000 Nancy, France

## ARTICLE INFO

### Article history:

Received 30 June 2020

Received in revised form 16 July 2020

Accepted 18 July 2020

Available online 23 July 2020

### Keywords:

Few-layer graphene nanofluids

Propylene-glycol/water

Shear flow stability

Shear flow behavior

Dynamic viscosity

## ABSTRACT

We report the shear flow behavior of few layer graphene (FLG) based nanofluids produced with a commercial mixture of water and propylene glycol and three nonionic surfactants, Triton X-100, Pluronic® P123, and Gum Arabic respectively. The flow properties of these nanofluids were experimentally investigated between 283.15 and 323.15 K and for FLG content from 0.05 to 0.5 wt%. The nanofluids were subjected to different experiments, at rest at fixed temperature, under steady shear flow at fixed temperature and under temperature ramp at fixed shear rate in order to evaluate their stability and behavior under shear and temperature influence. These results were compared and correlated to visual aspect of the samples at the end of measurements. This experimental study evidences that the temperature, the shearing and the shearing duration have an important influence on the stability under shear of nanofluids in function of concentration and surfactant used. Finally, for all stable nanofluids under shear, the dynamic viscosity evolution of nanofluids with temperature is correlated to Vogel-Fulcher-Tammann model.

© Published by Elsevier B.V.

## 1. Introduction

The progressive depletion of fossil fuels and world energy demand necessitate the development of new technologies based on alternative energy sources [1,2]. Nanofluids (nanoparticles dispersed in a conventional fluid) have become a research topic of immense interest worldwide. They have potential applications in many important fields such as in cooling technologies or advanced heat transfer, energy harvesting, medical, micro-electromechanical systems, microfluidics, microelectronics, numerous thermal management systems and transportation [3–10]. Most studies have mainly focused on the determination of thermal properties of nanofluids, especially thermal conductivity, their modeling and their use in simulations, due to the potential benefits compared to suspensions of microparticles as well as conventional fluids [3,11–20]. Likewise, dynamic viscosity also becomes an important property when it comes to practical applications related to heat transfer and fluid flow. For instance, the pumping power, pressure drop and convective heat transfer in flow systems are directly dependent to the viscosity of the fluids. Consequently, the interest in investigation and analysis of nanofluid viscosity is recently growing than those regarding thermal conductivity which was the topic of extensive studies for a longer time [3]. Among the different types of nanoparticles used in

literature, carbon-based nanomaterials, especially graphene, can be excellent thermal conductivity enhancers for nanofluid design, due to their excellent intrinsic thermal property compared to that of metal oxide or metallic nanoparticles [21–23].

Available literature shows that nanofluids can exhibit either a Newtonian or a non-Newtonian behavior, depending on nanoparticle shape, size or concentration [3,21,24]. Such an evaluation, as well as in what extend the viscosity of the base fluid is modified with the presence of graphene nanosheets, is of great interest for possible applications. With this aim, Moghaddam et al. [25] investigated graphene nanosheets with size of about 15–50 nm thick dispersed in glycerol. The prepared nanofluids were in the concentration range of 0.25–2.0 wt%, and their viscosity was measured at temperatures between 293.15 and 323.15 K. A non-Newtonian behavior was reported by these authors and a strong enhancement in viscosity of glycerol by 401.49% with the 2 wt% loading of graphene nanosheets at shear rate  $6.32 \text{ s}^{-1}$  and at temperature equal to 293.15 K was also observed. On the other hand, Sarsam et al. [26] prepared 0.1 wt% of graphene nanoplatelets (GNP)/water nanofluids without any surfactant assistance (samples labeled as “pristine” in that article) or stabilized using different surfactants like sodium dodecyl benzene sulfonate (SDBS), sodium dodecyl sulfate (SDS), cetyl trimethylammonium bromide (CTAB) and gum arabic (GA). Authors investigated the shear rate dependence of dynamic viscosity in the range from 20 to  $200 \text{ s}^{-1}$  and at temperatures from 298.15–328.15 K. Without any surfactant assistance, a slight shear

\* Corresponding author.

E-mail address: [patrice.estelle@univ-rennes1.fr](mailto:patrice.estelle@univ-rennes1.fr) (P. Estellé).

thinning behavior was observed for nanofluid in the region of low shear rates for all studied temperatures expect for 308.15 K. A more remarkable pseudoplastic behavior was reported for the dispersions stabilized with GA (at a GA-GNP ratio of 0.5:1) in the studied temperature range. Conversely, suspensions containing the ionic surfactants (SDBS, SDS and CTAB) at a surfactant-nanoparticle ratios of 1:1 behaved in a Newtonian manner. Additionally, the (1:1) SDBS-GNP sample showed the highest stability and nearly the lowest viscosity (7.4% higher than distilled water). And based on the average values of viscosity, the water based nanofluids could be sequenced as (0.5:1) GA-GNPs  $\gg$  pristine GNP  $>$  (1:1) SDBS-GNP  $>$  (1:1) SDS-GNP  $>$  (1:1) CTAB-GNP. The dispersion of GNPs, with thickness of about 5–10 nm and 15  $\mu\text{m}$  of large dimension, in a mixture of deionized water:ethylene glycol (70:30 volume ratio) using 0.75 vol% of sodium deoxycholate (SDC) as surfactant was studied by Selvam et al. [27]. The investigation was done for nanofluids in the GNP concentration range of 0.1–0.5 vol%. The obtained results showed that the viscosity ratios ( $\mu_{nf}/\mu_{bf}$ ) of nanofluids increased from 1.06 to 1.16 and 1.13 to 1.39 at 0.1 and 0.5 vol%, respectively. In another work, Wang et al. [28] investigated single layer graphene (SLG)/water nanofluids that contain a special dispersant (not specified in the article). They found that the viscosity decreased with increasing temperature from 278.15 to 298.15 K increases with increasing concentration from 0.2 to 1 wt% with a viscosity increment ratio between SLG nanofluids and water ranging from 1.24 to 2.35 and a non-Newtonian shear thinning behavior was reported. Vallejo et al. [29] studied functionalized GNP (fGNP) nanofluids based on water and propylene glycol:water mixture at 30:70 and 50:50 wt%. Rheological investigation was performed at shear rates from 10 to 1000  $\text{s}^{-1}$  with at different weight concentrations between 0.25 and 1 wt% and in the temperature range 283.15–353.15 K. The authors obtained a non-Newtonian behavior at low shear rates (up to 100) and a Newtonian behavior at higher shear rates. Additionally, they found that in the case of base fluid with higher viscosity, the nanofluid viscosity decrease with temperature was higher and in the case of the base fluid with lower viscosity, the nanofluid viscosity increase with weight content of fGNP was higher.

On another hand, Vallejo et al. [30] investigated the rheological properties of sulfonic acid- fGNP nanofluids based on ethylene glycol:water mixture 50:50 vol%. Different weight concentrations of fGNPs in the range 0.25–2% were prepared and studied in the shear rate range 1–1000  $\text{s}^{-1}$  between 283.15 and 353.15 K. With increasing temperature within the tested range, the measurements showed a viscosity decrease by around 82 and 80% for the base fluid and nanofluids, respectively. An increase in viscosity values was found with the increase of graphene loading. For example, a viscosity enhancement of 16% was obtained for the nanofluid with 0.5 wt% of fGNPs with respect to the base fluid, independently on the temperature. In addition, the studied nanofluids exhibited a shear thinning behavior at low shear rates with higher

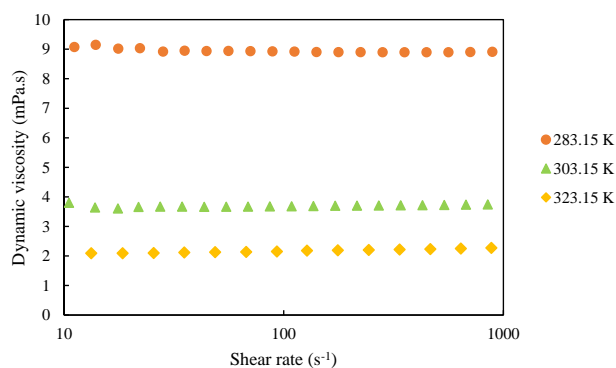
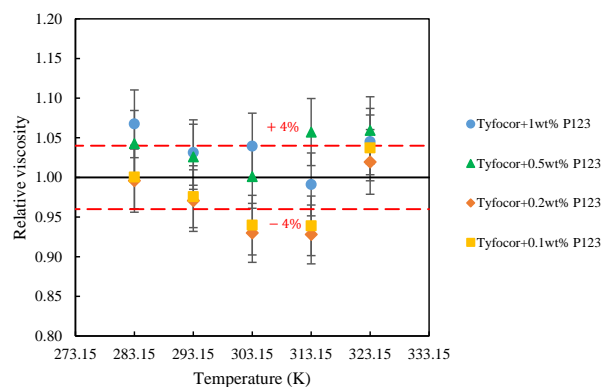


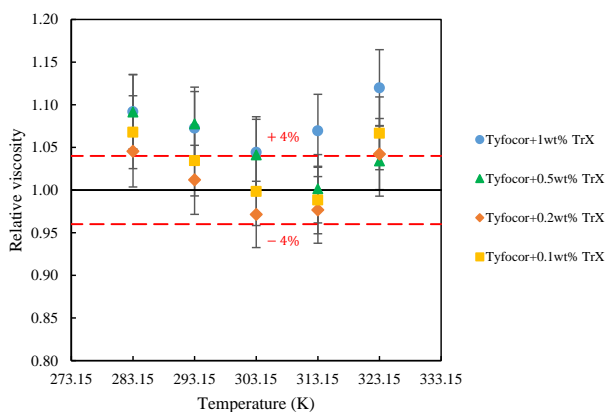
Fig. 1. Flow curves for the base fluid Tyfocor and 0.2 wt% of Triton X-100 at 283.15, 303.15 and 323.15 K.

pseudoplasticity for higher graphene concentration; and a Newtonian behavior was found at higher shear rates.

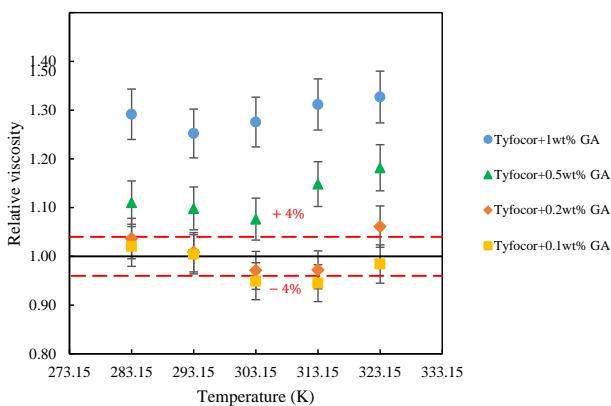
In another study, functionalized fGNPs were dispersed in propylene glycol:water mixture at (30:70) wt% by Vallejo et al. [31]. The authors prepared nanofluids with weight content between 0.25 and 1% and



(a)



(b)



(c)

Fig. 2. Relative viscosity of the studied base fluids prepared with Tyfocor with Pluronic® P-123 (a), Triton X-100 (b), and Gum Arabic (c) as a function of temperature. Solid line represents no viscosity enhancement for Tyfocor with surfactant compared to Tyfocor alone and dotted lines at  $\pm 4\%$  represent the uncertainty in dynamic viscosity measurement.

their viscosity was tested in the temperature range 293.15–323.15 K by imposing constant shear rates in the range of 1000–4000 s<sup>-1</sup>. The viscosity was found independent on shear rate (Newtonian behavior) and on testing time (100 s). In addition, the temperature rise caused a decrease in viscosity between 31 and 57%. On the other hand, with increasing the graphene loading, the viscosity increase attained 44 and 214% for the lowest and highest fGNP concentration, respectively.

The rheological properties of graphene oxide (GO) and reduced graphene oxide (rGO)/water nanofluids were studied by Cabaleiro et al. [21] at 293.15 and 303.15 K. The prepared nanofluids were in the volume concentration range of 0.0005–0.1%. The results showed a Newtonian behavior for the prepared nanofluids with graphene content lower than 0.01 vol% and shear-thinning behavior was observed for higher graphene concentrations. Additionally, maximum increases of 100–130% and 70–80% was obtained respectively for the non-Newtonian GO and rGO based nanofluids. The largest increase was found for the highest concentration at 303.15 K. The results regarding the relative viscosity showed an enhancement by about 130 and 70% in the tested range of concentration for GO and rGO based nanofluids, respectively, without any significant influence of temperature. On the other hand, the authors showed that for the highest graphene content studied, rGO based nanofluids exhibited lower apparent viscosities than for GO-based nanofluids, and weaker shear-thinning behaviors.

In this study, high quality few layer graphene (FLG) was dispersed in a commercial mixture of propylene-glycol/water using three different nonionic surfactants, Pluronic® P-123, Triton X-100 and Gum Arabic. The studied nanoparticle weight concentrations are: 0.05, 0.1, 0.25, and 0.5%. The rheological behavior of all corresponding base fluids and nanofluids were investigated at temperatures between 283.15 and 323.15 K and correlated to the visual aspect of the nanofluids after shearing. The results are discussed according to the influence of concentration and type of surfactant, concentration of FLG, temperature and shearing time. For well-stable nanofluids under shear, the viscosity evolution with temperature and FLG concentration is finally predicted by a comprehensive viscosity model. This study is the last step of the thermophysical characterizations of these FLG-based nanofluids, as the stability at rest and thermal conductivity [32] and the volumetric and surface tension properties [33] were recently reported.

## 2. Materials and methods

As reported in our recent works [32,33], the nanofluids presently investigated are produced with high quality few-layer graphene (3–5 layers, mean lateral size 5 μm, average thickness 1.5 nm) that was synthesized from ultrasound exfoliation of expanded graphene in water assisted by tannic acid. The full morphological and structural characterization of this FLG was previously performed in [32].

Graphene-based nanofluids were obtained from the dispersion of the FLG, previously washed, freeze-dried and dried after the exfoliation process, in a commercial heat transfer fluid, namely Tyfocor® LS, that is a mixture of water and propylene glycol 60:40 wt% using nonionic surfactants. Hence, Triton X-100 and Pluronic® P123 provided by Sigma Aldrich (Germany) and Gum Arabic by Acros Organics (France) were used as received. As also explained previously [32,33], a starting suspension with 0.5 wt% of FLG was added to the base fluid, Tyfocor + surfactant (1 wt%) and sonicated with a probe sonicator (Biolock Scientific Vibra cell 75042, 125 W with a pulse mode 2 s ON/1 s OFF) for several cycles of 15 min to avoid sample overheating. Samples with lower concentration were obtained from the dilution of the starting suspension with Tyfocor alone using the same sonication procedure. The surfactant:FLG ratio remain constant and equal to 2 for each FLG content that varies between 0.5 and 0.05 wt%. The procedure was similarly followed for the three used surfactants. More details can be found in [32]. In the following, Pluronic® P-123, Triton X-100 and Gum Arabic will be referred to as P123, TrX and GA, respectively and Tyfocor is used in the text and the figures instead of Tyfocor® LS, for sake of clarity.

### 2.1. Rheological characterizations

Dynamic viscosity studies were performed on a Malvern Kinexus Pro rotational rheometer (Malvern Instruments Ltd., United Kingdom) equipped with a cone-plate geometry appropriate to investigate low-viscosity colloidal suspensions. The measuring geometry has a diameter of 60 mm and a cone angle of 1°, while the gap between the cone and the plate is 0.03 mm. Stress-controlled measurements were done at temperatures between 283.15 and 323.15 K with an interval of 10 K. Temperature was controlled with a precision of ±0.01 K by means of a Peltier temperature control device placed below the lower surface. Special thermal clovers were used to ensure constant temperature throughout the sample gap during experiments. A sample volume of 1 cm<sup>3</sup>, considered optimal for the analysis with this geometry, was placed on the lower plate and a stabilization time of 5 min was allowed before experiments. Before starting the rheological measurements and in order to evaluate the temperature effect on nanofluid state at rest, every nanofluid was tested under controlled temperature at each single studied temperature for 10 min (+5 min stabilization time) and without shearing the sample.

Afterwards, two rheological analyses were performed. First, shear-viscosity flow curves were collected in state regimen at shear stresses in logarithmic scale corresponding to shear rates between 10 and 1000 s<sup>-1</sup>. Finally, with the aim of analyzing the combined effect of both temperature and shearing time on nanofluid state, samples were also subject to a temperature ramp (in which temperature was continuously increased in the range from 283.15 to 323.15 K by steps of 10 K)

**Table 1**

Observed states of the prepared nanofluid series at the end of the rheological measurements. Each visible aspect are noticed as (⊕) for the stable nanofluids without or with visually observed small aggregates, (□) for visible aggregates, (•) for a gel-like aspect, (▲) for a noticeable phase separation between FLG and the base fluid, (-) no measurement was done, (◇) no available photo. An example of each state mentioned in this table is shown in Fig. 3.

	T(K)	T fixed, shear rate fixed at 0 s <sup>-1</sup>					T fixed, shear rate ↑					T ↑, shear rate fixed at 500 s <sup>-1</sup>				
		283.15	293.15	303.15	313.5	323.15	283.15	293.15	303.15	313.15	323.15	283.15	293.15	303.15	313.15	323.15
P123	0.05%	⊕	⊕	⊕	⊕	⊕	⊕	-	-	-	⊕	◇	◇	◇	◇	⊕
	0.1%	⊕	⊕	⊕	⊕	⊕	⊕	-	-	-	⊕	◇	◇	◇	◇	⊕
	0.25%	⊕	⊕	⊕	⊕	⊕	⊕	-	-	-	⊕	◇	◇	◇	◇	⊕
	0.5%	⊕	⊕	⊕	⊕	⊕	⊕	-	-	-	⊕	◇	◇	◇	⊕	•
TrX	0.05%	□	□	□	□	▲	□	□	▲	▲	▲	◇	◇	◇	◇	▲
	0.1%	⊕	⊕	⊕	□	□	⊕	⊕	⊕	-	◇	◇	◇	◇	▲	-
	0.25%	⊕	⊕	⊕	⊕	▲	⊕	⊕	•	▲	◇	◇	◇	⊕	•	-
	0.5%	⊕	⊕	⊕	⊕	•	⊕	•	•	-	-	◇	◇	•	-	-
GA	0.05%	⊕	⊕	⊕	⊕	⊕	⊕	-	-	-	⊕	◇	◇	◇	◇	□
	0.1%	⊕	⊕	⊕	⊕	⊕	⊕	-	-	⊕	⊕	◇	◇	◇	◇	□
	0.25%	⊕	⊕	⊕	⊕	⊕	⊕	⊕	⊕	⊕	□	◇	◇	⊕	□	-
	0.5%	⊕	⊕	⊕	⊕	□	⊕	⊕	⊕	□	-	◇	◇	•	-	-

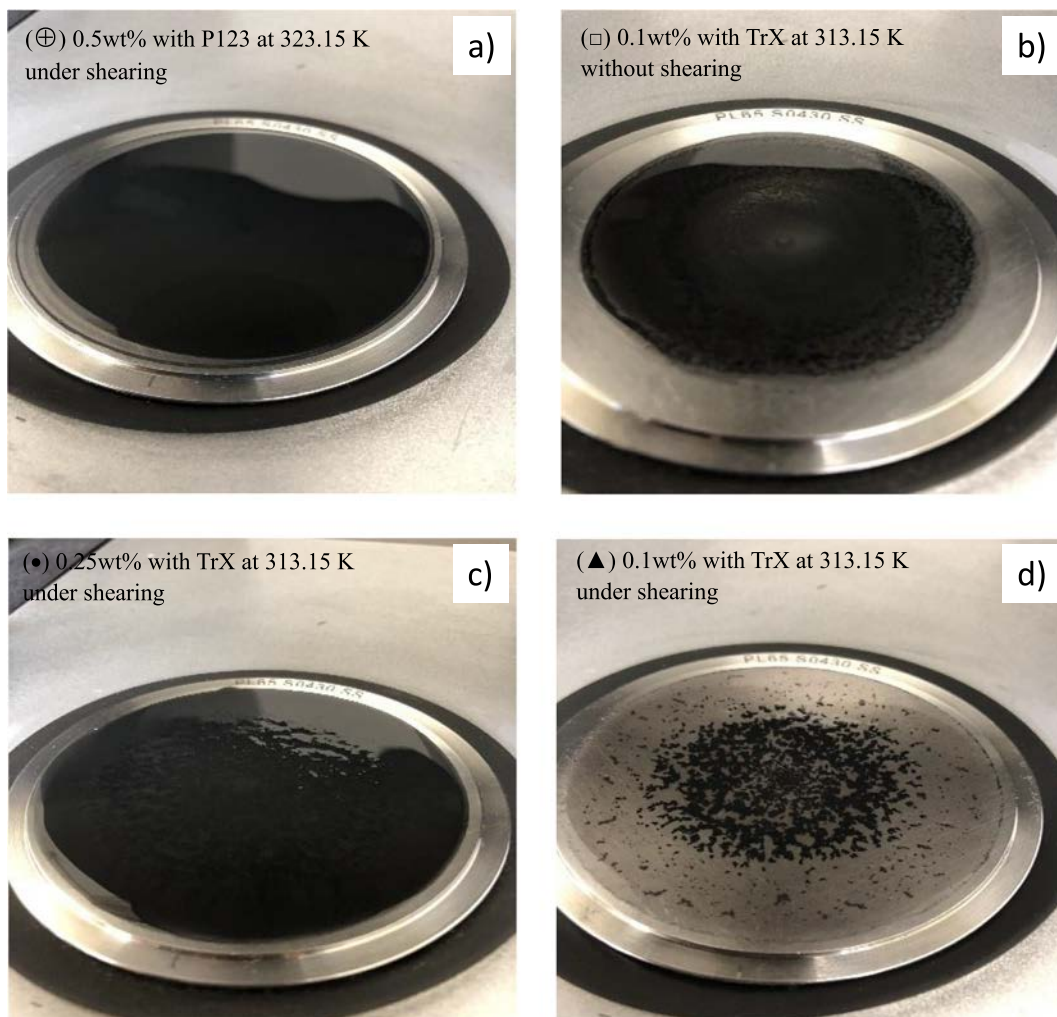


**Fig. 3.** Representative examples of the different nanofluid states observed after performing the measurements: a) stable nanofluids without or with visually observed small aggregates ( $\oplus$ ), b) visible aggregates unseparated to the base fluid ( $\square$ ), c) gel-like aspect ( $\bullet$ ), and d) visible phase separation between the FLG aggregates and the solvent ( $\blacktriangle$ ).

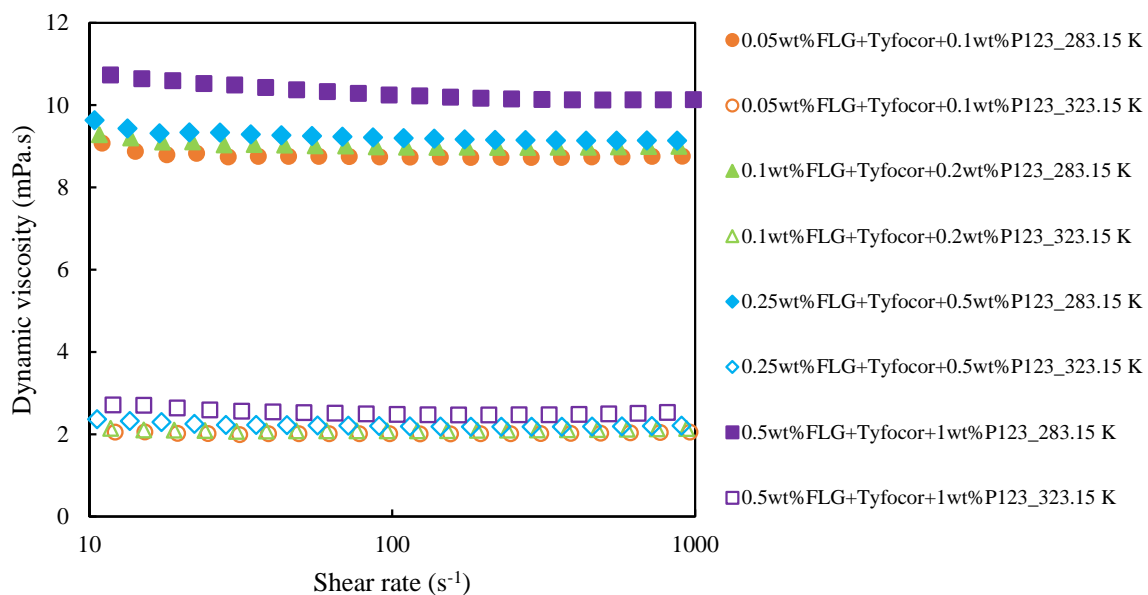


**Fig. 4.** Dynamic viscosity of nanofluids with Pluronic® P-123 at 283.15 and 323.15 K as a function of shear rate.

while shear rate was hold to  $500 \text{ s}^{-1}$ . This shear rate was selected based on shear flow curves and corresponded to the region where Newtonian plateau was reached for all samples.

In an original way, pictures of the samples were taken at the end of the measurements to evaluate the stability of the nanofluids and to correlate the shear flow behavior with the visual aspect of the nanofluids.

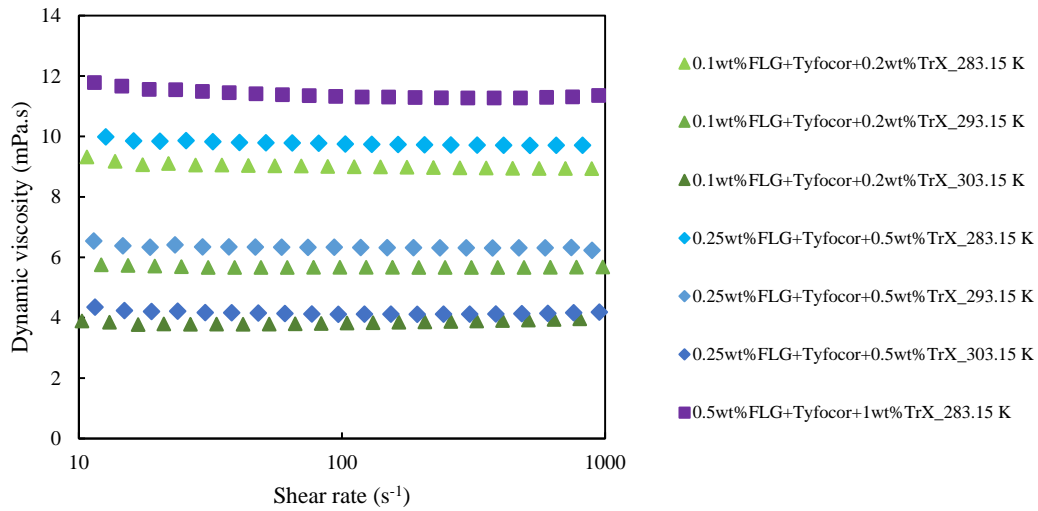
Additional details about the experimental device can be found in Halefadi et al. [34]. Experiments for each fluid and nanofluid and studied conditions were performed at least in duplicate and obtained flow curves did not show any significant difference. To validate the experimental shear flow protocol described above, dynamic viscosity measurements were done between 283.15 and 313.15 K for distilled water and between 273.15 and 373.15 K for Tyfocor thermal fluid. As

expected, the results showed a Newtonian behavior for these two fluids. To confirm the accuracy of the measure instrument, our experimental results were compared with those reported in the literature. The absolute average deviation obtained with water was about 3.5% [35] and that of Tyfocor was less than 5% [36] in the tested temperature range.

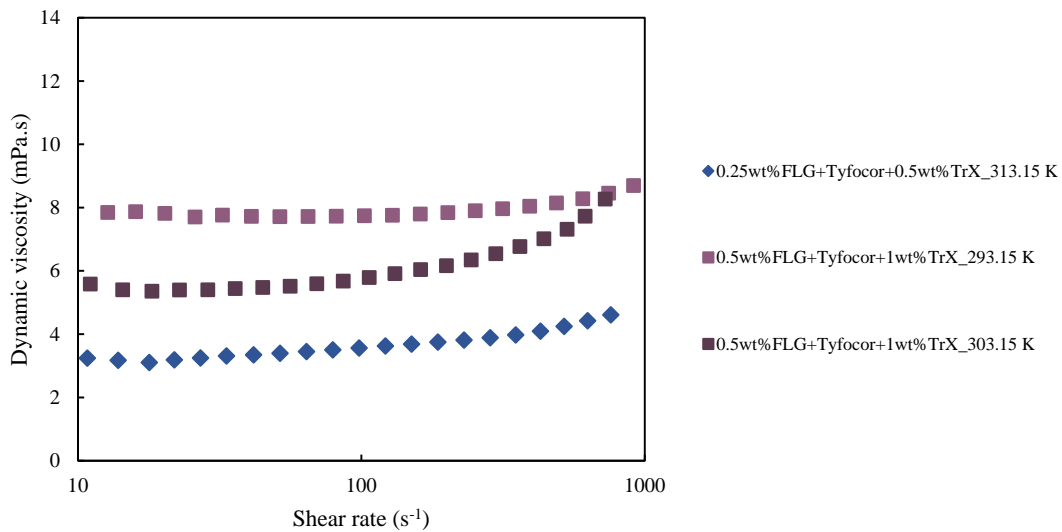
### 3. Results and discussion

#### 3.1. Effect of surfactant on viscosity of propylene-glycol/water mixture

To evaluate the effect of surfactant (type and concentration) on the dynamic viscosity of Tyfocor, this transport property was investigated in the temperature range 283.15–323.15 K for surfactant-Tyfocor



(a)



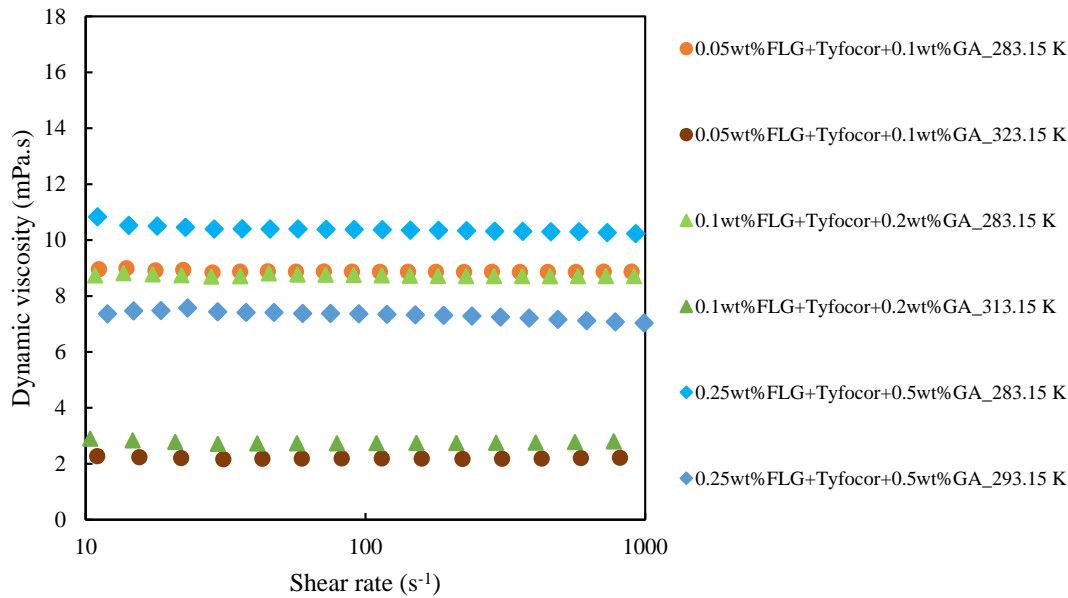
(b)

**Fig. 5.** Dynamic viscosity of FLG-based nanofluids prepared with Triton X-100 between 283.15 and 313.15 K as a function of shear rate; FLG based nanofluids showing a (a) stable or dispersed state and a (b) gel-like aspect.

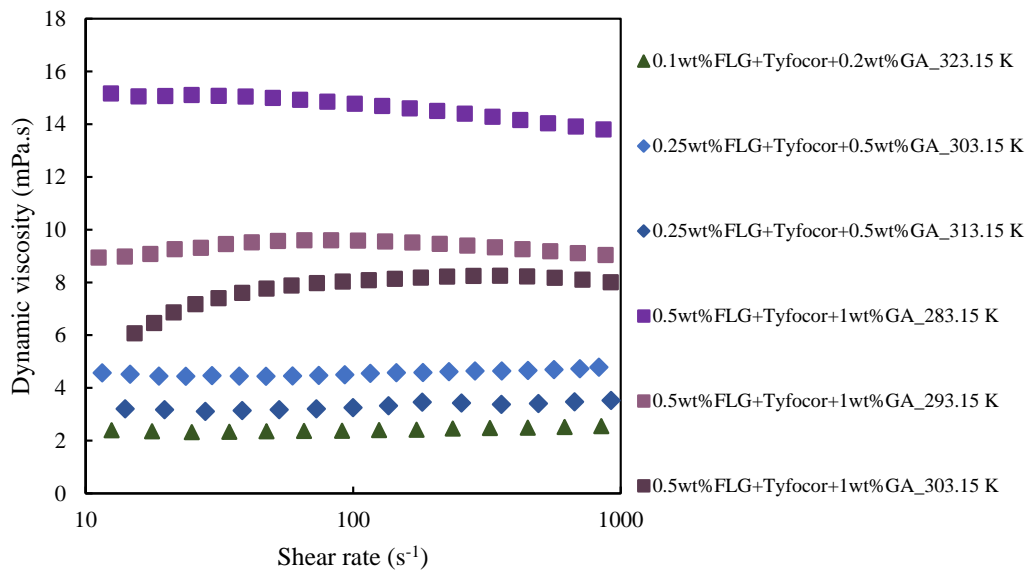
mixtures prepared at surfactant concentrations of 0.1, 0.2, 0.5 and 1.0 wt % with either Triton X-100, Pluronic® P-123 or Gum Arabic. At the investigated conditions, all studied surfactant-Tyfocor mixtures (which were also used as base fluids) exhibited a Newtonian behavior. As an example, Fig. 1 shows the obtained flow curves for the mixture of Tyfocor and 0.2 wt% of Triton X-100 at 283.15, 303.15 and 323.15 K.

Relative viscosity of the base fluids was determined in the tested temperature range as presented in Fig. 2. The results show that the

addition of Pluronic® P-123 (all concentrations), Triton X-100 (0.1, 0.2 and 0.5 wt%) and Gum Arabic (0.1 and 0.2 wt%) has no significant effect on the viscosity of the starting fluid (Tyfocor) within the experimental uncertainty. The highest concentration of Triton X-100 (1 wt%) increased the viscosity of Tyfocor by 7.9% on average in the tested temperature range. With Gum Arabic, the dynamic viscosity was increased by 12.3 and 29.2% after the addition of 0.5 and 1% of weight concentrations, respectively, without any dependence on the temperature.



(a)



(b)

Fig. 6. Dynamic viscosity of FLG based nanofluids prepared with gum arabic between 283.15 and 323.15 K as a function of shear rate; (a) Newtonian and (b) non-Newtonian samples.

### 3.2. Effect of temperature and concentration on nanofluids behavior

#### 3.2.1. Nanofluids at rest

All the nanofluids produced with the three different surfactants were tested between 283.15 and 323.15 K, without and under shearing in order to discriminate between the temperature and the shearing effects. The observed aspects of each nanofluid after each measurement are gathered in Table 1. An example of each nanofluid state described in Table 1 is shown in Fig. 3. Table 1 evidences that the dispersion state of the prepared FLG nanofluids can strongly vary after the different experiments depending on the experimental protocol (no shear and shear), the type of surfactant used, the temperature and the shearing time. Four states or aspects were mainly observed after the rheological measurements. The FLG-based nanofluids showing a dark homogeneous aspect without visible aggregates or with only few small aggregates, thus, appearing mainly as a well dispersed phase are named ( $\oplus$ ) for 'stable nanofluids' (Fig. 3a). When black FLG aggregates are visible, the aspect is noted aggregation ( $\square$ ) (Fig. 3b) and if these aggregates form a well-separated phase from the solvent, phase separation ( $\blacktriangle$ ) is recorded (Fig. 3d). In some cases, a homogeneous aspect is observed but in the form of a viscous gel ( $\bullet$ ) (Fig. 3c). Concisely, the FLG-based nanofluid samples produced with Pluronic® P-123 and Gum Arabic were rather stable at rest, while the dispersion state of the nanofluids prepared with Triton X-100 seemed much more sensitive to temperature. An aggregation phenomenon and a clear phase separation were indeed noticed when temperature increased especially for the highest FLG concentration.

#### 3.2.2. Nanofluid under shear

The shear flow behavior of the prepared FLG-based nanofluids is discussed in the following considering the type of surfactant used and the FLG concentration. With Pluronic® P-123, see Fig. 4, the FLG-based nanofluids were mainly Newtonian in the investigated temperature range and they exhibited a slight shear-thinning behavior at low shear rates. Such a shear-thinning trend is more pronounced at 0.5 wt% in FLG as the dynamic viscosity decreases up to  $200 \text{ s}^{-1}$  before to reach a Newtonian plateau. In addition, as noticed in Table 1, they stayed stable during all shear flow measurements. From this rheological study, the dynamic viscosity was found to increase with the FLG content in the nanofluids and to decrease with temperature.

FLG-based nanofluids prepared with Triton X-100 were observed to lose their stability at high temperature at rest (Table 1). Viscosity measurements with varying the shear rate between 10 and  $1000 \text{ s}^{-1}$

showed the shear flow behavior of the samples at the selected temperatures. The results of stable (dispersed state) nanofluids under shearing are presented in Fig. 5(a), those showing a gel-like appearance at end of the measurement (Table 1) are shown in Fig. 5(b). The stable FLG-based nanofluids behave as Newtonian fluids in the tested shear rate range with a slight decrease in viscosity at very low shear rates indicating a weak shear-thinning. For the other FLG-based nanofluids after a slight reduction at very low shear rates, it is observed that the dynamic viscosity mainly increases with increasing shear rate indicating a shear-thickening behavior. This behavior under shearing can be related to the observed gelation phenomenon and the presence of a disordered structure of aggregates. This behavior seems to be sensitive to high temperature and concentration. Actually, it produces for the FLG nanofluids having a relatively high amount of surfactant and FLG (see also Table 1) i.e. 0.25 wt% of FLG (and 0.5 wt% of Triton X-100) at 323.15 K or for the suspensions containing 0.5 wt% of FLG (and 1 wt% of Triton X-100) at 293.15 and 303.15 K.

In the case of nanofluids prepared with Gum Arabic, they were stable with the presence of some aggregates for high FLG concentrations at high temperatures without shearing. After shearing measurements at selected temperatures, no significant change of their aspect was observed. These measurements showed different behaviors for these nanofluids, like quite Newtonian (Fig. 6a and b), or shear-thinning and shear-thickening at low shear rates up to  $200 \text{ s}^{-1}$  (Fig. 6b) before to reach a Newtonian plateau. For example, a slight shear-thinning behavior was obtained for 0.1 wt% of Gum Arabic at 323.15 K, 0.25 wt% of Gum Arabic at 303.15 K and 313.15 K and also for 0.5 wt% of Gum Arabic at 283.15 K, respectively. A significant shear-thickening behavior was noticed for the highest concentration of FLG 0.5 wt% (containing 1 wt% of Gum Arabic) at 293.15 and 303.15 K at low shear rates ( $<200 \text{ s}^{-1}$ ). This trend could be attributed to the organization of the aggregates (see Table 1) under shear before to reach a stabilized state.

The fact that certain Newtonian fluids become non-Newtonian after the dispersion of nanoparticles can be explained by the formation of possible nanoparticle-based fluid networks whose structure gets modified under shear stress [30,37–39]. Accordingly, a shear thinning behavior could indicate that nanoparticle networks could break once oriented in the flow direction of the shear. This would lessen the interaction forces, decreasing the flow resistance and, consequently, the apparent viscosity of the dispersion decreases [30,37–39]. Inversely, and as mentioned earlier, shear-thickening could be attributed the presence of the disordered structure of aggregates and their interaction.

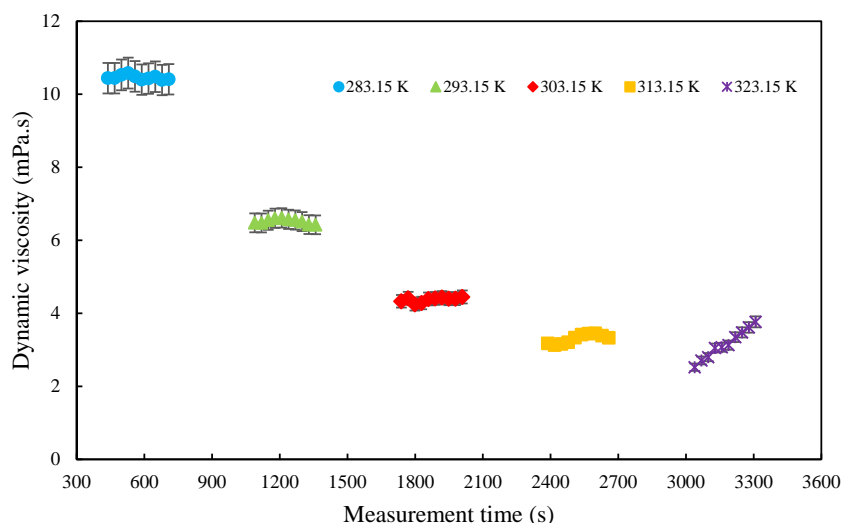


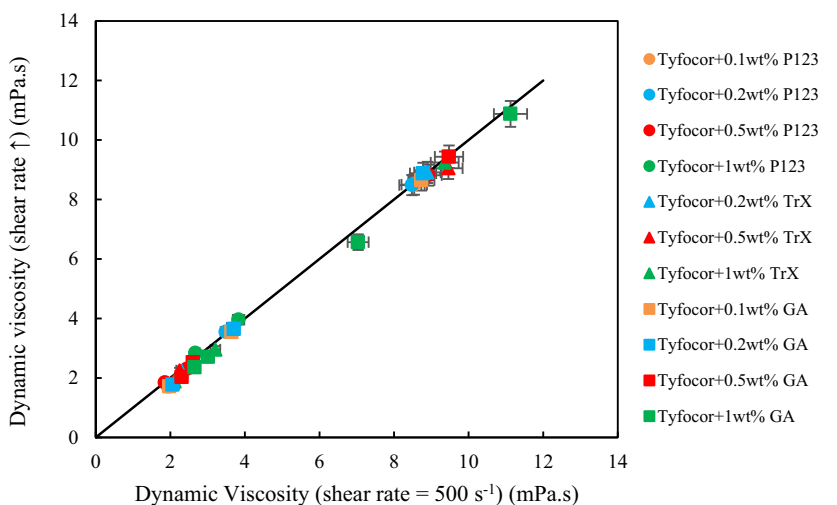
Fig. 7. Dynamic viscosity of the nanofluid prepared with 0.5 wt% of FLG and 1 wt% Pluronic® P-123 between 283.15 and 323.15 K as a function of measurement time.

### 3.2.3. Effect of shearing time and temperature

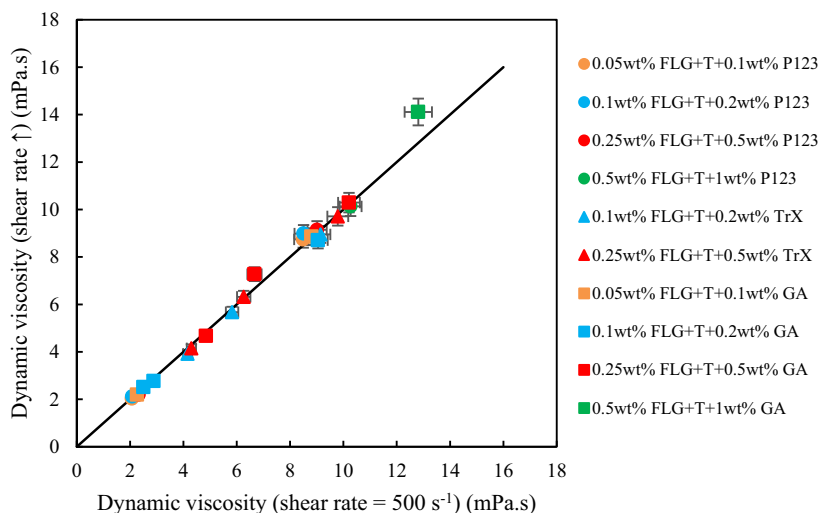
As explained before, a last measurement was performed with all stable nanofluids, selected from the previous experiments, by applying a fixing shear rate of  $500 \text{ s}^{-1}$  (this shear rate being in the Newtonian region) and increasing the temperature from 283.15 to 323.15 K with the same sample.

Concerning the nanofluids prepared with Pluronic® P-123, the dynamic viscosity was stable with time at all the temperatures between 283.15 and 323.15 K. However, with the highest concentration of 0.5 wt% of FLG, Fig. 7 shows that the viscosity started to increase at 323.15 K after 3040 s from the beginning of the measurement e.g. after a total shearing time equal to 1200 s due to delay between each temperature change) and the sample looked like a gel at the end of measurement. Another measurement performed from 283.15 to 313.15 K

did not show any significant change in the state of the nanofluid, which may indicate that such increase in viscosity at 323.15 K may be related to the instability of the sample and change in structure. Similar phenomenon was observed with the other two series, an increasing in the dynamic viscosity with time related to the loss of nanofluid stability after a certain shearing time and from certain temperature. Taking as an example the nanofluids prepared with Triton X-100, an increasing in viscosity is observed at measurement time equal to 2390 s, 1960 s, and 499.6 s (total shearing time equal to 900, 720 and 90 s) and that produces at the temperature 313.15, 303.15 and 283.15 K for the FLG concentrations of 0.1, 0.25 and 0.5 wt%, respectively. With Gum Arabic nanofluids, the rise in viscosity was detected at measurement times equal to 3210, 3190, 1220, and 656 s (that corresponds to a total shearing times equal to 1440, 1380, 450 and 240 s respectively) which

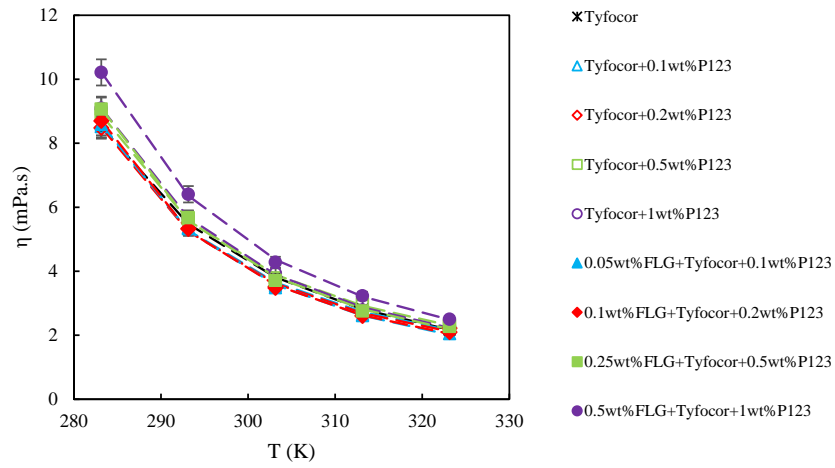


(a)

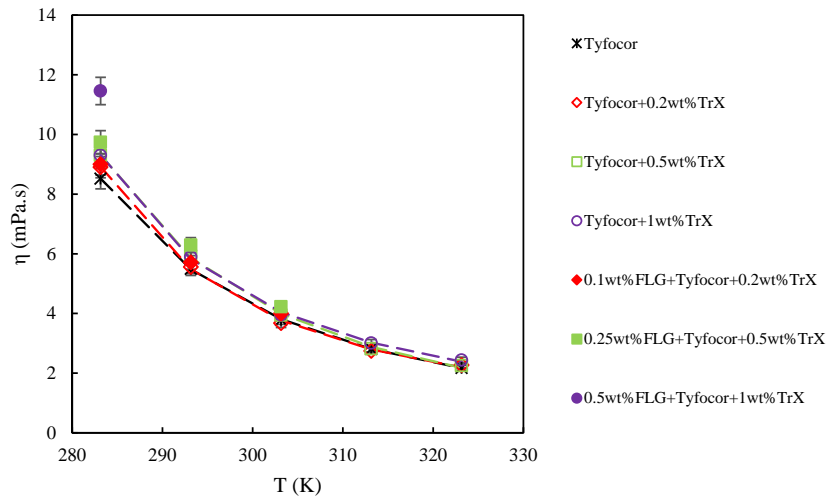


(b)

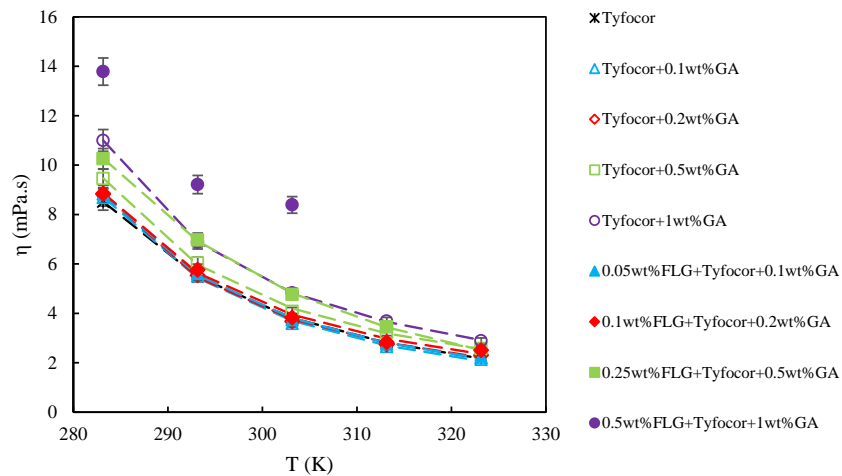
**Fig. 8.** Comparison between the dynamic viscosity with varying shear rate and fixing it at  $500 \text{ s}^{-1}$  at different temperatures for the base fluids (a) and the corresponding FLG nanofluids (b). The solid line represents the bisector.



(a)



(b)



(c)

**Fig. 9.** Dynamic viscosity of the FLG based nanofluids and the corresponding base fluids with Pluronic® P-123 (a), Triton X-100 (b) and Gum Arabic (c) as a function of temperature. The dashed lines represent the fitted values from Eq. (1).

corresponds to the temperatures of 323.15, 293.15, 293.15 and 283.15 K for the FLG concentrations of 0.05, 0.1, 0.25 and 0.5 wt%, respectively. From Table 1, the difference between the nanofluid states observed with the three different kinds of measurements evidences that the temperature, the concentration, the shearing and the duration of shearing have an important role in the stability of nanofluids under shear. Based on the analysis compiled in Table 1, the nanofluid samples produced with Pluronic® P-123 seem to be the most resistant against shear and temperature. Nanofluids with Gum Arabic are relatively stable while nanofluids containing Triton X-100 have the lowest stability. It should be finally noted that the viscosities of the base fluids (mixtures of Tyfocor and surfactant) are not sensitive to this kind of test and all the values were stable with time and for all the temperatures from 283.15 to 323.15 K.

### 3.3. Nanofluid viscosity

Now to compare the results of the two different measurements for stable nanofluids, by fixing the temperature with increasing the shear rate from 10 to 1000 s<sup>-1</sup> and by fixing the shear rate at 500 s<sup>-1</sup> with increasing the temperature, the obtained viscosity values are represented in Fig. 8.

In Fig. 8, the viscosity results obtained from flow curve experiments (y-axis) correspond to the average value of data collected at shear rates higher than 200 s<sup>-1</sup> (common Newtonian region for all stable nanofluids). Regarding the temperature ramps at a constant shear rate of 500 s<sup>-1</sup> (x-axis), viscosity values are the average of all data that were constant during the measurement (before the rise in viscosity observed at certain temperatures as explained before). Fig. 8 shows clearly that these two different tests are compatible since they lead to values belonging quite well to same bisector (taking into account the experimental uncertainty). That is why in the following section, the considered viscosity values are the average of the results obtained with the two tests.

The effect of temperature on the viscosity of both base fluids and nanofluids is shown in Fig. 9. It is known that increasing temperature leads to decrease the viscosity of a fluid. This universal behavior in liquids is attributed to the lessening of molecular cohesive forces with increasing temperature, which reduces the shear stress and then the viscosity [40]. For all the studied base fluids and nanofluids, as expected, dynamic viscosity decreases with the increase of temperature in the range 283.15–323.15 K. The decreasing rate with Tyfocor alone and all base fluids is around 74% from 283.15 to 323.15 K. For the nanofluids,

the dynamic viscosity decreases with a similar trend as the corresponding base fluids, except for the highest concentration of FLG (0.5 wt%) with Gum Arabic where it decreases from 293.15 to 303.15 K by 9%, while this rate is 30% for the corresponding base fluid.

One of the most used models describing the temperature dependence of viscosity is the Vogel-Fulcher-Tammann (VFT) equation [30,41–43]. This model has been previously used for graphene nanofluids [29,30,44].

$$\eta = \eta_0 \times e^{\frac{A \times T_0}{T - T_0}} \quad (1)$$

where  $\eta_0$ , A, and  $T_0$  are the fitting parameters. These parameters are gathered in Table 2 for both base fluids and nanofluids (that have results at more than three temperatures). Low absolute average deviations (AADs) and standard deviations between the experimental and fitted values around 1.53% and 0.0961 mPa·s in average were obtained, respectively.

The decrease in viscosity with increasing temperature has also been found previously with graphene-based nanofluids with water [21,45–51] and glycoled water mixtures in different proportions [23,31,44,52,53], respectively.

Addition of nanoparticles to a liquid was reported to induce an increase in fluid resistance to flow because of the greater friction occurring within the mixture [44,54]. Thus, once a nanofluid flows, to overcome this augmentation in internal friction resistance a higher energy consumption is required (in comparison to the base fluid without nanoparticles) [35,54]. Hence, the addition of nanoparticles in a liquid increases its viscosity. The viscosity enhancement of the studied stable FLG based nanofluids under shear as function of FLG concentration and temperature is shown in Fig. 10.

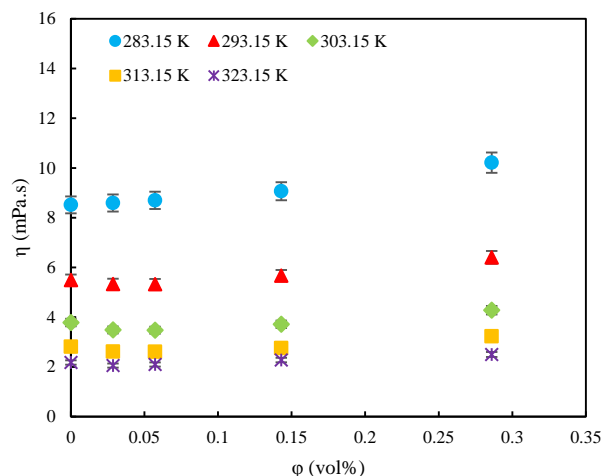
It worth noting that the volume concentration  $\varphi$ , used in Fig. 10 is calculated from the  $\varphi_m$  using the following equation [32]:

$$\varphi = \frac{\varphi_m \times \frac{\rho_{bf}}{\rho_{np}}}{\left(1 - \varphi_m \times \left(1 - \frac{\rho_{bf}}{\rho_{np}}\right)\right)} \quad (2)$$

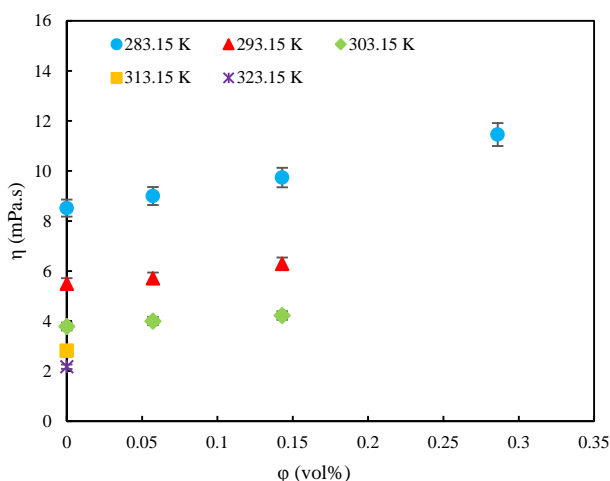
where  $\rho_{bf}$  and  $\rho_{np}$  are the experimental densities of base fluids at all temperatures and the one of the nanoparticles at ambient temperature, respectively, as reported in [33]. The increase rate in dynamic viscosity (with respect to Tyfocor fluid) is maximal for the highest FLG tested concentrations. Thus, it reaches 19.9, 34.5 and 121.6% in the case of

**Table 2**  
Dynamic viscosity values ( $\eta$ ) for base fluids and nanofluids and fitting parameters ( $\eta_0$ , A, and  $T_0$ ), standard deviation (s) and AAD obtained from the VFT equation, Eq. (1).

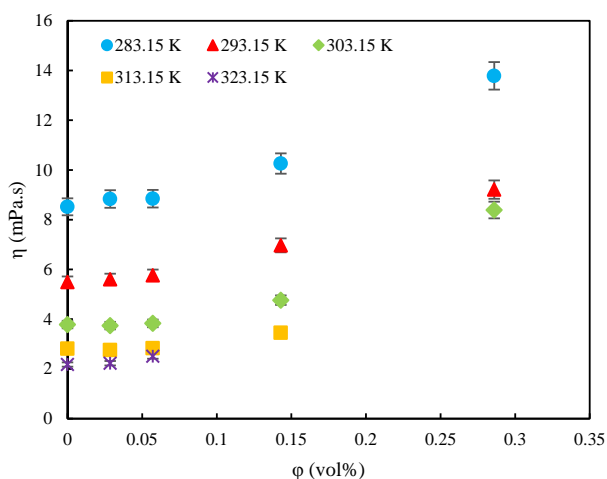
Sft	$\varphi_{m, sft}$ %	$\varphi_{m, np}$ %	Temperature (K)					Fitting parameters and deviations				
			283.15	293.15	303.15	313.15	323.15	$\eta_0$ (mPa·s)	A	$T_0$ (K)	s (mPa·s)	AAD (%)
P123	0	0	8.52	5.48	3.81	2.81	2.17	0.0906	2.22	190.28	0.022	0.28
	0.1	0	8.538	5.272	3.646	2.725	2.153	0.2296	1.08	218.15	0.131	2.47
	0.2	0	8.500	5.242	3.614	2.690	2.116	0.2069	1.15	216.26	0.131	2.49
	0.5	0	8.889	5.582	3.891	2.917	2.306	0.2237	1.19	214.01	0.091	1.13
	1	0	9.094	5.669	3.895	2.870	2.228	0.1479	1.54	206.01	0.073	1.22
	0.1	0.05	8.603	5.269	3.576	2.612	2.015	0.1306	1.52	207.74	0.083	1.17
	0.2	0.1	8.710	5.257	3.567	2.624	2.044	0.1850	1.18	216.85	0.088	1.42
	0.5	0.25	9.082	5.581	3.815	2.811	2.188	0.1724	1.34	211.73	0.121	2.07
	1	0.5	10.222	6.357	4.359	3.206	2.485	0.1611	1.56	205.76	0.068	0.80
	TrX	0.2	0	8.918	5.482	3.766	2.795	2.192	0.2053	1.18	215.65	0.106
	0.5	0	9.309	5.862	3.989	2.882	2.181	0.0597	2.72	183.97	0.087	1.57
	1	0	9.318	5.822	4.044	3.024	2.385	0.2271	1.20	214.10	0.092	1.29
GA	0.1	0	8.708	5.426	3.700	2.696	2.067	0.0971	1.93	198.09	0.118	1.99
	0.2	0	8.844	5.455	3.765	2.808	2.213	0.2265	1.11	217.32	0.123	2.22
	0.5	0	9.468	5.961	4.197	3.187	2.553	0.3259	0.96	220.33	0.107	1.28
	1	0	10.997	6.891	4.830	3.653	2.916	0.3552	0.99	219.72	0.032	0.42
	0.1	0.05	8.844	5.542	3.810	2.802	2.168	0.1254	1.71	202.06	0.085	1.49
	0.2	0.1	8.871	5.630	3.948	2.969	2.351	0.2210	1.24	211.95	0.195	3.40
	0.5	0.25	10.971	6.926	4.813	3.436	2.512	0.0005	58.11	41.30	0.0707	0.58



(a)



(b)



(c)

**Fig. 10.** Dynamic viscosity of the PLG-based nanofluids with Pluronic® P-123 (a), Triton X-100 (b) and Gum Arabic (c) as a function of PLG volume concentration.

Pluronic® P-123, Triton X-100 and Gum Arabic at 283.15, 283.15 and 303.15 K, respectively for the nanofluids containing 0.5 wt% of FLG. From an insight of Fig. 10, it can be observed that the nanofluids with Pluronic® P-123 have lower viscosities than samples containing Triton X-100 and the highest viscosities were obtained for Gum Arabic series.

#### 4. Concluding remarks

This study concerned the rheological characterization of PLG-based nanofluids produced with a commercial heat transfer fluid based on a mixture of water and propylene glycol and different non-ionic surfactants. In an original way, nanofluid samples were subjected to different experiments, at rest at fixed temperature, under steady shear flow at fixed temperature and under temperature ramp at fixed shear rate, which allowed evaluating their stability and behavior under shear and temperature influence. These results were compared and correlated to visual aspect of the sample at the end of measurements. These experiments were performed in the temperature range 283.15–323.15 K and varying the mass content in PLG from 0.05 to 0.5%. The difference between the nanofluids states observed with the different measurement methods showed that the temperature, the shearing and the duration of shearing have an important role on the nanofluids stability in function of their concentration and surfactant. This also allows the best nanofluid and surfactant to be evaluated in terms of stability under flow. Finally, for the stable nanofluids under shear, the dynamic viscosity evolution with temperature was correlated to Vogel-Fulcher-Tammann (VFT) equation.

#### CRediT authorship contribution statement

**Samah Hamze:** Investigation, Visualization, Data curation, Formal analysis, Writing - original draft. **David Cabaleiro:** Investigation, Visualization, Data curation, Writing - review & editing. **Thierry Maré:** Supervision. **Brigitte Vigolo:** Resources, Supervision, Writing - review & editing. **Patrice Estellé:** Conceptualization, Methodology, Supervision, Project administration, Writing - review & editing.

#### Declaration of competing interest

The authors declare that they have no known competing financial interests or personal relationships that could have appeared to influence the work reported in this paper.

#### Acknowledgements

The authors would like to thank Dr. D. Bégin for providing PLG samples, Dr. N. Berrada for her help in the preparation of the PLG based nanofluids and Dr. A. Desforges for fruitful discussions. D.C. is recipient of a postdoctoral fellowship from Xunta de Galicia (Spain). This investigation is a contribution to the COST (European Cooperation in Science and Technology) Action CA15119: Overcoming Barriers to Nanofluids Market Uptake (NanoUptake).

#### References

- [1] M. Mehrli, S. Tahan Latibari, M.A. Rosen, A.R. Akhiani, M.S. Naghavi, E. Sadeghinezhad, H.S.C. Metselaar, M. Mohammadi Nejad, M. Mehrli, From rice husk to high performance shape stabilized phase change materials for thermal energy storage, *RSC Adv.* 6 (2016) 45595–45604, <https://doi.org/10.1039/C6RA03721F>.
- [2] S. Iranmanesh, H.C. Ong, B.C. Ang, E. Sadeghinezhad, A. Esmaeilzadeh, M. Mehrli, Thermal performance enhancement of an evacuated tube solar collector using graphene nanoplatelets nanofluid, *J. Clean. Prod.* 162 (2017) 121–129, <https://doi.org/10.1016/j.jclepro.2017.05.175>.
- [3] S.M.S. Murshed, P. Estellé, A state of the art review on viscosity of nanofluids, *Renew. Sust. Energ. Rev.* 76 (2017) 1134–1152, <https://doi.org/10.1016/j.rser.2017.03.113>.

- [4] S.U.S. Choi, Z.G. Zhang, P. Keblinski, *Nanofluids*, in: H.S. Nalwa (Ed.), *Encyclopedia of Nanoscience and Nanotechnology*, American Scientific Publishers, Los Angeles 2004, pp. 757–773.
- [5] S.K. Das (Ed.), *Nanofluids: Science and Technology*, Wiley-Interscience, Hoboken, N. J., 2008.
- [6] S.M.S. Murshed, K.C. Leong, C. Yang, Thermophysical and electrokinetic properties of nanofluids – a critical review, *Appl. Therm. Eng.* 28 (2008) 2109–2125, <https://doi.org/10.1016/j.applthermaleng.2008.01.005>.
- [7] K.V. Wong, O. De Leon, Applications of nanofluids: current and future, *Adv. Mech. Eng.* 2 (2010), 519659, <https://doi.org/10.1155/2010/519659>.
- [8] R. Saidur, K.Y. Leong, H.A. Mohammed, A review on applications and challenges of nanofluids, *Renew. Sust. Energ. Rev.* 15 (2011) 1646–1668, <https://doi.org/10.1016/j.rser.2010.11.035>.
- [9] S.M.S. Murshed, C.A.N. de Castro, Nanofluids as advanced coolants, in: Inamuddin, A. Mohammad (Eds.), *Green Solvents I*, Springer Netherlands, Dordrecht 2012, pp. 397–415, [https://doi.org/10.1007/978-94-007-1712-1\\_14](https://doi.org/10.1007/978-94-007-1712-1_14).
- [10] S.M.S. Murshed, C.A.N. de Castro (Eds.), *Nanofluids: Synthesis, Properties, and Applications*, Nova Science Publishers, Inc, New York, 2014.
- [11] W. Yu, D.M. France, J.L. Routbort, S.U.S. Choi, Review and comparison of nanofluid thermal conductivity and heat transfer enhancements, *Heat Transf. Eng.* 29 (2008) 432–460, <https://doi.org/10.1080/01457630701850851>.
- [12] S. Thomas, C. Balakrishna Panicker Sobhan, A review of experimental investigations on thermal phenomena in nanofluids, *Nanoscale Res. Lett.* 6 (2011) 377, <https://doi.org/10.1186/1556-276X-6-377>.
- [13] S. Özerinç, S. Kakaç, A.G. Yazıcıoğlu, Enhanced thermal conductivity of nanofluids: a state-of-the-art review, *Microfluid. Nanofluidics*, 8 (2010) 145–170, <https://doi.org/10.1007/s10404-009-0524-4>.
- [14] O. Mahian, L. Kolsi, M. Amani, P. Estellé, G. Ahmadi, C. Kleinstreuer, J.S. Marshall, M. Siavashi, R.A. Taylor, H. Niazmand, S. Wongwises, T. Hayat, A. Kolanjiyil, A. Kasaeian, I. Pop, Recent advances in modeling and simulation of nanofluid flows—part I: fundamentals and theory, *Phys. Rep.* 790 (2019) 1–48, <https://doi.org/10.1016/j.physrep.2018.11.004>.
- [15] O. Mahian, L. Kolsi, M. Amani, P. Estellé, G. Ahmadi, C. Kleinstreuer, J.S. Marshall, R.A. Taylor, E. Abu-Nada, S. Rashidi, H. Niazmand, S. Wongwises, T. Hayat, A. Kasaeian, I. Pop, Recent advances in modeling and simulation of nanofluid flows—part II: applications, *Phys. Rep.* 791 (2019) 1–59, <https://doi.org/10.1016/j.physrep.2018.11.003>.
- [16] S.M.S. Murshed, K.C. Leong, C. Yang, Thermophysical properties of nanofluids, in: K.D. Sattler (Ed.), *Handbook of Nanophysics: Nanoparticles and Quantum Dots*, Taylor & Francis, Boca Raton, 2010.
- [17] C. Kleinstreuer, Y. Feng, Experimental and theoretical studies of nanofluid thermal conductivity enhancement: a review, *Nanoscale Res. Lett.* 6 (2011) 229, <https://doi.org/10.1186/1556-276X-6-229>.
- [18] S.M.S. Murshed, C.A. Nieto de Castro, Superior thermal features of carbon nanotubes-based nanofluids – a review, *Renew. Sust. Energ. Rev.* 37 (2014) 155–167, <https://doi.org/10.1016/j.rser.2014.05.017>.
- [19] H.Ş. Aybar, M. Sharifpur, M.R. Azizian, M. Mehrabi, J.P. Meyer, A review of thermal conductivity models for nanofluids, *Heat Transf. Eng.* 36 (2015) 1085–1110, <https://doi.org/10.1080/01457632.2015.987586>.
- [20] P. Estellé, S. Halelfadl, T. Maré, Thermal conductivity of CNT water based nanofluids: experimental trends and models overview, *J. Therm. Eng.* 1 (2015) 381, <https://doi.org/10.18186/jte.92293>.
- [21] D. Cabaleiro, P. Estellé, H. Navas, A. Desforges, B. Vigolo, Dynamic viscosity and surface tension of stable graphene oxide and reduced graphene oxide aqueous nanofluids, *J. Nanofluids*, 7 (2018) 1081–1088, <https://doi.org/10.1166/jon.2018.1539>.
- [22] A.A. Balandin, Thermal properties of graphene and nanostructured carbon materials, *Nat. Mater.* 10 (2011) 569–581, <https://doi.org/10.1038/nmat3064>.
- [23] D. Cabaleiro, L. Colla, S. Barison, L. Lugo, L. Fedele, S. Bobbo, Heat transfer capability of (ethylene glycol + water)-based nanofluids containing graphene nanoplatelets: design and thermophysical profile, *Nanoscale Res. Lett.* 12 (2017) 53, <https://doi.org/10.1186/s11671-016-1806-x>.
- [24] G. Żyła, Nanofluids containing low fraction of carbon black nanoparticles in ethylene glycol: an experimental study on their rheological properties, *J. Mol. Liq.* 297 (2020), 111732, <https://doi.org/10.1016/j.molliq.2019.111732>.
- [25] M.B. Moghaddam, E.K. Goharshadi, M.H. Entezari, P. Nancarrow, Preparation, characterization, and rheological properties of graphene–glycerol nanofluids, *Chem. Eng. J.* 231 (2013) 365–372, <https://doi.org/10.1016/j.cej.2013.07.006>.
- [26] W.S. Sarsam, A. Amiri, S.N. Kazi, A. Badarudin, Stability and thermophysical properties of non-covalently functionalized graphene nanoplatelets nanofluids, *Energy Convers. Manag.* 116 (2016) 101–111, <https://doi.org/10.1016/j.enconman.2016.02.082>.
- [27] C. Selvam, D. Mohan Lal, S. Harish, Enhanced heat transfer performance of an automobile radiator with graphene based suspensions, *Appl. Therm. Eng.* 123 (2017) 50–60, <https://doi.org/10.1016/j.applthermaleng.2017.05.076>.
- [28] Y. Wang, H.A.I. Al-Saaidi, M. Kong, J.L. Alvarado, Thermophysical performance of graphene based aqueous nanofluids, *Int. J. Heat Mass Transf.* 119 (2018) 408–417, <https://doi.org/10.1016/j.ijheatmasstransfer.2017.11.019>.
- [29] J.P. Vallejo, G. Żyła, J. Fernández-Seara, L. Lugo, Rheological behaviour of functionalized graphene nanoplatelet nanofluids based on water and propylene glycol: water mixtures, *Int. Commun. Heat Mass Transf.* 99 (2018) 43–53, <https://doi.org/10.1016/j.icheatmasstransfer.2018.10.001>.
- [30] J. Vallejo, G. Żyła, J. Fernández-Seara, L. Lugo, Influence of six carbon-based nanomaterials on the rheological properties of nanofluids, *Nanomaterials* 9 (2019) 146, <https://doi.org/10.3390/nano9020146>.
- [31] J.P. Vallejo, J. Pérez-Tavernier, D. Cabaleiro, J. Fernández-Seara, L. Lugo, Potential heat transfer enhancement of functionalized graphene nanoplatelet dispersions in a propylene glycol–water mixture, *Thermophysical profile, J. Chem. Thermodyn.* 123 (2018) 174–184, <https://doi.org/10.1016/j.jct.2018.04.007>.
- [32] S. Hamze, N. Berrada, D. Cabaleiro, A. Desforges, J. Ghanbaja, J. Gleize, D. Bégin, F. Michaux, T. Maré, B. Vigolo, P. Estellé, Few-layer graphene-based nanofluids with enhanced thermal conductivity, *Nanomaterials* 10 (2020) 1258, <https://doi.org/10.3390/nano10071258>.
- [33] S. Hamze, D. Cabaleiro, D. Bégin, A. Desforges, T. Maré, B. Vigolo, L. Lugo, P. Estellé, Volumetric properties and surface tension of few-layer graphene nanofluids based on a commercial heat transfer fluid, *Energies* 13 (2020) 3462, <https://doi.org/10.3390/en13133462>.
- [34] S. Halelfadl, P. Estellé, B. Aladag, N. Doner, T. Maré, Viscosity of carbon nanotubes water-based nanofluids: influence of concentration and temperature, *Int. J. Therm. Sci.* 71 (2013) 111–117, <https://doi.org/10.1016/j.ijthermalsci.2013.04.013>.
- [35] J.V. Sengers, J.T.R. Watson, Improved international formulations for the viscosity and thermal conductivity of water substance, *J. Phys. Chem. Ref. Data* 15 (1986) 1291–1314, <https://doi.org/10.1063/1.555763>.
- [36] L.S. Tyfocor, Technical information, available at <https://tyfo.de/en/produkt/tyfocor-ls/>.
- [37] M. Pastoriza-Gallego, L. Lugo, J. Legido, M.M. Piñeiro, Rheological non-Newtonian behaviour of ethylene glycol-based Fe<sub>2</sub>O<sub>3</sub> nanofluids, *Nanoscale Res. Lett.* 6 (2011) 560, <https://doi.org/10.1186/1556-276X-6-560>.
- [38] S. Genc, B. Derin, Synthesis and rheology of ferrofluids: a review, *Curr. Opin. Chem. Eng.* 3 (2014) 118–124, <https://doi.org/10.1016/j.coche.2013.12.006>.
- [39] C. Hermida-Merino, M. Pérez-Rodríguez, M.M. Piñeiro, M.J. Pastoriza-Gallego, Evidence of viscoplastic behavior of exfoliated graphite nanofluids, *Soft Matter* 12 (2016) 2264–2275, <https://doi.org/10.1039/C5SM02932E>.
- [40] J.F. Douglas, *Fluid Mechanics*, 5th ed Pearson/Prentice Hall, Harlow, England; New York, 2006.
- [41] G.S. Fulcher, Analysis of recent measurements of the viscosity of glasses, *J. Am. Ceram. Soc.* 8 (1925) 339–355, <https://doi.org/10.1111/j.1151-2916.1925.tb16731.x>.
- [42] G. Tammann, W. Hesse, The dependence of viscosity upon the temperature of supercooled liquids, *Z. Anorg. Allg. Chem.* 156 (1926) 245–257, <https://doi.org/10.1002/ange.192601560016>.
- [43] H. Vogel, The law of the relation between the viscosity of liquids and the temperature, *Phys. Z.* 22 (1921) 645–646.
- [44] J.P. Vallejo, S. Gómez-Barreiro, D. Cabaleiro, C. Gracia-Fernández, J. Fernández-Seara, L. Lugo, Flow behaviour of suspensions of functionalized graphene nanoplatelets in propylene glycol–water mixtures, *Int. Commun. Heat Mass Transf.* 91 (2018) 150–157, <https://doi.org/10.1016/j.icheatmasstransfer.2017.12.001>.
- [45] P. Dhar, M.H.D. Ansari, S.S. Gupta, V.M. Siva, T. Pradeep, A. Pattamatta, S.K. Das, Percolation network dynamics and sheet dynamics governed viscous behavior of polydispersed graphene nanosheet suspensions, *J. Nanopart. Res.* 15 (2013) 2095, <https://doi.org/10.1007/s11051-013-2095-2>.
- [46] M. Mehrali, E. Sadeghinezhad, S. Latibari, S. Kazi, M. Mehrali, M.N.B.M. Zubir, H.S. Metselaar, Investigation of thermal conductivity and rheological properties of nanofluids containing graphene nanoplatelets, *Nanoscale Res. Lett.* 9 (2014) 15, <https://doi.org/10.1186/1556-276X-9-15>.
- [47] E. Sadeghinezhad, M. Mehrali, S. Tahan Latibari, M. Mehrali, S.N. Kazi, C.S. Oon, H.S.C. Metselaar, Experimental investigation of convective heat transfer using graphene nanoplatelet based nanofluids under turbulent flow conditions, *Ind. Eng. Chem. Res.* 53 (2014) 12455–12465, <https://doi.org/10.1021/ie501947u>.
- [48] M. Mehrali, E. Sadeghinezhad, M.A. Rosen, S. Tahan Latibari, M. Mehrali, H.S.C. Metselaar, S.N. Kazi, Effect of specific surface area on convective heat transfer of graphene nanoplatelet aqueous nanofluids, *Exp. Thermal Fluid Sci.* 68 (2015) 100–108, <https://doi.org/10.1016/j.expthermflusci.2015.03.012>.
- [49] M. Mehrali, E. Sadeghinezhad, M.A. Rosen, A.R. Akhiani, S. Tahan Latibari, M. Mehrali, H.S.C. Metselaar, Heat transfer and entropy generation for laminar forced convection flow of graphene nanoplatelets nanofluids in a horizontal tube, *Int. Commun. Heat Mass Transf.* 66 (2015) 23–31, <https://doi.org/10.1016/j.icheatmasstransfer.2015.05.007>.
- [50] M.R. Esfahani, E.M. Languri, M.R. Nunna, Effect of particle size and viscosity on thermal conductivity enhancement of graphene oxide nanofluid, *Int. Commun. Heat Mass Transf.* 76 (2016) 308–315, <https://doi.org/10.1016/j.icheatmasstransfer.2016.06.006>.
- [51] M. Hadadian, E.K. Goharshadi, A. Youssefi, Electrical conductivity, thermal conductivity, and rheological properties of graphene oxide-based nanofluids, *J. Nanopart. Res.* 16 (2014) 2788, <https://doi.org/10.1007/s11051-014-2788-1>.
- [52] A. Ijam, R. Saidur, P. Ganesan, A. Moradi Golshaiikh, Stability, thermo-physical properties, and electrical conductivity of graphene oxide-deionized water/ethylene glycol based nanofluid, *Int. J. Heat Mass Transf.* 87 (2015) 92–103, <https://doi.org/10.1016/j.ijheatmasstransfer.2015.02.060>.
- [53] M. Kole, T.K. Dey, Investigation of thermal conductivity, viscosity, and electrical conductivity of graphene based nanofluids, *J. Appl. Phys.* 113 (2013), 084307, <https://doi.org/10.1063/1.4793581>.
- [54] Materials Science & Technology Conference et al., Ed., *Processing and Properties of Advanced Ceramics and Composites V*, 2013.

## **IV.6- Conclusion**

The characterization of the thermophysical properties of the FLG based nanofluids studied allowed us to highlight the influence of the FLG volume fraction, the temperature, and the type and content of surfactant. The results show that:

- The nanofluids with Gum Arabic surfactant are more stable at rest than those with Pluronic® P-123, while nanofluids with Triton X-100 have the lowest stability at rest.
- The addition of FLG enhances the thermal conductivity of the base fluids. Maximum enhancement by 23.9%, 18.3% and 21.5% were found at the highest concentration (0.5 wt.%), independently on the temperature, with Triton X-100, Pluronic® P-123 and Gum Arabic, respectively. A comparison between the experimental thermal conductivity of the nanofluids and several theoretical models showed that the thermal conductivity enhancement of FLG-based nanofluids is governed by the thickness and size of the FLG nanosheets, their thermal resistance at the FLG interface and their flatness ratio.
- The isobaric heat capacity of nanofluids increases with the temperature rise and is independent on the surfactant and FLG concentration. The experimental values of isobaric heat capacity of base fluids and nanofluids were compared to the values calculated using the mixing theory obtaining a good agreement.
- The density decreases with the temperature rise and increases slightly with FLG content comparing to the base fluids. The evolution of the density of FLG-based nanofluids as a function of temperature and FLG content is well predicted by the weight-average density equation, taking into account the densities of all components.
- The isobaric thermal expansivity of the FLG based nanofluids increases with the temperature. It is independent on the content and type of surfactant used, except for the highest content of Pluronic® P-123 it increases slightly by about 1.4%.  $\alpha_p$  decreases after the addition of FLG.
- In comparison to the Tyfocor® LS fluid, the addition of surfactant decreases its surface tension unless in case of Gum Arabic that does not change it significantly. The surface tension of nanofluids is lower than that of Tyfocor in case of Triton X-100 and Pluronic P-123 surfactants and higher in case of Gum Arabic.

- For dynamic viscosity of nanofluids, the investigation shows that the temperature, the shearing, and the duration of shearing play an important role to possibly destabilize the nanofluids in function of their surfactant and content. Nanofluids with Pluronic® P-123 are more stable under shearing than the two other series. The addition of the highest concentration of FLG (0.5 wt.%) increases the viscosity of Tyfocor® LS fluid up to 19.9%, 34.5% and 121.6 % in case of Pluronic® P-123, Triton X-100 and Gum Arabic at 283.15, 283.15 and 303.15 K, respectively. The evolution of dynamic viscosity with temperature for the stable nanofluids under shear was well predicted by the Vogel-Fulcher-Tammann (VFT) viscosity model.

After the full thermophysical characterization of the FLG based nanofluids, the next step consists in the evaluation of their potential thermal performance as heat transfer fluids using a qualitative approach. This is the aim of the next chapter. Based on the reported results, this will only concern the nanofluids that have been demonstrated to be stable under shear.



# **Chapter V- Thermal performance of stable FLG nanofluids: qualitative approach**

V.1- Introduction.....	180
V.2- Laminar regime.....	180
V.3- Turbulent regime.....	186
V.4- Conclusion.....	191
V.5- References.....	192

## **V.1- Introduction**

In forced convection processes, the heat transfer performance of fluid can only be tested in an actual installation equipped with a heat exchanger, which is used to induce the thermal energy transfer between two media separated by a heat exchange surface [1,2]. Heat exchangers are used in many daily activities, both domestic and industrial. Sectors such as refrigeration, power generation, transport or food processing, petroleum manufacturing, and day-to-day procedures such as air conditioning, driving a car or refrigerating food in the refrigerator are just a few examples [3]. So, nanofluids seem attractive if we only consider their remarkable thermal conductivity. The thermal performance of the nanofluid can be improved by the addition of nanoparticles, but on the other hand, this addition can lead to an unfavorable increase in hydrodynamic properties.

In this chapter, a qualitative approach is used to evaluate the potential thermal performance of the studied FLG nanofluids that were stable under shearing, as discussed in the previous chapter. Such an approach theoretically provides, without using a heat exchanger, the limits of nanofluids use according to the flow regime (laminar or turbulent). This approach is based on the thermophysical properties values of the nanofluids [4,5] that were previously reported in chapter IV. However, in this approach, the possible rearrangement of flowing nanoparticles in a heat exchanger is not taking into account. A relation between hydrodynamic and thermal properties exists, depending on the flow regime, laminar or turbulent. A part of this theoretical approach was presented in chapter II and it is recalled. Some other relationships about pumping power consumption increase are presented and used.

## **V.2- Laminar regime**

According to the literature [4,5], only nanofluids satisfying equation V.1 can be potentially used as heat transfer fluids under steady-state laminar flow conditions.

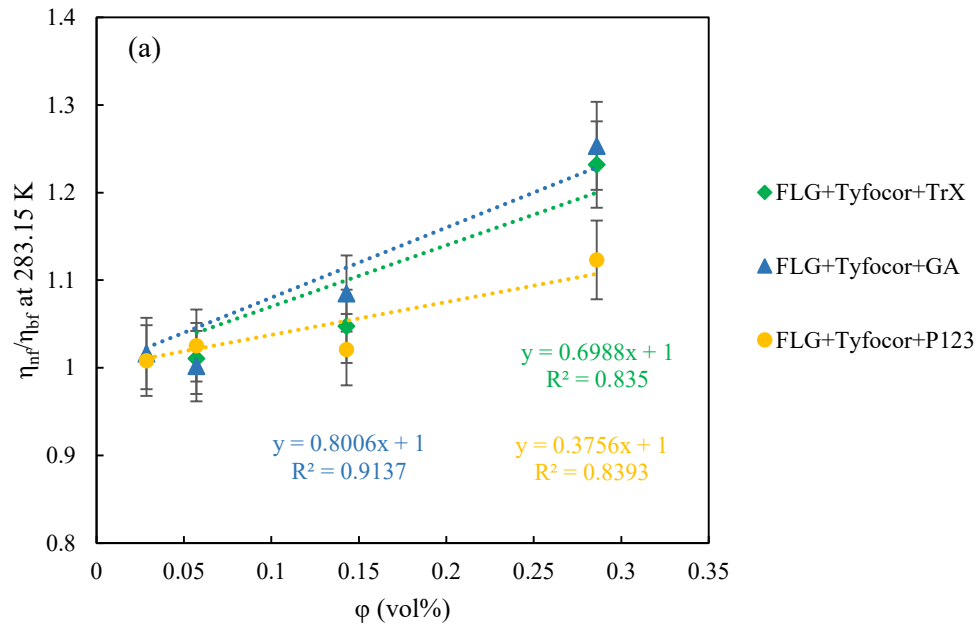
$$\frac{C_{\eta}}{C_k} < 4 \quad \text{Eq.V.1}$$

where  $C_{\eta}$  and  $C_k$  are the coefficients of the dynamic viscosity and thermal conductivity improvements of the nanofluids with volume concentrations, respectively.

$$\frac{\eta_{nf}}{\eta_{bf}} \approx 1 + C_{\eta} \phi_v \quad \text{Eq.V.2}$$

$$\frac{k_{nf}}{k_{bf}} \approx 1 + C_k \phi_v \quad \text{Eq.V.3}$$

These coefficients can be determined from the previous empirical simplified relationships that predicts a linear evolution of the experimental results for the relative dynamic viscosity (Eq.V.2) and the relative thermal conductivity (Eq.V.3) as a function of the nanoparticles volume fraction [4–6]. An example at 283.15 K is shown in Figure V.1.



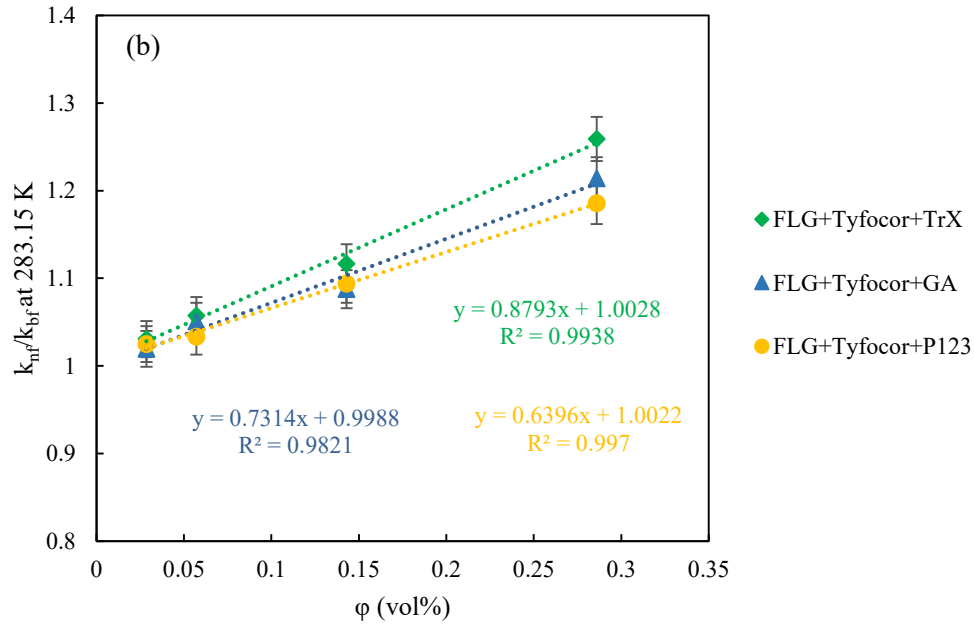


**Figure V.1.** Relative viscosity (a) and relative thermal conductivity (b) as a function of volume concentration of the nanofluids with Triton X-100, Pluronic® P-123 and Gum Arabic at 283.15 K. The dashed lines represent the equations Eq.V.2 (a) and Eq.V.3 (b).

These empirical models are valid regardless of the size, shape and dispersion state of the nanoparticles in the base fluid [4,5].

The two coefficients,  $C_\eta$  and  $C_k$ , of all stable studied nanofluids with Triton X-100, Pluronic® P-123, and Gum arabic were determined at all tested temperatures between 283.15 and 323.15 K.  $C_\eta$  was determined at two different shear rates: the first one,  $30 \text{ s}^{-1}$ , that corresponds to the region where the shear-thinning or shear-thickening behavior can be pronounced for non-Newtonian nanofluids, and in the range  $200\text{-}1000 \text{ s}^{-1}$  where the dynamic viscosity is constant that corresponds to the Newtonian region for all tested nanofluids. The results of the ratio  $C_\eta/C_k$  and the corresponding Reynolds numbers are shown in Table V.1. It should be noted here that, at a constant temperature, the values of  $C_\eta$  are only evaluated when dynamic viscosity values for stable nanofluids are available for at least three concentrations (see Figure V.1.a).

**Table V.1.** The ratio of viscosity enhancement coefficient to thermal conductivity enhancement coefficient of nanofluids with Triton X-100, Pluronic® P-123 and Gum Arabic, and the corresponding Reynolds numbers at different temperatures and shear rates.

	Temperature (K)				
	283.15	293.15	303.15	313.15	323.15
<i>FLG nanofluids based on Tyfocor® LS and Triton X-100</i>					
$C_\eta/C_k$ at 30 s <sup>-1</sup>	0.81	-	-	-	-
Re at 30 s <sup>-1</sup>	20-25	-	-	-	-
$C_\eta/C_k$ at 200-1000 s <sup>-1</sup>	0.78	-	-	-	-
Re at 200-1000 s <sup>-1</sup>	20-127	-	-	-	-
<i>FLG nanofluids based on Tyfocor® LS and Pluronic® P-123</i>					
$C_\eta/C_k$ at 30 s <sup>-1</sup>	0.80	-	-	-	0.35
Re at 30 s <sup>-1</sup>	22-26	-	-	-	87-112
$C_\eta/C_k$ at 200-1000 s <sup>-1</sup>	0.58	0.53	0.31	0.51	0.31
Re at 200-1000 s <sup>-1</sup>	22-133	36-213	53-324	70-430	89-542
<i>FLG nanofluids based on Tyfocor® LS and Gum Arabic</i>					
$C_\eta/C_k$ at 30 s <sup>-1</sup>	1.15	-	-	-	-
Re at 30 s <sup>-1</sup>	15-26	-	-	-	-
$C_\eta/C_k$ at 200-1000 s <sup>-1</sup>	1.10	1.64	2.97	0.69	-
Re at 200-1000 s <sup>-1</sup>	17-129	25-202	27-302	65-406	-

The results show that Eq.V.1 is always verified, which mean that all nanofluids are potentially good candidates to be used in heat exchangers, especially those with Pluronic® P-123 that have the lowest ratio values. These results correspond to a Reynolds number between 15 and 542, which has been evaluated using Eq.V.4 for cone-plate geometry [7].

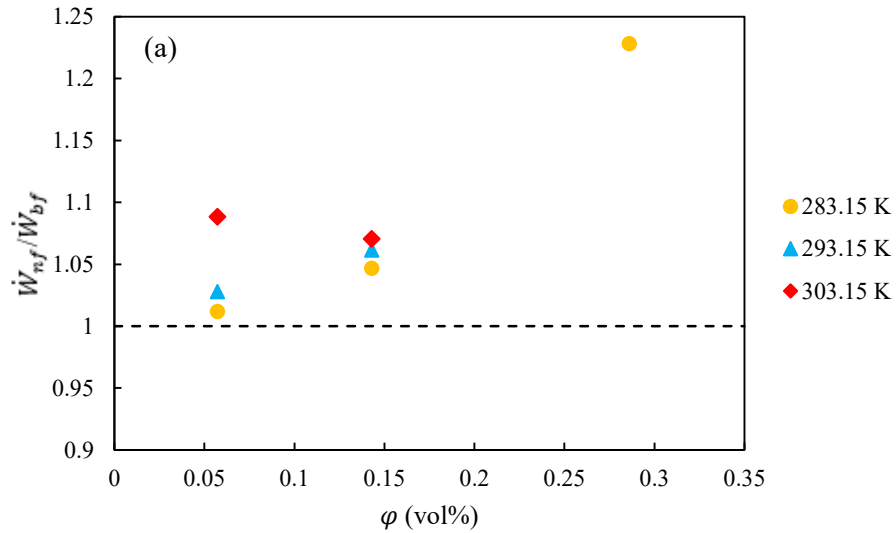
$$Re \approx \frac{\dot{\gamma} \rho_{nf}}{\eta_{nf}} \left( \frac{\pi R \alpha}{180} \right)^2 \quad \text{Eq.V.4}$$

where  $\dot{\gamma}$  is the shear rate (in s<sup>-1</sup>),  $\rho_{nf}$  is the density of nanofluids (in kg.m<sup>-3</sup>),  $\eta_{nf}$  is the viscosity of nanofluid (in Pa.s),  $R$  is the cone and plate diameter (in m) and  $\alpha$  is the cone angle (in °).

Obtaining Reynolds number values up to 542 following the shear rate, the temperature and the volume concentration means that all rheological measurements are well carried out under laminar flow regime.

To predict the magnitude of the expected pumping power consumption increase derived from the nanofluids use in forced convection processes through a tube where the heat flux is uniform at the wall, the following expression (Eq.V.5) has been proposed in the literature for laminar flow [8]:

$$\left[ \frac{\dot{W}_{nf}}{\dot{W}_{bf}} \right]_{laminar\ flow} = \frac{\eta_{nf}}{\eta_{bf}} \cdot \left( \frac{\rho_{bf}}{\rho_{nf}} \right)^2 \quad Eq.V.5$$



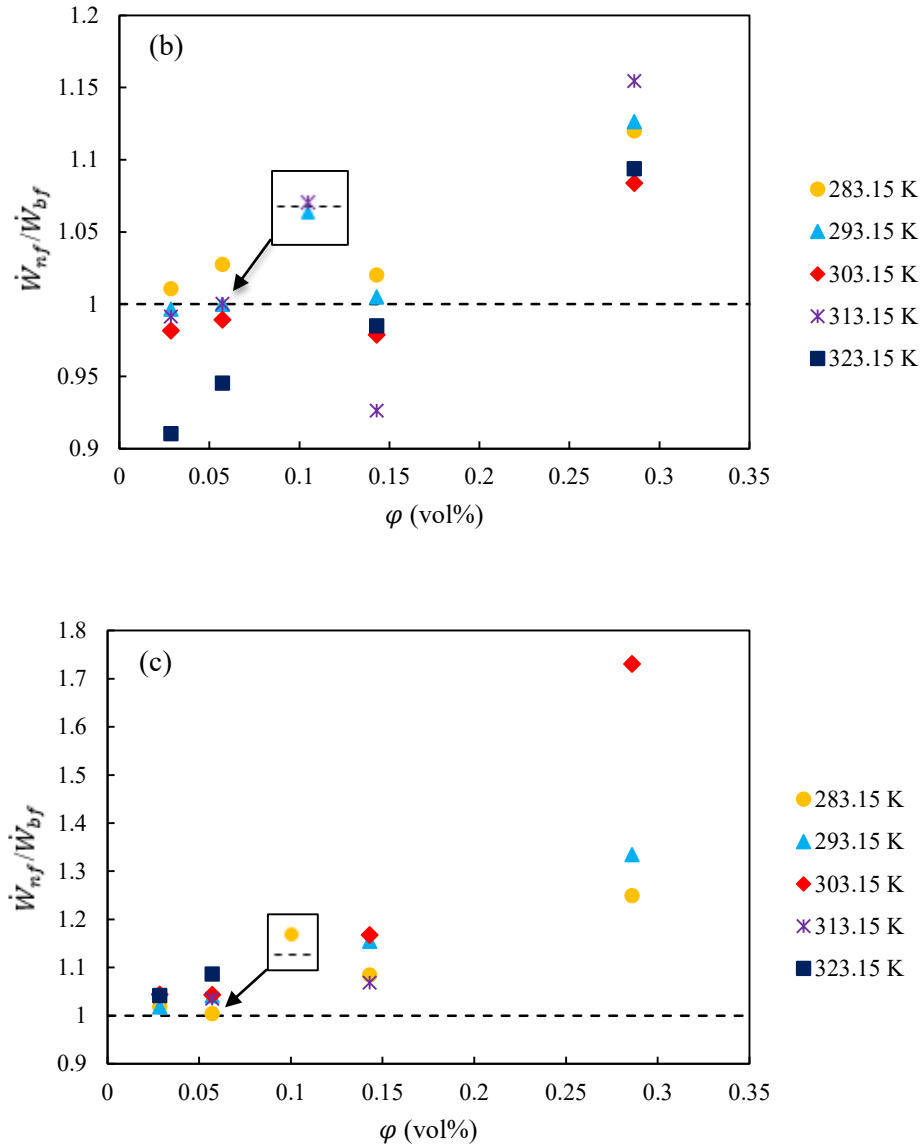


**Figure V.2.** Pumping power consumptions of FLG based nanofluids with Triton X-100 (a), Pluronic® P-123 (b) and Gum arabic (c) between 283.15 and 323.15 K in laminar regime.

Considering the pumping power consumption, lower values are preferable. It is shown in Figure V.2 that the increase in FLG loading enhances the pumping power consumption of the fluid as both the nanofluids viscosity and density increases with FLG content. The relative pumping power values were obtained in the range 1.01-1.23, 0.91-1.15 and 1.00-1.73 for nanofluids with Triton X-100, Pluronic® P-123 and Gum arabic, respectively. So the results of pumping power increase show that the FLG based nanofluids with Pluronic® P-123 as surfactant have the lowest values. A

maximum enhancement rate by 15.4% was found for the highest concentration of this series at 313.15 K. These results, with those obtained for  $C_\eta/C_k$  ratio showed that the series of nanofluids produced with Pluronic® P-123 is the best one for potential heat transfer exchanger application under laminar flow.

### V.3- Turbulent regime

The nanofluids heat transfer rate, under turbulent flow regime, depends on the overall of thermo-physical properties of the fluid (density, thermal conductivity, isobaric heat capacity and viscosity), and can be assessed from the Mouromtseff number,  $Mo$  [5,9,10]. This number is a figure of merit (FOM) widely used for comparing the capacity of a fluid as a working liquid in a heat transfer process [5,9,11,12].  $Mo$  of single-phase fluids in internal turbulent flows fully developed is defined according to the following equations, Eq.V.6 defined by Dittus–Boelter equation [13] for base fluids, and Pak and Cho equation [14], Eq.V.7, for nanofluids.

$$Mo_{bf} = \frac{\rho^{0.8} k^{0.6} C_p^{0.4}}{\eta^{0.4}} \quad \text{Eq.V.6}$$

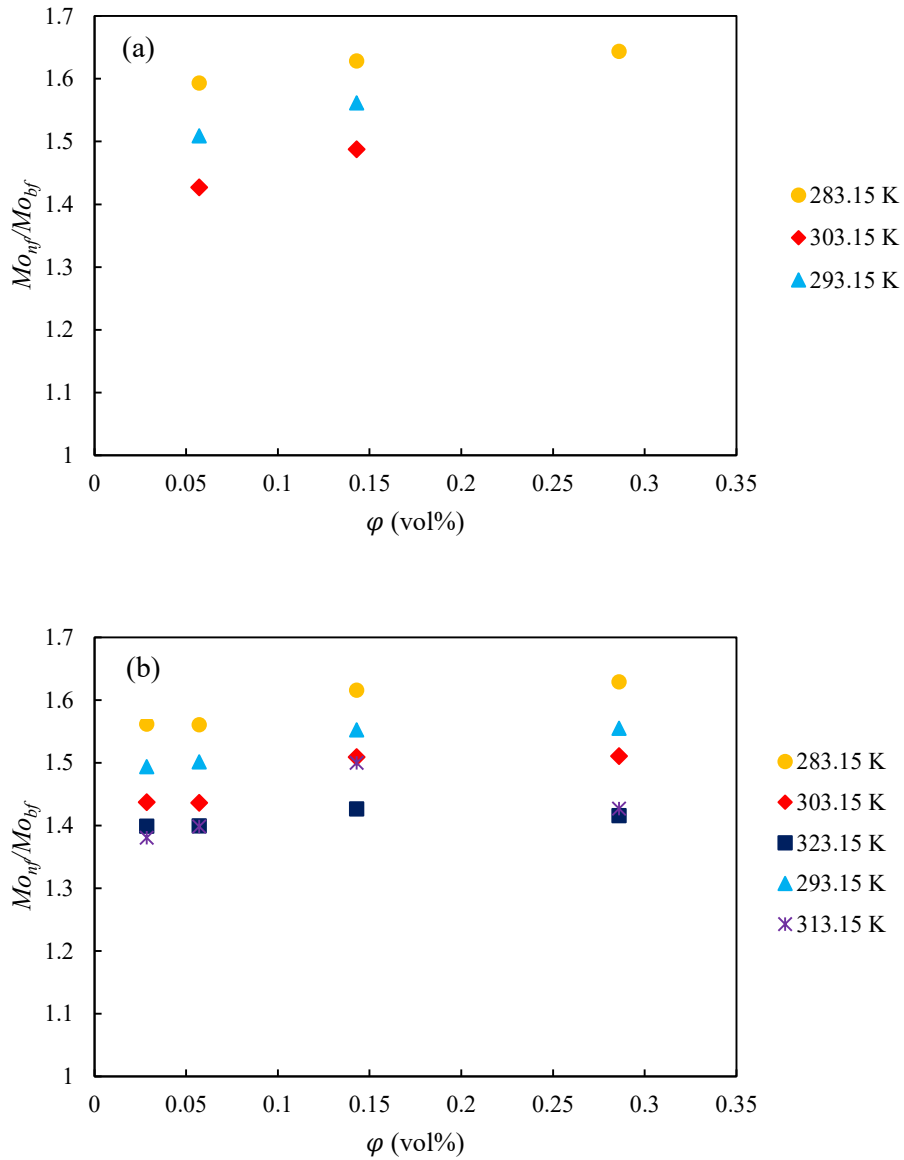
$$Mo_{nf} = \frac{\rho^{0.8} k^{0.5} C_p^{0.5}}{\eta^{0.3}} \quad \text{Eq.V.7}$$

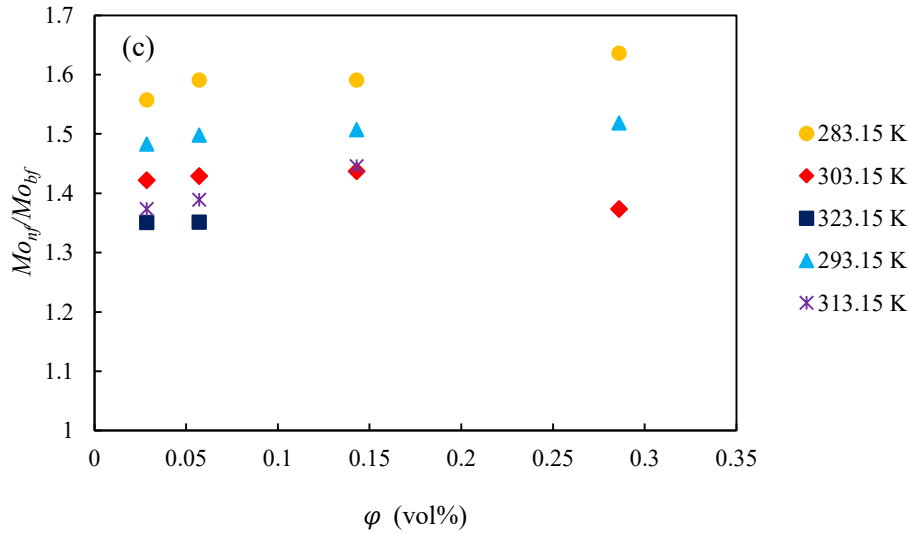
where  $\rho$  is the density (in  $\text{kg.m}^{-3}$ ),  $k$  is the thermal conductivity (in  $\text{W.m}^{-1}.\text{K}^{-1}$ ),  $C_p$  is the isobaric heat capacity (in  $\text{J.kg}^{-1}.\text{K}^{-1}$ ) and  $\eta$  is the dynamic viscosity (in  $\text{Pa.s}$ ) of the nanofluid. As the rheological measurements have been carried out in laminar regime, the dynamic viscosity value of base fluids and nanofluids within the Newtonian plateau has been considered in Eq.V.6 and Eq.V.7 respectively. It is assumed that dynamic viscosity value is not changed in turbulent flow.

Here, it is assumed that the ratio  $Mo_{nf}/Mo_{bf}$  is equivalent to the heat transfer improvement ratio. Compared to the base fluid, the nanofluid is considered advantageous if the condition of Eq.V.8 is verified [5,9].

$$\frac{Mo_{nf}}{Mo_{bf}} > 1 \quad \text{Eq.V.8}$$

This ratio for FLG based nanofluids with Triton X-100, Pluronic® P-123 and Gum arabic in the temperature range 283.15-323.15 K is shown in Figure V.3.





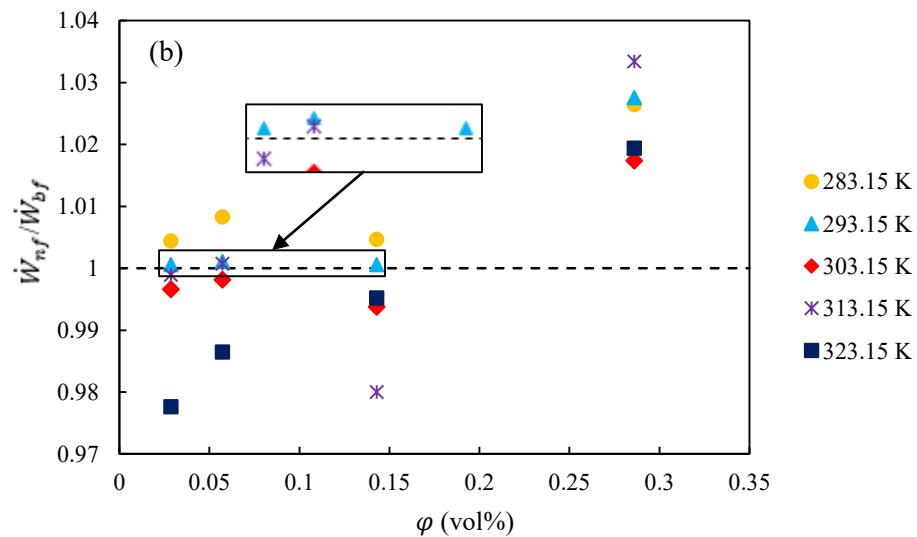
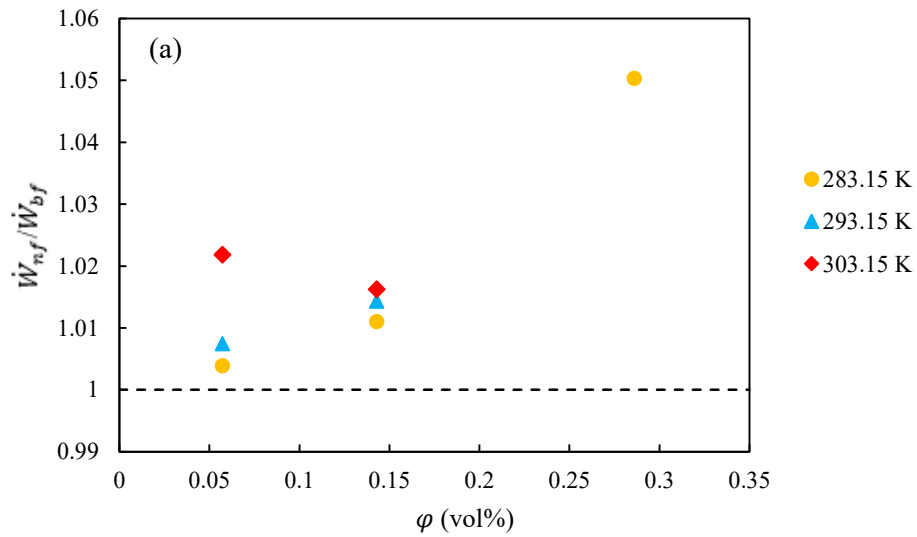
**Figure V.3.** Enhancements of Mouromtseff number of FLG based nanofluids with Triton X-100 (a), Pluronic® P-123 (b) and Gum arabic (c) between 283.15 and 323.15 K.

Figure V.3 shows that the heat transfer enhancement ratio  $Mo_{nf}/Mo_{bf}$  is higher than one for all nanofluids. The criteria of the Eq.V.8 is verified for all these nanofluids. Consequently, they appear as good candidates to be used in a real heat exchanger instead of Tyfocor® LS fluid alone. In addition, we can see in the above figures that this ratio increases with the FLG content and decreases with temperature rise. For example in case of nanofluids with Triton X-100 (see Figure V.3.a), the nanofluid with the highest volume concentration 0.286 % (0.5 % in weight) at 283.15 K is the best candidate in heat transfer performance under turbulent flow. Regarding Pluronic® P-123 (see Figure V.3.b) and Gum Arabic (see Figure V.3.c), the best nanofluid corresponds also to the same concentration and temperature. The enhancement rates with this nanofluid at this temperature are equal to 64.4%, 62.9% and 63.6% with Triton X-100, Pluronic® P-123 and Gum Arabic, respectively. Considering all temperatures, nanofluids with Pluronic® P-123 have approximately the highest heat transfer enhancement values. This makes them the best candidates especially the highest concentration 0.286 vol.% (0.5 wt.%) where the enhancement rate is between 41.6% and 62.9%. Unless at 313.15 K, the best nanofluid is that with the volume concentration 0.143% (0.25 wt.%), and the increase in the  $Mo_{nf}/Mo_{bf}$  ratio is about 50%.

For the prediction of the magnitude of the pumping power consumption increase expected derived from the use of nanofluids for fully developed turbulent flow, the following equation (Eq.V.9) has been proposed from the literature [8]:

$$\left[ \frac{\dot{W}_{nf}}{\dot{W}_{bf}} \right]_{turbulent\ flow} = \left( \frac{\eta_{nf}}{\eta_{bf}} \right)^{0.25} \cdot \left( \frac{\rho_{bf}}{\rho_{nf}} \right)^2 \quad Eq.V.9$$

The results are shown in the following figures (Figure V.4) as a function of FLG concentration and temperature.



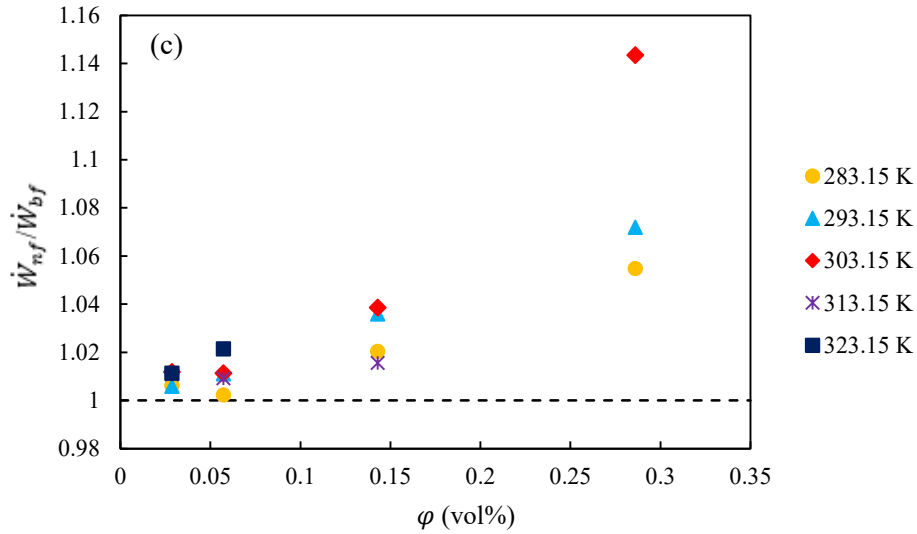


**Figure V.4.** Pumping power consumptions of FLG based nanofluids with Triton X-100 (a), Pluronic® P-123 (b) and Gum arabic (c) between 283.15 and 323.15 K in turbulent regime.

For the results of pumping power consumptions, we can see that the ratio  $\dot{W}_{nf}/\dot{W}_{bf}$  increases with the FLG content. The values were obtained in the range 1.00-1.05, 0.98-1.03 and 1.00-1.14 for nanofluids with Triton X-100, Pluronic® P-123 and Gum arabic, respectively. The lowest ratio values of all concentrations and at all tested temperatures are obtained with FLG based nanofluids containing Pluronic® P-123 as a surfactant. For this series, the highest increase in pumping power consumption is 3.3%, which was obtained for the highest concentration at 313.15 K. So these results, in addition to the results of the heat transfer enhancement ratio  $Mo_{nf}/Mo_{bf}$ , showed that the best candidates for heat transfer exchanger application are the nanofluids with Pluronic® P-123, especially with higher concentrations. If we want to compare the two highest concentrations of FLG based nanofluids with Pluronic® P-123, the results of  $Mo_{nf}/Mo_{bf}$  ratio are close together (the enhancement for 0.143 vol.% nanofluid is between 42.6% and 61.6%), but in case of  $\dot{W}_{nf}/\dot{W}_{bf}$ , the ratio is lower for 0.143 vol.% (0.25 wt.%) (maximum increase is 0.5% at 283.15 K). So based on this comparison, the nanofluid with this concentration and this surfactant presents the most promising prospects for its utilization practical situation.

The heat transfer performance of graphene-based nanofluids under turbulent flow was also previously studied in the literature using this qualitative approach. A lower heat transfer performance and higher pumping power consumption were obtained comparing to our results. For

example, Vallejo *et al.* [12] investigated functionalized graphene nanoplatelets dispersed in propylene glycol:water mixture with a ratio of 30:70% in mass. They prepared nanofluids in the weight concentration range 0.25-1% and evaluated their thermophysical properties between 293.15 and 323.15 K. The best nanofluid was the one with 0.25 wt.% where the  $Mo_{nf}/Mo_{bf}$  ratio values were obtained between 16% and 36% and the pumping power rises was found in the range 3.4%-9.0%. In addition, a graphene nanofluids based on a commercial industrial antifreeze, Havoline® XLC Premixed 50/50, with different concentrations up to 1 wt.% were also investigated by Vallejo *et al.* [15] between 293.15 and 343.15 K using sodium dodecylbenzene sulfonate as a surfactant. The nanofluid with weight concentration of 0.75% was found the most favorable one under turbulent flow as it showed a conspicuous heat transfer enhancement of about 45%, while the pumping power increase only reached 0.41% at 293.15 K. The better heat transfer performance and lower pumping power consumption found in our study can be explained by the higher thermal conductivities of nanofluids comparing to the two previous studies, and lower nanofluids viscosities comparing to the values obtained by Vallejo *et al.* [12]. This difference could be due to the better dispersion state of FLG in the base fluid and/or to the high quality of FLG obtained from their original method of synthesis.

## **V.4- Conclusion**

A theoretical approach was used to assess, as a preliminary step, the benefits provided by FLG nanofluids in comparison to Tyfocor® LS. This approach can be used to predict experimental conditions and particle contents that would tend towards a favorable energy balance [9] and identify the nanofluids that could be tested in real heat exchange condition.

As a conclusion, the study of heat transfer performance of FLG nanofluids based on Tyfocor® LS with the use of Triton X-100, Pluronic® P-123, and Gum Arabic as surfactants showed that the series of Pluronic® P-123 is the best one for possible use in a heat exchanger between 283.15 and 323.15 K, especially the volume concentration 0.143% which correspond to the mass content 0.25%, under both laminar and turbulent flow.

## V.5- References

1. K. Thulukkanam, Heat exchanger design handbook, CRC Press, Boca Raton, FL, USA, 2013.
2. *Heat Exchangers - Design, Experiment and Simulation*; Murshed, S.M.S., Lopes, M.M., Eds.; InTech, 2017; ISBN 978-953-51-3093-2.
3. Vallejo, J. P. Design, characterization and heat transfer performance evaluation of carbon-based nanofluids for renewable energy applications, Universida de Vigo, 2019.
4. Prasher, R.; Song, D.; Wang, J.; Phelan, P. Measurements of nanofluid viscosity and its implications for thermal applications. *Appl. Phys. Lett.* **2006**, *89*, 133108, doi:10.1063/1.2356113.
5. Timofeeva, E.V.; Routbort, J.L.; Singh, D. Particle shape effects on thermophysical properties of alumina nanofluids. *Journal of Applied Physics* **2009**, *106*, 014304, doi:10.1063/1.3155999.
6. Chen, L.; Xie, H.; Li, Y.; Yu, W. Nanofluids containing carbon nanotubes treated by mechanochemical reaction. *Thermochimica Acta* **2008**, *477*, 21–24, doi:10.1016/j.tca.2008.08.001.
7. J.W. Goodwin, R.W. Hughes, Rheology for Chemists: An Introduction, Royal Society of Chemistry Publishing, 2008. 264 p.
8. Mansour, R.B.; Galanis, N.; Nguyen, C.T. Effect of uncertainties in physical properties on forced convection heat transfer with nanofluids. *Applied Thermal Engineering* **2007**, *27*, 240–249, doi:10.1016/j.applthermaleng.2006.04.011.
9. Halefadi, S.; Maré, T.; Estellé, P. Efficiency of carbon nanotubes water based nanofluids as coolants. *Experimental Thermal and Fluid Science* **2014**, *53*, 104–110, doi:10.1016/j.expthermflusci.2013.11.010.
10. Mouromtseff, I.E. Water and Forced-Air Cooling of Vacuum Tubes Nonelectronic Problems in Electronic Tubes. *Proc. IRE* **1942**, *30*, 190–205, doi:10.1109/JRPROC.1942.234654.
11. Cabaleiro, D.; Colla, L.; Agresti, F.; Lugo, L.; Fedele, L. Transport properties and heat transfer coefficients of ZnO/(ethylene glycol + water) nanofluids. *International Journal of Heat and Mass Transfer* **2015**, *89*, 433–443, doi:10.1016/j.ijheatmasstransfer.2015.05.067.
12. Vallejo, J.P.; Pérez-Tavernier, J.; Cabaleiro, D.; Fernández-Seara, J.; Lugo, L. Potential heat transfer enhancement of functionalized graphene nanoplatelet dispersions in a propylene glycol-water mixture. Thermophysical profile. *The Journal of Chemical Thermodynamics* **2018**, *123*, 174–184, doi:10.1016/j.jct.2018.04.007.
13. Dittus, F.W.; Boelter, L.M.K. Heat transfer in automobile radiators of the tubular type. *International Communications in Heat and Mass Transfer* **1985**, *12*, 3–22, doi:10.1016/0735-1933(85)90003-X.
14. American Society of Heating, Refrigerating and Air-conditioning Engineers, ASHRAE Handbook Fundamentals, Atlanta, GA, 2009.
15. Vallejo, J.P.; Álvarez-Regueiro, E.; Cabaleiro, D.; Fernández-Seara, J.; Fernández, J.; Lugo, L. Functionalized graphene nanoplatelet nanofluids based on a commercial industrial antifreeze for the thermal performance enhancement of wind turbines. *Applied Thermal Engineering* **2019**, *152*, 113–125, doi:10.1016/j.applthermaleng.2019.02.046.

# **Chapter VI - General conclusion and perspectives**

### ***General conclusion***

The main objectives of this PhD thesis were the development of graphene-based nanofluids, including the characterization of graphene and the evaluation of their stability, and the full experimental investigation of their thermal and hydrodynamic properties in view of their possible applications in heat and energy systems. This study allowed us to quantify and analyze the effects of different parameters that can influence the stability and the thermophysical properties of nanofluids based on graphene, i.e. graphene concentration, temperature, type and concentration of surfactant, and shear rate (for rheological behavior). The study was divided into five main chapters, the main conclusions are as follows:

The first chapter presented the general context and the objectives of this study. The second one gave a bibliographical overview of the design of nanofluids based on graphene and the literature background concerning the characterization of their thermo-physical properties and their use as a heat transfer fluid in thermal systems. This literature review has enabled us to highlight the main parameters affecting the properties of graphene-based nanofluids. Better control of graphene production and structural quality is particularly needed and the thermophysical properties of nanofluids must be rigorously evaluated in view of their applications in heat systems.

The materials and experimental methods, in particular for the graphene production, its characterization and stability evaluation in the base fluid, of all the performed measurements were presented in chapter III. The results about dispersion state and stability coupled to shear flow and the thermo-physical properties are presented in the next chapter including thermal conductivity, isobaric heat capacity, dynamic viscosity, density, isobaric thermal expansivity and surface tension, in the form of published articles. Such a comprehensive characterization was performed for graphene concentration of 0.05, 0.1, 0.25 and 0.5 wt.% and temperature varying between 283.15 and 323.15 K.

First of all, it was shown that the liquid exfoliation method of graphite assisted with mechanical stirring and tannic acid allows producing few-layer graphene of really high quality and controlled size. Then, it was demonstrated that the nanofluids presently studied, produced with a commercial heat transfer fluid, Tyfocor® LS, and different nonionic surfactants, Triton X-100, Pluronic® P-123 and Gum Arabic, respectively, are relatively stable at rest at ambient condition. For the thermal conductivity, a significant enhancement up to 23.9%, 18.3% and 21.5%, independent on the

temperature, was found at the highest concentrations of nanofluids with Triton X-100, Pluronic® P-123 and Gum Arabic, respectively. The thermal conductivity of the nanofluids was compared to several theoretical models demonstrating that the thermal conductivity enhancement of FLG-based nanofluids is governed by the size and thickness of the FLG nanosheets, their flatness ratio and thermal resistance at the FLG interface.

The isobaric heat capacity of nanofluids was found to be independent on FLG concentration and surfactant, not significantly different than the isobaric heat capacity of the Tyfocor® LS, and in increasing with the temperature rise. Consequently, thermal properties enhancement for the nanofluids in view of possible applications could only be attributed to thermal conductivity.

The density of nanofluids was found to decrease with temperature rise and slightly increase with FLG loading in comparison to the base fluids. Its evolution with the graphene content and temperature is well predicted by the weight-average equation for density taking into consideration all components densities.

The isobaric thermal expansivity of nanofluids, evaluated from the experimental results of density, was found to decrease with temperature rise, similarly for all base fluids without any effect of the surfactant used, and to decrease with the presence of FLG.

The surface tension of nanofluids was found more sensitive to surfactant type and its loading in relation to their adsorption phenomenon or critical micelle concentration in the base fluid. It evolved differently following the FLG concentration and the surfactant used. Thus the surface tension of base fluids could decrease or be not modified following the surfactant, and the FLG addition can induce an increase in surface tension of nanofluids or do not strongly modify it.

For dynamic viscosity investigation of nanofluids, different methods of measurements have shown that the stability under shear of nanofluids depends on the shearing condition, the duration of shearing, and the temperature as well as the type of surfactant and its content. In addition, it was shown that the shear flow behavior of nanofluids also varied with the same parameters and can be related to the visual aspect of the nanofluids after shear. Finally, the evolution of dynamic viscosity of stable nanofluids with temperature was well predicted by the Vogel-Fulcher-Tammann (VFT) viscosity model.

Finally, in the last part, a qualitative approach was used to evaluate the potential of stable nanofluids to be used in a heat exchanger.

From all the obtained results, the best promising FLG based nanofluid to be used in energy systems for the temperature range considered is prepared with an FLG weight concentration of 0.25 wt.% and Pluronic® P-123 as a surfactant. The results of the surface tension also confirm this choice as nanofluids with Pluronic® P-123 has the lowest surface tensions compared to Tyfocor® LS.

Generally, the choice of the best sample would depend largely on the type of application. The results showed that all samples have a good thermal performance in the tested temperature range, especially the nanofluids with Pluronic® P-123. The best thing would be to experimentally evaluate the thermal performance of the nanofluid in the exact thermal facility (the best sample for one facility could not be the best for another).

Certainly, nanofluid temporal stability is a major concern when it comes to practical implementation. When the material is at rest, nanoparticles tend to settle and so the enhance in thermal conductivity disappears. Unfortunately, that is a disadvantage that most nanofluids have. If there is a pumping system, the sedimentation would be less remarkable.

It is true that, in general, heat transfer performance and pumping power/pressure drop do not strongly depend on the surface tension (when compared with other properties such as thermal conductivity, viscosity, density and isobaric heat capacity). However, surface tension may also play an important role when the nanofluid undergoes a phase change (if it works in a boiler, for instance, surface tension controls the formation of bubbles) or when working in a facility in which the diameter of the pipes is really small (capillarity systems, capillary forces may become much more important than gravitational or viscous forces).

### ***Perspectives***

As a continuation of this work, it would be relevant to study the thermal performance of the selected nanofluid(s) using a quantitative approach, e.g. performing experiments in a heat exchanger and investigate its performance in a real situation. This will also confirm the potential heat transfer of this nanofluid and will give an overview of its stability in the real system, due to high nanofluid content involved in this kind of devices. Such a study was initially planned in the last months of the PhD, but the sanitary situation due to Covid-19 did not allow it. Note that a

double-pipe heat exchanger experimental setup has been yet developed in that direction, as shown in Figure VI.1.

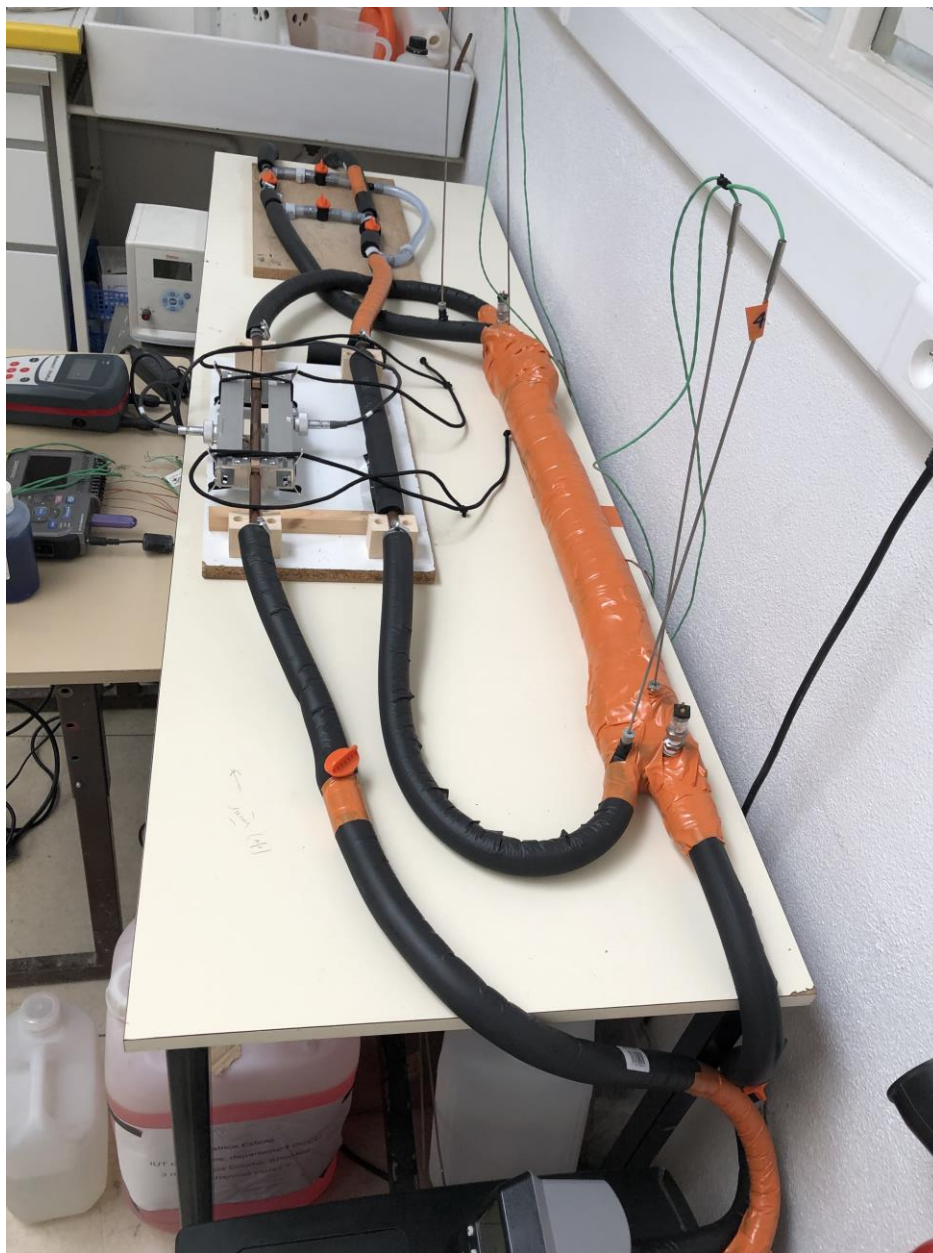


**Figure VI.1.** Photo of the double-pipe heat exchanger.

Also, regarding the stability of nanofluids, different actions could be performed:

- Tyfocor® LS, that is a commercial heat transfer fluid used here as base fluid contains some corrosion and ageing agents. It will be interesting to determine their nature and evaluate their influence on the stability of nanofluids.

- In the same way, develop similar nanofluids replacing this base fluid by a mixture of pure compounds of propylene glycol and water with the same weight ratio (40:60)% could help in this direction.
- In addition, a study of the interactions between few-layer graphene and both surfactants and base fluid could be realized.

Of course, the high-quality few-layer graphene investigated and used in this work can be employed to produce nanofluids with different base fluids and/or surfactants, and the present study could be extended to a wider range of temperatures.

Finally, the wide experimental database of thermophysical properties of nanofluids produced in this work can be used for numerical investigations in different configurations.

# Appendix

# TYFOCOR<sup>®</sup> LS<sup>®</sup>

**Frost Protection -28 °C**

Ready-to-Use Heat Transfer Fluid for  
Solar Thermal Systems with High Thermal Loads



TYFOROP Chemie GmbH

## Characteristics of TYFOCOR® LS®

Appearance	clear, red-fluorescent liquid	
Boiling point	102–105 °C	ASTM D 1120
Frost protection	–28 °C	ASTM D 1177
Density (20 °C)	1.032–1.035 g/cm <sup>3</sup>	DIN 51757
Viscosity (20 °C)	4.5–5.5 mm <sup>2</sup> /s	DIN 51562
Refraction nD20	1.380–1.384	DIN 51423
pH value (20 °C)	9.0–10.5	ASTM D 1287
Water content	55–58 %	DIN 51777
Flash point	none	DIN 51758
Reserve alkalinity	> 12 ml 0.1 m HCl	ASTM D 1121

The above data represent average values that were valid when this Technical Information Bulletin went into print. They do not have the status of a product specification. Specified values are the subject of a special leaflet.

## Properties

**TYFOCOR® LS®** is a liquid based on an aqueous solution of physiologically unobjectionable propylene glycol with a faint odour. The fluid was developed especially for use in solar thermal systems with high thermal loads (vacuum tube collectors).

The corrosion inhibitors contained in the product reliably protect the metals normally used in solar technology even in mixed installations against corrosion, ageing and deposits over long periods of time. It keeps the surfaces of heat exchangers clean, and thus ensures consistently high thermal efficiency of the solar thermal system.

## Miscibility

In order to maintain its specific properties, **TYFOCOR® LS®** must neither be mixed with other heat transfer fluids, nor it must be diluted with water! If any leakages occur, the system must be topped up with **TYFOCOR® LS®** only!

## Temperature Stability

**TYFOCOR® LS®** can be used in solar thermal systems with high stagnation temperatures provided it is ensured that the solar fluid will completely drain out of the collectors into the membrane expansion vessel in case of stagnation.

**TYFOCOR® LS®** must not be exposed to sustained temperatures higher than 170 °C. Temperatures higher than 200 °C lead to slow thermal decomposition of propylene glycol, which is indicated by darkening of the heat transfer fluid. The lifetime of the fluid thus may be strongly reduced, and the reliability of the system may be endangered.

## Anticorrosion Effect

The following table demonstrates the anticorrosion effect of **TYFOCOR® LS®** after two weeks of testing at 88 °C under permanent aeration. Corrosion test according to ASTM D 1384 (American Society for Testing and Materials).

Material		Average change of weight
Copper	(SF Cu)	–2.0 g/m <sup>2</sup>
Soft solder	(L Sn 30)	–6.0 g/m <sup>2</sup>
Brass	(MS 63)	–4.0 g/m <sup>2</sup>
Steel	(HI)	–0.1 g/m <sup>2</sup>
Cast Iron	(GG 26)	–0.2 g/m <sup>2</sup>
Cast Aluminium	(G-ALSi6Cu4)	–0.3 g/m <sup>2</sup>

## Compatibility with Sealing Materials

**TYFOCOR® LS®** does not attack the sealings that are normally used in solar technology. The following table of sealants, elastomers and plastics that are resistant to **TYFOCOR® LS®** has been compiled from experimental results, experience, and from literature data:

Examples of sealants are Fermit®, Fermitol® (registered trademarks of Nissen & Volk GmbH, Hamburg, Germany), hemp

Butyl rubber	IIR
Chloroprene	CR
Ethylene-propylene-diene-rubber	EPDM
Fluorocarbon elastomers	FPM
Natural rubber below 80 °C	NR
Nitrile rubber	NBR
Polyacetal	POM
Polyamides below 115 °C	PA
Polybutene	PB
Polyethylene, soft, hard	PE-LD/HD
Polyethylene, crosslinked	PE-X
Polypropylene	PP
Polytetrafluorethylene	PTFE
Polyvinylchloride, rigid	PVC h
Silicone rubber	Si
Styrene butadiene rubber below 100 °C	SBR
Unsaturated polyester resins	UP

Phenolic, urea-formaldehyde resins, plasticized PVC and polyurethane elastomers are not resistant.

An important point to note is that the performance of elastomers is not only governed by the properties of the rubber itself, e.g. EPDM, but also by the nature and amount of the constituent additives and the vulcanisation conditions. For this reason, it is recommended that their resistance to **TYFOCOR® LS®** is checked by performance tests before these elastomers are taken into use for the first time. This applies in particular to elastomers intended as membranes for expansion vessels as described in DIN EN 12828 and in DIN 4807 Part 2, respectively.

Gaskets that have proved to be resistant to hot **TYFOCOR® LS®** are: up to 160 °C gaskets made from 70 EPDM 281 (Carl Freudenberg GmbH, D-69465 Weinheim). Up to 200 °C: flat gaskets such as REINZ-AFM 34 (REINZ-Dichtungs-GmbH, D-89229 Neu-Ulm) or Centellen 3820 based on aramide/special-NBR. (Hecker Werke GmbH, D-71093 Weil im Schönbuch).

## Application guidelines

In view of the specific properties of **TYFOCOR® LS®** the following instructions must be observed to ensure long-term protection for the installations.

- 1.** Installations must be designed as closed circuits, as otherwise the contact with atmospheric oxygen will accelerate the consumption of inhibitors.
- 2.** Flexible-membrane expansion tanks must conform to DIN EN 12828 and DIN 4807 Part 2, resp.
- 3.** Silver or copper brazing solders are preferably to be used on joints. Fluxes used in combination with soft solder usually contain chlorides. Their residues must be removed from the system by thorough flushing. Otherwise, an increased content of chlorides in the heat transfer fluid may lead for example to pitting corrosion on stainless steel.
- 4.** The only flexible connections that are permitted for use are hoses, preferably made of metal, that are resistant to oxygen diffusion.
- 5.** The systems must not be equipped with internally galvanised heat exchangers, tanks or pipes, because zinc can be detached by propylene glycol/water mixtures.
- 6.** Chemically speaking, **TYFOCOR® LS®** is largely inert, but it is important to ensure that the manufacturer's recommendations state that all the seals and connector materials used are resistant up to the maximum fluid temperature.
- 7.** Scaling on copper surfaces must be removed from the system before filling. Otherwise, these particles will be removed by the hot heat transfer fluid and transported into other areas of the system, which may subsequently lead to formation of deposits and obstruction of the fluid flow rate.
- 8.** It must be ensured that no external voltages are applied between parts of the system that come into contact with the solar fluid.
- 9.** The layout of the piping must ensure that the circulation of the heat transfer fluid will not be disturbed by gas pockets or deposits.
- 10.** The fluid level must never be allowed to fall below the highest point in the system.
- 11.** If automatic bleed valves are used, they must not allow subsequent suction of air into the system.
- 12.** Dirt and water must not be allowed to enter the installation or its components during assembly and before filling. After the assembly has been completed, the system should be flushed to remove e.g. swarf, fluxes, assembly aids and any other impurities. Following to the flushing process and the leak test, the installation should be completely drained and then filled immediately with **TYFOCOR® LS®**.
- 13.** It must be ensured that no air remains in the solar thermal system after it has been filled. It is essential to eliminate any existing air or

gas pockets, because their collapse following a temperature drop would give rise to a vacuum and thus cause air to be sucked into the system. An insufficient deaeration furthermore affects the heat transfer efficiency of the system.

- 14.** In-circuit filter elements must be cleaned within 14 days at the latest after the system was put into operation, in order to ensure that no obstruction to the fluid flow may occur.
- 15.** If fluid losses occur due to evaporation, the system must be topped up with demineralised water. Losses due to leakage or removal from the system must be replaced with **TYFOCOR® LS®** only!
- 16.** The frost protection of **TYFOCOR® LS®** can be checked by measuring the fluid density with a hydrometer or an antifreeze tester suitable for propylene glycol/water mixtures. An equally convenient and accurate way to determine the frost protection is the measurement of the refractive index by using a hand-held refractometer.

## Storage Stability

The product has a shelf life of at least three years in airtight containers. It must not be stored in galvanised containers.

## Delivery Form and Packaging

**TYFOCOR® LS®** is available in road tankers, in 1,000 litre IBCs, in 200 litre drums, and in 30, 25, 20 and 10 litre non-returnable plastic cans.

## Disposal

Spills of the product must be taken up with an absorbent binder and disposed of in accordance with the regulations. For further information please refer to the Safety Data Sheet.

## Ecology

**TYFOCOR® LS®** is classified in water hazard class (WGK) 1, (low-rate endangering, Germany) acc. German water hazard regulations (*Verwaltungsvorschrift für wassergefährdende Stoffe* of May 17, 1999). The product is readily biodegradable.

## Handling

The usual safety and industrial hygiene measures relating to chemicals and the information and instructions given in our Safety Data Sheet must be observed in handling **TYFOCOR® LS®**.

## Safety Data Sheet

A current Safety Data Sheet in accordance with EU Directive 1907/2006/EC [REACH] is available on our website [www.tyfo.de](http://www.tyfo.de)

## Thermophysical properties of TYFOCOR® LS®

as a function of temperature

T [°C]	Density [kg/m <sup>3</sup> ]	Specific heat capacity [kJ/kg·K]	Thermal conductivity [W/m·K]	Kinematic viscosity [mm <sup>2</sup> /s]	Cubic expansion coefficient [•10 <sup>-5</sup> /K]	Vapour pressure [bar]
200	-	-	-	-	-	14.9
190	-	-	-	-	-	12.0
180	-	-	-	-	-	9.20
170	-	-	-	-	-	7.10
160	-	-	-	-	-	5.60
150	-	-	-	-	-	4.20
140	-	-	-	-	-	3.20
130	-	-	-	-	-	2.50
120	959	3.990	0.483	0.50	87	1.80
110	969	3.960	0.476	0.63	84	1.40
100	977	3.920	0.469	0.76	81	0.90
90	986	3.880	0.462	0.91	78	0.62
80	993	3.840	0.456	1.08	75	0.42
70	1001	3.800	0.449	1.32	72	0.29
60	1008	3.760	0.442	1.66	69	0.19
50	1015	3.720	0.434	1.91	66	0.12
40	1021	3.680	0.427	2.52	63	0.07
30	1029	3.640	0.420	3.40	59	0.04
20	1034	3.600	0.413	4.95	56	-
10	1040	3.560	0.406	7.90	53	-
0	1045	3.520	0.399	14.5	49	-
-10	1049	3.480	0.392	26.9	46	-
-20	1053	3.440	0.385	57.1	43	-

### Note

The information submitted in this publication is based on our current knowledge and experience. In view of the many factors that may affect processing and application these data do not relieve processors of the responsibility of carrying out their own tests and experiments, neither do they imply any legally binding assurance of certain properties or of suitability for a specific purpose. It is the responsibility of those to whom we supply our products to ensure that any proprietary rights and existing laws and legislations are observed.

# The TYFO product range

**TYFOCOR®** is a long-life, corrosion-inhibiting antifreeze based on ethylene glycol for cooling and heating, air-conditioning, heat pump, and under-soil heating systems. It can be supplied as a concentrate or a pre-mixed, ready-to-use product as desired.

**TYFOCOR® GE** is a long-life, corrosion-inhibiting antifreeze based on ethylene glycol specially formulated for use in geothermal heat pump systems, air conditioning units, and under-soil heating. It can be supplied as desired in the form of a concentrate or a pre-mixed, ready-to-use product.

**TYFOCOR® L** is a long-life corrosion-inhibiting antifreeze based on propylene glycol for heating and air-conditioning, solar thermal, and heat pump systems. It is also used as a special food-grade brine by food and beverage manufacturers and is supplied both as a concentrate and a pre-mixed, ready-to-use product.

**TYFOCOR® Leco®** is a long-life corrosion-inhibiting antifreeze based on propylene glycol that covers the same applications as **TYFOCOR® L**. Practically all of the substances contained in the product are derived from 100% renewable resources.

**TYFOCOR® LS®** is a special, ready-to-use, almost completely vaporizable, propylene-glycol-based heat transfer fluid for use in solar systems that are subject to extreme thermal conditions.

**TYFOCOR® G-LS** is a special, ready-to-use, almost completely vaporizable, propylene-glycol-based heat transfer fluid for use in solar systems that are subject to extreme thermal conditions. It contains a glass protection additive that makes it suitable for use in all-glass solar collectors.

**TYFOCOR® HTL** is a special, ready-to-use heat transfer fluid based on non-toxic glycols for use in solar systems that are subject to extreme thermal conditions.

**TYFO-SPEZIAL** is a special, high-performance brine formulated for geothermal heat pumps located in areas subject to special government regulations. Due to its lack of glycols, it does not cause any underground biological oxygen depletion in the event of a leak.

**TYFOXIT® 1.15–1.25** are non-toxic, high-performance, glycol-free secondary coolants based on potassium acetate with very low viscosities for chiller systems with secondary cooling. They are available as concentrates (**TYFOXIT® 1.25**) and ready-to-use mixtures ranging from  $-20\text{ °C}$  (**TYFOXIT® 1.15**) to  $-55\text{ °C}$  (**TYFOXIT® 1.25**).

**TYFOXIT® F15–50** are non-toxic, high-performance, glycol-free, potassium-formate-based secondary coolants with very low viscosities for chiller systems with secondary cooling. They are available as ready-to-use mixtures ranging from  $-15\text{ °C}$  (**TYFOXIT® F15**) to  $-50\text{ °C}$  (**TYFOXIT® F50**).

To learn more about our products, visit [www.tyfo.de](http://www.tyfo.de)





Edition: 2015 © TYFOROP Chemie GmbH. Technical information is subject to change without notice.

---

**TYFOROP** Chemie GmbH

Anton-Rée-Weg 7  
20537 Hamburg, Germany

Phone: +49 (0) 40/20 94 97-0  
Fax: +49 (0) 40/20 94 97-20  
205

info@tyfo.de  
www.tyfo.de



**TYFOROP** Chemie GmbH



# Publications and communications

## Publications

1. **Hamze, S.**; Berrada, N.; Cabaleiro, D.; Desforges, A.; Ghanbaja, J.; Gleize, J.; Bégin, D.; Michaux, F.; Maré, T.; Vigolo, B.; Estellé, P. Few-Layer Graphene-Based Nanofluids with Enhanced Thermal Conductivity. *Nanomaterials* **2020**, *10*, 1258, doi:10.3390/nano10071258.
2. **Hamze, S.**; Cabaleiro, D.; Bégin, D.; Desforges, A.; Maré, T.; Vigolo, B.; Lugo, L.; Estellé, P. Volumetric Properties and Surface Tension of Few-Layer Graphene Nanofluids Based on a Commercial Heat Transfer Fluid. *Energies* **2020**, *13*, 3462, doi:10.3390/en13133462.
3. **Hamze, S.**; Cabaleiro, D.; Maré, T.; Vigolo, B.; Estellé, P. Shear flow behavior and dynamic viscosity of few-layer graphene nanofluids based on propylene glycol-water mixture. *Journal of Molecular Liquids* **2020**, *316*, 113875, doi:10.1016/j.molliq.2020.113875.
4. **Hamze, S.**; Berrada, N.; Desforges, A.; Vigolo, B.; Gleize, J.; Ghanbaja, J.; Maré, T.; Cabaleiro, D.; Estellé, P. Dynamic viscosity of purified MWCNT water and water-propylene glycol based nanofluids. *Heat transfer Eng.*, accepted.
5. Berrada, N.; **Hamze, S.**; Desforges, A.; Ghanbaja, J.; Gleize, J.; Maré, T.; Vigolo, B.; Estellé, P. Surface tension of functionalized MWCNT-based nanofluids in water and commercial propylene-glycol mixture. *Journal of Molecular Liquids* **2019**, *293*, 111473, doi:10.1016/j.molliq.2019.111473.
6. Cabaleiro, D.; **Hamze, S.**; Fal, J.; Marcos, M.A.; Estellé, P.; Żyła, G. Thermal and Physical Characterization of PEG Phase Change Materials Enhanced by Carbon-Based Nanoparticles. *Nanomaterials* **2020**, *10*, 1168, doi:10.3390/nano10061168.
7. Cabaleiro, D.; **Hamze, S.**; Agresti, F.; Estellé, P.; Barison, S.; Fedele, L.; Bobbo, S. Dynamic Viscosity, Surface Tension and Wetting Behavior Studies of Paraffin-in-Water Nano-Emulsions. *Energies* **2019**, *12*, 3334, doi:10.3390/en12173334.
8. Wanic, M.; Cabaleiro, D.; **Hamze, S.**; Fal, J.; Estellé, P.; Żyła, G. Surface tension of ethylene glycol-based nanofluids containing various types of nitrides: An experimental study. *J Therm Anal Calorim* **2020**, *139*, 799–806, doi:10.1007/s10973-019-08512-1.
9. Marcos, M.A.; Cabaleiro, D.; **Hamze, S.**; Fedele, L.; Bobbo, S.; Estellé, P.; Lugo, L. NePCM Based on Silver Dispersions in Poly(Ethylene Glycol) as a Stable Solution for Thermal Storage. *Nanomaterials* **2019**, *10*, 19, doi:10.3390/nano10010019.
10. Gómez-Villarejo, R.; Aguilar, T.; **Hamze, S.**; Estellé, P.; Navas, J. Experimental analysis of water-based nanofluids using boron nitride nanotubes with improved thermal properties. *Journal of Molecular Liquids* **2019**, *277*, 93–103, doi:10.1016/j.molliq.2018.12.093.
11. Kujawska, A.; Mulka, R.; **Hamze, S.**; Żyła, G.; Zajaczkowski, B.; Buschmann, M. H.; Estellé, P. The effect of boiling in a thermosyphon on surface tension and contact angle of silica and graphene oxide nanofluids. *International Journal of Heat and Mass Transfer*, submitted.
12. Sobczak, J.; Vallejo, J. P.; Traciak, J.; **Hamze, S.**; Fal, J.; Estellé, P.; Lugo, L.; Żyła, G. Thermophysical profile of ethylene glycol based nanofluids containing two types of carbon black nanoparticles with different specific surface areas. *International Journal of Heat and Mass Transfer*, submitted.

**Communications**

1. **Hamze, S.**; Berrada, N.; Desforges, A.; Vigolo, B.; Maré, T.; Cabaleiro, D.; Estellé, P. Dynamic viscosity of purified MWCNT water and water-propylene glycol based nanofluids. *First International Conference on Nanofluids (ICNf)*, Castellon, Spain, June 2019 (Oral presentation).
2. Cabaleiro, D.; **Hamze, S.**; Agresti, F.; Estellé, P.; Barison, S.; Fedele, L.; Bobbo, S. Dynamic viscosity and surface tension characterization of paraffin-in-water nanoemulsions. *First International Conference on Nanofluids (ICNf)*, Castellon, Spain, June 2019 (Oral presentation).
3. Berrada, N.; Desforges, A.; Ghanbaja, J.; Gleize, J.; Bégin, D.; Estellé, P.; **Hamze, S.**; Vigolo, B. Graphene-based nanofluids: structural quality of graphene vs. dispersion quality. *First International Conference on Nanofluids (ICNf)*, Castellon, Spain, June 2019 (Oral presentation).
4. Kujawska, A.; **Hamze, S.**; Mulka, R.; Zajaczkowski, B.; Estellé, P. The influence of boiling process on surface tension, contact angle, and viscosity of nanofluids. *IV International Caparica Symposium on Nanoparticles/nanomaterials and Applications 2020*, Caparica, Portugal, January 2020 (Poster).



**Titre :** Nanofluides à base de graphène: développement, caractérisation et application aux systèmes énergétiques et de chaleur

**Mots clés :** Graphène à quelques couches, Tyfocor® LS, nanofluides, performance thermique

**Résumé :** Dans notre vie quotidienne, le transfert de la chaleur et de l'énergie constitue la base de nombreux processus industriels. L'épuisement progressif des énergies fossiles conduit à améliorer et optimiser les rendements de ces échanges par de nouveaux procédés. Pour cela, une idée d'améliorer la performance thermique des fluides dans les échangeurs de chaleur a été proposée pour réduire l'énergie consommée pour l'échange de chaleur. Cette idée est basée sur l'introduction des nanoparticules solides qui présentent des propriétés thermiques beaucoup plus importantes que les liquides caloporteurs dans ces derniers, en obtenant un nanofluide. Cette introduction a pour effet d'augmenter la conductivité thermique du fluide mais d'autre part provoque une augmentation défavorable de sa viscosité qui résulte en une augmentation de la puissance de pompage. Alors il faut faire un compromis entre la stabilité, la conductivité thermique et la viscosité des nanofluides. Dans cette étude, des nanofluides à base de

graphène à quelques couches et un fluide commercial, Tyfocor® LS, ont été préparés dans la gamme de concentration massique 0,05-0,5% en utilisant trois surfactants différents. Une étude complète sur ces nanofluides est présentée, y compris la synthèse des feuillets de graphène, la préparation des nanofluides et l'étude de leur stabilité, ainsi que l'évaluation expérimentale de leurs propriétés thermophysiques en fonction de la concentration en graphène, du type de surfactant utilisé et de la température dans la gamme 283,15-323,15 K. Finalement, sur la base de ces résultats et par une approche qualitative, le potentiel applicatif des nanofluides dans des systèmes énergétiques est déterminé pour sélectionner le meilleur candidat. Les résultats ont montré une bonne amélioration de la performance thermique par rapport aux fluides de base dans la gamme de température testée et surtout le nanofluide de la série du surfactant Pluronic® P-123 de concentration massique 0,25%.

**Title :** Graphene based nanofluids: development, characterization and application for heat and energy systems

**Keywords :** Few layer graphene, Tyfocor® LS, nanofluids, thermal performance

**Abstract :** In our daily lives, the heat and energy transfer forms the basis of many industrial processes. The gradual depletion of fossil fuels leads to improving and optimizing the efficiency of these exchanges through new processes. To this end, the idea of improving the thermal performance of fluids in heat exchangers has been proposed forward to reduce the energy consumed for heat exchange. This idea is based on the introduction of solid nanoparticles, which have much greater thermal properties than heat-transfer fluids in the latter, obtaining a nanofluid. This introduction has the effect of increasing the thermal conductivity of the fluid but on the other hand causes an unfavorable increase in its viscosity, which results in an increase in pumping power. So a compromise has to be made between the stability, thermal conductivity and viscosity of nanofluids. In this study, few layer graphene based nanofluids and a commercial fluid,

Tyfocor® LS, were prepared in the weight concentration range 0.05-0.5% using three different surfactants. A complete study on these nanofluids is presented, including the synthesis of the graphene sheets, the preparation of the nanofluids and the study of their stability, as well as the experimental evaluation of their thermo-physical properties as a function of the graphene concentration, the type of surfactant used and the temperature in the range 283.15-323.15 K. Finally, on the basis of these results and through a qualitative approach, the potential application of nanofluids in energy systems is determined in order to select the best candidate. The results showed a good improvement of the thermal performance compared to the base fluids in the tested temperature range and especially the nanofluid of the Pluronic® P-123 surfactant series with a mass concentration of 0.25%.